Expanding the Utility of
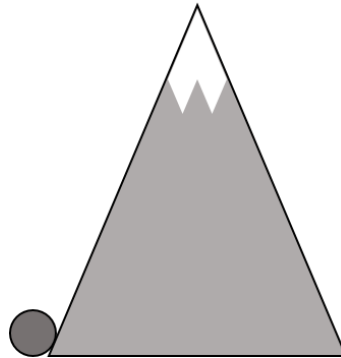# Catalyst-Transfer Polymerization

by

Mitchell Lee Smith

A dissertation submitted in partial fulfillment
of the requirements for the degree of
Doctor of Philosophy
(Chemistry)
in the University of Michigan
2017

Doctoral Committee:

       Professor Anne J. McNeil (Chair)
       Professor Jinsang Kim
       Professor Adam J. Matzger
       Professor John P. Wolfe

"There is much I wish to know
but neither books nor people will tell me"
Danil Kharms

"It is recommended to work in the fully relaxed regime"
Bruker imaging manual

Mitchell L. Smith

mlsmit@umich.edu

ORCID iD: 0000-0002-2271-2637

DEDICATION

To my family and to Laura– your confidence in me was the support I needed.

ACKNOWLEDGEMENTS

TABLE OF CONTENTS

LIST OF FIGURES

FIGURE

LIST OF TABLES

TABLE

LIST OF SCHEMES

LIST OF CHARTS

CHART

LIST OF APPENDICIES

APPENDIX

ABSTRACT

Conjugated polymers are electronically tunable semiconductors that can be solution-processed onto flexible substrates, making them valuable materials for electronic devices including bulk-heterojunction (BHJ) solar cells. Historical syntheses of π-conjugated polymers have been step-growth; however, the development of catalyst-transfer polymerization (CTP) has led to precise control over molecular weight, dispersity, and copolymer sequence. To date, CTP has not been widely adopted to prepare materials for devices. This thesis describes our efforts to improve the utility of CTP through developing new catalysts for the controlled synthesis of π-conjugated polymers, investigating the mechanism of non-living behavior in CTP of challenging substrates, and understanding the impact of dispersity on thin-film morphology.

Chapter 1 provides an overview of BHJ solar cells and a brief history of catalyst-transfer polymerization. Investigations of the mechanism of CTP are described, with a focus on the purported key intermediate, a catalyst-polymer π-complex formed following reductive elimination. We focus on the monomer scope, illustrating the current limitations, and connect the challenge posed by electron-deficient monomers to the proposed mechanism. The catalyst scope, and efforts to expand CTP catalysis to alternate ancillary ligand scaffolds, is also described.

Chapter 2 describes the use of a palladium-N-heterocyclic carbene catalyst for CTP. We observe the controlled polymerization of both phenylene and thiophene monomers, while the polymerization of fluorene is nonliving. Excitingly, block copolymers of thiophene and phenylene can be prepared regardless of addition order, indicating more complicated copolymer sequences

could be achieved. We suggest further investigation of this catalyst scaffold as an alternate path for new CTP conditions.

Chapter 3 describes mechanistic studies into the CTP of thiazole, an electron-deficient analogue of thiophene. Using reaction-discovery calculations, we identify a facile pathway for chain-transfer to monomer. The chain-transfer pathway is enabled by preferential association of the catalyst following reductive elimination, inhibiting catalyst transfer to the chain-end. We selectively inhibit this chain-transfer pathway and promote chain propagation via ancillary ligand modification. End-group analysis confirms the greatly enhanced living character of the polymerization. We also report the autopolymerization of certain thiazole Grignard monomers.

Chapter 4 reports initial investigations into the role of dispersity on thin-film morphology. The existing literature on dispersity's impact is in poor agreement, and we believe that the control CTP provides over molecular weight is necessary to properly investigate this question. We utilize two methods to vary dispersity, preparing three series of polymer samples with similar M_n or M_w. Using UV-vis spectroscopy and optical microscopy, we find that fullerene aggregation increases with dispersity, and tentatively attribute this to the presence of more low-molecular-weight polymer. Preparation and characterization of solar cells is underway. We expect the large morphological differences we observe to significantly impact device performance and lifetime. The control over molecular weight distribution that CTP provides will be invaluable for future BHJ research.

Chapter 5 summarizes our efforts expanding the scope of CTP and applying it towards the synthesis of polymers for bulk-heterojunction photovoltaic solar cells. Future directions are outlined for each chapter, highlighting areas of research needed to address limitations of CTP. Additionally, relevant external papers that have been influenced by our work are also briefly discussed. Widespread adoption of CTP will require continued expansion of the monomer scope to include polymers used in high-efficiency devices, and this thesis describes some fruitful strategies for targeting useful monomers.

Chapter 1
Introduction

Since the Nobel Prize-winning work demonstrating conductivity in polymers with extended π-conjugation,[1] there have been efforts to replace inorganic semiconductors with these novel materials. Devices prepared with conjugated polymers include field-effect transistors,[2] light-emitting diodes,[3] and photovoltaic solar cells.[4] In many applications, organic electronic devices are preferred to their inorganic analogues because of their favorable physical properties. They are lightweight, flexible, and have manufacturing cost advantages over traditional semiconductors arising from their solution processability and roll-to-roll manufacture.[5]

Organic photovoltaic solar cells (OPVs) operate via a three-step process analogous to that of inorganic solar cells.[6] First, absorption of a photon generates an exciton in the donor. The exciton migrates to the donor/acceptor interface, where charge separation occurs and the excited electron is transferred to the acceptor. The electron and hole are then conducted through the acceptor and donor phases to the anode and cathode, respectively, where they are collected and can perform work. While OPVs with acceptor phases comprised of polymers[7] or small molecules[8] have been developed, their performance lags those with fullerene acceptors; the soluble fullerene derivative phenyl-C_{61}-butyric acid methyl ester (PCBM) is the most commonly used acceptor due to its high electron affinity and conductivity. Soon after the first reports of photoinduced electron transfer from conjugated polymers to fullerenes,[9] bilayer OPV devices were prepared.[10] The power conversion efficiencies of these cells were very low due to their small interfacial area, but the proof of concept led researchers to explore alternate device architectures. Bulk heterojunction (BHJ) cells[11] are particularly attractive due to

their high interfacial surface area and their straightforward preparation. The active layer of a BHJ is made up of a physical blend of a semiconducting donor polymer and acceptor fullerene (Figure 1.1). During device preparation, this film is deposited from solution via spin-coating. The donor and acceptor undergo nanoscale phase separation driven by donor crystallization.[12] Alternate strategies to control the growth of the heterojunction and minimize isolated domains, e.g. controlled organic vapor-phase deposition,[13] provide moderately increased performance, but their arduous device manufacturing processes assure the continued dominance of comparatively simple BHJs.

Figure 1.1 Diagram of BHJ photovoltaic solar cell structure and energy levels.[14]
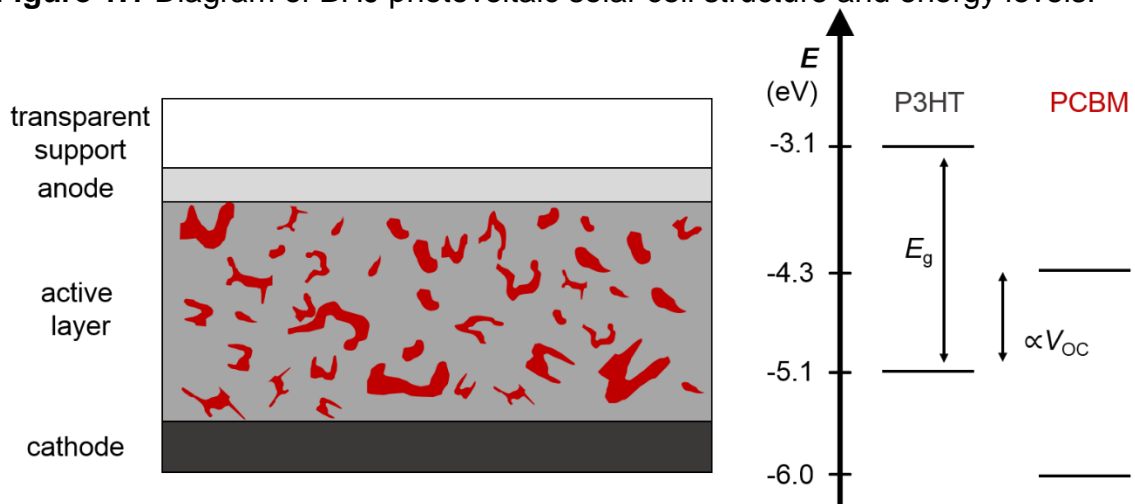
The maximum efficiency of BHJ OPVs is determined by the electronic properties of the donor and acceptor that make up the active layer. For example, the portion of the solar spectrum that is absorbed is determined by the band gap (E_g, the energy difference between the lowest unoccupied and highest occupied molecular orbitals) of the donor polymer, and the maximum output potential (V_{oc}) of the cell is proportional to the difference between the energies of the acceptor LUMO and donor HOMO.[15] Because fullerene derivatives dramatically outperform conjugated polymers and other small molecules as acceptor phases, electronic tuning of the active layer is usually carried out by modifying the polymer structure. The theoretical efficiency of a device employing PCBM as an acceptor is

maximized by a donor polymer whose LUMO sits at -4.0 eV with E_g = 1.6 eV.[14] To achieve these narrow band gaps and low-lying LUMOs, alternating copolymers combining electron-rich and electron-poor monomers are frequently employed.[16] In these donor-acceptor copolymers, the HOMO level is largely determined by the electron-rich donor monomer, while the LUMO level is determined by the electron-deficient acceptor monomer.[17] Power conversion efficiencies above 10% have been achieved using this design strategy (Chart 1.1).[18]

Chart 1.1 Active-layer components for selected high-performance BHJ OPVs.[18a,b]

PffBT4T-2OD
PCE: 10.5%

PTB7-Th
PCE: 10.6%

PC$_{71}$BM
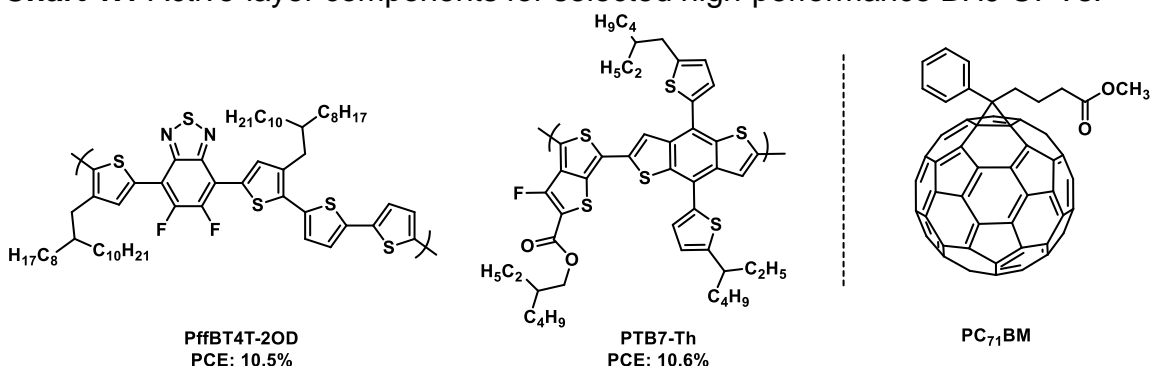
While the LUMO and bandgap of the donor polymer play a major role in determining a bulk heterojunction solar cell's theoretical efficiency, its realized efficiency depends heavily on that polymer's physical properties. After excitons are generated by photon absorption in the donor polymer, they must travel to the donor/acceptor interface to undergo charge separation. The charges must then be conducted to the electrodes and collected. Factors such as the size and crystallinity of polymer domains and the degree of polymer-fullerene intermixing influence these conduction processes and directly impact how much current is produced by the cell (measured as the short-circuit current J_{sc} and fill factor FF). In the active layer blend, donor crystallization during deposition leads to nanoscale phase separation to form homogenous domains. If the donor domain size is larger than the exciton diffusion length (ca. 10 nm), geminate recombination will limit charge generation. On the other hand, very small domains act as trap sites and lead to nongeminate recombination following charge separation.[19] Domain size is

strongly influenced by processing (i.e., spin rate, solvent choice, annealing temperature)[20] of the active layer as well as by the properties of the donor polymer. One key donor property is molecular weight: higher molecular weight polymers consistently outperform low-molecular weight polymers. The reduction of crystallinity in heavier polymers leads to improved intermixing with PCBM.[21]

Figure 1.2 Number-average molecular weight (M_n) versus conversion (A) and molecular weight distributions (B) of polymers synthesized via ideal step- and chain-growth methods.
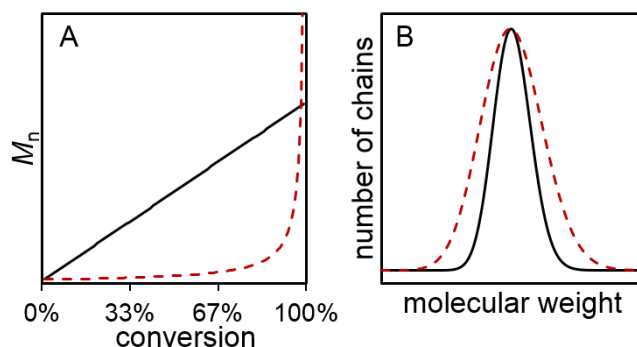
In the step-growth polymerizations used to synthesize most conjugated polymers, it can be difficult to target specific molecular weights, due to the rapid increase in M_n at high conversion (Figure 1.2A). In contrast, chain-growth polymerization enables simple targeting of molecular weight by adjusting catalyst loading. Because molecular weight strongly influences device properties, chain-growth synthesis of conjugated polymers may be important for optimizing and commercializing organic photovoltaic devices. Additionally, chain-growth polymerizations have a narrower distribution of molecular weights (dispersity, Đ, née PDI) (Figure 1.2B). However, there remains a lack of consensus on how dispersity affects device performance. Previous studies on the effect of dispersity employ polymers synthesized via step-growth methods, leading to confounding correlations between dispersity and regioregularity and/or molecular weight.[22,23,24] Synthetic limitations in existing studies of the role of dispersity in device performance may explain their contradictions regarding dispersity's effect. Using chain-growth synthesis techniques, M_n and M_w can be independently varied while

keeping potential confounders like regioregularity constant. Chapter 4 reports such a study on the impact of dispersity on the morphology of BHJ OPVs.

In many cases, BHJ active layer morphology is unstable. Aging or annealing these devices leads to continued growth of nanoscale domains, eventually generating micron-sized aggregates in the case of P3HT/PCBM.[25] The concomitant reduction in interfacial area, and therefore charge generation, limits the effective lifetime of BHJ solar cells. The power conversion efficiency of BHJs has been stabilized utilizing an active layer composed of a ternary blend of donor polymer, fullerene acceptor, and a polymer additive with portions similar to both the donor and acceptor.[26] The proposed mechanism involves the additive localizing at the donor/acceptor interface, stabilizing the initial morphology. The sequence of the additive plays a key role. Desirable sequences such as *gradient* and *block* copolymers (Figure 1.3) are difficult or impossible to access using step-growth polymerization methods. However, desirable copolymer sequences such as block and gradient are readily accessed via chain-growth methods by varying the comonomer ratio over the course of the reaction.

Figure 1.3 Copolymer sequences and corresponding composition diagrams.
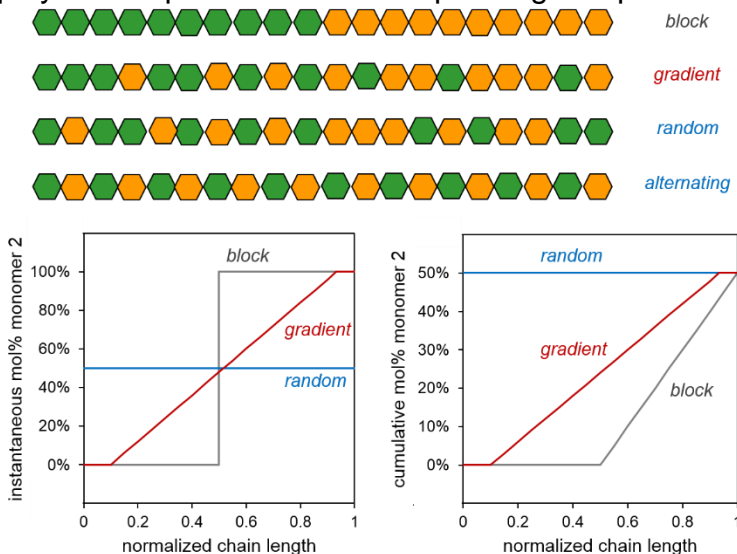
Conjugated polymers were first observed to undergo chain-growth polymerization, in which monomers are added one at a time to the growing chain

end, in 2004 by McCullough and Yokozawa, who were independently investigating the synthesis of poly(3-hexylthiophene) from organometallic/bromide difunctionalized monomers with (1,3-bis(diphenylphosphino)propane)nickel(II) dichloride.[27] Several possibilities were proposed to explain the observed chain propagation. However, most researchers favor a model involving formation of a catalyst-polymer π-complex[28] (Scheme 1.1) over alternate hypotheses such as coordination to a heteroatom lone pair, diffusion-controlled oxidative addition, or enhanced reactivity of the polymer chain-end.[27a,29] While efforts to directly observe this intermediate have been unsuccessful, Ni-arene π-complexes have been reported in the literature[30] and analogous intermediates are observed in small-molecule studies.[31] This associative intermediate promotes intramolecular oxidative addition, ensuring that each catalyst remains associated with a single polymer chain throughout the polymerization. This mechanism has been termed catalyst-transfer polymerization (CTP).

Scheme 1.1 Proposed mechanism of Kumada catalyst-transfer polymerization.
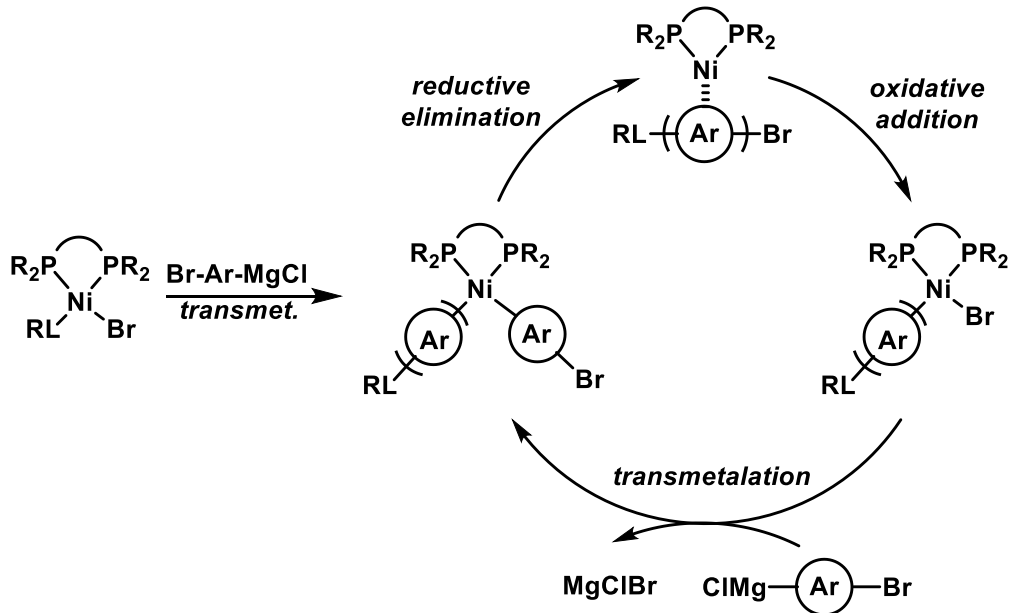
Catalyst-transfer polymerizations do not exhibit perfectly living behavior: both termination and chain-transfer reactions are observed. While deviations from ideal behavior can be observed as a broader distribution of molecular weights, this

metric gives little insight into the non-living behavior's origin. Additionally, broad dispersity can arise even in a living polymerization; for example, if initiation is slow relative to propagation.[32] Of the three common non-living pathways – chain-transfer, disproportionation, and termination – two give rise to unique end-groups (Scheme 1.2). With appropriate choice of initiator reactive ligand, these end-groups can be readily identified using mass spectrometry, and the cause of non-living behavior ascertained.

Scheme 1.2 Non-living pathways and their characteristic end-groups. (A) Chain-transfer (B) Disproportionation
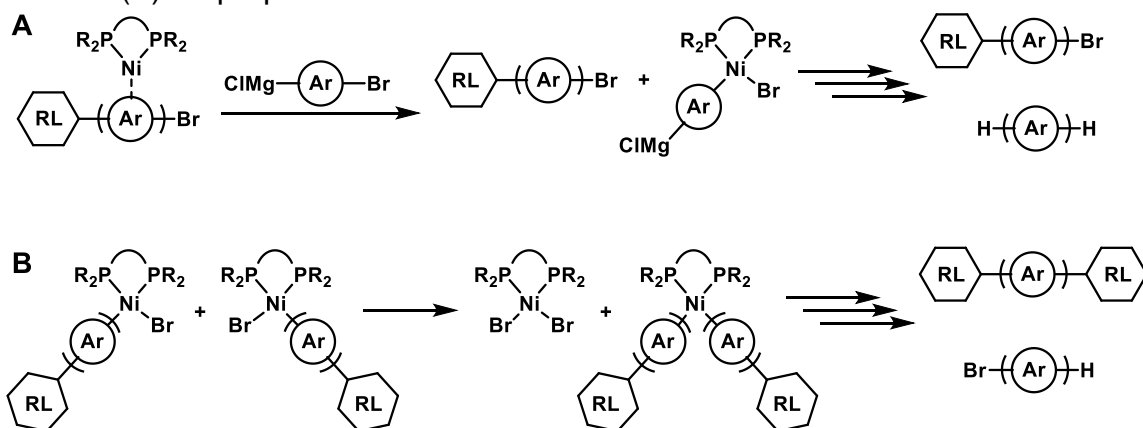
As CTP has been further developed, the ability to target comonomer sequences has been exploited. Block[33] and gradient[34] copolymers, inaccessible via step-growth methods, have been synthesized. The two most-studied monomers for CTP are the thiophene derivative **1** and phenylene derivative **2**. While several catalysts have been demonstrated to mediate living, chain-growth polymerizations of both **1** and **2**, the synthesis of their copolymers nevertheless proved problematic.[35] The order of monomer addition played a key role in the synthesis of **PPP-*block*-P3HT**: while **P3HT-NiL₂X** macroinitiators are readily extended with a **PPP** block, the inverse chain-extension fails. Instead, a mixture of the desired copolymer and both homopolymers is produced. Preferential association between the catalyst and poly(thiophene) may inhibit catalyst migration to the chain-end following installation of a phenylene monomer, leading to chain-transfer rather than the desired chain extension (Scheme 1.3). This

hypothesis is supported by MALDI-TOF-MS analysis showing that many of the **P3HT** homopolymers are capped with bromobis(hexyloxy)phenylene on each end.[35a] This cross-propagation failure renders the synthesis of copolymer sequences such as triblock, gradient, or random impossible. Synthesis of these interesting sequences using both electron-rich and electron-poor monomers, as are used in high-performing devices, will require a broader comonomer scope for chain-growth polymerization.

Scheme 1.3 Order of polymerization is critical in the synthesis of electronically differentiated block copolymers with commonly-used Ni-phosphine catalysts.[35a]
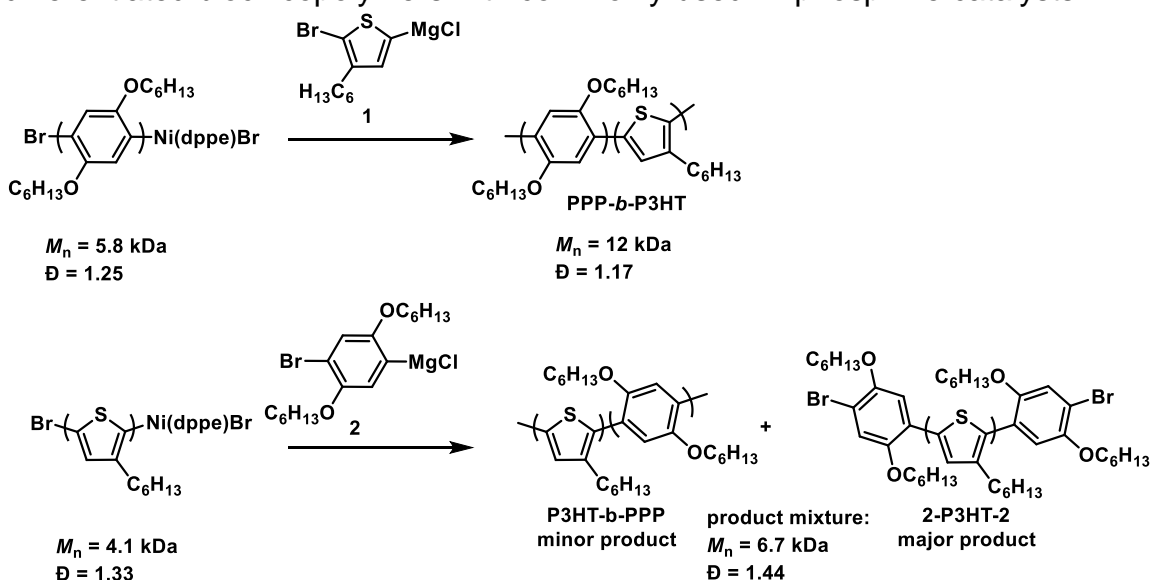
The limits on cross-propagation with nickel phosphine catalysts motivates the investigation of alternate catalyst systems for CTP to achieve broader comonomer scope. In systematic studies of nickel bisphosphine-catalyzed polymerizations,[36] it was demonstrated that moderate steric crowding promotes chain growth, while unhindered ligands led to catalyst decomposition and sterically encumbering ligands inhibited transmetalation. Additionally, more electron-donating ligands were shown to give more-ideal chain-growth behavior, possibly due to a stabilized metal-polymer π-complex intermediate.[37] This work suggests that electron-rich ligands with moderate steric encumbrance are suitable targets to investigate as alternate ancillary ligands for chain-growth polymerizations.

8

Although CTP catalysts have historically employed nickel, palladium phosphine catalysts have been demonstrated to mediate chain-growth polymerizations. These Pd catalysts outperform Ni in polymerizations that employ less-reactive monomer types, such as those based on direct arylation[38] or Suzuki,[39] Stille,[40] and Heck[41] couplings (Chart 1.2).

Chart 1.2 Selected Pd-catalyzed catalyst-transfer polymerizations.
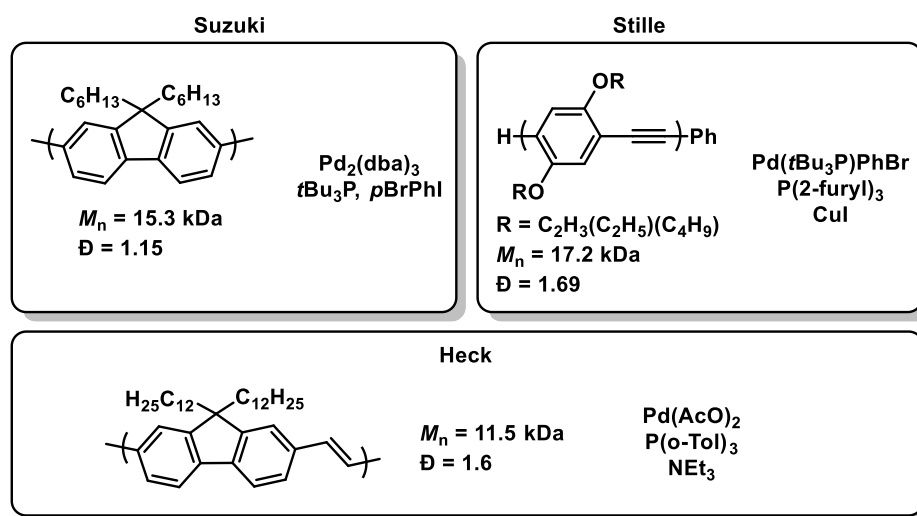
Chapter 2 reports the use of a palladium-N-heterocyclic carbene precatalyst, which is air- and moisture-stable and sold commercially as PEPPSI-IPr, in CTP. N-Heterocyclic carbenes (NHCs) are stronger σ-donors than phosphines,[42] and their steric encumbrance is readily modified by choice of 'arm', similar to the features observed to promote chain-growth polymerization with phosphines. In addition, PEPPSI-IPr was reported to selectively difunctionalize 1,4-dibromobenzene upon treatment with a single equivalent of phenylmagnesium bromide.[43] This result suggests preferential intramolecular oxidative addition following reductive elimination. Because chain-growth polymerization proceeds via selective intramolecular oxidative addition, this behavior in a small-molecule system suggested that this precatalyst is potentially suitable for CTP. Using PEPPSI-IPr, we report the chain-growth synthesis of **P3HT** and **PPP**, as well as their block copolymers with both orders of addition. This result suggests the

importance of the catalyst-polymer association in determining the monomer scope for copolymerizations. Too weak an interaction may lead to frequent chain-transfer in homopolymerizations; too strong an interaction may inhibit propagation to a comonomer. Recent work exploring alternate ligand scaffolds for nickel, including N-heterocyclic carbenes[44] and diimines,[45] is also promising in this regard, including demonstrations of copolymerizations of electronically differentiated monomers.[45b,d]

Extending CTP to synthesizing low-bandgap polymers for use in high-efficiency devices will also require expansion of the monomer scope. While CTP conditions have been identified for some electron-rich monomers,[46] CTP of electron-deficient monomers remains challenging. This contradicts naïve expectation, as the catalyst-polymer π-complex that promotes intramolecular oxidative addition should be stabilized in electron-deficient monomers, which are stronger π-acceptors.[47] While these substrates are challenging, there have been several reported non-living chain-growth syntheses of n-type conjugated polymers.

The first significant demonstration of CTP with an electron-deficient monomer was Rasmussen's work with polythienopyrazine derivative **PTPz**.[48] The narrow band-gap of **PTPz** (E_g = 0.93 eV) makes it desirable for a variety of applications; however, poor solubility prevented the synthesis of high molecular weight materials. Limited characterization of insoluble materials also hinders determination of the polymerization mechanism, but the narrow dispersity of the soluble fraction suggests some chain-growth character. Yokozawa also encountered low solubility during studies of polypyridine derivatives **PpPy** and **PmPy**. In **PpPy**, the position of the side-chain greatly impacted polymerization control; with the ethereal substituent in the 2-position, frequent disproportionation led to very broad dispersity and poor end-group control.[49a] Facile disproportionation is attributed to coordination between a N lone pair at the chain end and Ni associated with another polymer chain. This side reaction is suppressed when the side chain is installed at the monomer 3-position, giving poly(pyridine) with moderate molecular weight and good dispersity.[49b] The chain-growth nature of the polymerization is further improved in the synthesis of **PmPy**. This polymer was prepared with good dispersity and control over end-groups;

however, as **PmPy** is not through-conjugated it is of limited interest.[49c] Very high molecular weights were achieved in Kiriy's synthesis of poly(napthelene diimide) derivative **PNDI**, albeit with moderate dispersities due to slow initiation.[50] Unusually, activation of the perylene diimide monomer with Zn^0 did not give the expected Negishi reagent; instead, a stable radical anion was proposed to form. This alternate mechanism limits extension to non-radical-forming monomers and comonomers.

Chart 1.3 CTP homopolymerization of electron-deficient substrates.[48-54]
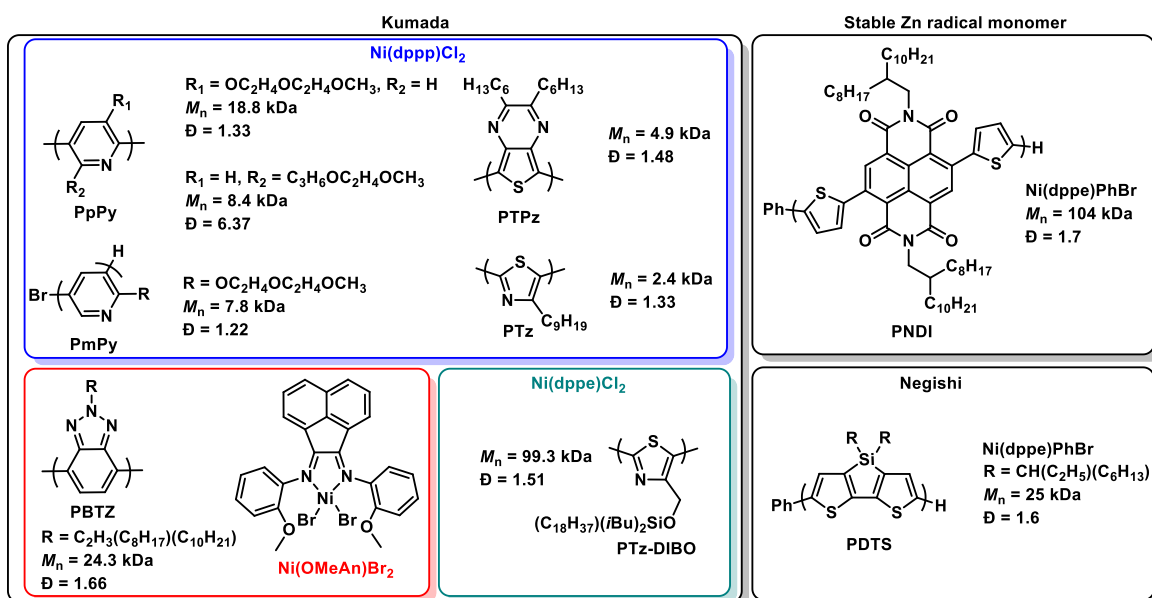
Pammer's work with polythiazole derivative **PTz**, like Yokozawa's with pyridine, was complicated by poor solubility. The narrow dispersity and good end-group control observed with an alkyl-functionalized monomer was promising, but the bulk of the recovered polymer was insoluble.[51a] By using a highly solubilizing silane-functionalized monomer, **PTz-DIBO** was prepared at very high molecular weights with moderate dispersities.[50b] However, the bulky side chain disrupted π-stacking in films of **PTz-DIBO**, which has been demonstrated to lower charge-carrier mobility and thereby limit utility in devices.[52] Kiriy's synthesis of polydithienosilole **PDTS** is more promising for device applications. In addition to the chain-growth synthesis of **PDTS**, **P3HT-block-PDTS** is prepared with good control over molecular weight and end-groups.[53] Seferos recently demonstrated

that several nickel diimine catalysts are competent in the chain-growth synthesis of polybenzotriazole derivative **PBTZ**.[54] As with phosphine ligands, the more strongly-donating diimines gave better polymerization performance; the most electron-rich gave **PBTZ** with moderate molecular weight and dispersity and good end-group control.

Even in these examples of CTP with electron-deficient monomers, dispersities are broader and end-group control is generally poor compared to electron-rich examples. There is currently no consensus on the origin of non-living polymerizations with these substrates; however, several researchers have proposed that the Ni-polymer π-complex intermediate may play a detrimental role by hindering transfer to the chain-end.[55] For example, initially formed oligomers have been invoked as trapping ligands: strong interactions with these oligomers are proposed to inhibit catalyst migration to the chain-end (Scheme 1.4). Kiriy and Sommer observed that nickel bisphosphines do not 'ring-walk' across a benzothiadiazole moiety during the polymerization of **1**, leading to exclusively unidirectional growth despite the presence of reactive bromides on both ends of the polymer chain.[55a] Koeckelbergs reports a similar 'trapping' of Ni^0 in a stable π-complex after a single turnover during the polymerization of thienothiophene derivative **4**.[55b] Kiriy attributes reduced control in the synthesis of **PTiI** compared to the similar **PNDI** to its increased double-bond character. Frequent chain-transfer is facilitated by a strong π-complex inhibiting chain-walking.[55c] Whether this issue of too-stable or too-localized coordination of Ni^0 can be generalized is unknown.

Scheme 1.4 Catalyst trapping via preferential association during catalyst-transfer polymerization. [55]

exclusive product

not observed

no polymer formation

observed spectroscopically

step-growth
M_n = 18 kDa
Đ = 20.5
R = $C_2H_3(C_8H_{17})(C_{10}H_{21})$

PTiI
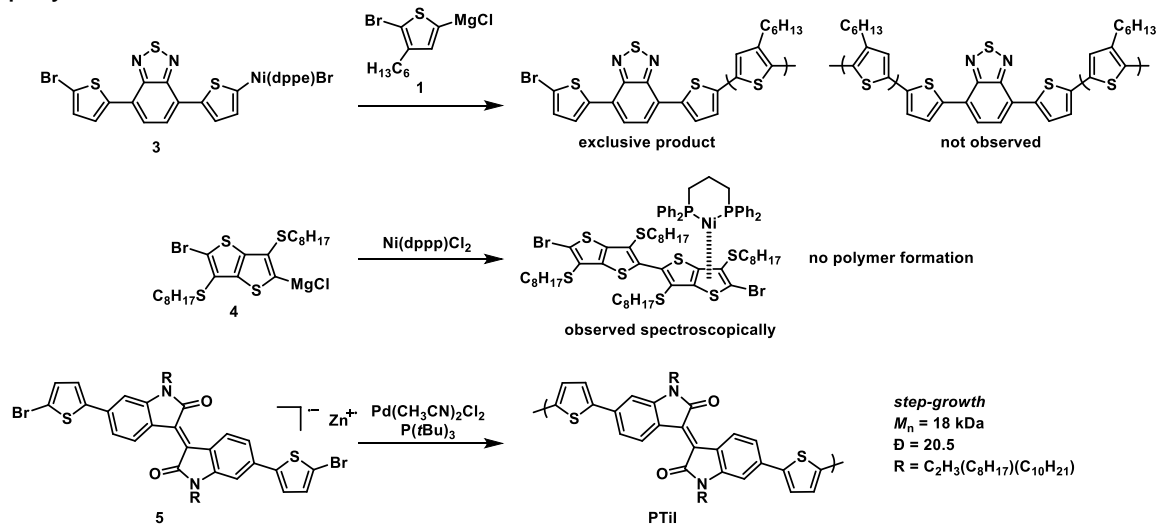
To address this question, Chapter 3 reports an investigation into non-chain-growth behavior in the polymerization of thiazole derivatives. Thiazole was chosen due to its structural similarity to thiophene, the most-studied monomer for CTP. While structurally analogous to **P3HT**, **PTz**'s LUMO is 0.55 eV lower, similar to valuable electron-deficient monomer targets.[51a] We identified a chain-transfer pathway using computational reaction discovery in collaboration with Prof. Paul Zimmerman. Inhibiting this chain-transfer pathway via ancillary ligand modification led to improved CTP performance. Frequent chain-transfer in other nonsymmetric monomers may have a similar origin. The synthesis of alternating copolymers via CTP involves monomers that incorporate electron-rich and electron-poor moieties;[56] chain-walking in these polymerizations presents similar challenges.

This thesis aims to improve the utility of CTP for synthesizing conjugated polymers used in organic photovoltaic solar cells. To this end, it reports a new class of catalysts for the polymerization of dissimilar comonomers, mechanistic insight into non-chain-growth behavior in CTP of an electron-deficient monomer and improved end-group control via ligand modification, and a clarification of the importance of dispersity in BHJ optimization. These key discoveries provide a promising path for continued CTP development. The control that CTP provides over sequence and molecular weight will be invaluable in future attempts to

13

improve understanding and performance of OPVs. Furthermore, chain-growth synthesis of conjugated polymers opens the door to novel materials, such as donor-acceptor gradients, and grafting from surfaces, nanoparticles, and polymers.

References

(1) (a) Chiang, C. K.; Fincher, C. R., Jr.; Park, Y. W.; Heeger, A. J.; Shirakawa, H.; Louis, E. J.; Gau, S. C.; MacDiarmid, A. G. *Physical Review Letters*, **1977**, *39*, 1098–1101. (b) Shirakawa, H. *Angew. Chem.* **2001**, *40*, 2575-2580. (c) MacDiarmid, A. G. *Angew. Chem.* **2001**, *40*, 2581-2590. (d) Heeger, A. J. *Angew. Chem.* **2001**, *40*, 2591–2611.

(2) For recent reviews, see: (a) Sirringhaus, H. *Adv. Mat.* **2014**, *26*, 1319– 1335. (b) Holliday, S.; Donaghey, J. E.; McCulloch, I. *Chem. Mat.* **2014**, *26*, 647–663.

(3) For recent examples, see: (a) McDowell, J. J.; Maier-Flaig, F.; Wolf, T. J. A.; Unterreiner, A.-N.; Lemmer, U.; Ozin, G. *ACS Appl. Mater. Interfaces* **2014**, *6*, 83– 93. (b) Schelkle, K. M.; Bender, M.; Jeltsch, K.; Buckup, T.; Müllen, K.; Hamburger, M.; Bunz, U. H. F. *Angew. Chemie* **2015**, *54*, 14545–14548. (c) Dumur, F. *Org. Electron.* **2015**, *25*, 345–361.

(4) For recent examples, see: (a) Guo, X.; Zhang, M.; Ma, W.; Ye, L.; Zhang, S.; Liu, S.; Ade, H.; Huang, F.; Hou, *J. Adv. Mater.* **2014**, *26*, 4043–4049. (b) Hwang, Y.-J.; Courtright, B. A. E.; Ferreira, A. S.; Tolbert, S. H.; Jenekhe, S. A. *Adv. Mater.* **2015**, *27*, 4578–4584. (c) Liu, C.; Yi, C.; Wang, K.; Yang, Y.; Bhatta, R. S.; Tsige, M.; Xiao, S.; Gong, X. *ACS Appl. Mater. Interfaces* **2015**, *7*, 4928–4935. (d) Sun, D.; Meng, D.; Cai, Y.; Fan, B.; Li, Y.; Jiang, W.; Huo, L.; Sun, Y.; Wang, Z. *J. Am. Chem. Soc.* **2015**, *137*, 11156–11162.

(5) (a) Dennler, G.; Scharber, M. C.; Brabec, C. J. *Adv. Mater.* **2009**, *21*, 1323– 1338. (b) Søndergaard, R. R.; Hösel, M.; Krebs, F. C. *J. Polym. Sci. Part B Polym. Phys.* **2013**, *51*, 16–34.

(6) For a review, see Blom, P. W. M.; Mihailetchi, V. D.; Koster, L. J. A.; Markov, D. E. *Adv. Mater.* **2007**, *19*, 1551–1566.

(7) (a) Mori, D.; Benten, H.; Ohkita, H.; Ito, S.; Miyake, K. *ACS Appl. Mater. Interfaces,* **2012**, *4*, 3325–3329. (b) Zhou, Y.; Kurosawa, T.; Ma, W.; Guo, Y.; Fang, L.; Vandewal, K.; Diao, Y.; Wang, C.; Yan, Q.; Reinspach, J.; Mei, J.; Appleton, A. L.; Koleilat, G. I.; Gao, Y.; Mannsfeld, S. C. B.; Salleo, A.; Ade, H.; Zhao, D.; Bao, Z. *Adv. Mater.* **2014**, *26*, 3767–3772. (c) Gao, L.; Zhang, Z.-G.; Xue, L.; Min, J.; Zhang, J.; Wei, Z.; Li, Y. *Adv. Mater.* **2016**, *28*, 1884–1890.

(8) (a) Sun, D.; Meng, D.; Cai, Y.; Fan, B.; Li, Y.; Jiang, W.; Huo, L.; Sun, Y.; Wang, Z. J. *Am. Chem. Soc.* **2015**, *137*, 11156-11162. (b) Li, H.; Earmme, T.; Ren, G.; Saeki, A.; Yoshikawa, S.; Murari, N. M.; Subramaniyan, S.; Crane, M. J.; Seki, S.; Jenekhe, S. A. *J. Am. Chem. Soc.* **2014**, *136*, 14589-14597.

(9) Sariciftci, N. S.; Smilowitz, L.; Heeger, A. J.; Wudl, F. *Science*, **1992**, *258*, 1474–1476.

(10) Sariciftci, N. S.; Braun, D.; Zhang, C.; Srdanov, V. I.; Heeger, A. J.; Stucky, G.; Wudl, F. *Appl. Phys. Lett.*, **1993**, *62*, 585–587.

(11) Yu, G.; Gao, J.; Hummelen, J.C.; Wudl, F.; Heeger, A. J. *Science,* **1995**, *270*, 1789–1791.

(12) (a) Chou. K. W.; Yan, B.; Li. R.; Li, E.Q.; Zhao, K. *Adv. Mater.* 2013., *25*, 1923–29. (b) Schmidt-Hansberg, B.; Klein, M. F. G.; Sanyal, M.; Buss, F.; de Medeiros G.Q.G. *Macromolecules* **2012,** *45*, 7948–55. (c) Schmidt-Hansberg, B.; Sanyal, M.; Klein, M. F. G.; Pfaff, M.; Schnabel, N. *ACS Nano* **2011**, *5*, 8579–90.

(13) Yang, F.; Shtein, M.; Forrest, S. R. *Nature Mat.* **2005**, *4*, 37–41.

(14) Scharber, M. C.; Muhlbacher, D.; Koppe, M.; Denk, P.; Waldauf, C.; Heeger, A. J.; Brabec, C. J. *Adv. Mater.* **2006**, *18*, 789–794.

(15) V_{oc} is typically 0.2–0.3 V less than the difference between acceptor LUMO and donor HOMO; see ref. 14.

(16) For recent reviews, see: (a) Nakabayashi, K.; Mori, H. *Materials* **2014**, *7*, 3274–3290. (b) Kularatne, R. S.; Magurudeniya, H. D.; Sista, P.; Biewer, M. C.; Stefan, M. C. *J. Polym. Sci. Part A Polym. Chem.* **2013**, *51*, 743–768. (c) Zhou, H.; Yang, L.; You, W. *Macromolecules* **2012**, *45*, 607–632.

(17) Zhou, H.; Yang, L.; Stoneking, S.; You, W. *ACS App. Mater. Interfaces*, **2010**, *2*, 1377–1383.

(18) (a) Liu, Y. H.; Zhao, J. B.; Li, Z. K.; Mu, C.; Ma, W.; Hu, H. W.; Jiang, K.; Lin, H. R.; Ade, H.; Yan, H. *Nat. Commun.* **2014**, *5*, 5293–5300. (b) He, Z. C.; Xiao, B.; Liu, F.; Wu, H. B.; Yang, Y. L.; Xiao, S.; Wang, C.; Russell, T. P.; Cao, Y. *Nat. Photonics* **2015**, *9*, 174–179. (c) Zhang, J.; Zhang, Y.; Fang, J.; Lu, K.; Wang, Z.; Ma, W.; Wei, Z. *J. Am. Chem. Soc.* **2015**, *137*, 8176– 8183.

(19) Foertig, A.; Kniepert, J.; Gluecker, M.; Brenner, T.; Dyakonov, V.; Neher, D.; Deibel, C. *Adv. Func. Mat.* **2013**, *24*, 1306–1311.

(20) For a review, see Hoppe, H.; Sariciftci, N. S. *J. Mater. Chem.* **2005**, *16*, 45–61.

(21) Kang, H.; Uddin, M. A.; Lee, C.; Kim, K. H.; Nguyen, T. L.; Lee, W.; Li, Y.; Wang, C.; Woo, H. Y.; Kim, B. J. *J. Am. Chem. Soc.* **2015**, *137*, 2359–2365.

(22) Li, W.; Yang, L.; Tumbleston, J. R.; Yan, L.; Ade, H.; You, W. *Adv. Mater.* **2014**, *26*, 4456–4462.

(23) Lu, L.; Zheng, T.; Xu, T.; Zhao, D.; Yu, L. *Chem. Mater.* **2015**, *27*, 537–543.

(24) Meager, I.; Ashraf, R. S.; Nielsen, C. B.; Donaghey, J. E.; Huang, Z.; Bronstein, H.; Durrant, J. R.; McCulloch, I. *J. Mater. Chem. C* **2014**, *2*, 8593–8598.

(25) (a) Pearson, A. J.;Wang, T.; Jones, R. A. L.; Lidzey, D. G.; Staniec, P. A.; Hopkinson, P. E.; Donald, A. M. *Macromolecules*, **2012**, *45*, 1499–1508. (b) Verploegen, E.; Miller, C. E.; Schmidt, K.; Bao, Z. N.; Toney, M. F. *Chem. Mater.* **2012**, *24*, 3923–3931.

(26) Palermo, E. F.; Darling, S. B.; McNeil, A. J. *J. Mater. Chem. C* **2014**, *2*, 3401–3406.

(27) (a) Sheina, E. E.; Liu, J.; Iovu, M. C.; Laird, D. W.; McCullough, R. D. *Macromolecules* **2004**, *37*, 3526–3528. (b) Yokoyama, A.; Miyakoshi, R.; Yokozawa, T. *Macromolecules* **2004**, *37*, 1169–1171. (c) Miyakoshi, R.; Yokoyama, A.; Yokozawa, T. *Macromol. Rapid Commun.* **2004**, *25*, 1663–1666.

(28) Bryan, Z. J.; McNeil, A. J. *Chem. Sci.*, **2013**, *4*, 1620–1624.

(29) Miyakoshi, R.; Yokoyama, A.; Yokozawa, T. *J. Am. Chem. Soc.* **2005**, *127*, 17542− 17547.

(30) (a) Hatnean, J. A.; Shoshani, M.; Johnson, S. A. *Inorg. Chim. Acta* **2014**, *422*, 86–94. (b) Hatnean, J. A.; Beck, R.; Borrelli, J. D.; Johnson, S. A.; *Organometallics* **2010**, *29*, 6077–6091. (c) Johnson, S.; Huff, C.; Mustafa, F.; Saliba, M. *J. Am. Chem. Soc.* **2008**, *130*, 17278–17280. (d) Bennett, M.; Kopp, M.; Wenger, E.; Willis, A. *J. Organomet. Chem.* **2003**, *667*, 8–15. (e) Bach, I.; Pörschke, K.-R.; Goddard, R.; Kopiske, C.; Krüger, C.; Rufińska, A.; Seevogel, K. *Organometallics* **1996**, *15*, 4959–4966. (f) Stanger, A.; Vollhardt, K. P. C. *Organometallics* **1992**, *11*, 317–320. (g) Stanger, A. *Organometallics* **1991**, *10*, 2979–2982. (h) Jonas, K. *J. Organomet. Chem.* **1974**, *78*, 273–279.

(31) (a) Hatnean, J. A.; Johnson, S. A. *Organometallics* **2012**, *31*, 1361−1373. (b) Li, T.; García, J. J.; Brennessel, W. W.; Jones, W. D. *Organometallics* **2010**, *29*, 2430−2445. (c) Yoshikai, N.; Matsuda, H.; Nakamura, E. *J. Am. Chem. Soc.* **2009**, *131*, 9590−9599. (d) Yoshikai, N.; Matsuda, H.; Nakamura, E. *J. Am. Chem. Soc.* **2008**, *130*, 15258−15259. (e) Zenkina, O. V.; Karton, A.; Freeman, D.; Shimon, L. J. W.; Martin, J. M. L.; L, J. W.; van der Boom, M. E. *Inorg. Chem.* **2008**, *47*, 5114−5121.

(32) Lee, S. R.; Bloom, J. W. G.; Wheeler, S. E.; McNeil, A. J. *Dalton Trans.* **2013**, *41,* 4218–4222.

(33) (a) Bridges, C. R.; Yan, H.; Pollit, A. A; Seferos, D. S. *ACS Macro Lett.* **2014**, *3,* 671–674. (b) Gao, L. M.; Hu, Y. Y.; Yu, Z. P.; Liu, N.; Yin, J.; Zhu, Y. Y.; Ding, Y.; Wu, Z. Q. *Macromolecules* **2014**, *47,* 5010–5018. (c) Ono, R. J.; Todd, A. D.; Hu, Z.; Vanden Bout, D. A; Bielawski, C. W. *Macromol. Rapid Commun.* **2013**, *35,* 204–209. (d) Javier, A. E.; Varshney, S. R.; McCullough, R. D. *Macromolecules* **2010**, *43,* 3233–3237. (e) Wu, S.; Sun, Y.; Huang, L.; Wang, J.; Zhou, Y.; Geng, Y.; Wang, F. *Macromolecules* **2010**, *43,* 4438–4440. (f) Van den Bergh, K.; Huybrechts, J.; Verbiest, T.; Koeckelberghs, G. *Chem. Eur. J.* **2008**, *14,* 9122–9125. (g) Yokozawa, T.; Adachi, I.; Miyakoshi, R.; Yokoyama, A. *High Perform. Polym.* **2007**, *19,* 684–699.

(34) (a) Locke, J. R.; McNeil, A. J. *Macromolecules* **2010**, *43,* 8709–8710. (b) Palermo, E. F.; McNeil, A. J. *Macromolecules* **2012**, *45,* 5948–5955. (c) Palermo, E. F.; van der Laan, H. L.; McNeil, A. J. *Polym. Chem.* **2013**, *4,* 4606–4611. (d) Palermo, E. F.; Darling, S. B.; McNeil, A. J. *J. Mater. Chem. C* **2014**, *2,* 3401–3406.

(35) (a) Wu, S.; Bu, L.; Huang, L.; Yu, X.; Han, Y.; Geng, Y.; Wang, F. *Polymer* **2009**, *50,* 6245–6251. (b) Miyakoshi, R.; Yokoyama, A.; Yokozawa, T. *Chem. Lett.* **2008**, *37,* 1022–1023. (c) Yokoyama, A.; Kato, A.; Miyakoshi, R.; Yokozawa, T. *Macromolecules* **2008**, *41,* 7271–7273. (d) Van den Bergh, K.; Cosemans, I.; Verbiest, T.; Koeckelberghs, G. *Macromolecules* **2010**, *43,* 3794–3800.

(36) (a) Lanni, E. L.; McNeil, A. J. *J. Am. Chem. Soc.* **2009**, *131,* 16573–16579. (b) Lanni, E. L.; McNeil, A. J. *Macromolecules* **2010**, *43,* 8039–8044. (c) Lanni, E. L.; Locke, J. R.; Gleave, C. M.; McNeil, A. J. *Macromolecules* **2011**, *44,* 5136–5145.

(37) Lee, S. R.; Bryan, Z. J.; Wagner, A. M.; McNeil, A. J. *Chem. Sci.* **2012**, *3,* 1562–1566.

(38) (a) Rudenko, A. E.; Thompson, B. C. *Macromolecules* **2015**, *48,* 569–575. (b) Rudenko, A. E.; Wiley, C. A.; Tannaci, J. F.; Thompson, B. C. *J. Polym. Sci., Part A: Polym. Chem.* **2013**, *2,* 135–147. (c) Wang, Q.; Takita, R.; Kikuzaki, Y.; Ozawa, F. *J. Am. Chem. Soc.* **2010**, *132,* 11420−11421.

(39) (a) Zhang, Z.; Hu, P.; Li, X.; Zhan, H.; Cheng, Y. *J. Polym. Sci., Part A: Polym. Chem.* **2015**, *53,* 1457−1463. (b) Zhang, H.-H.; Xing, C.-H.; Hu, Q.-S. *J. Am. Chem. Soc.* **2012**, *134,* 13156−13159. (b) Yokozawa, T.; Suzuki, R.; Nojima, M.; Ohta, Y.; Yokoyama, A. *Macromol. Rapid Commun.* **2011**, *32,* 801–806. (b)

Elmalem, E.; Kiriy, A.; Huck, W. T. S. *Macromolecules* **2011**, *44*, 9057–9061. (c) Yokozawa, T.; Kohno, H.; Ohta, Y.; Yokoyama, A. *Macromolecules* **2010**, *43*, 7095–7100. (d) Huang, W.; Su, L.; Bo, Z. *J. Am. Chem. Soc.* **2009**, *131*, 10348–10349. (e) Beryozkina, T.; Boyko, K.; Khanduyeva, N.; Senkovskyy, V.; Horecha, M.; Oertel, U.; Simon, F.; Stamm, M.; Kiriy, A. *Angew. Chem. Int. Ed.* **2009**, *48*, 2695–2698. (f) Yokoyama, A.; Suzuki, H.; Kubota, Y.; Ohuchi, K.; Higashimura, H.; Yokozawa, T. *J. Am. Chem. Soc.* **2007**, *129*, 7236–7237.

(40) Kang, S.; Ono, R. J.; Bielawski, C. W. *J. Am. Chem. Soc.* **2013**, *135*, 4984−4987.

(41) Grisorio, R.; Suranna, G. P.; Mastrorilli, P. *Chem. Eur. J.* **2010**, *16*, 8054–8061.

(42) (a) Chianese, A. R.; Li, X.; Janzen, M. C.; Faller, J. W.; Crabtree, R. H. *Organometallics* **2003**, *22*, 1663–1667. (b) Herrmann, W. A.; Schütz, J.; Frey, G. D.; Herdtweck, E. *Organometallics* **2006**, *25*, 2437–2448.

(43) Larrosa, I.; Somoza, C.; Banquy, A.; Goldup, S. M. *Org. Lett.* **2011**, *13*, 146–149.

(44) (a) Fuji, K.; Tamba, S.; Shono, K.; Sugie, A.; Mori, A. *J. Am. Chem. Soc.* **2013**, *135*, 12208−12211. (b) Qiu, Y.; Worch, J. C.; Fortney, A.; Gayathri, C.; Gil, R. R.; Noonan, K. J. T. *Macromolecules* **2016**, *49*, 4757−4762. (c) Murakami, K.; Tanaka, S.; Mori, A. *Polym. Chem.* **2015**, *6*, 6573− 6578.

(45) (a) Magurudeniya, H. D.; Sista, P.; Westbrook, J. K.; Ourso, T. E.; Nguyen, K.; Maher, M. C.; Alemseghed, M. G.; Biewer, M. C.; Stefan, M. C. *Macromol. Rapid Commun.* **2011**, *32*, 1748−1752. (b) Bridges, C. G.; McCormick, T. M.; Gibson, G. L.; Hollinger, J.; Seferos, D. S. *J. Am. Chem. Soc.* **2013**, *135*, 13212−13219. (c) Bridges, C. R.; Yan, H.; Pollit, A. A.; Seferos, D. S. *ACS Macro Lett.* **2014**, *3*, 671−674. (d) Pollit, A. A.; Bridges, C. R.; Seferos, D. S. *Macromol. Rapid Commun.* **2015**, *36*, 65−70.

(46) For reviews, see: (a) Grisorio, R.; Suranna, G. P. *Polym. Chem.* **2015**, *6*, 7781–7795. (b) see (2)

(47) (a) Ateşin, T. A.; Li, T.; Lachaize, S.; García, J. J.; Jones, W. D. Organometallics 2008, 27, 3811−3817. (b) Radonovich, L. J.; Koch, F. J.; Albright, T. A. *Inorg. Chem.* **1980**, *19*, 3373–3379.

(48) Wen, L.; Duck, B. C.; Dastoor, P. C.; Rasmussen, M. C. *Macromolecules* **2008**, *41*, 4576–4578.

(49) (a) Nanashima, Y.; Shibata, R.; Miyakoshi, R.; Yokoyama, A.; Yokozawa, T. *J. Polym. Sci., Part A: Polym. Chem.* **2012**, *50*, 3628–3640. (b) Nanashima, Y.; Yokoyama, A.; Yokozawa, T. *J. Polym. Sci., Part A: Polym. Chem.* **2012**, *50*, 1054–1061. (c) Nanashima, Y.; Yokoyama, A.; Yokozawa, T. *Macromolecules* **2012**, *45*, 2609–2613.

(50) (a) Senkovskyy, V.; Tkachov, R.; Komber, H.; Sommer, M.; Heuken, M.; Voit, B.; Huck, W. T. S.; Kataev, V.; Petr, A.; Kiriy, A. *J. Am. Chem. Soc.* **2011**, *133*, 19966–19970. (b) Senkovskyy, V.; Tkachov, R.; Komber, H.; John, A.; Sommer, J.-U.; Kiriy, A. *Macromolecules* **2012**, *45*, 7770–7777.

(51) (a) Pammer, F.; Passlack, U. *ACS Macro Lett.* **2014**, 3, 170–174. (b) Pammer, F.; Jäger, J.; Rudolf, B.; Sun, Y. *Macromolecules* **2014**, *47*, 5904–5912.

(52) Jäger, J.; Tchamba Yimga, N.; Urdanpilleta, M.; von Hauff, E.; Pammer, F. *J. Mater. Chem. C* **2016**, *4*, 2587–2597.

(53) Bridges, C. R.; McCormick, T. M.; Gibson, G. L.; Hollinger, J.; Seferos, D. S. *J. Am. Chem. Soc.* **2013**, *135*, 13212–13219.

(54) Erdmann, T.; Back, J.; Tkachov, R.; Ruff, A.; Voit, B.; Ludwigs, S.; Kiriy, A. *Polym. Chem.* **2014**, *5*, 5383–5390.

(55) (a) Komber, H.; Senkovskyy, V.; Tkachov, R.; Johnson, K.; Kiriy, A.; Huck, W. T. S.; Sommer, M. *Macromolecules* **2011**, *44*, 9164–9172. (b) Willot, P.; Koeckelberghs, G. *Macromolecules* **2014**, *47*, 8548–8555. (c) Karpov, Y.; Maiti, J.; Tkachov, R.; Beryozkina, T.; Bakulev, V.; Liu, W.; Komber, H.; Lappan, U.; Al-Hussein, M.; Stamm, M.; Voita, B.; Kiriy, A. *Polym. Chem.* **2016**, *7*, 2691–2697.

(56) Ono, R. J.; Kang, S.; Bielawski, C. W. *Macromolecules* **2012**, *45*, 2321–2326.

Chapter 2

Chain-growth polymerization of aryl Grignards initiated by a stabilized NHC-Pd precatalyst

The recent discovery of chain-growth methods for synthesizing π-conjugated polymers[1] has generated significant interest because copolymers with specific sequences and potentially advantageous properties can now be targeted.[2] For example, all-conjugated block[3] and gradient[4] copolymers as well as surface-grafted[5] and end-functionalized[6] polymers have been prepared. These chain-growth methods largely consist of cross-coupling reactions between difunctionalized arenes (e.g., Br/MgX) using Ni catalysts ligated by chelating phosphines.[7] One current limitation is the narrow scope of monomers that are capable of undergoing chain-growth homo- and copolymerizations. As a consequence, there is an ongoing search for a more universal catalyst.

One approach is to modify the steric and electronic properties of the ligand. In 2011, we reported on a series of bis(dialkylphosphino)ethane-based ligands and demonstrated that unhindered ligands led to facile catalyst decomposition while hindered ligands interfered with the chain-growth pathway.[8] More recently, we examined the influence of ligand electronic properties and found that electron-rich ligands promoted the chain-growth pathway.[9] We hypothesized that this electronic effect was due, in part, to stabilization of the key intermediate (complex **I** in Scheme 2.2). Combined, these results suggest that electron-donating ligands with moderate steric properties are ideal for chain-growth polymerizations. Because N-heterocyclic carbenes (NHCs) are stronger σ-donors than phosphines,[10,11] and their steric

properties are easily modified, we anticipated that they would be ideal ligands for the chain-growth polymerizations.[12]

An alternative approach for developing new catalysts is to change the nature of the metal species. Pd catalysts have recently emerged as an alternative to Ni in the chain-growth polymerizations.[13,14,15] For example, using (t-Bu$_3$P)Pd(Ph)Br as the catalyst, both Suzuki-Miyaura[13] and Suzuki-Heck[14] conditions have led to chain-growth polymerizations. Excitingly, the scope of monomers is broad and even includes n-type monomers, which have been rare in the Ni-catalyzed processes.[16] Nevertheless, these methods need further improvement. For example, in most cases the MALDI-TOF MS analysis of the resulting polymers revealed a significant amount of polymers with Ph/Br end-groups. These end-groups indicate that either the catalyst fails to undergo an intramolecular oxidative addition into the growing polymer chain or the propagating species is unstable, leading to premature reductive elimination of polymer-Br.

We selected NHC-ligated Pd precatalyst **1**[17,18] based on a recent report by Larrosa, Goldup, and co-workers, who observed an unexpected difunctionalization of 1,4-dibromobenzene when one equivalent of PhMgCl was used.[19] A diffusion-controlled oxidative addition was invoked to rationalize this selectivity.[20] This mechanism is similar to that proposed for the Ni-catalyzed chain-growth polymerizations (see Scheme 2.2),[21,22] suggesting that this Pd precatalyst might also mediate chain-growth polymerization of aryl monomers. In addition, Organ and co-workers demonstrated that this precatalyst could facilitate cross-coupling reactions between two hindered arenes,[17c] suggesting that precatalyst **1** will readily polymerize the *ortho*-functionalized monomers typically used to make soluble π-conjugated polymers. Finally, these pyridine-stabilized Pd precatalysts have additional advantages in that they are air- and moisture-stable as well as commercially available.

We report herein the homo- and copolymerizations of (4-bromo-2,5-bis(hexyloxy)phenyl)magnesium chloride (**2**), (5-bromo-4-hexylthiophen-2-yl)magnesium chloride (**3**), and (7-bromo-9,9-dioctyl-fluoren-2-yl)magnesium chloride (**4**) mediated by Pd precatalyst **1** (Scheme 2.1). A chain-growth homopolymerization was observed for both monomers **2** and **3**, with linear increases in the number-average molecular weight (M_n) with conversion as well

as narrow molecular weight distributions (Đ). Block copolymerizations gave the expected chain extension when the second monomer was added soon after complete consumption of the first monomer. In contrast, polymerization of monomer **4** was neither living nor perfectly chain-growth. Overall, these studies indicate that further modifications to the catalyst scaffold, either by selecting an alternative NHC ligand or by varying the steric and electronic properties of the stabilizing ligand (i.e., 3-chloropyridine),[23] are needed to further improve the chain-growth polymerizations.
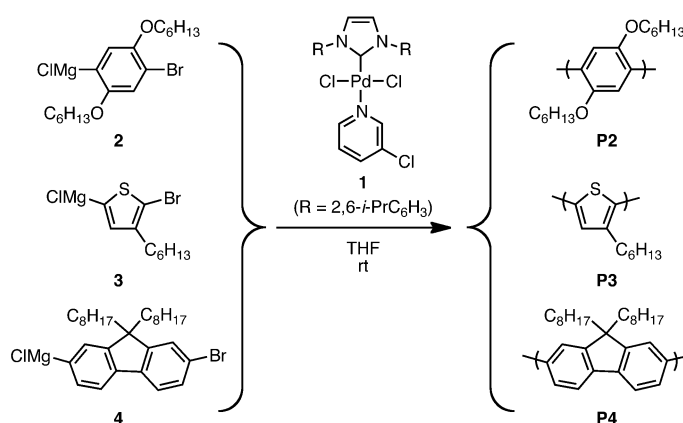
Scheme 2.1 Syntheses of π-conjugated polymers **P2**-**P4** mediated by Pd precatalyst **1**.

Experimental Section

Monomer Preparation

Monomers **2**, **3**, and **4** were generated in situ via Grignard metathesis of the dibromo precursors using *i*-PrMgCl (see Supporting Information, Appendix 1).[24, 25]

General Procedure for Homopolymerizations

A 25 mL Schlenk flask was equipped with a stir bar, precatalyst **1** (10.2 mg, 0.0150 mmol, 1 equiv), and THF (7.5 mL) in a glovebox under an N_2 atmosphere. The flask was then equipped with a septum (secured with copper wire), removed from the glovebox, and put under an N_2 atmosphere. Monomer **2** (2.25 mL, 1.01 mmol) was then added via syringe and stirred for 90 min at rt. The reaction was then quenched with aq. HCl (5 M, 10 mL) and extracted with CH_2Cl_2 (3 x 10 mL). The combined organic extracts were dried over $MgSO_4$,

filtered, and the solvent was removed in vacuo. The resulting white solid was then washed with MeOH and dried under vacuum. (209 mg, 75% yield) M_n = 28.2 kDa, Đ = 1.19.

General Procedure for Block Copolymerizations

A 25 mL Schlenk flask was equipped with a stir bar, precatalyst **1** (10.2 mg, 0.0150 mmol, 1 equiv), and THF (5.0 mL) in a glovebox under an N_2 atmosphere. The flask was then equipped with a septum (secured with copper wire), removed from the glovebox, and put under an N_2 atmosphere. Monomer **2** (1.8 mL, 0.50 mmol) was then added via syringe and stirred for 180 min at rt. After 180 min, an aliquot (0.5 mL) was withdrawn via syringe and immediately quenched with aq. HCl (12 M, 1 mL). The mixture was extracted with $CHCl_3$ (3 x 1 mL) with mild heating and the combined aliquots were dried over $MgSO_4$, filtered, and analyzed by GPC (M_n = 9.2 kDa, Đ = 1.24). Monomer **3** (3.2 mL, 0.90 mmol) was then added via syringe and stirred for 60 min at rt. After 60 min, the reaction was quenched with aq. HCl (5 M, 10 mL) and extracted with $CHCl_3$ (3 x 10 mL). The combined organic extracts were dried over $MgSO_4$, filtered, and the solvent was removed in vacuo. The resulting purple solid was then dissolved in a minimum amount of $CHCl_3$ and precipitated into MeOH. The precipitate was collected and dried under vacuum (223 mg, 78% yield). M_n = 17.8 kDa, Đ = 1.32.

Results and Discussion

Homopolymerizations

The homopolymerizations of **2** and **3** mediated by precatalyst **1** showed linear increases in the number-average molecular weight (M_n) with conversion and narrow molecular weight distributions (Đ) (Figure 2.1A/B). Both results are consistent with a chain-growth mechanism. Further support was provided by examining the relationship between the [monomer]/[catalyst] ratio and the M_n (Figure 2.1C/D). The observed linear relationship suggests that each Pd precatalyst initiates a single-polymer chain.
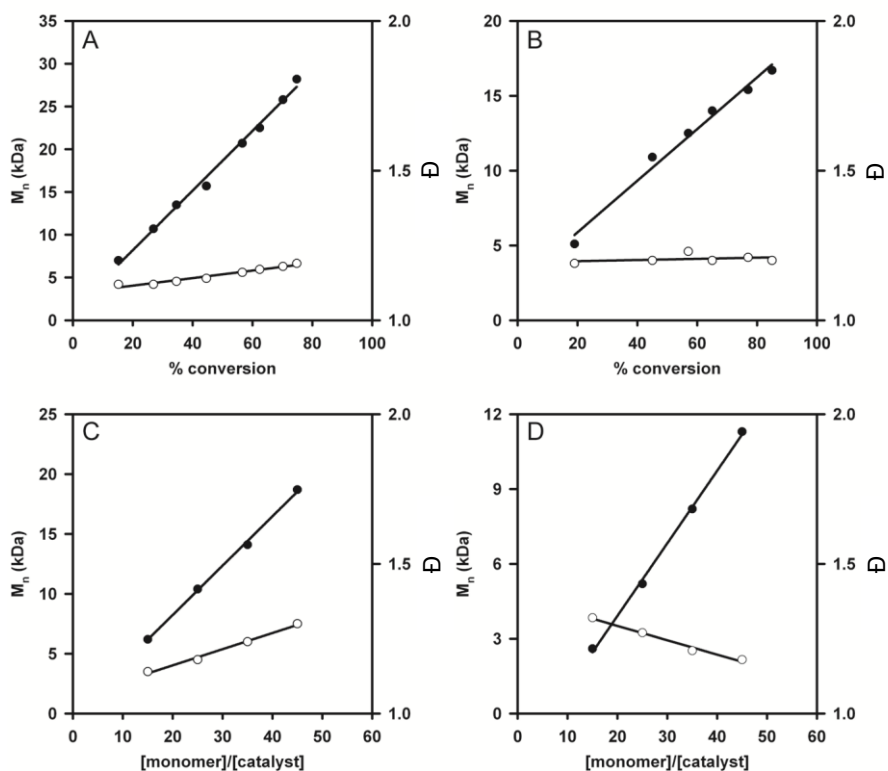
Figure 2.1 Plots of M_n (●) and Đ (○) versus conversion for the polymerization of monomers (A) **2** and (B) **3** using precatalyst **1** ([**1**] = 1.5 mM; [**2**] = 77 mM; [**3**] = 98 mM; 25 °C; THF). Plots of M_n (●) and Đ (○) versus [monomer]/[catalyst] ratio for polymerization of monomers (C) **2** and (D) **3** using precatalyst **1** (25 °C, THF).

Low molecular weight polymers were subjected to MALDI-TOF MS analysis after quenching, which revealed predominantly polymers with H/Br end-groups. These end-groups reveal that the catalyst is located at the polymer chain end, as evidenced by its replacement with a proton during the acidic quench. To support the living nature of these polymerizations, a second aliquot of the same monomer was added immediately after consumption of the first aliquot. The observed increases in M_n with only minor broadening of Đ indicates that most polymer chains remain living under these conditions (Appendix 1).

The regioregularity of the poly(3-hexylthiophene) will depend on the relative reactivities of the regioisomers of monomer **3** (~80:20 mixture, major isomer is shown in Scheme 2.1). By monitoring their relative conversions, we observed that the major regioisomer is predominantly consumed within the first 50% conversion (Appendix 1). As the concentration of the major regioisomer decreased, the minor regioisomer was consumed. As a consequence, the poly(3-hexylthiophene) regioregularity was low (80%). The increased reactivity

of the major regioisomer has been attributed to the lack of a substituent *ortho* to the reactive carbon, which leads to a faster transmetalation onto the catalyst compared to the minor regioisomer.[26] Though not explored herein, if the I/Br functionalized precursor is used to regioselectively generate **3**, a highly regioregular poly(3-hexylthiophene) is expected using this method.[27,28]

In contrast to both monomers **2** and **3**, the polymerization of fluorene monomer **4** with precatalyst **1** is pseudo-chain-growth but not living. For example, MALDI-TOF MS analysis at low monomer conversions indicated a variety of different end-groups, suggesting that chain-transfer and/or chain-termination were occurring, even at early conversions (Appendix 1). It is interesting to note that the largest peak corresponded to polymers with iPr/H end-groups. These end-groups could arise via competitive transmetalation of iPrMgCl (leftover from the Grignard metathesis)[29] or oxidative addition of the iPrBr (formed via Grignard metathesis) into "free" $L_nPd(0)$.[17a] ^{1}H NMR analysis of a sample before and after polymerization (referenced to an internal standard) revealed complete consumption of iPrMgCl and no consumption of the iPrBr, consistent with the transmetalation hypothesis.

Adding a second aliquot of monomer **4** immediately following consumption of the first aliquot did not result in a significant amount of chain extension. Instead, a broadening of the molecular weight distribution was observed and new chains were initiated (Appendix 1). These results suggest that either the Pd catalyst is not efficiently transferred to the chain end during the polymerization of **4**[15] or there may be a stability issue with the catalyst at the chain end. In both cases, "free" $L_nPd(0)$ is generated and can initiate new chains. Between 5-30% of the dibromo precursor (leftover from an incomplete Grignard metathesis) is consumed during polymerization, consistent with "free" Pd(0) forming during polymerization (Appendix 1). As discussed below, some time-dependent catalyst stability issues are observed with both monomers **2** and **3** after complete consumption of monomer. Thus, the observed uncontrolled polymerization of monomer **4** may be due to a similar decomposition pathway.

Block Copolymerizations

Previous studies with both Pd and Ni catalysts have shown that copolymerizations can be challenging even when homopolymerizations were successful.[30] For example, the order of monomer addition can influence the results of these block copolymerizations. In contrast to these previous studies, we observed the expected increases in the polymer molecular weights regardless of the order of monomer addition in the copolymerizations of monomers **2** and **3** with Pd precatalyst **1** (Figure 2.2A/B). These results were obtained when the second monomer was added within 3 h after addition of the first monomer. If longer periods between monomer additions were used, some chain termination was observed. This result is most consistent with a catalyst stability issue at the end of the polymerization, once the monomer concentration is depleted.
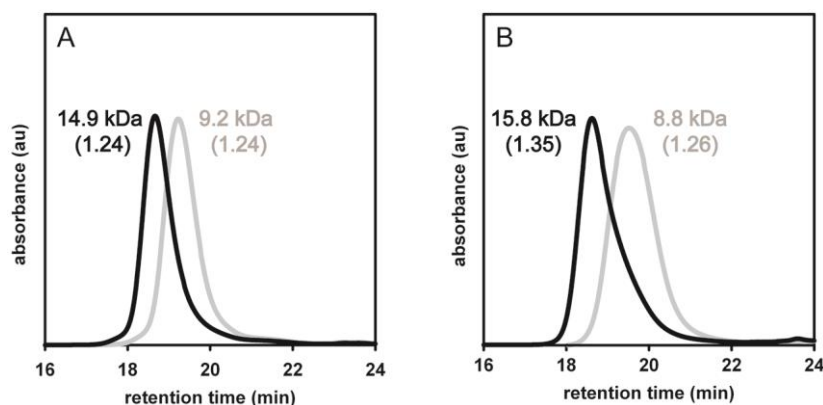
Figure 2.2 Gel permeation chromatograms (GPC) for block copolymerizations using Pd precatalyst **1** to generate (A) **P2**-*block*-**P3** and (B) **P3**-*block*-**P2**. The grey line represents the GPC curve immediately before second monomer addition. The black line represents the GPC curves after copolymerization is complete.

It is important to note that there is no evidence of catalyst decomposition during the polymerization. For example, at low conversions, the MALDI-TOF MS analysis revealed predominantly H/Br end-groups, whereas Br/Br end-groups would have resulted if catalyst stability was an issue (Appendix 1). In addition, a control experiment, wherein only 50% of the dibromo precursor was activated with *i*-PrMgCl, revealed no significant consumption of the dibromo starting material, even up to 80% conversion of the Grignard monomer (Appendix 1). This result suggests that "free" Pd(0) is not formed during the polymerization. The fact that the decomposition does not occur during

polymerization suggests that a different catalyst resting state is present under those conditions. We[8,9,22] and others[15,21] have been probing the mechanistic details with Ni catalysts chelated by phosphine ligands, and these studies have revealed structures similar to both complexes **II** and **III** as catalyst resting states during polymerization, depending on the ligand structure.[8,9,22] At the end of these Ni-catalyzed polymerizations, structures similar to complex **II** are observed, regardless of the ligand structure. Roy and Hartwig previously reported that reductive eliminations of Ar-Br can occur from LPd(Ar)Br complexes (similar to complex **II**) when sufficiently hindered ligands are used.[31] Thus, one mechanism for decomposition is the reductive elimination of polymer-Br from this complex. Mechanistic studies of the Pd-catalyzed polymerizations described herein are needed to address these catalyst stability issues.
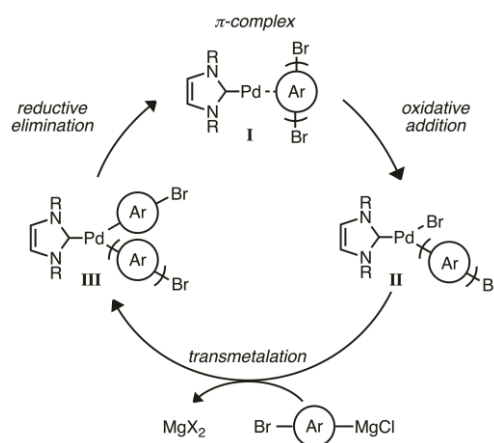
Scheme 2.2 Proposed mechanism for the observed chain-growth behavior.

Conclusions

NHC-ligated Pd precatalyst **1** mediates chain-growth homo- and copolymerizations of both phenylene- and thiophene-based monomers. On the other hand, polymerization of a fluorene-based monomer was problematic, with evidence of both chain-termination and re-initiation pathways occurring. In addition, the catalyst appears to be moderately unstable once monomer consumption is complete. Although not explored herein, the "throw-away" ligand (3-chloropyridine) may play a non-innocent role in the mechanism.[32] In addition, less sterically encumbered NHCs might represent a promising alternative to IPr.[31] Mechanistic studies are needed to elucidate the precise

role of ligand steric and electronic properties, as well as monomer structure, on the chain-growth and competing reaction pathways. Studies aimed at addressing these issues, as well as examining the substrate scope (e.g., electron-poor monomers) for precatalyst **1** and related NHC-Pd catalysts are currently underway.

References

(1) (a) Sheina, E. E.; Liu, J.; Iovu, M. C.; Laird, D. W.; McCullough, R. D. *Macromolecules*, **2004**, *37*, 3526–3528. (b) Yokoyama, A.; Miyakoshi, R.; Yokozawa, T. *Macromolecules*, **2004**, *37*, 1169–1171. (c) Miyakoshi, R.; Yokoyama, A.; Yokozawa, T. *Macromol. Rapid Commun.*, **2004**, *25*, 1663–1666.

(2) For recent reviews, see: (a) Kiriy, A.; Senkovskyy, V.; Sommer, M.; *Macromol. Rapid Commun.*, **2011**, *32*, 1503–1517. (b) Okamoto, K.; Luscombe, C. K. *Polym. Chem.*, **2011**, *2*, 2424–2434.

(3) For recent examples of block copolymers prepared via this method, see: (a) Verswyvel, M.; Monnaie, F.; Koeckelberghs, G. *Macromolecules*, **2011**, *44*, 9489–9498. (b) Kim, J.; Siva, A.; Song, I. Y.; Park, T. *Polymer*, **2011**, *52*, 3704–3709. (c) Higashihara, T.; Ohshimizu, K.; Ryo, Y.; Sakurai, T.; Takahashi, A.; Nojima, S.; Ree, M.; Ueda, M. *Polymer*, **2011**, *52*, 3687–3695. (d) Ohshimizu, K.; Takahashi, A.; Higashihara, T.; Ueda, M. *J. Polym. Sci., Part A: Polym. Chem.*, **2011**, *49*, 2709–2714. (e) Hollinger, J.; Jahnke, A. A.; Coombs, N.; Seferos, D. S. *J. Am. Chem. Soc.*, **2010**, *132*, 8546–8547. (f) Van den Bergh, K.; Cosemans, I.; Verbiest, T.; Koeckelberghs, G. *Macromolecules*, **2010**, *43*, 3794–3800. (g) Javier, A. E.; Varshney, S. R.; McCullough, R. D. *Macromolecules*, **2010**, *43*, 3233–3237. (h) Miyanishi, S.; Zhang, Y.; Tajima, K.; Hashimoto, K. *Chem. Commun.*, **2010**, *46*, 6723–6725.

(4) Locke, J. R.; McNeil, A. J. *Macromolecules*, **2010**, *43*, 8709–8710.

(5) For a recent review, see: Marshall, N.; Sontag, S. K.; Locklin, J. *Chem. Commun.*, **2011**, *47*, 5681–5689.

(6) For recent examples, see: (a) Doubina, N.; Paniagua, S. A.; Soldatova, A. V.; Jen, A. K. Y.; Marder, S. R.; Luscombe, C. K. *Macromolecules*, **2011**, *44*, 512–520. (b) Smeets, A.; Willot, P.; De Winter, J.; Gerbaux, P.; Verbiest, T.; Koeckelberghs, G. *Macromolecules*, **2011**, *44*, 6017–6025.

(7) For a recent example of an non-phosphine based Ni-catalyst, see: Magurudeniya, H. D.; Sista, P.; Westbrook, J. K.; Ourso, T. E.; Nguyen, K.; Maher, M. C.; Alemseghed, M. G.; Biewer, M. C.; Stefan, M. C. *Macromol. Rapid Commun.*, **2011**, *32*, 1748–1752.

(8) Lanni, E. L.; Locke, J. R.; Gleave, C. M.; McNeil, A. J. *Macromolecules*, **2011**, *44*, 5136–5145.

(9) Lee, S. R.; Bryan, Z. J.; Wagner, A. M.; McNeil, A. J. *Chem. Sci.*, **2012**, *3*, 1562–1566.

(10) (a) Chianese, A. R.; Li, X.; Janzen, M. C.; Faller, J. W.; Crabtree, R. H. *Organometallics*, **2003**, *22*, 1663–1667. (b) Herrmann, W. A.; Schütz, J.; Frey, G. D.; Herdtweck, E. *Organometallics*, **2006**, *25*, 2437–2448.

(11) For recent reviews, see: (a) Fortman, G. C.; Nolan, S. P.; *Chem. Soc. Rev.*, **2011**, *40*, 5151–5169. (b) Díez-González, S.; Marion, N.; Nolan, S. P. *Chem. Rev.*, **2009**, *109*, 3612–3676. (c) Kantchev, E. A. B.; O'Brien, C. J.; Organ, M. G. *Angew. Chem. Int. Ed.*, **2007**, *46*, 2768–2813.

(12) Tamba, S.; Shono, K.; Sugie, A.; Mori, A. *J. Am. Chem. Soc.*, **2011**, *133*, 9700–9703.

(13) (a) Yokozawa, T.; Suzuki, R.; Nojima, M.; Ohta, Y.; Yokoyama, A. *Macromol. Rapid Commun.*, **2011**, *32*, 801–806. (b) Elmalem, E.; Kiriy, A.; Huck, W. T. S. *Macromolecules*, **2011**, *44*, 9057–9061. (c) Yokozawa, T.; Kohno, H.; Ohta, Y.; Yokoyama, A. *Macromolecules*, **2010**, *43*, 7095–7100. (d) Huang, W.; Su, L.; Bo, Z. *J. Am. Chem. Soc.*, **2009**, *131*, 10348–10349. (e) Beryozkina, T.; Boyko, K.; Khanduyeva, N.; Senkovskyy, V.; Horecha, M.; Oertel, U.; Simon, F.; Stamm, M.; Kiriy, A. *Angew. Chem. Int. Ed.*, **2009**, *48*, 2695–2698. (f) Yokoyama, A.; Suzuki, H.; Kubota, Y.; Ohuchi, K.; Higashimura, H.; Yokozawa, T. *J. Am. Chem. Soc.*, **2007**, *129*, 7236–7237.

(14) Grisorio, R.; Suranna, G. P.; Mastrorilli, P. *Chem. Eur. J.*, **2010**, *16*, 8054–8061.

(15) Verswyvel, M.; Verstappen, P.; De Cremer, L.; Verbiest, T.; Koeckelberghs, G. *J. Polym. Sci., Part A: Polym. Chem.*, **2011**, *49*, 5339–5349.

(16) Senkovskyy, V.; Tkachov, R.; Komber, H.; Sommer, M.; Heuken, M.; Voit, B.; Huck, W. T. S.; Kataev, V.; Petr, A.; Kiriy, A.; *J. Am. Chem. Soc.*, **2011**, *133*, 19966–19970.

(17) (a) O'Brien, C. J.; Kantchev, E. A. B.; Valente, C.; Hadei, N.; Chass, G. A.; Lough, A.; Hopkinson, A. C.; Organ, M. G. *Chem. Eur. J.*, **2006**, *12*, 4743–4748. (b) Organ, M. G.; Avola, S.; Dubovyk, I.; Hadei, N.; Kantchev, E. A. B.; O'Brien, C. J.; Valente, C. *Chem. Eur. J.*, **2006**, *12*, 4749–4755. (c) Organ, M. G.; Abdel-Hadi, M.; Avola, S.; Hadei, N.; Nasielski, J.; O'Brien, C. J.; Valente, C. *Chem. Eur. J.*, **2007**, *13*, 150–157.

(18) For recent reviews, see: (a) Valente, C.; Çalimsiz, S.; Hoi, K. H.; Mallik, D.; Sayah, M.; Organ, M. G. *Angew. Chem. Int. Ed.*, **2012**, *51*, 2-21. (b) Organ, M. G.; Chass, G. A.; Fang, D.-C.; Hopkinson, A. C.; Valente, C. *Synthesis*, **2008**, *17*, 2776–2797.

(19) Larrosa, I.; Somoza, C.; Banquy, A.; Goldup, S. M. *Org. Lett.*, **2011**, *13*, 146–149.

(20) Unusually selective difunctionalizations have previously been observed with other Pd catalysts. Similar mechanisms have been proposed. For examples, see: (a) Weber, S. K.; Galbrecht, F.; Scherf, U. *Org. Lett.*, **2006**, *8*, 4039–4041. (b) Sinclair, D. J.; Sherburn, M. S. *J. Org. Chem.*, **2005**, *70*, 3730–3733. (c) Dong, C.-G.; Hu, Q.-S. *J. Am. Chem. Soc.*, **2005**, *127*, 10006–10007.

(21) (a) Tkachov, R.; Senkovskyy, V.; Komber, H.; Kiriy, A. *Macromolecules*, **2011**, *44*, 2006-2015. (b) Tkachov, R.; Senkovskyy, V.; Komber, H.; Sommer,

J.-U.; Kiriy, A. *J. Am. Chem. Soc.*, **2010**, *132*, 7803–7810. (c) Beryozkina, T.; Senkovskyy, V.; Kaul, E.; Kiriy, A. *Macromolecules*, **2008**, *41*, 7817–7823. (d) Miyakoshi, R.; Yokoyama, A.; Yokozawa, T. *J. Am. Chem. Soc.*, **2005**, *127*, 17542–17547. (e) Iovu, M. C.; Sheina, E. E.; Gil, R. R.; McCullough, R. D. *Macromolecules*, **2005**, *38*, 8649–8656.

(22) (a) Lanni, E. L.; McNeil, A. J. *Macromolecules*, **2010**, *43*, 8039–8044. (b) Lanni, E. L.; McNeil, A. J. *J. Am. Chem. Soc.*, **2009**, *131*, 16573–16579. (c) See also, ref 8.

(23) Nasielski, J.; Hadei, N.; Achonduh, G.; Kantchev, E. A. B.; O'Brien, C. J.; Lough, A.; Organ, M. G. *Chem. Eur. J.*, **2010**, *16*, 10844–10853.

(24) (a) Shi, L.; Chu, Y.; Knochel, P.; Mayr, H. *Org. Lett.*, **2009**, *11*, 3502–3505. (b) Shi, L.; Chu, Y.; Knochel, P.; Mayr, H. *J. Org. Chem.*, **2009**, *74*, 2760–2764.

(25) Excess iPrMgCl (or tBuMgCl) can be detrimental. For example, see: Lohwasser, R. H.; Thelakkat, M. *Macromolecules* **2011**, *44*, 3388-3397.

(26) (a) Lamps, J.-P.; Catala, J.-M. *Macromolecules*, **2011**, *44*, 7962–7968. (b) See also, ref 21a.

(27) For example, see ref 1b.

(28) Note that the radical-based mechanisms have been proposed when iPrI is generated in situ. For reference, see: (a) Kienle, M.; Knochel, P. *Org. Lett.*, **2010**, *12*, 2702–2705. (b) Manolikakes, G.; Knochel, P. *Angew. Chem. Int. Ed.*, **2009**, *48*, 205–209.

(29) Stefan, M. C.; Javier, A. E.; Osaka, I.; McCullough, R. D. *Macromolecules*, **2009**, *42*, 30–32.

(30) (a) Wu, S.; Bu, L.; Huang, L.; Yu, X.; Han, Y.; Geng, Y.; Wang, F. *Polymer*, **2009**, *50*, 6245–6251. (b) Miyakoshi, R.; Yokoyama, A.; Yokozawa, T. *Chem. Lett.*, **2008**, *37*, 1022–1023. (c) Yokoyama, A.; Kato, A.; Miyakoshi, R.; Yokozawa, T. *Macromolecules*, **2008**, *41*, 7271–7273. (e) See also, ref 3f.

(31) Roy, A. H.; Hartwig, J. F. *J. Am. Chem. Soc.*, **2003**, *125*, 13944–13945. See also: Roy, A. H.; Hartwig, J. F. *Organometallics*, **2004**, *23*, 1533–1541.

(32) (a) Chen, M.-T.; Vicic, D. A.; Turner, M. L.; Navarro, O. *Organometallics*, **2011**, *30*, 5052–5056. (b) See also, ref 23.

Chapter 3

Impact of preferential π-binding in catalyst-transfer polymerization of thiazole derivatives

Few living, chain-growth methods exist for polymerizing electron-deficient arenes.[1,2,3,4,5] As a consequence, accessing n-type and low band-gap polymers with precisely defined sequences and molecular weights is still challenging. In contrast, several living, chain-growth methods have been discovered for electron-rich arenes.[6,7,8] Sommer[9] and Kiriy[10] suggest that with the electron-deficient arenes, catalyst turnover might be inhibited due to strong binding by oligomers formed initially during polymerization.[11] Stalling the polymerization at this point can lead to nonproductive pathways such as chain-transfer to monomer. Consistent with this hypothesis, we show herein that the nonliving behavior with thiazole derivatives can be attributed to both preferential π-binding and a high barrier for catalyst chain-walking to the reactive chain end. Consequently, a chain-transfer pathway via Mg-N coordination and ancillary ligand dissociation becomes competitive. We demonstrate that this pathway can be attenuated with a more rigid ancillary ligand, improving the polymerization. Overall, our studies provide mechanistic insight into the nonliving behavior of electron-deficient heteroarene polymerizations.

We selected thiazole because it is an electron-deficient analogue of thiophene,[12] and it exhibits n-type behavior in electronic devices.[13] Until recent reports by Pammer et al.,[2a,3a] thiazole[14] and bithiazole[15] had only been polymerized via step-growth methods.[16] We began our studies with thiazole precursor **1**, which was prepared in modest yield (see Appendix 2).[17] Activation of **1** with iPrMgCl was regioselective, although the ^{1}H NMR spectrum suggested

---

[1] Reproduced with permission from Smith, M. L.; Leone, A. K.; Zimmerman, P. M.; McNeil, A. J. "Impact of Preferential π-Binding in Catalyst-Transfer Polycondensation of Thiazole Derivatives" *ACS Macro Lett.* **2016**, *5*, 1411-1415.

[2] A.K.L. conducted the synthesis of **3** and improved the synthesis of **1**. P.M.Z. performed all calculations.

surprising activation at the more hindered carbon (**2a**). Two-dimensional heteronuclear magnetic resonance spectroscopic analysis (^{1}H/^{13}C HSQC and HMBC) confirmed the structural assignment (Appendix 2). In the absence of Ni catalyst, we observed oligomerization of **2a** (avg ~ 4–6 repeat units) after 16 h, and with regioisomer **2b**, oligomers formed within 10 min. These results are similar to those of Pammer et al., who observed that **2b** (with C_9H_{19} instead of $C_{10}H_{21}$) will "decompose rapidly" in the presence of coordinating solvents (e.g., THF).[3a] We suspected that the oligomerization proceeded via spontaneous radical anion generation, with subsequent halide cleavage, followed by a radical-mediated nucleophilic aromatic substitution ($S_{RN}1$). Hayashi and co-workers proposed a similar $S_{RN}1$ pathway to explain metal-free coupling between Grignard reagents and haloarenes.[18] Consistent with the proposed mechanism, the electron paramagnetic resonance (EPR) spectrum of **2b** showed a signal matching an organic radical (Figure 3.1). Using an external standard, it was found that only 0.07% of **2b** contained a radical (Appendix 2). This low concentration is reasonable for an uncontrolled radical polymerization with spontaneous initiation and termination reactions occurring. Negligible radical concentrations were observed in either thiazole **1** or iPr$_3$PhMgBr. Combined, these studies reveal that spontaneous oligomerization occurs in THF at room temperature with Mg/Br-functionalized thiazole derivatives, regardless of the regioisomer, and therefore these monomers should not be used for polymerizations.
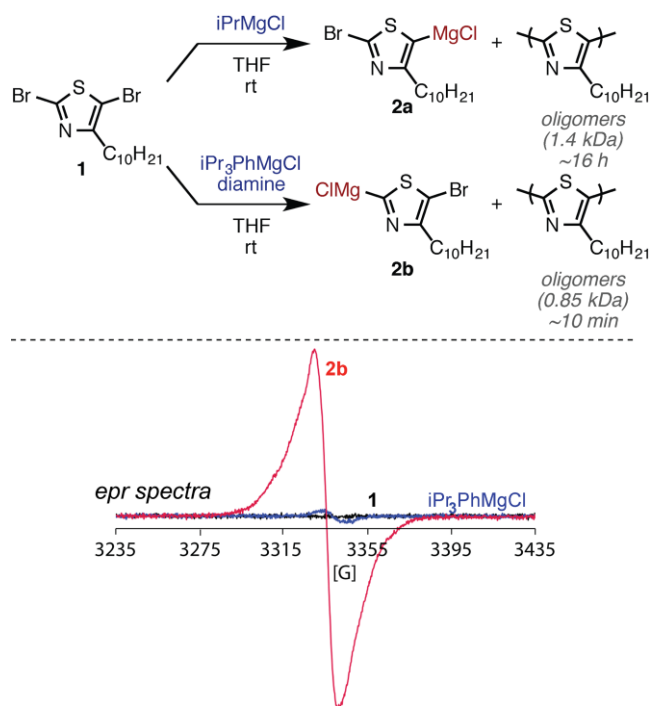
Figure 3.1 Spectroscopic evidence of radical-mediated oligomer formation during the Grignard metathesis reaction with thiazole **1**.

To circumvent the spontaneous oligomerization, we prepared Cl/Br-functionalized thiazole **3**,[2a] rationalizing that the C–Cl bond will be less likely to cleave during the $S_{RN}1$ pathway. Indeed, no oligomers were observed after 24 h when **3** was activated with iPrMgCl (eq 1 and Appendix 2). Although more hindered regioisomer 4 was formed, related thiophenes[19] and thiazoles[2a] have been polymerized in a chain-growth fashion. Both soluble and insoluble polymer formed when monomer 4 was reacted with precatalyst **5** in THF at rt over 10 h (eq 1). The soluble material was highly regioregular (Appendix 2)[3a] and exhibited a low number-average molecular weight (M_n = 0.9 kDa, ~ 4 repeat units). The presence of higher molecular weight polymer suggests a chain-growth mechanism, especially in light of the 42% conversion of monomer **4**. While this work was in progress, Pammer and co-workers reported polymerizing a more soluble thiazole derivative mediated by precatalyst **5**.[2a] Evidence for a chain-growth mechanism was demonstrated by the near-linear relationship between M_n and monomer/catalyst ratio. Nevertheless, the observed bimodal peaks in the gel permeation chromatogram suggested a nonliving polymerization.

$$\text{(1)}$$
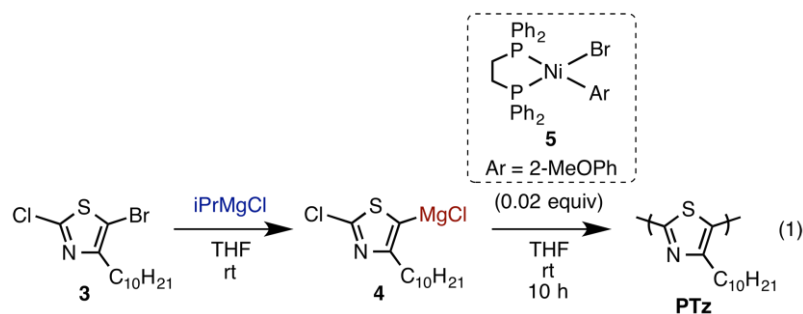
To determine the origin of this nonliving polymerization, chain-growth and chain-transfer pathways were evaluated computationally using model systems (Appendix 2). These quantum chemical simulations were performed starting with a dppe-ligated Ni catalyst similar to **Ni$_{RE}$** (Scheme 1 and Appendix 2). After reductive elimination, a π-complex forms preferentially between (dppe)Ni and the C=C bond in the terminal thiazole (**Ni$_\pi$**). The barrier for chain-walking to the chloro-substituted C=N bond to form **Ni$_{\pi\text{-cw}}$** was surprisingly high ($\Delta G^\ddagger$ = 18.6 kcal/mol). In contrast, the corresponding chain-walking barrier for thiophene is more than 8 kcal/mol lower. This preferential binding and slower chain-walking enables unproductive pathways to become competitive. Using reaction discovery computations, a possible chain-transfer pathway was identified (Scheme 3.1).[20] Chain-transfer is initiated when the N lone pair binds to a Mg atom on a monomer, an energetically downhill process, displacing one THF molecule. The N-Mg coordination brings a monomer proximate to the Ni center, which is facilitated by temporary dissociation of one P from Ni. Rate-limiting Ni migration with concomitant ligand reassociation displaces the π-bound oligothiazole, completing the chain-transfer. The overall barrier for this process is 11.2 kcal/mol higher than chain-walking, making it a plausible pathway to account for nonliving behavior.
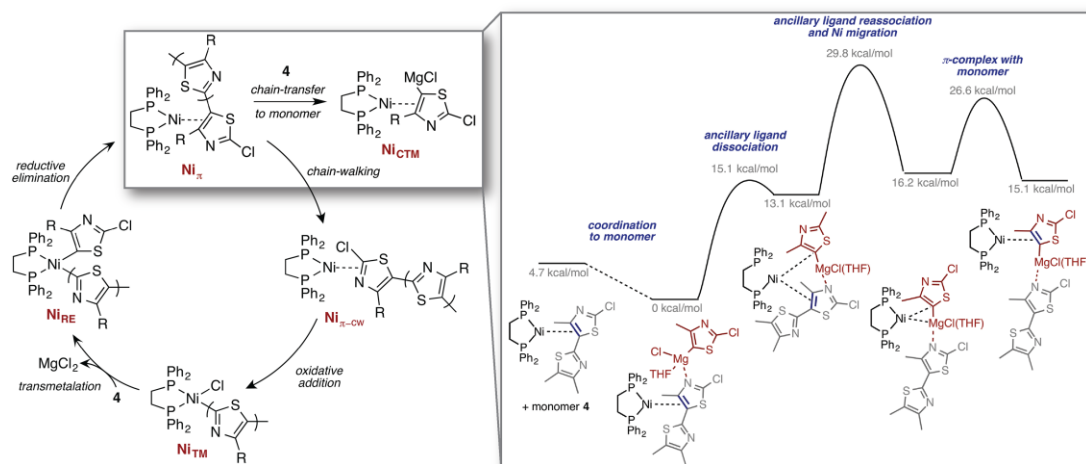
Scheme 3.1 Proposed Mechanisms for the Chain-Growth Catalytic Cycle and the Competing Chain-Transfer to Monomer Pathway.

Because our studies suggest preferential binding in the Ni(0)-thiazole π-complex, we attempted to characterize this species using a model system. Specifically, we added 2 equiv of 4-methylthiazole to known Ni(0)-anthracene π-complex **6**,[21] rationalizing that the stronger π-accepting thiazole would displace anthracene. Indeed, a new species was observed downfield (Figure 3.2); however, the relatively narrow coupling constants ($J_{P\text{-}P}$ = 18 Hz) were inconsistent with known Ni(0)-arene π-complexes (e.g., **6**, $J_{P\text{-}P}$ = 68 Hz),[22,23] and were more consistent with Ni(II) complexes.[24,25] The ^{1}H NMR spectrum of the new species revealed a small upfield shift (Δ = 0.2 ppm) for proton H_A and a significantly larger upfield shield (Δ = 0.6 ppm) for H_B. These signals appeared to be a doublet of doublets rather than the expected doublets from the H_A/H_B splitting. In addition, the magnetic field strength had no influence on the coupling constants, suggesting the peaks correspond to a single species (Appendix 2). Using 2D heteronuclear multiple bond correlation (^{1}H/^{31}P HMBC) spectroscopy, the additional coupling was traced to the phosphorus atoms in the ancillary ligand ($J_{P\text{-}H}$ = 11.9 and 36.5 Hz, Appendix 2). No metal-hydride signals were observed in the ^{1}H NMR spectrum, ruling out a Ni-mediated C-H insertion.[26] Instead, the unknown species is most consistent with complex **7**, which is generated from oxidative addition into the C–S bond.[27] Oxidative additions into both the C–H or C–S bond were evaluated computationally (Appendix 2). While the activation barrier for C–S oxidative addition is slightly higher, the reaction is exothermic (ΔG^0 = -7.2 kcal/mol) whereas C–H cleavage

has a lower barrier but is endothermic (ΔG^0 = +7.7 kcal/mol). As a consequence, the equilibrium should favor the C–S oxidative addition (i.e., complex **7**). Although this reaction pathway is novel for thiazole, we do not believe it is relevant under the polymerization conditions since oxidative addition into the C–Cl bond is near barrierless ($\Delta G^{\ddagger}$ = 0.4 kcal/mol) and effectively irreversible (ΔG^0 = -36.9 kcal/mol).
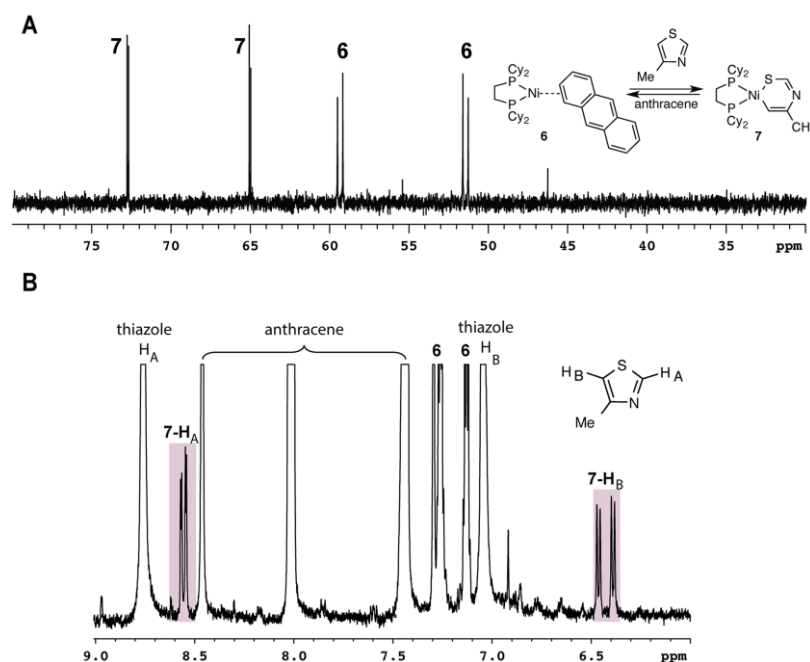
Figure 3.2 (A) ^{31}P NMR spectrum of anthracene π-complex **6** (7 mM) with 4-methylthiazole (14 mM) in THF at rt after 10 min. (B) ^{1}H NMR spectrum of the same sample after 20 min.

Because the chain-transfer pathway involves ancillary ligand dissociation, we reasoned that a more rigid ligand framework (e.g., 1,2-bis(diphenylphosphino)benzene (dppbz)) should suppress this pathway by making dissociation more unfavorable. Consistent with this hypothesis, we found that the chain-transfer pathway is 4.9 kcal/mol higher with dppbz than dppe. As a consequence, a dppbz-ligated catalyst (e.g., **10**) should undergo more productive turnovers than dppe during a polymerization. To evaluate this hypothesis, we performed side-by-side polymerizations using the more soluble thiazole monomer (**9**) reported by Pammer et al.,[2a] to minimize polymer precipitation and access higher molecular weight polymers. To provide the best ligand comparison, each set of polymerizations (i.e., dppe versus dppbz at a single monomer/catalyst ratio) used the same monomer batch and were performed in tandem (Appendix 2). Both catalysts showed a linear relationship

between M_n and the monomer/catalyst ratio, however, dppbz consistently yielded polymers with higher M_n and slightly narrower dispersities, suggesting fewer chain-transfer events (Figure 3.3A).[28] This conclusion is supported by analysis of the matrix-assisted laser desorption/ionization time-of-flight mass spectrometry (MALDI-TOF-MS) data, which showed that the major polymer species when dppbz was used has an end-group consistent with a living, chain-growth mechanism (PhOMe/H), whereas the major polymer species when dppe was used is consistent with at least one chain-transfer event (H/Cl, Figure 3.3B). Combined, these data suggest that rigid ancillary ligands can minimize the chain-transfer pathway in thiazole polymerization.
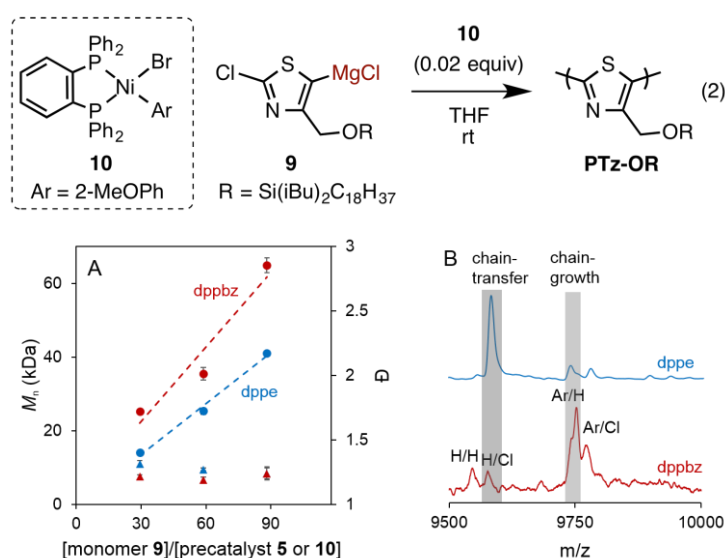
Figure 3.3 (A) Plot of M_n and dispersity (Đ) of **PTz-OR** versus the monomer/catalyst ratio using either precatalyst **5** (blue) or precatalyst **10** (red) and monomer **9**. (B) MALDI-TOF-MS analysis of **PTz-OR** obtained via either precatalyst **5** or **10** and monomer **9**.

To summarize, our studies identified one significant challenge for polymerizing electron-deficient (hetero)arenes: preferential binding of the catalyst to the C=C bond, which hinders catalyst migration to the active polymer chain end and enables unproductive pathways to become competitive. These results provide insight into why N-containing electron-deficient monomers might fail to under-go living, chain-growth polymerization despite their strong binding in the π-complex. Our computational studies point to rigid ancillary ligands as a potential solution and our experimental results supported this hypothesis. Further studies evaluating alternative ancillary ligands and monomers are

needed to generalize this approach and make progress toward synthesizing higher performing materials containing both electron-rich and electron-deficient monomers.

References

(1) For reviews, see: (a) Yokozawa, T.; Ohta, Y. *Chem. Rev.* **2016**, *116*, 1950–1968. (b) Yokozawa, T.; Nanashima, Y.; Nojima, M.; Ohta, Y. *Macromol. Symp.* **2015**, *350*, 22–33. (c) Yokozawa, T.; Nanashima, Y.; Ohta, Y. *ACS Macro Lett.* **2012**, *1*, 862–866.

(2) For examples of chain-growth (but not perfectly living) behavior with electron-deficient monomers, see: (a) Pammer, F.; Jäger, J.; Rudolf, B.; Sun, Y. *Macromolecules* **2014**, *47*, 5904–5912. (b) Bridges, C. R.; McCormick, T. M.; Gibson, G. L.; Hollinger, J.; Seferos, D. S. *J. Am. Chem. Soc.* **2013**, *135*, 13212–13219. (c) Nanashima, Y.; Yokoyama, A.; Yokozawa, T. *Macromolecules* **2012**, *45*, 2609–2613.

(3) Mostly nonliving behavior has been observed with electron-deficient monomers containing nitrogen. For examples, see: (a) Pammer, F.; Passlack, U. *ACS Macro Lett.* **2014**, 3, 170–174. (b) Nanashima, Y.; Shibata, R.; Miyakoshi, R.; Yokoyama, A.; Yokozawa, T. *J. Polym. Sci., Part A: Polym. Chem.* **2012**, *50*, 3628–3640. (c) Senkovskyy, V.; Tkachov, R.; Komber, H.; John, A.; Sommer, J.-U.; Kiriy, A. *Macromolecules* **2012**, *45*, 7770–7777. (d) Nanashima, Y.; Yokoyama, A.; Yokozawa, T. *J. Polym. Sci., Part A: Polym. Chem.* **2012**, *50*, 1054–1061. (e) Senkovskyy, V.; Tkachov, R.; Komber, H.; Sommer, M.; Heuken, M.; Voit, B.; Huck, W. T. S.; Kataev, V.; Petr, A.; Kiriy, A. *J. Am. Chem. Soc.* **2011**, *133*, 19966–19970. (f) Wen, L.; Duck, B. C.; Dastoor, P. C.; Rasmussen, S. C. *Macromolecules* **2008**, *41*, 4576–4578.

(4) Copolymerization with electron-rich monomers (e.g., block, statistical and alternating) have been more successful. For examples, see: (a) Pollit, A. A.; Bridges, C. R.; Seferos, D. S. *Macromol. Rapid Commun.* **2015**, *36*, 65–70. (b) Todd, A. D.; Bielawski, C. W. *ACS Macro Lett.* **2015**, *4*, 1254–1258. (c) Goto, E.; Ando, S.; Ueda, M.; Higashihara, T. *ACS Macro Lett.* **2015**, *4*, 1004–1007. (d) Tkachov, R.; Komber, H.; Rauch, S.; Lederer, A.; Oertel, U.; Häußler, L.; Voit, B.; Kiriy, A. *Macromolecules* **2014**, *47*, 4994–5001. (e) Willot, P.; Moerman, D.; Leclère, P.; Lazzaroni, R.; Baeten, T.; Van der Auweraer, M.; Koeckelberghs, G. *Macromolecules* **2014**, *47*, 6671–6678. (f) Elmalem, E.; Kiriy, A.; Huck, W. T. S. *Macromolecules* **2011**, *44*, 9057–9061. (g) Bronstein, H.; Hurhangee, M.; Collado Fregoso, E.; Beatrup, D.; Soon, Y. W.; Huang, Z.; Hadipour, A.; Tuladhar, P. S.; Rossbauer, S.; Sohn, E.-H.; Shoaee, S.; Dimitrov, S. D.; Frost, J. M.; Ashraf, R. S.; Kirchartz, T.; Watkins, S. E.; Song, K.; Anthopoulos, T.; Nelson, J.; Rand, B. P.; Durrant, J. R.; McCulloch, I. *Chem. Mater.* **2013**, *25*, 4239–4249. (h) Wang, J.; Ueda, M.; Higashihara, T. *ACS Macro Lett.* **2013**, *2*, 506–510.

(5) Alternatively, electron-deficient monomers without nitrogen atoms have been polymerized via CTP. For an example, see Erdmann, T.; Back, J.; Tkachov, R.; Ruff, A.; Voit, B.; Ludwigs, S.; Kiriy, A. *Polym. Chem.* **2014**, *5*, 5383–5390.

(6) (a) Sheina, E. E.; Liu, J.; Iovu, M. C.; Laird, D. W.; McCullough, R. D. *Macromolecules* **2004**, *37*, 3526–3528. (b) Yokoyama, A.; Miyakoshi, R.;

Yokozawa, T. *Macromolecules* **2004**, *37*, 1169–1171. (c) Miyakoshi, R.; Yokoyama, A.; Yokozawa, T. *Macromol. Rapid Commun.* **2004**, *25*, 1663−1666.

(7) For recent reviews, see (a) Leone, A. K.; McNeil, A. *J. Acc. Chem. Res.* **2016**, *49*, 2822−2831. (b) Verheyen, L.; Leysen, P.; Van Den Eede, M.-P.; Ceunen, W.; Hardeman, T.; Koeckelberghs, G. *Polymer* **2017**, *108*, 521−546. (c) Grisorio, R.; Suranna, G. P. *Polym. Chem.* **2015**, *6*, 7781–7795. (d) Bryan, Z. J.; McNeil, A. J. *Macromolecules* **2013**, *46*, 8395–8405. (e) Stefan, M. C.; Bhatt, M. P.; Sista, P.; Magurudeniya, H. D. *Polym. Chem.* **2012**, *3*, 1693–1701.

(8) For recent examples, see (a) Suraru, S.-L.; Lee, J. A.; Luscombe, C. K. *ACS Macro Lett.* **2016**, *5*, 533–536. (b) Ye, S.; Steube, M.; Carrera, E. I.; Seferos, D. S. *Macromolecules* **2016**, *49*, 1704–1711. (c) Miyane, S.; Mori, H.; Higashihara, T. *Microsyst. Technol.* **2016**, *22*, 3–10. (d) Yang, X.; Ge, J.; He, M.; Ye, Z.; Liu, X.; Peng, J.; Qiu, F. *Macromolecules* **2016**, *49*, 287–297. (e) Hardeman, T.; Koeckelberghs, G. *Macromolecules* **2015**, *48*, 6987–6993. (f) Bridges, C. R.; Guo, C.; Yan, H.; Miltenburg, M. B.; Li, P.; Li, Y.; Seferos, D. S. *Macromolecules* **2015**, *48*, 5587–5595. (g) He, L.-Y.; Urrego-Riveros, S.; Gates, P. J.; Näther, C.; Brinkmann, M.; Abetz, V.; Staubitz, A. *Tetrahedron* **2015**, *71*, 5399–5406. (h) Sui, A.; Shi, X.; Wang, Y.; Geng, Y.; Wang, F. *Polym. Chem.* **2015**, *6*, 4819–4827. (i) Shi, X.; Sui, A.; Wang, Y.; Li, Y.; Geng, Y.; Wang, F. *Chem. Commun.* **2015**, *51*, 2138–2140. (j) Zhang, H.-H.; Xing, C.-H.; Hu, Q.-S.; Hong, K. *Macromolecules* **2015**, *48*, 967–978. (k) Qiu, Y.; Mohin, J.; Tsai, C.-H.; Tristram-Nagle, S.; Gil, R. R.; Kowalewski, T.; Noonan, K. J. T. *Macromol. Rapid Commun.* **2015**, 36, 840–844. (l) see also, ref 4a

(9) Komber, H.; Senkovskyy, V.; Tkachov, R.; Johnson, K.; Kiriy, A.; Huck, W. T. S.; Sommer, M. *Macromolecules* **2011**, *44*, 9164–9172.

(10) Karpov, Y.; Maiti, J.; Tkachov, R.; Beryozkina, T.; Bakulev, V.; Liu, W.; Komber, H.; Lappan, U.; Al-Hussein, M.; Stamm, M.; Voita, B.; Kiriy, A. *Polym. Chem.* **2016**, *7*, 2691–2697.

(11) For another example of a stalled catalytic cycle due to strong binding, see: Willot, P.; Koeckelberghs, G. *Macromolecules* **2014**, *47*, 8548–8555.

(12) The reduction potential of poly(3-alkylthiazole) is shifted by 0.3 V compared to poly(3-alkylthiophene). For more information, see ref 3a.

(13) For a recent review of thiazole-based semiconductors, see Lin, Y.; Fan, H.; Li, Y.; Zhan, X. *Adv. Mater.* **2012**, *24*, 3087–3106.

(14) For thiazole homopolymers, see (a) Mori, S.; Yamamoto, T.; Asakawa, N.; Yazawa, K.; Inoue, Y. *Polym. J.* **2008**, *40*, 475–478. (b) Mori, S.; Inoue, Y.; Yamamoto, T.; Asakawa, N. *Phys. Rev. B - Condens. Matter Mater. Phys.* **2005**, *71*, 1–11. (c) Yamamoto, T.; Komarudin, D.; Arai, M.; Lee, B.-L.; Suganuma, H.; Asakawa, N.; Inoue, Y.; Kubota, K.; Sasaki, S.; Fukuda, T.; Matsuda, H. *J. Am. Chem. Soc.* **1998**, *120*, 2047–2058. (d) Maruyama, T.; Suganuma, H.; Yamamoto, T. *Synth. Met.* **1995**, *74*, 183–185. (e) Bolognesi, A.; Catellani, M.; Destri, S.; Porzio, W. *Synth. Met.* **1987**, *18*, 129–132.

(15) For bithiazole homopolymers, see (a) Kuwabara, J.; Kuramochi, M.; Liu, S.; Yasuda, T.; Kanbara, T. *Polym. J.* **2017**, *49*, 123–131. (b) Politis, J. K.; Curtis, M. D.; González-Ronda, L.; Martin, D. C. *Chem. Mater.* **2000**, *12*, 2798–2804. (c) Politis, J. K.; Curtis, M.; He, Y.; Kanicki, J. *Macromolecules* **1999**, *32*, 2484–2489. (d) Politis, J. K.; Somoza, F. B.; Kampf, J. W.; Curtis, M. D.; Ronda, L. G.; Martin, D. C. *Chem. Mater.* **1999**, *11*, 2274–2284. (e) González-Ronda, L.; Martin, D. C.; Nanos, J. I.; Politis, J. K.; Curtis, M. D. *Macromolecules* **1999**, *32*, 4558–4565. (f) Curtis, M. D.; Cheng, H.; Johnson, J. A.; Nanos, J. I.; Kasim, R.; Elsenbaumer, R. L.; Ronda, L. G.; Martin, D. C. *Chem. Mater.* **1998**, *10*, 13–16. (g) Yamamoto, T.; Suganuma, H.; Maruyama, T.; Inoue, T.; Muramatsu, Y.; Arai, M.; Komarudin, D.; Ooba, N.; Tomaru, S.; Sasaki, S.; Kubota, K. *Chem. Mater.* **1997**, *9*, 1217–1225. (h) Nanos, J. I.; Kampf, J. W.; Curtis, M. D.; Gonzalez, L.; Martin, D. C. *Chem. Mater.* **1995**, *7*, 2232–2234. (i) Yamamoto, T.; Suganuma, H.; Maruyama, T.; Kubota, K. *J. Chem. Soc., Chem. Commun.* **1995**, 1613–1614.

(16) For recent examples of thiazole-containing copolymers, see (a) Li, W.; Hendriks, K. H.; Furlan, A.; Wienk, M. M.; Janssen, R. A. J. *J. Am. Chem. Soc.* **2015**, *137*, 2231–2234. (b) Saeki, A.; Tsuji, M.; Yoshikawa, S.; Gopal, A.; Seki, S. *J. Mater. Chem. A*, **2014**, *2*, 6075–6080. (c) Osaka, I.; Saito, M.; Koganezawa, T.; Takimiya, K. *Adv. Mater.* **2014**, *26*, 331–338. (d) Usta, H.; Sheets, W. C.; Denti, M.; Generali, G.; Capelli, R.; Lu, S.; Yu, X.; Muccini, M.; Facchetti, A. *Chem. Mater.* **2014**, *26*, 6542–6556. (e) Beatrup, D.; Wade, J.; Biniek, L.; Bronstein, H.; Hurhangee, M.; Kim, J.-S.; McCulloch, I.; Durrant, J. R. *Chem. Commun.* **2014**, *50*, 14425–14428. (f) Ustamehmetoğlu, B. *Electrochim. Acta* **2014**, *122*, 130–140. (g) Li, W.; Roelofs, W. S. C.; Turbiez, M.; Wienk, M. M.; Janssen, R. A. J. *Adv. Mater.* **2014**, *26*, 3304–3309. (h) Wang, Y.; Kadoya, T.; Wang, L.; Hayakawa, T.; Tokita, M.; Mori, T.; Michinobu, T. *J. Mater. Chem. C* **2015**, *3*, 1196–1207. (i) Li, W.; An, Y.; Wienk, M. M.; Janssen, R. A. J. *J. Mater. Chem. A* **2015**, *3*, 6756–6760.

(17) (a) Fan, P.; Goto, H.; He, X.; Kakutani, M.; Labelle, M.; McMinn, D. L.; Powers, J. P.; Rew, Y.; Sun, D.; Yan, X. U.S. Patent WO2005110980 A2, Nov 24, 2005. (b) Siméon, F. G.; Wendahl, M. T.; Pike, V. W. *J. Org. Chem.* **2009**, *74*, 2578–2580. (c) Cardwell, H. M. E.; Kilner, A. E. H. *J. Chem. Soc.* **1951**, 2430–2441.

(18) (a) Shirakawa, E.; Okura, K.; Uchiyama, N.; Murakami, T.; Hayashi, T. *Chem. Lett.* **2014**, *43*, 922–924. (b) Uchiyama, N.; Shirakawa, E.; Hayashi, T. *Chem. Commun.* **2013**, *49,* 364–366. (c) Shirakawa, E.; Hayashi, Y.; Itoh, K.-I.; Watabe, R.; Uchiyama, N.; Konagaya, W.; Masui, S.; Hayashi, T. *Angew. Chem. Int. Ed.* **2012**, *51*, 218–221. (d) See also Haines, B. E.; Wiest, O. *J. Org. Chem.* **2014**, *79*, 2771–2774.

(19) (a) Wu, S.; Huang, L.; Tian, H.; Geng, Y.; Wang, F. *Macromolecules* **2011**, *44*, 7558–7567. (b) Tkachov, R.; Senkovskyy, V.; Komber, H.; Kiriy, A. *Macromolecules* **2011**, *44*, 2006–2015.

(20) (a) Pendleton, I. M.; Pérez-Temprano, M. H.; Sanford, M. S.; Zimmerman, P. M. *J. Am. Chem. Soc.* **2016**, 138, 6049-6060. (b) Zimmerman, P. M. *J. Comput. Chem.* **2013**, *34*, 1385–1392. (c) Zimmerman, P. M. *J. Comput. Chem.*

2015, *36*, 601–611. (d) Zimmerman, P. M. *J. Chem. Phys.* **2013**, *138*, 184102. (e) Zimmerman, P. M. *J. Chem. Theory Comput.* **2013**, *9*, 3043–3050.

(21) (a) Stanger, A.; Vollhardt, K. P. C. *Organometallics* **1992**, *11*, 317–320. (b) Jonas, K. *J. Organomet. Chem.* **1974**, *78*, 273–279.

(22) For other examples of Ni(0) π-complexes, see (a) Hatnean, J. A.; Shoshani, M.; Johnson, S. A. *Inorg. Chim. Acta* **2014**, *422*, 86–94. (b) Hatnean, J. A.; Beck, R.; Borrelli, J. D.; Johnson, S. A.; *Organometallics* **2010**, *29*, 6077–6091. (c) Johnson, S.; Huff, C.; Mustafa, F.; Saliba, M. *J. Am. Chem. Soc.* **2008**, *130*, 17278–17280. (d) Bennett, M.; Kopp, M.; Wenger, E.; Willis, A. *J. Organomet. Chem.* **2003**, *667*, 8–15. (e) Bach, I.; Pörschke, K.-R.; Goddard, R.; Kopiske, C.; Krüger, C.; Rufińska, A.; Seevogel, K. *Organometallics* **1996**, *15*, 4959–4966. (f) Stanger, A. *Organometallics* **1991**, *10*, 2979–2982.

(23) For related Ni(0) π-complexes containing a N heteroatom, see: (a) Guan, W.; Sakaki, S.; Kurahashi, T.; Matsubara, S. *ACS Catal.* **2015**, *5*, 1–10. (b) Hatnean, J.; Johnson, S. *Organometallics* **2012**, *31*, 1361–1373. (c) Atesin, T. A.; Li, T.; Lachaize, S.; Garcia, J. J.; Jones, W. D. *Organometallics* **2008**, *27*, 3811–3817. (d) Garcia, J. J.; Brunkan, N. M.; Jones, W. D. *J. Am. Chem. Soc.* **2002**, *124*, 9547–9555. (e) Garcia, J. J.; Jones, W. D. *Organometallics* **2000**, *19*, 5544–5545.

(24) For example, see Lee, S. R.; Bloom, J. W. G.; Wheeler, S. E.; McNeil, A. J. *Dalton Trans.* **2013**, *42*, 4218–4222.

(25) (a) Lee, S. R.; Bryan, Z. J.; Wagner, A. M.; McNeil, A. J. *Chem. Sci.* **2012**, *3*, 1562–1566. (b) Lanni, E. L.; Locke, J. R.; Gleave, C. M.; McNeil, A. J. *Macromolecules* **2011**, *44*, 5136–5145. (c) Lanni, E. L.; McNeil, A. J. *Macromolecules* **2010**, *43*, 8039–8044. (d) Lanni, E. L.; McNeil, A. J. *J. Am. Chem. Soc.* **2009**, *131*, 16573–16579.

(26) For example, see: Ateşin, T. A.; Li, T.; Lachaize, S.; Brennessel, W. W.; García, J. J.; Jones, W. D. *J. Am. Chem. Soc.* **2007**, *129*, 75627569.

(27) Jones et al. reported a similar oxidative addition into 2-cyanothiophene using [Ni(dippe)H]$_2$. For ref, see (a) Grochowski, M. R.; Li, T.; Brennessel, W. W.; Jones, W. D. *J. Am. Chem. Soc.* **2010**, *132*, 12412–12421. (b) Vicic, D. A.; Jones, W. D. *J. Am. Chem. Soc.* **1999**, *121*, 7606–7617.

(28) Note that conversion could not be measured due to nonsensical fluctuations in the quenched monomer concentration, presumably due to side-chain cleavage during the acidic workup.

Chapter 4

Synthesis of P3HT with targeted dispersity and its role in thin-film morphology

Morphological factors such as domain size, crystallinity, and polymer-fullerene intermixing influence charge generation, mobility and quantum efficiency in bulk heterojunction solar cells.[1] Thin-film morphology is influenced by processing conditions[2] as well as polymer properties. It has long been understood that regioregular polymers have higher charge mobility than regiorandom due to improved lamellar ordering.[3] The impact of average molecular weight has also seen significant investigation; higher molecular weights are associated with improved charge mobility[4] and improved PCE[5] up to a critical value (ca. 20 kDa in poly(3-hexylthiophene) (P3HT)). After decades of investigation into these devices, there remains a surprising lack of information on how the donor polymer's dispersity affects device performance. Previous studies on the effect of dispersity employ polymers synthesized via step-growth methods, leading to confounding correlations between dispersity and other factors, such as regioregularity or molecular weight. Catalyst-transfer polymerization, a chain-growth method for synthesizing conjugated polymers, enables the simple targeting of molecular weight and narrow dispersity in the resulting polymer. This control over the molecular weight distribution may make it an important technique in optimizing and commercializing organic photovoltaic devices.

Studies on the impact of dispersity in light-emitting diodes (LEDs) and organic field-effect transistors (OFETs) find contradictory effects (Chart 4.1). Some studies find that increased dispersity harms charge-carrier mobility: in LEDs constructed from low molecular weight **PPV**, the addition of high molecular weight **PPV** lowered device efficiency by an order of magnitude.[6] The lowered mobility
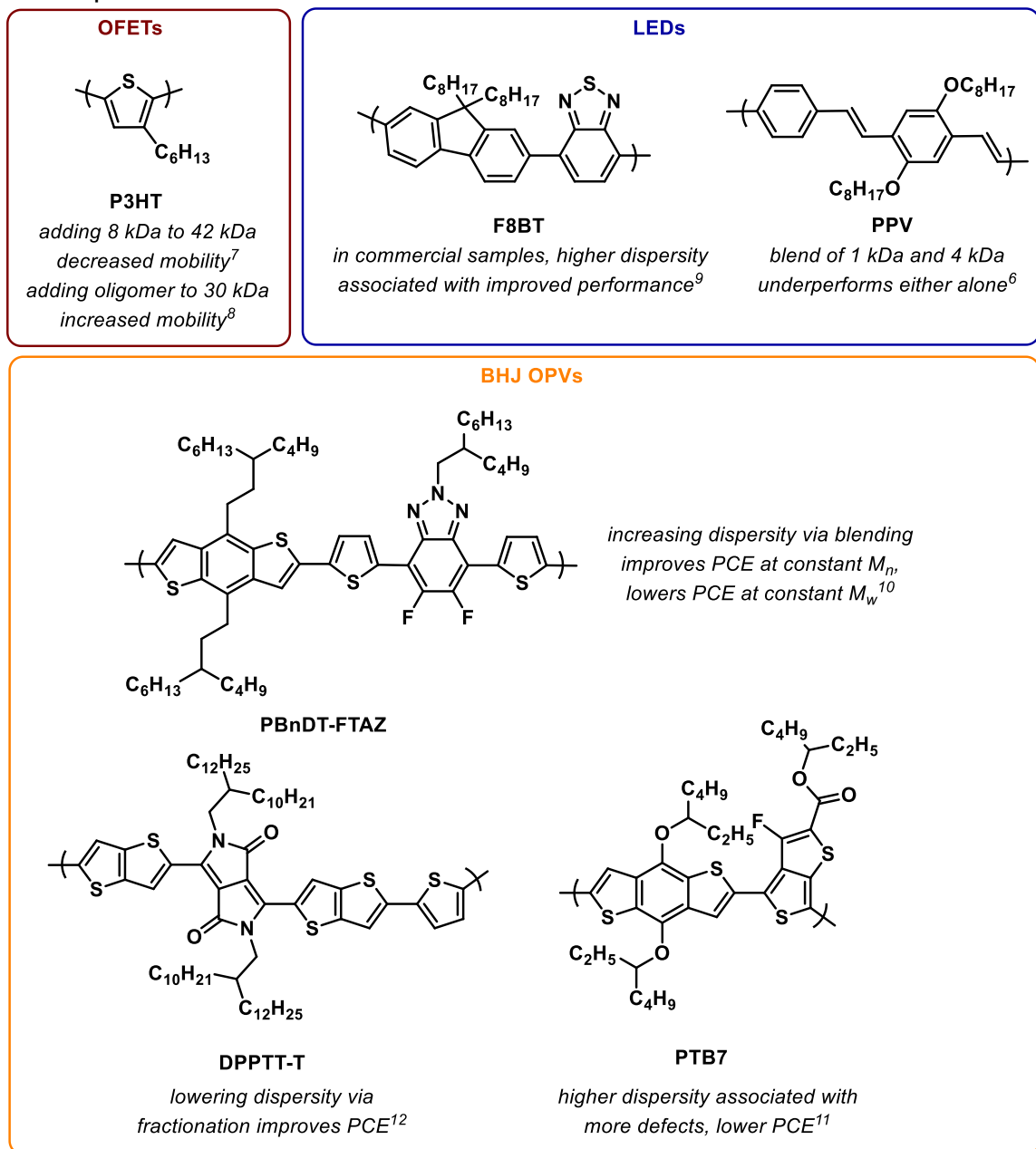
was attributed to charge carrier trapping by the high molecular weight polymer chains, which have lower LUMO energies. In OFETs utilizing **P3HT**, increased dispersity was again found to lower charge mobility; however, in these devices low molecular weight polymers were the culprit.[7] In binary blends of low- and high-molecular-weight **P3HT**, the presence of even 0.5 wt% low-molecular weight polymer degraded mobility. This finding is readily rationalized by a simple model of charge conduction in which intrachain transport is more efficient than interchain "hopping".

Other studies in these devices found the opposite effect. For example, OFETs constructed from blends of thiophene oligomers and **P3HT** outperformed devices made from either material alone.[8] This increase in conductivity was ascribed to low molecular weight oligomers forming highly crystalline domains connected by long "linker" polymers that prevent charge trapping at grain boundaries. Somewhat similarly, in PLEDs constructed utilizing commercially available **F8BT** with a broad range in both molecular weight and dispersity, higher dispersities were associated with larger domains and therefore better optical properties.[9] However, correlations to average molecular weight made the role of dispersity in this study difficult to interpret.

Results in bulk heterojunction solar cells (BHJs) are similarly mixed. Li et al. prepared broadly disperse **PBnDT-FTAZ** by blending 10 kDa and 60 kDa batches, then compared its properties to directly synthesized polymer samples with similar M_n or M_w and narrower dispersity.[10] They found that all three polymers had similar optical properties. The fill factor and power conversion efficiency of cells incorporating the broadly disperse **PBnDT-FTAZ** was enhanced relative to the sample with narrow Đ and similar M_n, but lower than those of the narrow Đ sample with similar M_w. The role of Đ apart from average molecular weight is therefore unclear. When comparing donor polymers with varied dispersities due to batch-to-batch variation in step-growth synthesis, **PTB7** with higher Đ had diminished device performance.[11] In these polymers, higher dispersity was correlated with

higher rates of homocoupling defects, which led to dramatically lowered hole mobility.

Chart 4.1 Selected studies on the role of polymer dispersity in optoelectronic device performance[6-12]

OFETs

P3HT
adding 8 kDa to 42 kDa decreased mobility[7]
adding oligomer to 30 kDa increased mobility[8]

LEDs

F8BT
in commercial samples, higher dispersity associated with improved performance[9]

PPV
blend of 1 kDa and 4 kDa underperforms either alone[6]

BHJ OPVs

PBnDT-FTAZ
increasing dispersity via blending improves PCE at constant M_n, lowers PCE at constant M_w[10]

DPPTT-T
lowering dispersity via fractionation improves PCE[12]

PTB7
higher dispersity associated with more defects, lower PCE[11]

McCulloch and coworkers also found that narrower dispersities were correlated with improved device performance.[12] By fractionating a broadly disperse sample

of **DPPTT-T** they obtained samples with narrower Đ and lower, similar, and higher average molecular weights. All of the narrowly disperse samples had improved device performance compared to the more-disperse unfractionated material. This improved performance was due to increased fill factor ascribed to removal of very low molecular weight impurities in all of the fractionated samples, leading to improved intermixing with PCBM. While this study suggests that high dispersities may harm BHJ efficiency, only a small range in Đ can be studied by this method.

Synthetic limitations in the methods used in existing studies on the role of dispersity in device performance may explain their contradictions regarding the magnitude and sign of increased dispersity's effect. The confounding correlations between dispersity and regioregularity or molecular weight, which arise from the step-growth syntheses employed, can be eliminated by use of living, chain-growth syntheses.

Results and Discussion

Preparation of P3HT with systematically varied Đ

Table 4.1 GPC data for P3HT prepared for blending
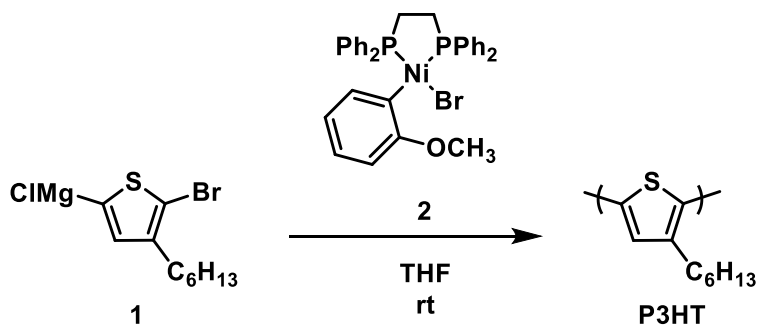
	mol% **2**	M_n (kDa)	M_w (kDa)	Đ
P3HT-A	1.66	13.4	15.8	1.18
P3HT-B	0.831	18.5	27.0	1.46
P3HT-C	0.554	33.8	45.3	1.34
P3HT-D	0.416	41.9	64.5	1.54
P3HT-E	0.333	51.0	69.4	1.36

Ni-catalyzed CTP with a dppe ligand provides highly regioregular, narrowly disperse P3HT whose molecular weight is readily targeted via catalyst loading.[13]

The dispersity of samples with narrow Đ can be increased via blending.[14] Five samples of P3HT with narrow dispersity and varied molecular weights were prepared by treating monomer **1** with varied loadings of initiator **2**. (Table 4.1). These polymers were then blended together in ratios calculated to keep either M_n or M_w constant while varying dispersity (Figure 4.1 and Table 4.2, see Appendix 3 for details).
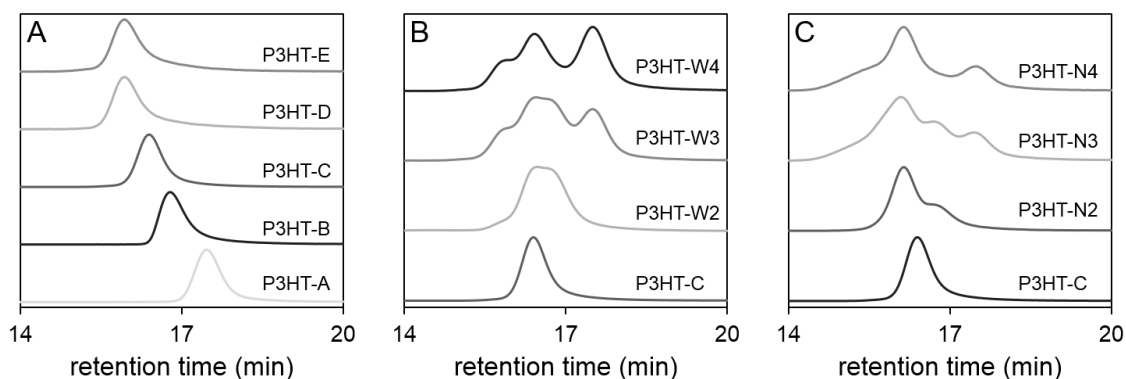
Figure 4.1 GPC traces of narrowly disperse P3HT for blending (A) and blended P3HT samples with constant M_w (B) and M_n (C).

Table 4.2 GPC data for blended P3HT samples

	M_n (kDa)	M_w (kDa)	Đ
P3HT-N2	36.6	50.9	1.39
P3HT-N3	36.0	60.1	1.67
P3HT-N4	33.2	61.8	1.86
P3HT-W2	29.9	46.0	1.54
P3HT-W3	24.3	39.9	1.64
P3HT-W4	20.9	37.8	1.81

While blending allows easy access to arbitrary molecular weights, the resulting distribution shapes are multimodal (Figure 4.1B and C), unlike broad dispersity caused by frequent chain-transfer or step-growth polymerization. There are alternative ways to systematically vary dispersity while retaining the advantages CTP provides with regard to regioregularity and molecular weight targeting. Initiation rates in these polymerizations can vary widely based on the reactive ligand with which the catalyst is functionalized, while propagation rates

are largely unaffected by this 'endcap'. Efforts to date have focused on increasing initiation rates relative to propagation rates to minimize dispersity.[15] These studies have identified arene-functionalized initiators with a wide range of initiation rates; judicious selection from this series would furnish a sequence of otherwise identical polymers with divergent dispersity and end-group. However, it would be experimentally simpler to use a single fast-initiating catalyst. Gradual addition of initiator to the polymerization artificially slows initiation such that the dispersity of the polymer is inversely proportional to the initiator addition rate.[16] In addition to its experimental simplicity, this approach permits targeting of arbitrary shapes in the molecular weight distribution (symmetrical, head- or tail-weighted, etc.) by use of a programmable syringe pump. Gradual addition of initiator has been applied in the nitroxide-mediated polymerization of styrene with successful targeting of molecular weights, dispersities, and peak shapes,[16] but has not previously been utilized in CTP. We generated P3HT with similar M_n and varied Đ via gradual addition of initiator **2** to a solution of monomer **1** (Table 4.3 and Figure 4.2, details in Appendix 3).

Table 4.3 P3HT with varied dispersity via gradual addition of **2**

	addition rate of **2** (µmol/min)	M_n (kDa)	M_w (kDa)	Đ
P3HT-G1	0.406	39.1	46.8	1.20
P3HT-G2	0.203	42.1	57.9	1.38
P3HT-G3	0.135	35.7	76.8	2.15
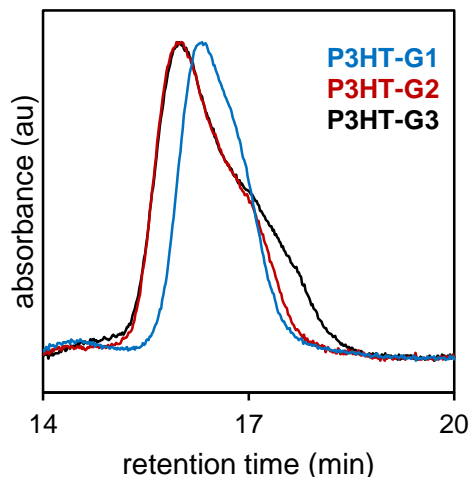
Figure 4.2 GPC traces of P3HT with varied dispersity prepared via gradual addition of **2**.

Analysis of polymer films

Thin films of each polymer sample were prepared by spin-coating from 1,2-dichlorobenzene onto glass slides, followed by annealing for 10 min at 150 °C in a vacuum oven (details in Appendix 3).[17] Regioregular P3HT has three characteristic absorbances: a broad π-π* excitation and two distinct vibronic transitions.[18] The low-energy absorbance at λ_{max} = 610 nm corresponds to the 0-0 absorbance and is made more pronounced by the formation of H-aggregates. The higher-energy absorbance at λ_{max} = 560 nm corresponds to the 0-1 absorption and arises from disordered chains. The ratio of these vibronic peaks provides a simple measurement of the degree of crystallinity of a P3HT film.[19] In both series of blended polymer samples, crystallinity appears to be maximized at an intermediate dispersity, while both broadly and narrowly disperse samples are less crystalline (Figure 4.3). A red-shift in the π-π* intrachain absorbance at λ_{max} = ca. 535 nm has also been attributed to increased crystallinity;[20] this metric is in agreement with the 0-0/0-1 absorption ratio (see Appendix 3 for absorbance maxima and magnitudes), indicating maximized crystallinity at intermediate dispersity. In samples prepared via gradual addition of monomer the trend is the same, although less pronounced than in the blended samples.
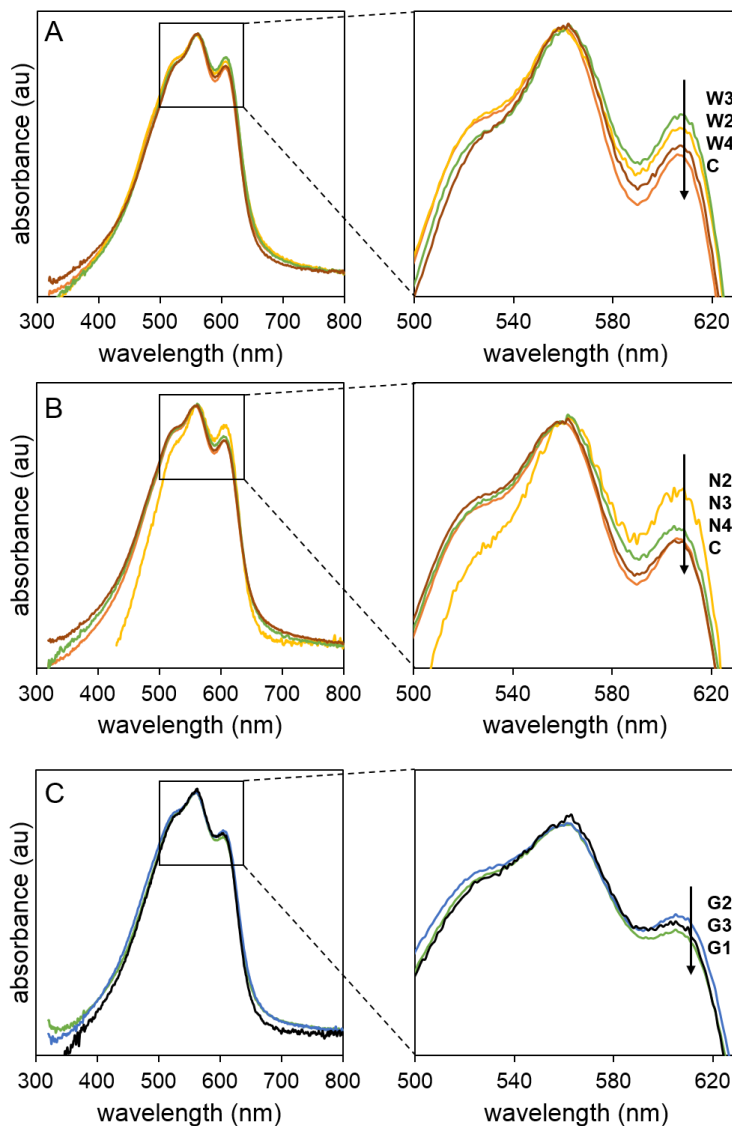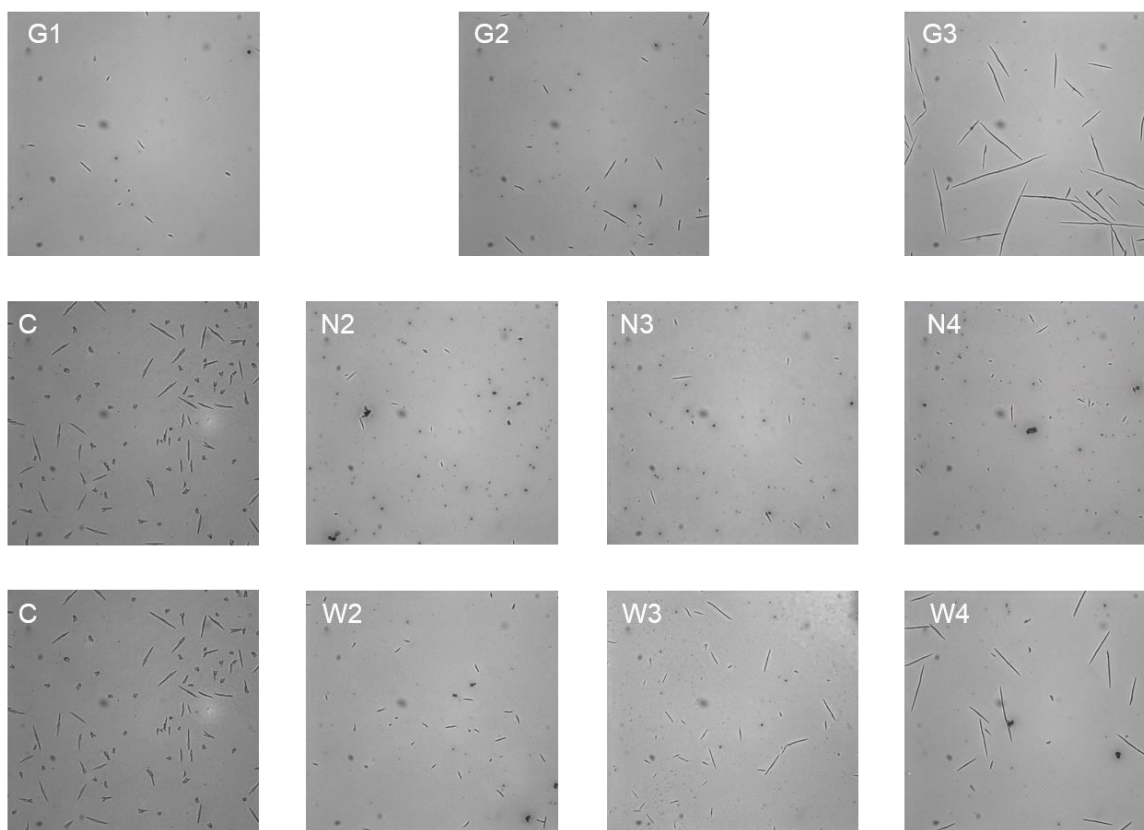
Figure 4.3 UV-vis spectra of polymer films spin-coated on glass slides and annealed at 150 °C for 30 min. (A) orange: **P3HT-C**; yellow: **P3HT-W2**; green: **P3HT-W3**; maroon: **P3HT-W4**. (B) orange: **P3HT-C**; yellow: **P3HT-N2**; green: **P3HT-N3**; maroon: **P3HT-N4**; (C) green: **P3HT-G1**; blue: **P3HT-G2**; black: **P3HT-G3**.

Analysis of polymer-fullerene blend films

To understand how the enhanced polymer crystallinity might impact the morphology of BHJ active layers, thin films of PCBM/P3HT (1:1 weight ratio) were prepared as above. PCBM has an absorbance at 335 nm, which is suppressed by aggregation due to reduced cross-sectional area.[21] The dispersity of the polymer with which the fullerene is blended appears to have a dramatic impact on PCBM

aggregation. As in the crystallinity of the polymer-only films, this influence is not linear with dispersity but is maximized at intermediate values in both constant-M_n and constant-M_w series (Figure 4.4). The PCBM absorbance is most suppressed in blends with narrowly-disperse P3HT, indicating the formation of large aggregates. With increasing Đ, PCBM aggregation is initially reduced at moderate dispersities then increases with continued broadening. The nonlinearity of the trend in both blended series is largely driven by significant aggregation in a single sample, **P3HT-C**. The trend is different in the samples prepared via slowed initiation: PCBM aggregation increases monotonically with Đ. In the P3HT absorbance region, the trends are reversed from the polymer-only films. Narrowly-disperse polymer is the most crystalline, with intermediate dispersity giving the least crystalline P3HT regions. This result is consistent with the formation of PCBM aggregates, as crystalline P3HT more effectively excludes fullerene.
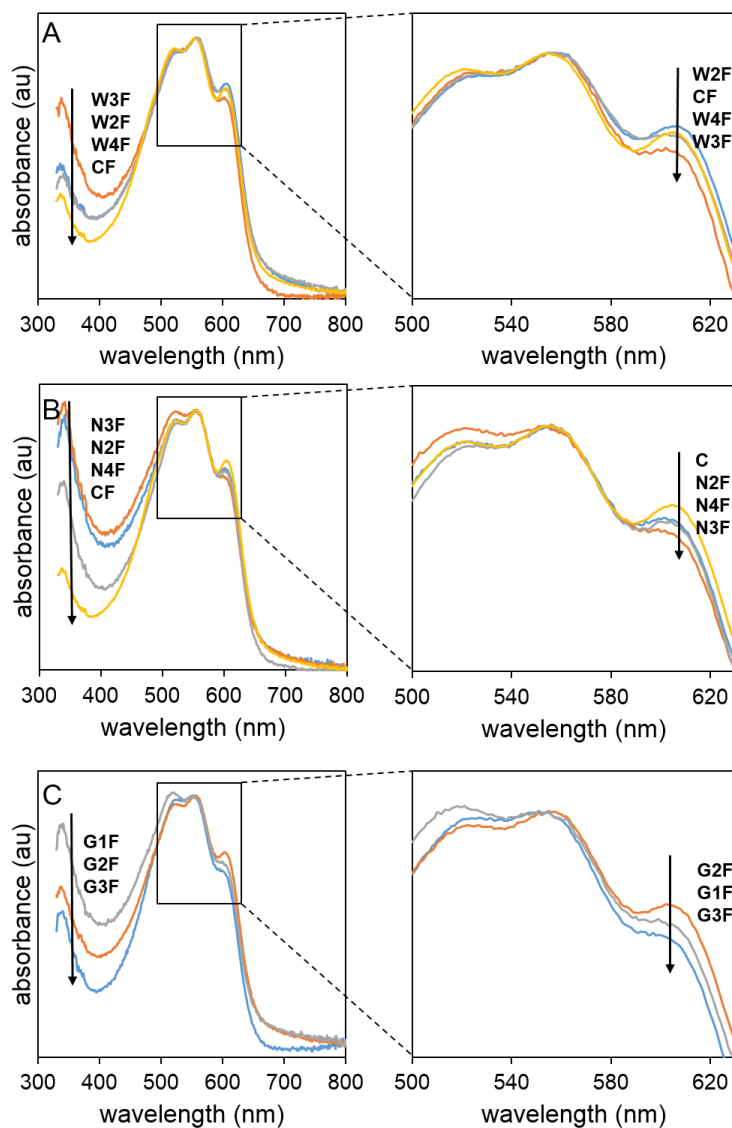
Figure 4.4 UV-vis spectra of polymer-fullerene blend films spin-coated on glass slides and annealed at 150 °C for 30 min. (A) yellow: **P3HT-CF**; blue: **P3HT-W2F**; orange: **P3HT-W3F**; gray: **P3HT-W4F**. (B) yellow: **P3HT-CF**; blue: **P3HT-N2F**; orange: **P3HT-N3F**; gray: **P3HT-N4F**. (C) gray: **P3HT-G1F**; orange: **P3HT-G2F**; blue: **P3HT-G3F**.

Microscale PCBM aggregates can be seen as needlelike crystals using optical microscopy (Figure 4.5). The trends in aggregate size broadly agree with the UV-vis results. In the blended samples, **P3HT-CF** gives moderate aggregate formation; increasing Đ initially suppresses aggregation, while continued broadening gives large aggregates. In the series prepared via gradual initiator addition, aggregate size increases with Đ. The differences in aggregate size are

much larger in the constant M_w blended series and gradual initiation series than in the constant M_n blended series. In these samples, increased Đ is largely driven by the inclusion of more low molecular weight P3HT, while the constant M_n blends are weighted towards high molecular weight components. This comports with our finding from UV-vis that PCBM aggregation is correlated with P3HT crystallinity, as lower molecular weight P3HT is more crystalline.[22]

Figure 4.5 Optical micrographs of polymer-fullerene blend films spin-coated on glass slides and annealed at 150 °C for 30 min.

To further support the morphological trends observed using optical microscopy and UV-vis spectroscopy, we subjected the thin films to X-ray diffraction. Initial attempts were inconclusive as to relative crystallinity and domain size. Due to low signal, only a peak corresponding to P3HT's lamellar spacing was observed, and not the expected peaks for P3HT π-π stacking or PCBM. We attribute the weak signal to the limited sample volume provided by a film thickness

expected to be on the order of 100 nm. Polymer-only and fullerene-containing films both give a peak at $2\theta = 5.3°$, corresponding to a lamellar spacing of 16.7 Å. This matches previously reported values well.[23] The scattering is highly anisotropic, indicating a preferred orientation within the film (See Appendix 3).

Conclusions

We demonstrated two methods of modifying dispersity in polymer samples with constant M_n or M_w using catalyst-transfer polymerization. Varying dispersity has significant impact on the thin-film morphology of both P3HT and P3HT/PCBM blends. In tests with P3HT/PCBM blends, increasing dispersity beyond moderate values (Đ = 1.6) led to significantly increased PCBM aggregation. This result suggests that narrow- to moderately-disperse P3HT is best-suited for optimizing BHJ morphology and lifetime. The impact of dispersity differs in magnitude between the blended and slowly initiated samples, suggesting that the shape of the molecular weight distribution also plays a role. The larger PCBM aggregates in the gradual addition and constant M_w blended series suggest that the differences in aggregation are largely driven by the amount of low molecular weight P3HT. This result is readily rationalized by the higher crystallinity of lower molecular weight P3HT.

These results are preliminary, and additional characterization will help to support the validity of the trends identified here. Specifically, thermogravimetric analysis to determine solvent inclusion and differential scanning calorimetry to characterize variations in T_g and crystallinity are underway. Additionally, P3HT film thickness has recently been shown to influence UV-vis absorption spectra,[24] and this factor should be measured via ellipsometry and controlled. Additionally, we are working to fabricate BHJs and measure PCE and current-voltage characteristics to compare the morphological results to solar cell performance. In future work, additional techniques such as photoluminescence spectroscopy and SEM should be applied to further identify the degree of intermixing in PCBM/P3HT blends.

References

(1) For reviews, see (a) Collins, B. A.; Tumbleston, J. R.; Ade, H. *J. Phys. Chem. Lett.*, **2011**, *2*, 3135–3145. (b) Hoppe, H.; Sariciftci, N. S. *J. Mater. Chem.* **2006**, *16*, 45–61.

(2) (a) Chang, J.; Sun, B.; Breiby, D. W.; Nielsen, M. M.; Solling, T. I.; Giles, M.; McCulloch, I.; Sirringhaus, H. *Chem. Mater.* **2004**, *16*, 4772–4776. (b) Yang, H.; Shin, T. J.; Yang, L.; Cho, K.; Ryu, C. Y.; Bao, Z. *Adv. Funct. Mater.* **2005**, *15*, 671–676.

(3) Bao, Z.; Dodabalapur, A.; Lovinger, A. *J. Appl. Phys. Lett.* **1996**, *69*, 4108−4110.

(4) (a) Koch, F. P. V.; Rivnay, J.; Foster, S.; Müller, C.; Downing, J. M.; Buchaca-Domingo, E.; Westacott, P.; Yu, L.; Yuan, M.; Baklar, M.; Fei, Z.; Luscombe, C.; McLachlan, M. A.; Heeney, M.; Rumbles, G.; Silva, C.; Salleo, A.; Nelson, J.; Smith, P.; Stingelin, N. *Prog. Polym. Sci.* **2013**, *38*, 1978–1989. (b) Zen, A.; Saphiannikova, M.; Neher, D.; Grenzer, J.; Grigorian, S.; Pietsch, U.; Asawapirom, U.; Janietz, S.; Scherf, U.; Lieberwirth, I.; Wegner, G. *Macromolecules* **2006**, *39*, 2162–2171. (c) Zhang, R.; Li, B.; Iovu, M. C.; Jeffries-El, M.; Sauvé, G.; Cooper, J.; Jia, S.; Tristram-Nagle, S.; Smilgies, D. M.; Lambeth, D. N.; McCullough, R. D.; Kowalewski, T. *J. Am. Chem. Soc.* **2006**, *128*, 3480–3481.

(5) (a) Liu, F.; Chen, D.; Wang, C.; Luo, K.; Gu, W.; Briseno, A. L.; Hsu, J. W. P.; Russell, T. P. *ACS Appl. Mater. Interfaces* **2014**, *6*, 19876–19887. (b) Hiorns, R. C.; de Bettignies, R.; Leroy, J.; Bailly, S.; Firon, M.; Sentein, C.; Khoukh, A.; Preud'homme, H.; Dagron-Lartigau, C. *Adv. Funct. Mater.* **2006**, *16*, 2263–2273.

(6) Menon, A.; Dong, H.; Niazimbetova, Z. I.; Rothberg, L. J.; Galvin, M. E. *Chem. Mater.* **2002**, *14*, 3668−3675.

(7) Himmelberger, S.; Vandewal, K.; Fei, Z.; Heeney, M.; Salleo, A. *Macromolecules* **2014**, *47*, 7151−7157.

(8) Chu, P.-H.; Zhang, L.; Colella, N. S.; Fu, B.; Park, J. O.; Srinivasarao, M.; Briseno, A. L.; Reichmanis, E. *ACS Appl. Mater. Interfaces* **2015**, *7*, 6652−6660.

(9) Martinez-Ferrero, E.; Grigorian, S.; Ryan, J. W.; Cambarau, W.; Palomares, E. *ACS Appl. Mater. Interfaces* **2015**, *7*, 1078−1086.

(10) Li, W.; Yang, L.; Tumbleston, J. R.; Yan, L.; Ade, H.; You, W. *Adv. Mater.* **2014**, *26*, 4456–4462.

(11) Lu, L.; Zheng, T.; Xu, T.; Zhao, D.; Yu, L. *Chem. Mater.* **2015**, *27*, 537–543.

(12) Meager, I.; Ashraf, R. S.; Nielsen, C. B.; Donaghey, J. E.; Huang, Z.; Bronstein, H.; Durrant, J. R.; McCulloch, I. *J. Mater. Chem. C* **2014**, *2*, 8593–8598.

(13) (a) Lanni, E.L.; McNeil, A. J. *J. Am. Chem. Soc.* **2009**, *131*, 16573–16579. (b) Adachi, I.; Miyakoshi, R.; Yokoyama, A.; Yokozawa, T. *Macromolecules* **2006**, *39*, 7793–7795. (c) Sheina, E. E.; Khersonsky, S. M.; Jones, E. G.; McCullough, R. D. *Chem. Mater.* **2005**, *17*, 3317–3319.

(14) For examples of blending to target composition distribution in nonconjugated polymers, see (a) Noro, A.; Iinuma, M.; Suzuki, J.; Takano, A.; Matsushita, Y. *Macromolecules* **2004**, *37*, 3804–3808. (b) Nguyen, D.; Zhong, X.-F.; Williams, C. E.; Eisenberg, A. *Macromolecules* **1994**, *27*, 5173–5181. (c) Hadziioannou, G.; Skoulios, A. *Macromolecules* **1982**, *15*, 267–271.

(15) Lee, S. R.; Bloom, J. W. G.; Wheeler, S. E.; McNeil, A. J. *Dalton Trans.* **2013**, *42*, 4218–4222.

(16) Gentekos, D. T.; Dupuis, L. N.; Fors, B. P. *J. Am. Chem. Soc.* **2016**, *138*, 1848–1851.

(17) These film preparation conditions are adapted from those that maximized PCE in a previous study in our lab; see Palermo, E. F.; Darling, S. B.; McNeil, A. J. *J. Mater. Chem. C* **2014**, *2*, 3401–3406.

(18) (a) Clark, J.; Chang, J. F.; Spano, F. C.; Friend, R. H.; Silva, C. *Appl. Phys. Lett.*, **2009**, *94*, 163306; (b) Clark, J.; Silva, C.; Friend, R. H.; Spano, F. C. *Phys. Rev. Lett.*, **2007**, *98*, 206406.

(19) Spano, F. C.; *J. Chem. Phys.* **2005**, *122*, 234701.

(20) (a) Li, G.; Shrotriya, V.; Huang, J.; Yao, Y.; Moriarty, T.; Emery, K.; Yang, Y. *Nature Mater.* **2005**, *4*, 864–868. (b) Shrotriya, V.; J. Ouyang, J.; Tseng, R. J.; Li, G. Yang, Y. *Chem. Phys. Lett.* **2005**, *411*, 138–143.

(21) (a) Turkovic, V.; Engmann, S.; Gobsch, G.; Hoppe, H. *Synth. Met.* **2012**, *161*, 2534–2539. (b) Zhang, Y.; Yip, H.-L.; Acton, O.; Hau, S. K.; Huang, F.; Jen, A. K.-Y. *Chem. Mater.*, **2009**, *21*, 2598–2600.

(22) Brinkmann, M.; Rannou, P. *Macromolecules* **2009**, *42*, 1125–1130.

(23) (a) Palermo, E. F.; van der Laan, H. L.; Mcneil, A. J. *Polym. Chem.* **2013**, *4*, 4606–4611. (b) Tashiro, K.; Kobayashi, M. Kawai, T. Yoshino, K. *Polymer* **1997**, *38*, 2867–2879.

(24) Ehrenreich, P.; Birkhold, S. T.; Zimmermann, E.; Hu, H.; Kim, K.-D.; Weickert, J.; Pfadler, T.; Schmidt-Mende, L. *Sci. Rep.* **2016**, *6*, 32434.

Chapter 5

Conclusions and Future Directions

Since the discovery of semiconducting polymers, significant research efforts have been focused on understanding how their chemical structure impacts their performance in organic electronic devices. These studies have established the importance of molecular weight[1] and orbital energies.[2] Catalyst transfer polymerization, a chain-growth method for the synthesis of conjugated polymers, enables the manipulation of molecular weight, dispersity, and copolymer sequence. While CTP has seen significant development since its discovery in 2004,[3] it has yet to achieve widespread use to prepare polymers for organic electronic devices. Limited monomer scope is the major challenge preventing increased use of CTP; the electron-deficient monomers used to achieve narrow bandgaps in high-performing polymers cannot be accessed by chain-growth methods. We believe that the increased control over molecular weight distribution and comonomer sequence that CTP provides will prove valuable tools to optimize organic electronic devices. Better mechanistic understanding of challenging monomers will lead to expanded monomer scope and the chain-growth production of high-efficiency polymers.

In the second chapter we discussed a new class of cataysts for the CTP of phenylene and thiophene.[4] Goldup demonstrated preferential multi-functionalization in small molecule reactions using the palladium-N-heterocyclic carbene precatalyst PEPPSI-IPr.[5] Because preferential intramolecular oxidative addition is key to CTP, we investigated this catalyst in polymerizations. Gratifyingly, we found that PEPPSI-IPr mediated CTP homopolymerizations of thiophene and phenylene under Kumada conditions, similar to current nickel catalysts. Additionally, we found that PEPPSI-IPr formed block copolymers with

both orders of monomer addition. Thiophene to phenylene chain-extension is a significant improvement over current nickel catalysts, which can only form block copolymers if thiophene is added following an initial phenylene block. A catalyst that can cross-propagate in both directions allows access to more interesting sequences, such as multi-block copolymers. PEPPSI-IPr was also used to polymerize fluorene, albeit in an uncontrolled chain-growth fashion with poor end-group control.

Since our demonstration of CTP promoted by a Pd-NHC catalyst, several notable studies have explored the potential for expanded monomer scope, with a focus on the use of milder monomer conditions. Using the same Pd-NHC catalyst, PEPPSI-IPr, Noonan reported polymerizing thiophene under Stille conditions[6] and Luscombe reported polymerizing an organogold thiophene monomer.[7] Catalyst modifications have also been productive. A computational study of PEPPSI-IPr found that the 3-chloropyridine "throw-away ligand" plays a key role in the catalytic cycle.[8] Wang reported polymerizing thiophene and fluorene under Suzuki conditions with a Pd-NHC precatalyst that replaces 3-chloropyridine with acetylacetonate (acac).[9] Using $Ni(IPr)(acac)_2$, a nickel analogue of this catalyst, they also report the Suzuki CTP of thiophene with record molecular weight (416 kDa) and moderate Đ (1.72).[10] Mori used a similar Ni-NHC catalyst, with triphenylphosphine as the throw-away ligand, in the polymerization of phenylene and thiophene organolithium derivatives,[11] as well as in the polymerization of oligothiophene Grignards.[12]

Future work in the area of Pd-NHC CTP should focus on expanding monomer scope. Modifications to the NHC ligand should be explored in conjunction with new monomers. Small-molecule studies have demonstrated that electronic and steric contributions dramatically impact substrate scope.[13] More sterically-demanding NHCs in particular appear attractive for further investigation.[14] Electron-deficient monomers remain challenging; while we observed poor end-group control when synthesizing polyfluorene, this is likely due to challenges with monomer activation rather than with the catalyst. Other monomers and monomer activation methods should be screened. Emphasis on

Kumada-type monomers may limit adoption of CTP methods. PEPPSI precatalysts are air- and moisture-stable and should be investigated with Suzuki- and Negishi-type monomers that tolerate a broader range of functional groups and reaction conditions. This work will benefit from elucidating the reaction mechanism. The detailed mechanistic work that has been performed on nickel phosphine catalysts[15] has led to optimization of the steric and electronic properties of their ancillary ligands, but this body of literature is underdeveloped for Pd-NHCs. Identifying the catalyst resting state could help explain the observed stability issues at low monomer concentrations. Understanding the role of the throw-away ligand would enable selection of either a more stabilizing or less 'trapping' ligand. Finally, development of Pd-NHC catalysts with reactive ligands is essential for the full exploitation of this class of catalysts. By transferring the reactive ligand to the polymer chain, these initiators incorporate an 'end-cap' and enforce unidirectional growth, preventing sequence scrambling via end-to-end chain-walking. Preliminary work in our lab has achieved only moderate incorporation of reactive ligands as polymer end-groups. Quantitative ligand transfer from a Pd-NHC initiator will allow the synthesis of complex copolymer sequences such as gradients with electronically differentiated monomers.
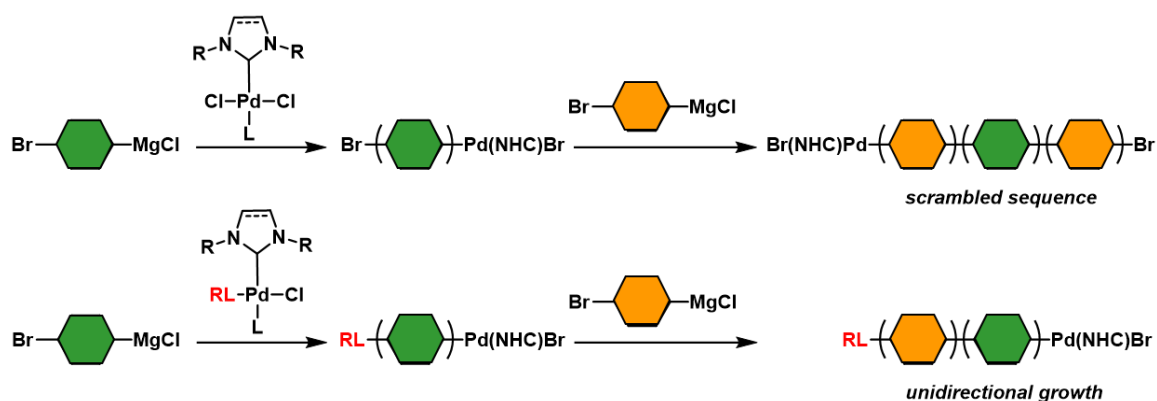
Scheme 5.1 Reactive ligand prevents copolymer sequence scrambling

In Chapter 3 we discussed investigations into polymerizing thiazole derivatives.[16] Though electron-deficient monomers are important targets for CTP, they remain challenging. Thiazole was chosen due to its similarity to thiophene;

however, it behaved quite differently in polymerizations. During the course of our study, Pammer and coworkers published two papers reporting the nonliving chain-growth polymerization of thiazole derivatives.[17] Using reaction-discovery calculations, we identified a facile pathway for chain-transfer to monomer. This pathway is operative due to the high barrier for transfer of the catalyst to the chain end arising from preferential association to the C=C following reductive elimination. By modifying the ancillary ligand to increase its rigidity, we were able to inhibit ancillary ligand dissociation, the key step in the chain-transfer pathway, and promote chain-growth propagation. We additionally identified a spontaneous polymerization during Grignard formation from dibromothiazole, accompanied by the detection of organic radicals.

This work provides experimental support to the hypothesis that stabilizing the catalyst-polymer π-complex can inhibit catalyst transfer to the chain end, and thereby hinder intramolecular oxidative addition rather than promote it.[18] This result reaffirms that optimizing ancillary ligands is a "Goldilocks problem" for each monomer or comonomer pair. While more electron-donating ligands promote more-ideal chain-growth in electron-rich monomers,[15b] this trend must be reexamined in electron-deficient monomers to avoid overstabilization of the π-complex.

Future work in this area should focus on extension to monomers which are used in high-efficiency optoelectronic devices. We demonstrate that identifying and understanding side reactions can assist catalyst optimization to promote chain propagation. Monomers such as thienothiophene present valuable targets for CTP homo- and copolymerization. Additionally, the chain-growth synthesis of alternating donor-acceptor 'copolymers' via monomers that incorporate electron-rich and electron-poor moieties should be further developed. Bielawski has reported the synthesis of poly(thiophene-*alt*-*p*-phenylene) using this strategy.[19] Application of our strategies to this class of monomer may lead to improved dispersity and end-group control in commonly utilized monomers. The radical-mediated polymerization that we observed also warrants further investigation. While polymerizations of stable radical monomers have been reported,[20] they still

proceed via Ni-mediated coupling. If initiation can be controlled via use of an electron donor[21] and termination can be prevented, the $S_{RN}1$ mechanism we propose could furnish high molecular weight material. This method may be particularly suited to electron-deficient monomers due to their lower reduction potentials.

Chart 5.1 Monomer targets for future CTP development

M = MgCl, ZnOPiv, Bpin, SnBu$_3$
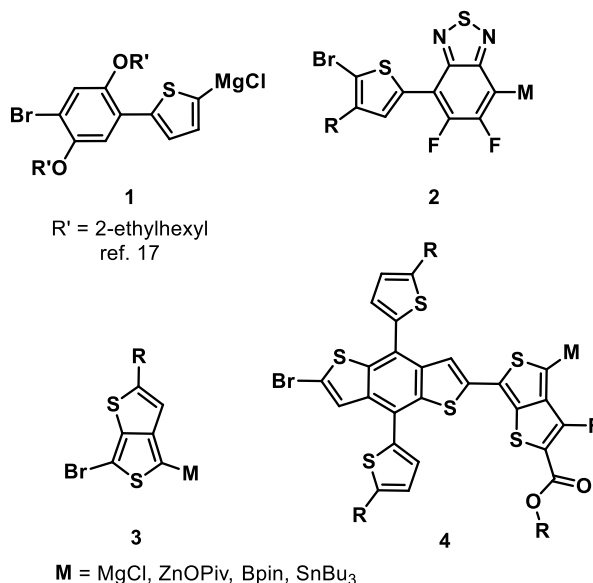
Finally, in Chapter 4 we discussed the effect of molecular weight dispersity on polymer and polymer-fullerene thin-films. The impact of dispersity had previously been studied in LEDs,[22] transistors,[23] and bulk heterojunction solar cells;[24] however, the conclusions of these studies are not in agreement. We believe that the step-growth methods used to generate polymers for these studies led to correlations between dispersity and confounding factors such as regioregularity and molecular weight. We utilized two different methods to generate series of polymer samples with varied Đ at constant M_n or M_w, eliminating these confounders. We observed that dispersity affected the degree of crystallinity of polymer films, as well as PCBM aggregation in films of polymer-fullerene blends. We tentatively conclude that increased dispersity leads to increased PCBM aggregation due to the presence of low molecular weight P3HT,

which is more crystalline. We hypothesize that the improved intermixing we observe with narrowly disperse P3HT will lead to increased device fill factor, efficiency, and lifetime in studies of bulk heterojunction solar cells currently underway.

While the use of sequence-controlled polymers to stabilize BHJ performance has demonstrated the utility of CTP for synthesizing solar cell active layer additives,[25] implications for the bulk donor have not been adequately explored. Our results suggest that the molecular weight distribution plays a key role in active layer morphology. Future work should examine the impact of donor dispersity on BHJ fill factor and short-circuit current, relating these properties to the morphological trends we identified. In BHJ processing studies, polymers synthesized via CTP should be employed whenever possible to better control the molecular weight distribution.

Since its discovery in 2004, CTP has been used to synthesize a variety of polymers,[26] including sequences like blocks[27] and gradients[28] that are otherwise difficult to access. However, it has seen limited adoption in the broader field of organic electronic devices, largely because its scope does not include the polymers used in the most efficient optoelectronic devices.[29] The work highlighted in this thesis develops CTP towards increased utility for device fabrication. A Pd-NHC catalyst was found to outperform current nickel catalysts in the copolymerization of thiophene and phenylene, expanding the possible sequences for electronically differentiated comonomers. In the polymerization of an electron-deficient monomer, a chain-transfer pathway was identified and ancillary ligand modification led to improved chain-growth. Improved understanding of the role of the polymer-catalyst π-complex in chain-walking was key to both these expansions of scope. Additionally, two methods to control Đ in CTP were demonstrated, and Đ was observed to affect the thin-film morphology of polymer-fullerene blends. Further development of this work may demonstrate the importance of molecular weight distribution in optimizing BHJ performance. With continued expansion of scope, CTP could become the preferred synthetic

route for π-conjugated polymers being used in LEDs, field-effect transistors, and photovoltaic solar cells.

References

(1) Liu, F.; Chen, D.; Wang, C.; Luo, K.; Gu, W.; Briseno, A. L.; Hsu, J. W. P.; Russell, T. P. *ACS Appl. Mater. Interfaces* **2014**, *6*, 19876–19887.

(2) Scharber, M. C.; Muhlbacher, D.; Koppe, M.; Denk, P.; Waldauf, C.; Heeger, A. J.; Brabec, C. J. *Adv. Mater.* **2006**, *18*, 789–794.

(3) For related reviews, see: (a) Leone, A. K.; McNeil, A. J. *Acc. Chem. Res.* **2016**, *49*, 2822–2831. (b) Higashihara, T.; Ueda, M. *Macromol. Res.* **2013**, *21*, 257-271. (c) Bryan, Z. J.; McNeil, A. J. *Macromolecules* **2013**, *46*, 8395–8405. (d) Yokozawa, T.; Nanashima, Y.; Ohta, Y. *ACS Macro. Lett.* **2012**, *1*, 862–866. (e) Marrocchi, A.; Lanari, D.; Facchetti, A.; Vaccaro, L. *Energy Environ. Sci.* **2012**, *5*, 8457–8474. (f) Stefan, M. C.; Bhatt, M. P.; Sista, P.; Magurudeniya, H. D. *Polym. Chem.* **2012**, *3*, 1693–1701. (g) Kiriy, A.; Senkovskyy, V.; Sommer, M. *Macro. Rapid Commun.* **2011**, *32*, 1503–1517. (h) Okamoto, K.; Luscombe, C. K. *Polym. Chem.* **2011**, *2*, 2424–2434. (i) Yokozawa, T.; Yokoyama, A. *Chem. Rev.* **2009**, *109*, 5595–5619. (j) Osaka, I.; McCullough, R. D. *Acc. Chem. Res.* **2008**, *41*, 1202–1214. (k) Miyakoshi, R.; Yokoyama, A.; Yokozawa, T. *J. Polym. Sci. Pol. Chem.* **2008**, *46*, 753–765. (l) Yokoyama, A.; Yokozawa, T. *Macromolecules* **2007**, *40*, 4093–4101.

(4) Bryan, Z. J.; Smith, M. L.; McNeil, A. J. *Macromol. Rapid Comm.* **2012**, *33*, 842–847.

(5) Larrosa, I.; Somoza, C.; Banquy, A.; Goldup, S. M. *Org. Lett.* **2011**, *13*, 146–149.

(6) Qiu, Y.; Mohin, J.; Tsai, C.-H.; Tristram-Nagle, S.; Gil, R. R.; Kowalewski, T.; Noonan, K. J. T. *Macromol. Rapid Comm.* **2015**, *36*, 840–844.

(7) Suraru, S.-L.; Lee, J. A.; Luscombe, C. K. *ACS Macro Lett.* **2016**, *5*, 533–536.

(8) Zhao, Y.; Nett, A. J.; McNeil, A. J.; Zimmerman, P. M. Macromolecules, **2016**, *49*, 7632–7641.

(9) Sui, A.; Shi, X.; Tian, H.; Geng, Y.; Wang, F. *Polym. Chem.* **2014**, *5*, 7072-7080.

(10) Shi, X.; Wang, Y.; Li, Y.; Geng, Y.; Wang, F. *Chem. Comm.* **2015**, *51*, 2138-2140.

(11) Fuji, K.; Tamba, S.; Shono, K.; Sugie, A.; Mori, A. Murahashi *J. Am. Chem. Soc.* **2013**, *135*, 12208−12211.

(12) Murakami, K.; Tanaka, S.; Mori, A. *Polym. Chem.* **2015**, *6*, 6573− 6578.

(13) (a) Tamba, S.; Shono, K.; Sugie, A.; Mori, A. *J. Am. Chem. Soc.* **2011**, *133*, 9700–9703. (b) Roy, A. H.; Hartwig, J. F. *J. Am. Chem. Soc.* **2003**, *125*, 13944–13945. (c) Roy, A. H.; Hartwig, J. F. *Organometallics* **2004**, *23*, 1533–1541.

(14) Nasielski, J.; Hadei, N.; Achonduh, G.; Kantchev, E. A. B.; O'Brien, C. J.; Lough, A.; Organ, M. G. *Chem. Eur. J.* **2010**, *16*, 10844–10853.

(15) (a) Lee, S. R.; Bloom, J. W. G.; Wheeler, S. E.; McNeil, A. J. *Dalton Trans.* **2013**, *42*, 4218–4222. (b) Lee, S. R.; Bryan, Z. J.; Wagner, A. M.; McNeil, A. J. *Chem. Sci.* **2012**, *3*, 1562–1566. (c) Lanni, E. L.; McNeil, A. J. *Macromolecules* **2010**, *43*, 8039–8044. (d) Lanni, E. L.; McNeil, A. J. *J. Am. Chem. Soc.* **2009**, *131*, 16573–16579. (e) Iovu, M. C.; Sheina, E. E.; Gil, R. R.; McCullough, R. D. *Macromolecules* **2005**, *38*, 8649–8656.

(16) Smith, M. L.; Leone, A. K.; Zimmerman, P. M.; McNeil, A. J. *ACS Macro Lett.* **2016**, *5*, 1411-1415.

(17) (a) Pammer, F.; Passlack, U. *ACS Macro Lett.* **2014**, 3, 170–174. (b) Pammer, F.; Jäger, J.; Rudolf, B.; Sun, Y. *Macromolecules* **2014**, *47*, 5904–5912.

(18) (a) Komber, H.; Senkovskyy, V.; Tkachov, R.; Johnson, K.; Kiriy, A.; Huck, W. T. S.; Sommer, M. *Macromolecules* **2011**, *44*, 9164–9172. (b) Willot, P.; Koeckelberghs, G. *Macromolecules* **2014**, *47*, 8548–8555. (c) Karpov, Y.; Maiti, J.; Tkachov, R.; Beryozkina, T.; Bakulev, V.; Liu, W.; Komber, H.; Lappan, U.; Al-Hussein, M.; Stamm, M.; Voita, B.; Kiriy, A. *Polym. Chem.* **2016**, *7*, 2691–2697.

(19) Ono, R. J.; Kang, S.; Bielawski, C. W. *Macromolecules* **2012**, *45*, 2321–2326.

(20) (a) Senkovskyy, V.; Tkachov, R.; Komber, H.; Sommer, M.; Heuken, M.; Voit, B.; Huck, W. T. S.; Kataev, V.; Petr, A.; Kiriy, A. *J. Am. Chem. Soc.* **2011**, *133*, 19966–19970. (b) see also ref. 1g.

(21) (a) Zhou, S., Anderson, G. M., Mondal, B., Doni, E., Ironmonger, V., Kranz, M., Murphy, J. *Chemical Science*, **2014** *5*, 476–482. (b) Shirakawa, E., Hayashi, Y., Itoh, K., Watabe, R., Uchiyama, N., Konagaya, W., Hayashi, T. *Angew. Chemie Int. Ed.*, **2012**, *51*, 218–221. (c) Murarka, S.; Studer, A. *Angew. Chemie Int. Ed.* **2012**, *51*, 12362–12366.

(22) (a) Martinez-Ferrero, E.; Grigorian, S.; Ryan, J. W.; Cambarau, W.; Palomares, E. *ACS Appl. Mater. Interfaces* **2015**, *7*, 1078−1086. (b) Menon, A.; Dong, H.; Niazimbetova, Z. I.; Rothberg, L. J.; Galvin, M. E. *Chem. Mater.* **2002**, *14*, 3668-3675.

(23) (a) Chu, P.-H.; Zhang, L.; Colella, N. S.; Fu, B.; Park, J. O.; Srinivasarao, M.; Briseno, A. L.; Reichmanis, E. *ACS Appl. Mater. Interfaces* **2015**, *7*, 6652−6660. (b) Himmelberger, S.; Vandewal, K.; Fei, Z.; Heeney, M.; Salleo, A. *Macromolecules* **2014**, *47*, 7151−7157.

(24) (a) Li, W.; Yang, L.; Tumbleston, J. R.; Yan, L.; Ade, H.; You, W. *Adv. Mater.* **2014**, *26*, 4456–4462. (b) Holmes, N. P.; Ulum, S.; Sista, P.; Burke, K. B.; Wilson, M. G.; Stefan, M. C.; Zhou, X.; Dastoor, P. C.; Belcher, W. J. *Solar Energy Materials & Solar Cells* **2014**, *128*, 369–377. (c) Koppe, M.; Brabec, C. J. *Macromolecules* **2009**, *42*, 4661–4666.

(25) Palermo, E. F.; Darling, S. B.; McNeil, A. J. *J. Mater. Chem C.* **2014**, *2*, 3401-3406.

(26) For representative examples, see: (1) Kang, S.; Ono, R. J.; Bielawski, C. W. J. Am. Chem. Soc. 2013, 135 (13), 4984–4987. (1) Alvey, P. M.; Ono, R. J.; Bielawski, C. W.; Iverson, B. L. Macromolecules 2013, 46 (3), 718–726. (a) Wu, Z. Q.; Radcliffe, J. D.; Ono, R. J.; Chen, Z.; Li, Z. C.; Bielawski, C. W. *Polym. Chem.* **2012**, *3*, 874–881. (b) Nanashima, Y.; Yokoyama, A.; Yokozawa, T. *J. Polym. Sci. Pol. Chem.* **2012**, *50*, 1054–1061. (c) Verswyvel, M.; Koeckelberghs, G. *Polym. Chem.* **2012**, *3*, 3203–3216. (e) Hollinger, J.; Jahnke, A. A.; Coombs, N.; Seferos, D. S. *J. Am. Chem. Soc.* **2010**, *132*, 8546–8547. (f) Li, L. S.; Hollinger, J.; Jahnke, A. A.; Petrov, S.; Seferos, D. S. *Chem. Sci.* **2011**, *2*, 2306–2310. (g) Van den Bergh, K.; Cosemans, I.; Verbiest, T.; Koeckelberghs, G. *Macromolecules* **2010**, *43*, 3794–3800. (h) Wang, Q.; Takita, R.; Kikuzaki, Y.; Ozawa, F. *J. Am. Chem. Soc.* **2010**, *132*, 11420–11421. (i) Hollinger, J.; Jahnke, A. A.; Coombs, N.; Seferos, D. S. *J. Am. Chem. Soc.* **2010**, *132*, 8546–8547. (j) Grisorio, R.; Suranna, G. P.; Mastrorilli, P. *Chem. Eur. J.* **2010**, *16*, 8054–8061. (k) Doubina, N.; Stoddard, M.; Bronstein, H. A.; Jen, A. K. Y.; Luscombe, C. K. *Macromol. Chem. Phys.* **2009**, *210*, 1966–1972. (l) Duck, B. C.; Dastoor, P. C.; Rasmussen, M. C. *Macromolecules* **2008**, *41*, 4576–4578.

(27) (a) Bridges, C. R.; Yan, H.; Pollit, A. A; Seferos, D. S. *ACS Macro Lett.* **2014**, *3*, 671–674. (b) Gao, L. M.; Hu, Y. Y.; Yu, Z. P.; Liu, N.; Yin, J.; Zhu, Y. Y.; Ding, Y.; Wu, Z. Q. *Macromolecules* **2014**, *47*, 5010–5018. (c) Ono, R. J.; Todd, A. D.; Hu, Z.; Vanden Bout, D. A; Bielawski, C. W. *Macromol. Rapid Commun.* **2013**, *35*, 204–209. (d) Javier, A. E.; Varshney, S. R.; McCullough, R. D. *Macromolecules* **2010**, *43*, 3233–3237. (e) Wu, S.; Sun, Y.; Huang, L.; Wang, J.; Zhou, Y.; Geng, Y.; Wang, F. *Macromolecules* **2010**, *43*, 4438–4440. (f) Van den Bergh, K.; Huybrechts, J.; Verbiest, T.; Koeckelberghs, G. *Chem. Eur. J.* **2008**, *14*, 9122–9125. (g) Yokozawa, T.; Adachi, I.; Miyakoshi, R.; Yokoyama, A. *High Perform. Polym.* **2007**, *19*, 684–699.

(28) (a) Palermo, E. F.; McNeil, A. J. *Macromolecules* **2012**, *45*, 5948–5955. (b) Locke, J. R.; McNeil, A. J. *Macromolecules* **2010**, *43*, 8709–8710. (c) Palermo, E. F.; van der Laan, H. L.; McNeil, A. J. *Polym. Chem.* **2013**, *4*, 4606-4611. (d) see also ref. 23.

(29) (a) Liu, Y. H.; Zhao, J. B.; Li, Z. K.; Mu, C.; Ma, W.; Hu, H. W.; Jiang, K.; Lin, H. R.; Ade, H.; Yan, H. *Nat. Commun.* **2014**, *5*, 5293–5300. (b) He, Z. C.; Xiao, B.; Liu, F.; Wu, H. B.; Yang, Y. L.; Xiao, S.; Wang, C.; Russell, T. P.; Cao, Y. *Nat. Photonics* **2015**, *9*, 174–179. (c) Zhang, J.; Zhang, Y.; Fang, J.; Lu, K.; Wang, Z.; Ma, W.; Wei, Z. *J. Am. Chem. Soc.* **2015**, *137*, 8176– 8183.

Appendix 1

Supporting Information for Chapter 2
Chain-growth polymerization of aryl Grignards initiated by a stabilized NHC-Pd precatalyst

I. Materials

Flash chromatography was performed on SiliCycle silica gel (40-63 µm) and thin layer chromatography was performed on Merck TLC plates pre-coated with silica gel 60 F254. *i*-PrMgCl (2 M in THF) was purchased in 100 mL quantities from Aldrich. [1,3-Bis(2,6-Diisopropylphenyl)imidazol-2-ylidene](3-chloropyridyl)palladium(II) dichloride was purchased from Aldrich. All other reagent grade materials and solvents were purchased from Aldrich, Acros, EMD, or Fisher and used without further purification unless otherwise noted. THF was dried and deoxygenated using an Innovative Technology (IT) solvent purification system composed of activated alumina, copper catalyst, and molecular sieves. All glassware was oven dried at 120 °C for at least 1 h before use. Compounds **S1**[1] and **S2**[2] were prepared according to literature procedures.

II. General Experimental

NMR Spectroscopy: ^{1}H NMR spectra for all compounds were acquired at rt in CDCl$_3$ on a Varian vnmrs 500 operating at 500 MHz. For ^{1}H NMR spectra in deuterated solvents, the chemical shift data are reported in units of δ (ppm) relative to tetramethylsilane (TMS) and referenced with residual solvent. Multiplicities are reported as follows: singlet (s), multiplet (m), pentet (p), and broad resonance (br).

MALDI-TOF MS: MALDI-TOF mass spectra were recorded using Waters Tofspec-2E in reflectron mode at a unit mass resolution of 4000. The matrix, α-cyano-4-hydroxy-cinnamic acid (CHCA), was prepared at a concentration of 10 mg/mL in a solution of 50/50 (v/v) CH$_3$CN/EtOH. The instrument was mass calibrated with a mixture of peptides in the CHCA matrix. The polymer sample was dissolved in CH$_2$Cl$_2$ to obtain a ~1 mg/mL solution. A 3 µL aliquot of the polymer solution was mixed with 3 µL of the matrix solution. 1 µL of this mixture was placed on the target plate and then air-dried.

Gel-Permeation Chromatography: Polymer molecular weights were determined by comparison with polystyrene standards (Varian, EasiCal PS-2 MW 580-377,400) on a Waters 1515 HPLC instrument equipped with Waters Styragel®

(7.8 x 300 mm) THF HR 0.5, THF HR 1, and THF HR 4 type columns in sequence and analyzed with Waters 2487 dual absorbance detector (254 nm). Samples were dissolved in THF (with mild heating) and passed through a 0.2 μm PTFE filter prior to analysis.

Titrations of the Grignard Reagents: An accurately weighed sample of salicylaldehyde phenylhydrazone (typically between 290-310 mg) was dissolved in 5.00 mL of THF. A 0.50 mL aliquot of this solution was stirred at rt while ArMgCl was added dropwise using a 500 μL syringe. The initial solution is yellow and turns bright orange at the end-point.[3]

Gas Chromatography: Gas chromatography was carried out using a Shimadzu GC 2010 containing a Shimadzu SHRX5 (crossbound 5% diphenyl – 95% dimethyl polysiloxane; 15 m 0.25 mm ID, 0.25 μm df) column.

IR Spectroscopy: Samples were recorded using a Mettler Toledo ReactIR iC10 fitted with a Mercury Cadmium Telluride (MCT) detector, and AgX probe (9.5 mm x 1.5 mm) with a SiComp tip. The spectra were processed using icIR 4.0 software and raw absorbances were exported into Microsoft Excel or Sigma Plot 10 for analysis.

III. Synthetic Procedures
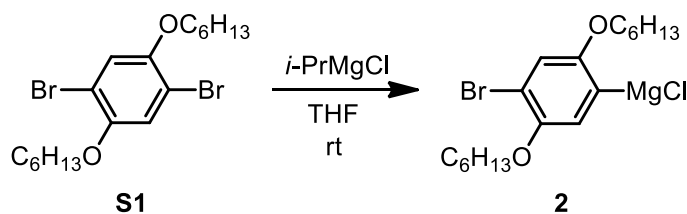
2. In the glovebox, **S1** (1.025 g, 2.350 mmol, 1.0 equiv) was dissolved in THF (2.5 mL) in a 20 mL vial equipped with a stir bar. Then, *i*-PrMgCl (1.07 mL, 2.12 mmol, 0.9 equiv) was added via syringe, the vial was capped, and the reaction was stirred overnight at rt.
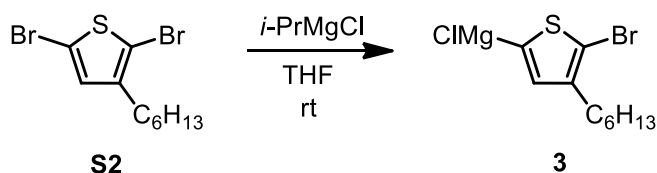
3. In the glovebox, **S2** (0.424 g, 1.30 mmol, 1.0 equiv) was dissolved in THF (3.5 mL) in a 20 mL vial equipped with a stir bar. Then, *i*-PrMgCl (0.59 mL, 1.2 mmol, 0.9 equiv) was added via syringe, the vial was capped, and the reaction was stirred for 30 min at rt.
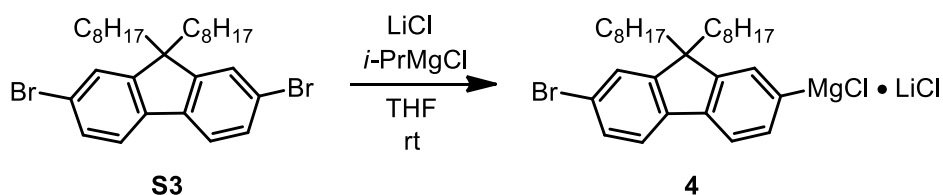
4. In the glovebox, 9,9-dioctyl-2,7-dibromofluorene (2.742 g, 5.000 mmol, 1.0 equiv) and lithium chloride (0.463 g, 5.00 mmol, 1.0 equiv) was dissolved in THF (5.0 mL) in a 20 mL vial equipped with a stir bar. Then, *i*-PrMgCl (2.25 mL, 4.50 mmol, 0.9 equiv) was added via syringe, the vial was capped, and the reaction was stirred overnight at rt.

2 → **P2**

___

P2. A 25 mL Schlenk flask was equipped with a stir bar, precatalyst **1** (10.2 mg, 0.0150 mmol, 1 equiv), and THF (7.75 mL) in a glovebox under an N_2 atmosphere. The flask was then equipped with a septum (secured with copper wire), removed from the glovebox, and put under an N_2 atmosphere. Monomer **2** (2.25 mL, 0.466 M, 1.01 mmol, 67 equiv) was then added via syringe and stirred for 90 min at rt. The reaction was quenched with aq. HCl (5 M, 10 mL), extracted with CH_2Cl_2 (3 x 10 mL), dried over $MgSO_4$, filtered, and the solvent was removed in vacuo. The resulting white solid was then washed with MeOH, and dried under vacuum (209 mg, 75% yield) M_n = 28.2 kDa, Đ = 1.19.

___

3 → **P3**

___

P3. A 25 mL Schlenk flask was equipped with a stir bar, precatalyst **1** (10.2 mg, 0.0150 mmol, 1 equiv), and THF (8.07 mL) in a glovebox under an N_2 atmosphere. The flask was then equipped with a septum (secured with copper wire), removed from the glovebox, and put under an N_2 atmosphere. Monomer **3** (1.93 mL, 0.466 M, 0.900 mmol, 60 equiv) was then added via syringe and stirred for 90 min at rt. The reaction was quenched with aq. HCl (5 M, 10 mL), extracted with $CHCl_3$ (3 x 10 mL), dried over $MgSO_4$, filtered, and the solvent was removed in vacuo. The resulting purple solid was then dissolved in a minimum amount of $CHCl_3$ and precipitated into MeOH. The precipitate was collected and dried under vacuum (130 mg, 87% yield) M_n = 18.1 kDa, Đ = 1.19.
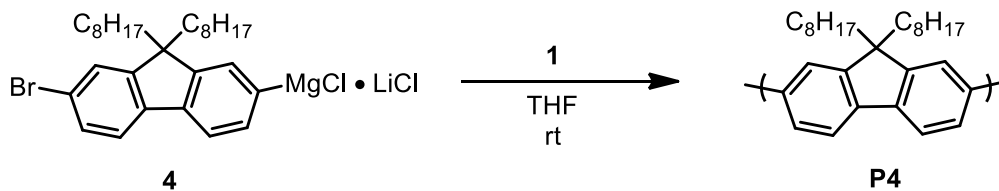
___

4 → **P4**

___

P4. A 25 mL Schlenk flask was equipped with a stir bar, precatalyst **1** (10.2 mg, 0.0150 mmol, 1 equiv), and THF (6.33 mL) in a glovebox under an N_2

73

atmosphere. The flask was then equipped with a septum (secured with copper wire), removed from the glovebox, and put under an N_2 atmosphere. Monomer **4** (3.67 mL, 0.286 M, 1.01 mmol, 67 equiv) was then added via syringe and stirred for 60 min at rt. The reaction was quenched with aq. HCl (5 M, 10 mL), extracted with $CHCl_3$ (3 x 10 mL), dried over $MgSO_4$, filtered, and the solvent was removed in vacuo. The resulting yellow solid was then washed with acetone, and dried under vacuum. (246 mg, 63% yield) M_n = 7.2 kDa, Đ = 1.73.
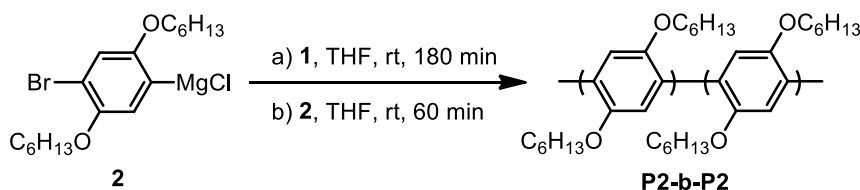
P2-b-P2. A 25 mL Schlenk flask was equipped with a stir bar, precatalyst **1** (10.2 mg, 0.0150 mmol, 1 equiv), and THF (4.6 mL) in a glovebox under an N_2 atmosphere. The flask was then equipped with a septum (secured with copper wire), removed from the glovebox, and put under an N_2 atmosphere. Monomer **2** (2.70 mL, 0.210 M, 0.567 mmol, 38 equiv) was then added via syringe and stirred for 180 min at rt. After 180 min, an aliquot was withdrawn via syringe and immediately quenched with aq. HCl (12 M, 1 mL). Monomer **2** (2.70 mL, 0.210 M, 0.567 mmol, 38 equiv) was then added via syringe and stirred for 60 min at rt. After 60 min, an aliquot was withdrawn via syringe and immediately quenched with aq. HCl (12 M, 1 mL). Each aliquot was then extracted with CH_2Cl_2 (3 x 1 mL) with mild heating, dried over $MgSO_4$, filtered, and concentrated in vacuo. The resulting solid was then dissolved in THF (~1.5 mL) with mild heating and passed through a 0.2 μm PTFE filter for GPC analysis. Block 1: M_n = 13.8 kDa, Đ = 1.13, Block 2: M_n = 21.8 kDa, Đ = 1.18.

P3-b-P3. A 25 mL Schlenk flask was equipped with a stir bar, precatalyst **1** (10.2 mg, 0.0150 mmol, 1 equiv), and THF (7.8 mL) in a glovebox under an N_2 atmosphere. The flask was then equipped with a septum (secured with copper wire), removed from the glovebox, and put under an N_2 atmosphere. Monomer **3** (1.06 mL, 0.525 M, 0.557 mmol, 37 equiv) was then added via syringe and stirred for 180 min at rt. After 180 min, an aliquot was withdrawn via syringe and immediately quenched with aq. HCl (12 M, 1 mL). Monomer **3** (1.06 mL, 0.525 M, 0.557 mmol, 37 equiv) was then added via syringe and stirred for 60 min at rt.

After 60 min, an aliquot was withdrawn via syringe and immediately quenched with aq. HCl (12 M, 1 mL). Each aliquot was then extracted with $CHCl_3$ (3 x 1 mL) with mild heating, dried over $MgSO_4$, filtered, and concentrated in vacuo. The resulting solid was then dissolved in THF (~1.5 mL) with mild heating and passed through a 0.2 µm PTFE filter for GPC analysis. Block 1: M_n = 11.2 kDa, Đ = 1.22, Block 2: M_n = 17.8 kDa, Đ = 1.35.
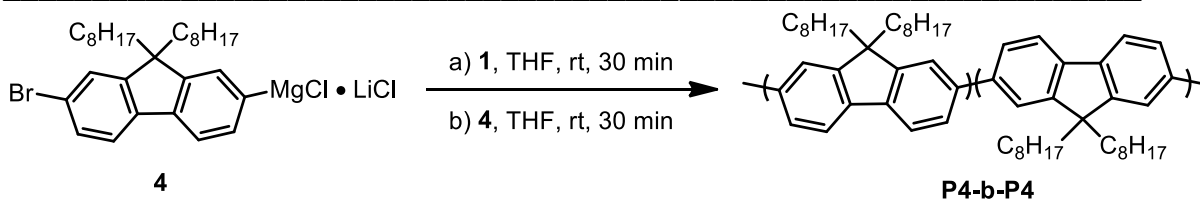
P4-b-P4. A 25 mL Schlenk flask was equipped with a stir bar, precatalyst **1** (10.2 mg, 0.0150 mmol, 1 equiv), and THF (6.48 mL) in a glovebox under an N_2 atmosphere. The flask was then equipped with a septum (secured with copper wire), removed from the glovebox, and put under an N_2 atmosphere. Monomer **3** (1.76 mL, 0.286 M, 0.503 mmol, 35 equiv) was then added via syringe and stirred for 30 min at rt. After 30 min, an aliquot was withdrawn via syringe and immediately quenched with aq. HCl (12 M, 1 mL). Monomer **3** (1.76 mL, 0.286 M, 0.503 mmol, 35 equiv) was then added via syringe and stirred for 30 min at rt. After 30 min, an aliquot was withdrawn via syringe and immediately quenched with aq. HCl (12 M, 1 mL). Each aliquot was then extracted with $CHCl_3$ (3 x 1 mL) with mild heating, dried over $MgSO_4$, filtered and concentrated in vacuo. The resulting solid was then dissolved in THF (~1.5 mL) with mild heating and passed through a 0.2 µm PTFE filter for GPC analysis. Block 1: M_n = 7.0 kDa, Đ = 1.97, Block 2: M_n = 7.3 kDa, Đ = 2.04.
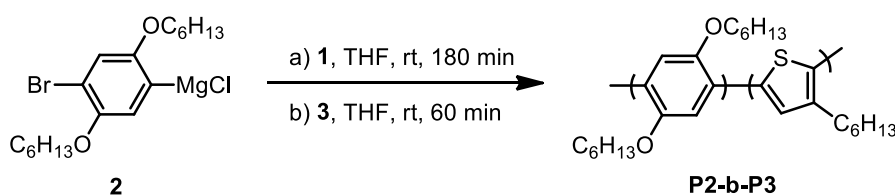
P2-b-P3. A 25 mL Schlenk flask was equipped with a stir bar, precatalyst **1** (10.2 mg, 0.0150 mmol, 1 equiv), and THF (7.11 mL) in a glovebox under an N_2 atmosphere. The flask was then equipped with a septum (secured with copper wire), removed from the glovebox, and put under an N_2 atmosphere. Monomer **2** (0.96 mL, 0.52 M, 0.50 mmol, 33 equiv) was then added via syringe and stirred for 180 min at rt. After 180 min, an aliquot was withdrawn via syringe and immediately quenched with aq. HCl (12 M, 1 mL). Monomer **3** (1.93 mL, 0.466 M, 0.900 mmol, 60 equiv) was then added via syringe and stirred for 60 min at rt. After 60 min, an aliquot was withdrawn via syringe and immediately quenched with aq. HCl (12 M, 1 mL). The aliquots were extracted with $CHCl_3$ (3 x 1 mL) with mild heating and the combined aliquots were dried over $MgSO_4$. The organic

phase was then concentrated in vacuo, redissolved in THF (~1.5 mL) with mild heating and passed through a 0.2 μm PTFE filter for GPC analysis (Block 1: M_n = 9.2 kDa, Đ = 1.24, Block 2: M_n = 17.8 kDa, Đ = 1.32). The reaction was quenched with aq. HCl (5 M, 10 mL), extracted with CHCl$_3$ (3 x 10 mL), dried over MgSO$_4$, filtered, and the solvent was removed in vacuo. The resulting purple solid was then dissolved in a minimum amount of CHCl$_3$ and precipitated into MeOH. The precipitate was collected and dried under vacuum (223 mg, 78% yield).
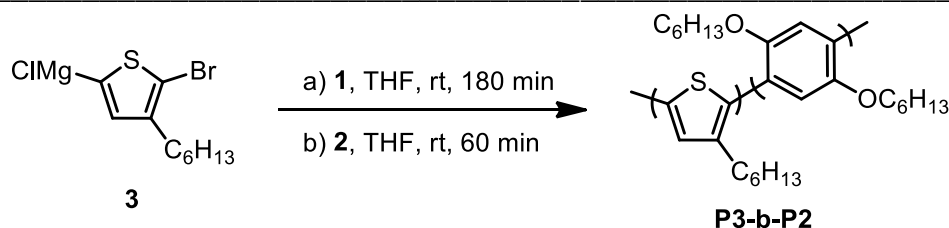
P3-b-P2. A 25 mL Schlenk flask was equipped with a stir bar, precatalyst **1** (10.2 mg, 0.0150 mmol, 1 equiv), and THF (7.11 mL) in a glovebox under an N$_2$ atmosphere. The flask was then equipped with a septum (secured with copper wire), removed from the glovebox, and put under an N$_2$ atmosphere. Monomer **3** (1.93 mL, 0.466 M, 0.900 mmol, 60 equiv) was then added via syringe and stirred for 180 min at rt. After 180 min, an aliquot was withdrawn via syringe and immediately quenched with aq. HCl (12 M, 1 mL). Monomer **2** (0.96 mL, 0.52 M, 0.50 mmol, 33 equiv) was then added via syringe and stirred for 60 min at rt. After 60 min, an aliquot was withdrawn via syringe and immediately quenched with aq. HCl (12 M, 1 mL). The aliquots were extracted with CHCl$_3$ (3 x 1 mL) with mild heating and the combined aliquots were dried over MgSO$_4$. The organic phase was then concentrated in vacuo, redissolved in THF (~1.5 mL) with mild heating and passed through a 0.2 μm PTFE filter for GPC analysis (Block 1: M_n = 8.8 kDa, Đ = 1.26, Block 2: M_n = 15.8 kDa, Đ = 1.35). The reaction was quenched with aq. HCl (5 M, 10 mL), extracted with CHCl$_3$ (3 x 10 mL), dried over MgSO$_4$, filtered, and the solvent was removed in vacuo. The resulting purple solid was then dissolved in a minimum amount of CHCl$_3$ and precipitated into MeOH. The precipitate was collected and dried under vacuum (238 mg, 83% yield).

IV. ^{1}H NMR Spectra
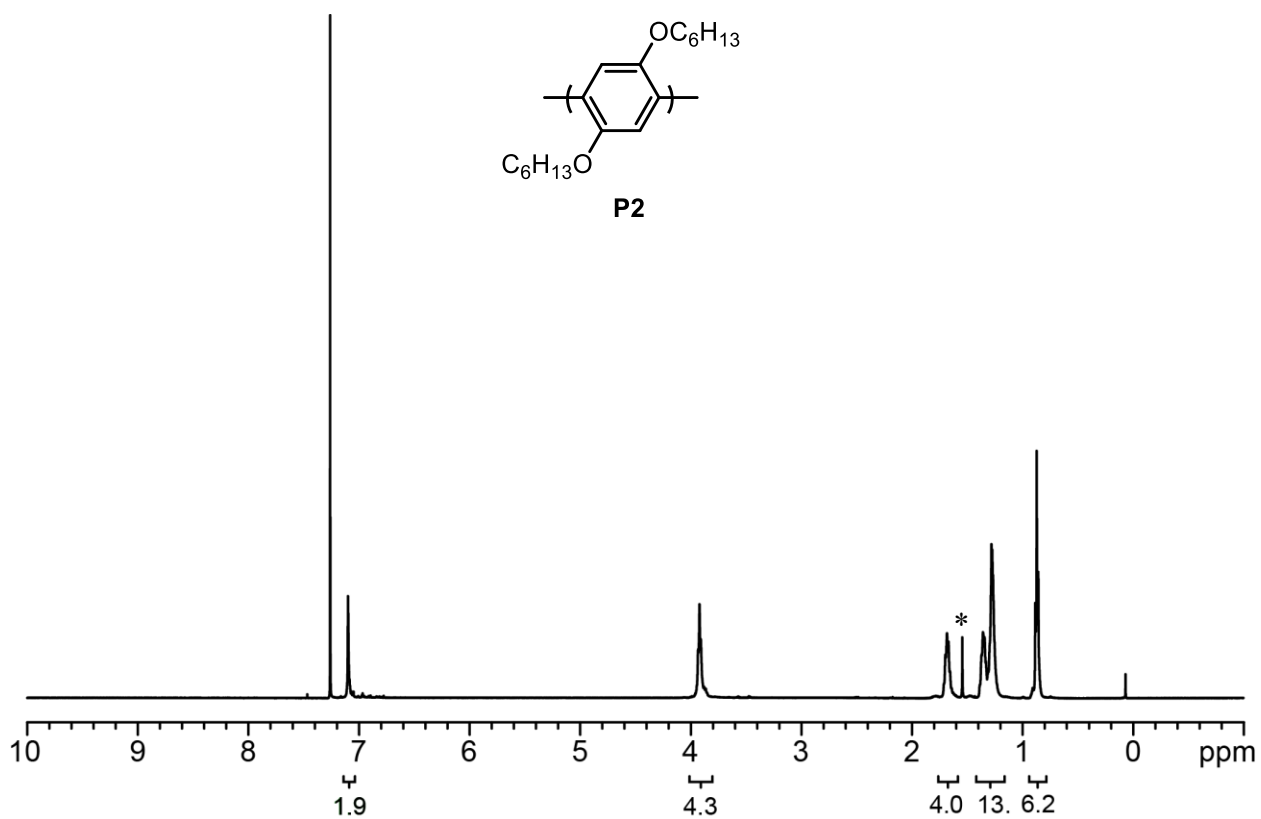
Figure S1.1 ^{1}H NMR spectrum for **P2**.
^{1}H NMR (500 MHz, CDCl$_3$) δ 7.10 (br s, 2H), 3.92 (br m, 4H), 1.68 (br m, 4H) 1.40-1.21 (br m, 12H), 0.87 (br m, 6H). * indicates residual H$_2$O
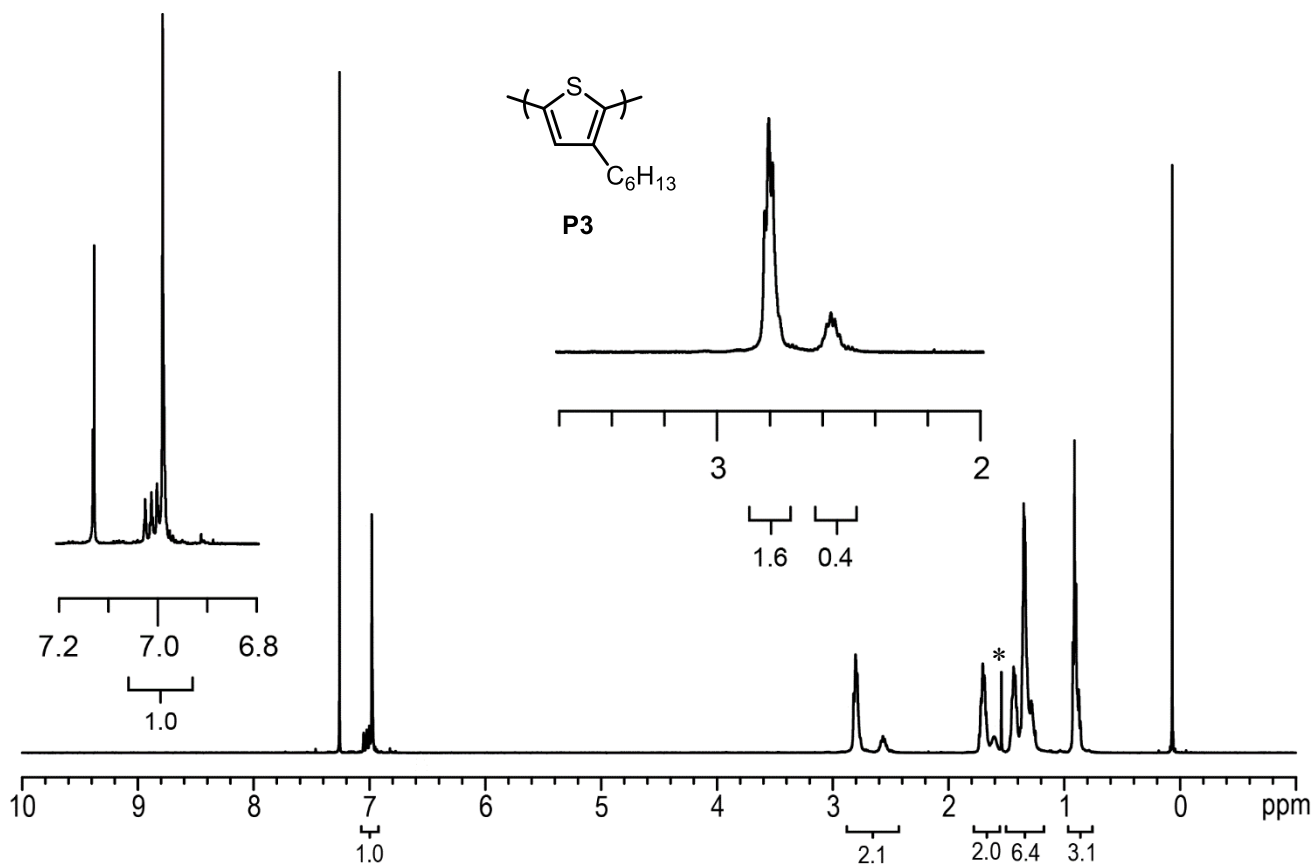
Figure S1.2 ^{1}H NMR spectrum for **P3**.
^{1}H NMR (500 MHz, CDCl$_3$) δ 6.98 (s, 1H), 2.83-2.50 (br m, 2H), 1.74-1.57 (m, 2H) 1.47-1.24 (br m, 6H), 0.91 (br m, 3H). * indicates residual H$_2$O
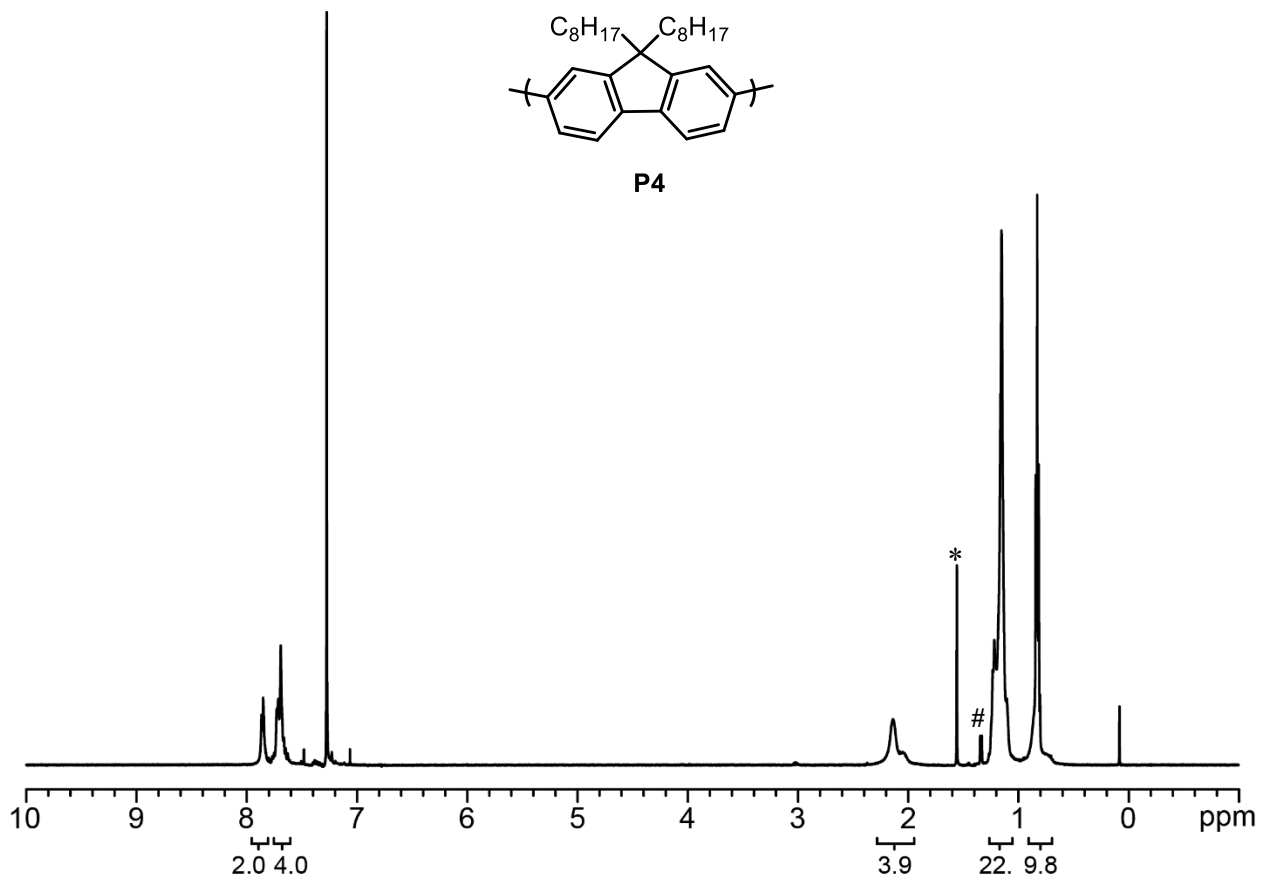
Figure S1.3 ^{1}H NMR spectrum for **P4**.
^{1}H NMR (500 MHz, CDCl$_3$) δ 7.85 (br m, 2H), 7.69 (br m, 4H), 2.22-1.89 (br m, 4H), 1.27-1.06 (br m, 20H), 0.90-0.71 (br m, 10H). * indicates residual H$_2$O, **#** indicates iPr end groups
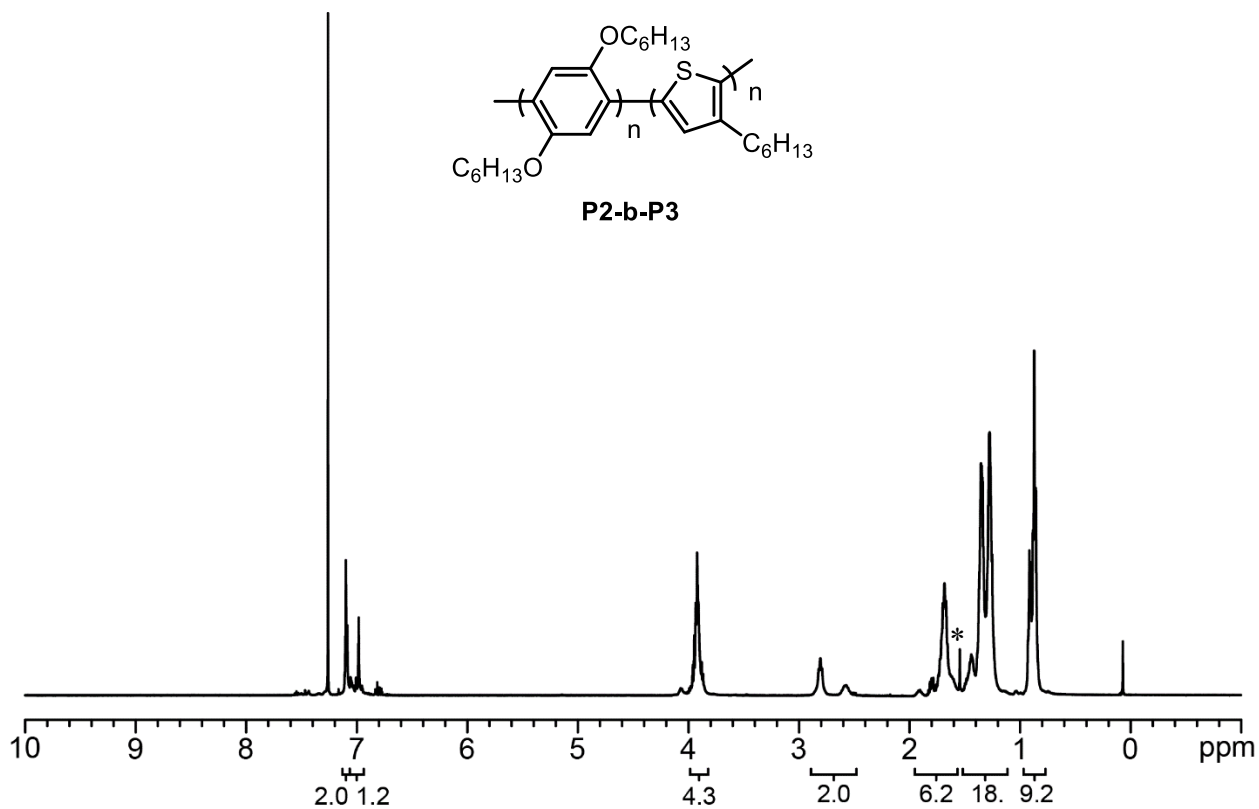
Figure S1.4 ^{1}H NMR spectrum for **P2-b-P3**.
^{1}H NMR (500 MHz, CDCl$_3$) δ 7.10 (br s, 2H), 6.98 (s, 1H), 4.09-3.84 (br m, 4H), 2.83-2.50 (br m, 2H), 1.74-1.57 (br m, 6H) 1.47-1.24 (br m, 18H), 0.94-0.84 (br m, 9H). * indicates residual H$_2$O
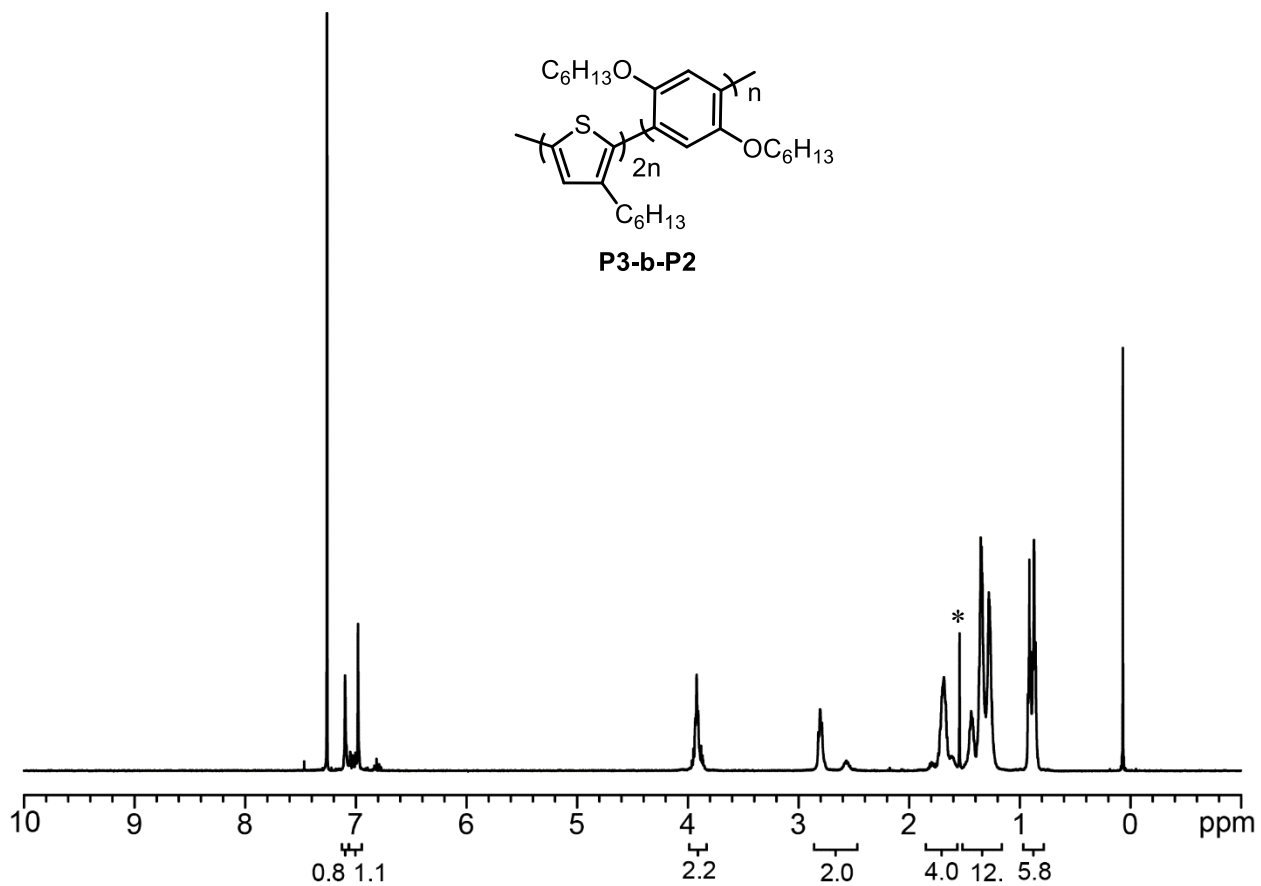
Figure S1.5 ^{1}H NMR spectrum for **P3-b-P2**
^{1}H NMR (500 MHz, CDCl$_3$) δ 7.10 (br s, 1H), 6.98 (m, 1H), 4.09-3.84 (br m, 2H), 2.83-2.50 (br m, 2H), 1.74-1.57 (br m, 4H) 1.47-1.24 (br m, 12H), 0.94-0.84 (br m, 6H). * indicates residual H$_2$O

V. M_n and Đ versus Conversion

Representative Procedure for M_n and Đ versus Conversion Studies utilizing GC analysis:
A 25 mL Schlenk flask was equipped with a stir bar, precatalyst **1** (10.2 mg, 0.0150 mmol, 1 equiv), and THF (7.75 mL) in a glovebox under an N_2 atmosphere. The flask was then equipped with a septum (secured with copper wire), removed from the glovebox, and put under an N_2 atmosphere. Monomer **2** (2.25 mL, 0.466 M, 1.01 mmol, 67 equiv), with docosane added (as an internal standard), was then added via syringe and stirred for 90 min at rt. Aliquots (~0.5 mL) were withdrawn via syringe and immediately quenched with aq. HCl (12 M, 1 mL). Each aliquot was then extracted with CH_2Cl_2 (3 x 1 mL) with mild heating and the combined aliquots were dried over $MgSO_4$. To monitor conversion, GC samples were prepared by taking aliquots (~0.25 mL) of this organic phase and diluting with CH_2Cl_2 (~0.75 mL). Conversion was determined relative to the initial concentration, using the internal standard as a reference. To measure molecular weight and molecular weight distribution, the remaining organic phase was concentrated in vacuo, redissolved in THF (~1.5 mL) with mild heating and passed through a 0.2 µm PTFE filter for GPC analysis.

Note: nonadecane was used as internal standard with monomer **3**, docosane was used as internal standard with monomer **4**.
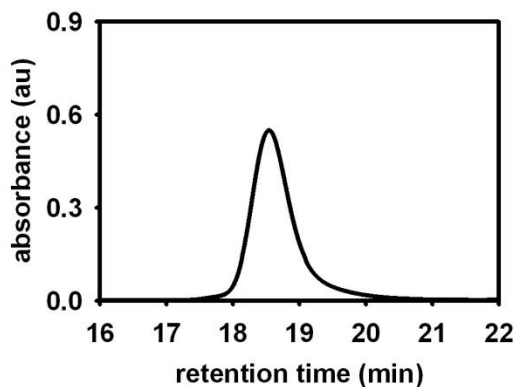
Figure S1.6. Representative GPC trace of **P2** at 60% conversion with precatalyst **1** (M_n: 22.5 kDa, Đ: 1.17).
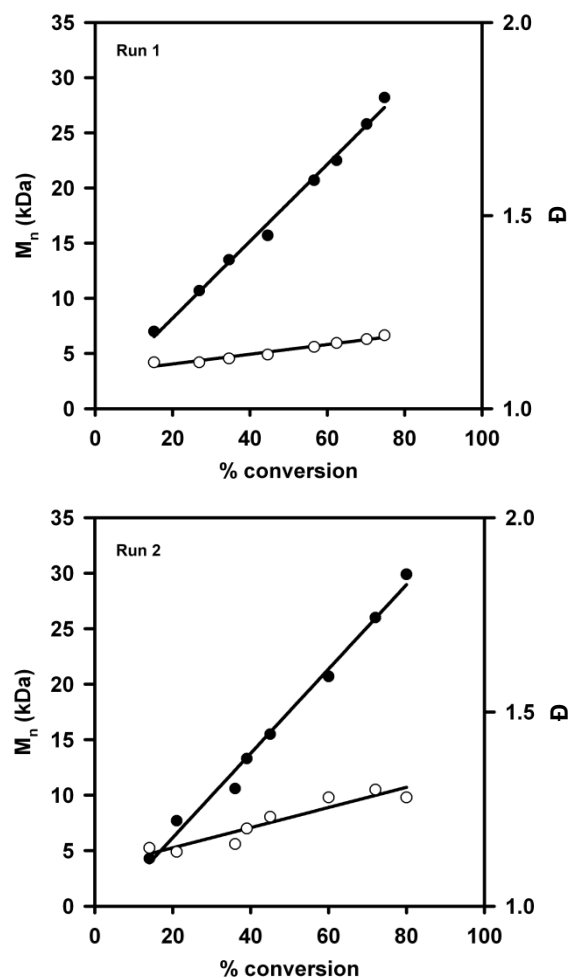
Figure S1.7 Plots of M_n (●) and Đ (○) versus conversion for the polymerization of monomer **2** using precatalyst **1** ([**1**] = 1.5 mM, [**2**] = 77 mM (run 1), 91 mM (run 2), 25 °C, THF).

Table S1.1 Data for the plot in Figure S1.7, run 1.

% Conversion	M_n (kDa)	Đ
15	7.0	1.12
27	10.7	1.12
35	13.5	1.13
45	15.7	1.14
57	20.7	1.16
62	22.5	1.17
70	25.8	1.18
75	28.2	1.19

Table S1.2 Data for the plot in Figure S1.7, run 2.

% Conversion	M_n (kDa)	Đ
14	4.3	1.15
21	7.7	1.14
36	10.6	1.16
39	13.3	1.20
45	15.5	1.23
60	20.7	1.28
72	26.0	1.30
80	29.9	1.28
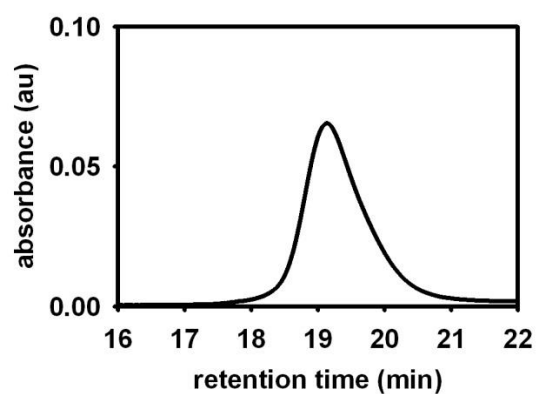
Figure S1.8 Representative GPC trace of **P3** at 60% conversion with precatalyst **1** (M_n: 11.5 kDa, Đ: 1.20).
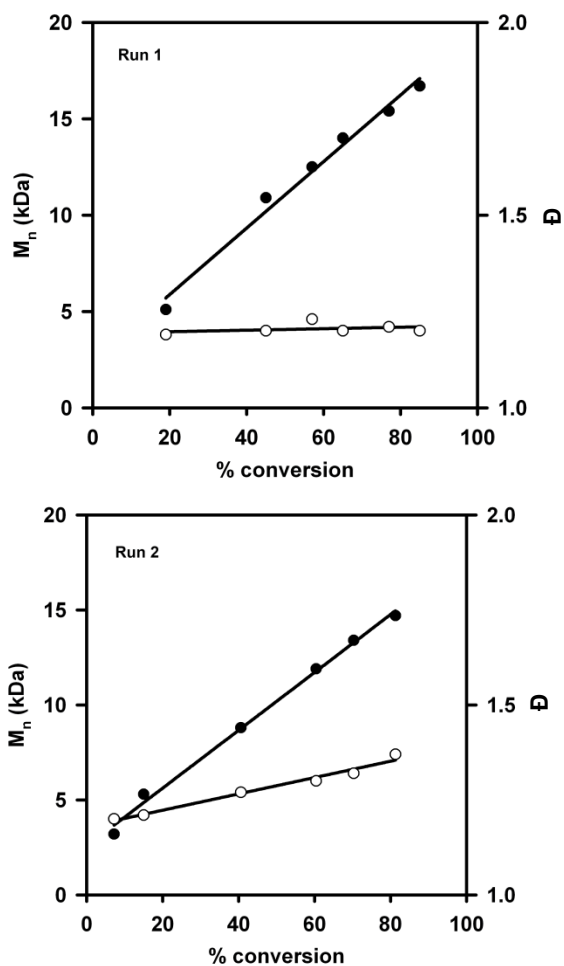
Figure S1.9 Plots of M_n (●) and Đ (○) versus conversion for the polymerization of monomer **3** using precatalyst **1** ([**1**] = 1.5 mM, [**3**] = 98 mM (run 1), 88 mM (run 2), 25 °C, THF).

Table S1.3 Data for the plot in Figure S1.9, run 1.

% Conversion	M_n (kDa)	Đ
19	5.1	1.19
45	10.9	1.20
57	12.5	1.23
65	14.0	1.20
77	15.4	1.21
85	16.7	1.20

Table S1.4 Data for the plot in Figure S1.9, run 2.

% Conversion	M_n (kDa)	Đ
7	3.2	1.20
15	5.3	1.21
41	8.8	1.27
60	11.9	1.30
70	13.4	1.32
81	14.7	1.37
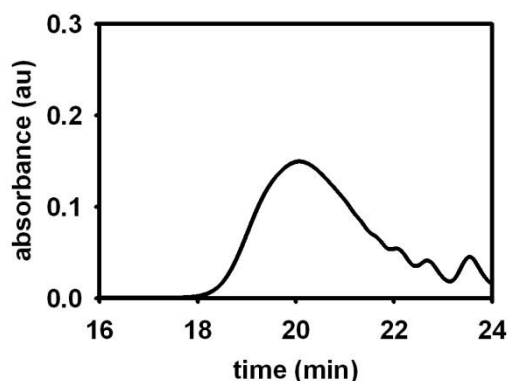
Figure S1.10 Representative GPC trace of **P4** at 60% conversion with precatalyst **1** (M_n: 4.3 kDa, Đ: 1.53).
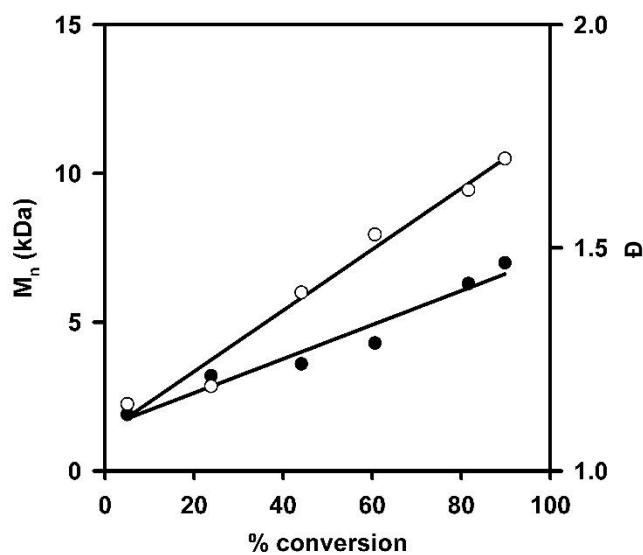
Figure S1.11 Plot of M_n (●) and Đ (○) versus conversion for the polymerization of monomer **4** using precatalyst **1** ([**1**] = 1.5 mM, [**2**] = 101 mM, 25 °C, THF).

Table S1.5 Data for the plot in Figure S1.11.

% Conversion	M_n (kDa)	Đ
5	1.9	1.15
24	3.2	1.19
44	3.6	1.40
61	4.3	1.53
82	6.3	1.63
90	7.0	1.70

VI. M_n and Đ versus [monomer]/[catalyst]
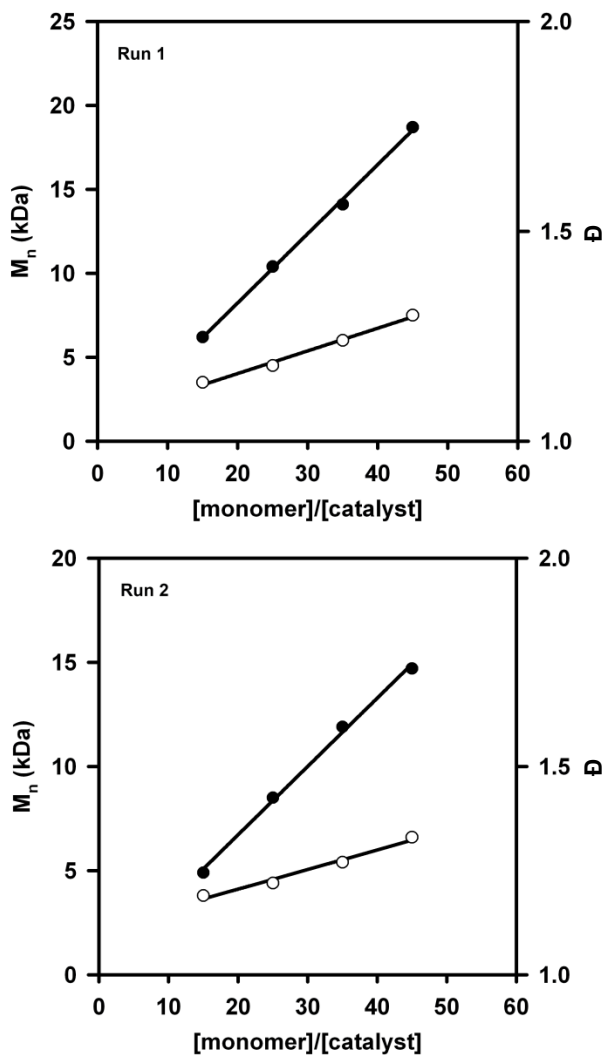
Figure S1.12 Plots of M_n (●) and Đ (○) versus [monomer]/[catalyst] for the polymerization of monomer **2** using precatalyst **1** ([**1**] = 1.5 mM, [**2**] = 23 mM, 38 mM, 53 mM, 68 mM, 25 °C, THF).

Table S1.6 Data for the plot in Figure S1.12, run 1.

[monomer]/[catalyst]	M_n (kDa)	Đ
15	6.2	1.14
25	10.4	1.18
35	14.1	1.24
45	18.7	1.30

Table S1.7 Data for the plot in Figure S1.12, run 2.

[monomer]/[catalyst]	M_n (kDa)	Đ
15	4.9	1.19
25	8.5	1.22
35	11.9	1.27
45	14.7	1.33
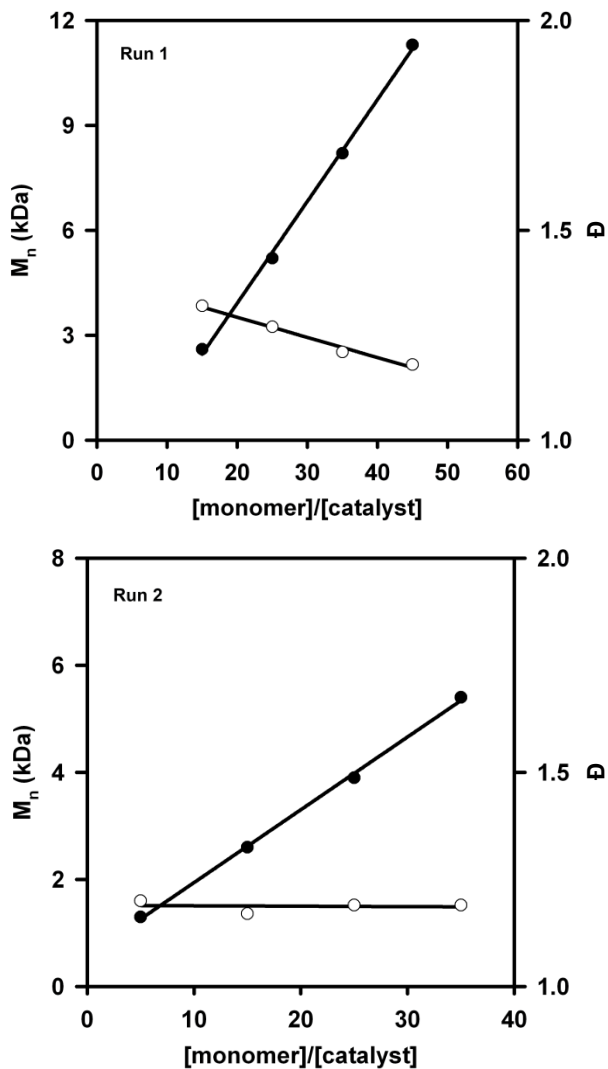
Figure S1.13 Plots of M_n (●) and Đ (○) versus [monomer]/[catalyst] for the polymerization of monomer **3** using precatalyst **1** ([**1**] = 1.5 mM, [**3**] = 23 mM, 38 mM, 53 mM, 68 mM (run 1), 8 mM, 23 mM, 38 mM, 53 mM (run 2), 25 °C, THF).

Table S1.8 Data for the plot in Figure S1.13, run 1.

[monomer]/[catalyst]	M_n (kDa)	Đ
15	2.6	1.37
25	5.2	1.27
35	8.2	1.21
45	11.3	1.18

Table S1.9 Data for the plot in Figure S1.13, run 2.

[monomer]/[catalyst]	M_n (kDa)	Đ
5	1.3	1.20
15	2.6	1.17
25	3.9	1.19
35	5.4	1.19

VII. Thiophene Regioregularity
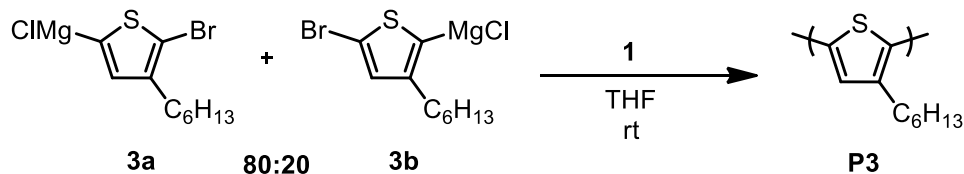
P3. A 25 mL Schlenk flask was equipped with a stir bar, precatalyst **1** (10.2 mg, 0.0150 mmol, 1 equiv), and THF (8.07 mL) in a glovebox under an N_2 atmosphere. The flask was then equipped with a septum (secured with copper wire), removed from the glovebox, and put under an N_2 atmosphere. Monomer **3** (1.93 mL, 0.466 M, 0.900 mmol, 60 equiv), with nonadecane added (as an internal standard), was then added via syringe and stirred for 90 min at rt. Aliquots (~0.5 mL) were withdrawn via syringe and immediately quenched with aq. HCl (12 M, 1 mL). Each aliquot was then extracted with $CHCl_3$ (3 x 1 mL) with mild heating and the combined aliquots were dried over $MgSO_4$. To monitor conversion, GC samples were prepared by taking aliquots (~0.25 mL) of this organic phase and diluting with CH_2Cl_3 (~0.75 mL). Conversion was determined by sum of areas (**3a** + **3b**) relative to a nonadecane internal standard.

Table S1.10 Data for the consumption of thiophene regioisomers, run 1.

% Conversion (**3a**)	% Conversion (**3b**)	Total Conversion
20	0*	14
46	3	36
58	0	44
71	5	56
85	13	68
94	20	76
98	48	87
99	95	98

* Within range of intrinsic GC error

Table S1.11 Data for the consumption of thiophene regioisomers, run 2.

% Conversion (**3a**)	% Conversion (**3b**)	Total Conversion
22	0	17
39	2	31
46	1	36
63	9	51
79	18	65
90	28	76
98	42	86

VIII. Competition Experiment
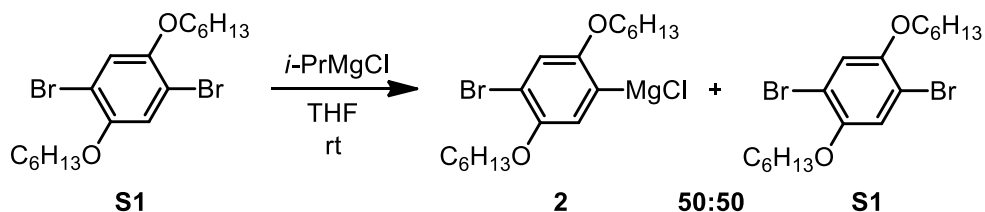
2:S1 Mixture. In the glovebox, **S1** (3.00 g, 6.88 mmol, 1.0 equiv) was dissolved in THF (7.5 mL) in a 20 mL vial equipped with a stir bar. Then, *i*-PrMgCl (1.72 mL, 3.44 mmol, 0.5 equiv) was added via syringe, the vial was capped, and the reaction was stirred overnight at rt. Approximate ratio was confirmed via GC analysis.
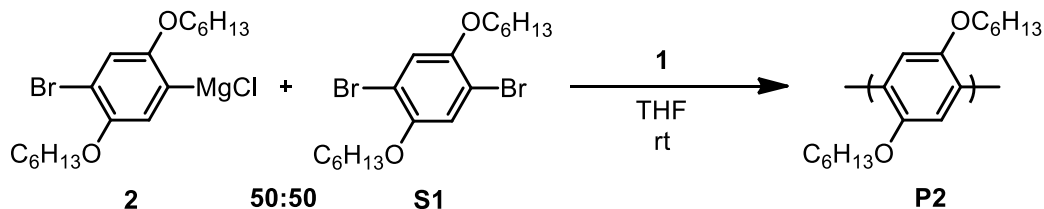
P2. A 25 mL Schlenk flask was equipped with a stir bar, precatalyst **1** (10.2 mg, 0.0150 mmol, 1 equiv), and THF (6.25 mL) in a glovebox under an N_2 atmosphere. The flask was then equipped with a septum (secured with copper wire), removed from the glovebox, and put under an N_2 atmosphere. A mixture of **2:S1** (~50:50) (3.75 mL, [**2**] = 0.268 M, 1.005 mmol, 67 equiv), with docosane added (as an internal standard), was then added via syringe and stirred for 90 min at rt. Aliquots (~0.5 mL) were withdrawn via syringe and immediately quenched with aq. HCl (12 M, 1 mL). Each aliquot was then extracted with CH_2Cl_2 (3 x 1 mL) with mild heating and the combined aliquots were dried over $MgSO_4$. To monitor conversion, GC samples were prepared by taking aliquots (~0.25 mL) of this organic phase and diluting with CH_2Cl_2 (~0.75 mL). Conversion was determined relative to docosane internal standard. To measure molecular weight and molecular weight distribution, the remaining organic phase was concentrated in vacuo, redissolved in THF (~1.5 mL) with mild heating and passed through a 0.2 μm PTFE filter for GPC analysis.

_____
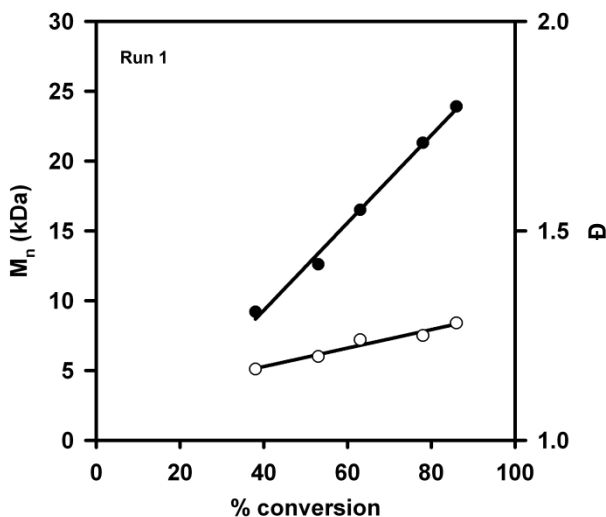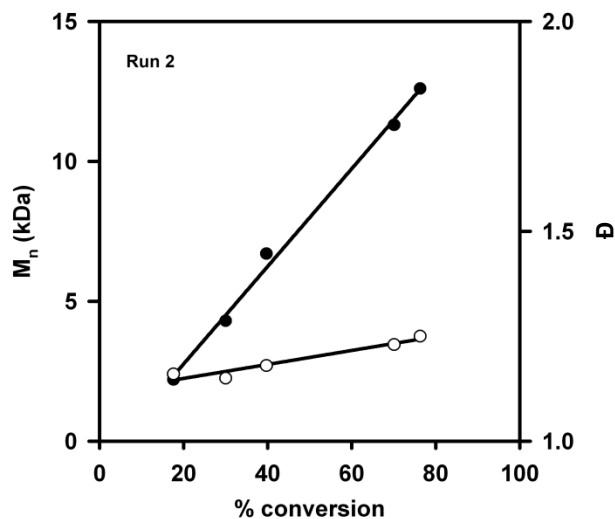
Figure S1.14 Plots of M_n (●) and Đ (○) versus conversion for the polymerization of monomer **2** with 50% **S1** using precatalyst **1** ([**1**] = 1.5 mM, [**2**] = 101 mM (run 1), 85 mM (run 2), 25 °C, THF).

Table S1.12 Data for the plot in Figure S1.14, run 1.

% Conversion (**2**)	% **S1**	M_n (kDa)	Đ
38	6	9.2	1.17
53	6	12.6	1.20
63	0*	16.5	1.24
78	1	21.3	1.25
86	7	23.9	1.28

* Within range of intrinsic GC error

Table S1.13 Data for the plot in Figure S1.14, run 2.

% Conversion (**2**)	% **S1**	M_n (kDa)	Đ
18	4	2.2	1.16
30	5	4.3	1.15
40	0*	6.7	1.18
70	1	11.3	1.23
76	0	12.6	1.25

* Within range of intrinsic GC error

IX. MALDI-TOF MS Data

Representative Procedure for Preparation of Oligomers for MALDI-TOF MS Studies:

All actions were performed in a glovebox under N_2 atmosphere. A 20 mL vial was equipped with a stir bar. Sequentially, precatalyst **1** (10.2 mg, 0.0150 mmol, 1.0 equiv), THF (4.75 mL), and **2** (0.25 mL, 0.45 M, 0.11 mmol, 7.0 equiv) were added to the flask. After 1 h, the reaction was removed from the glovebox, and poured into aq. HCl (5 M, 5 mL). This mixture was then extracted with CH_2Cl_2 (3 x 5 mL). The combined organic layers were dried over $MgSO_4$, filtered, and concentrated in vacuo. The resulting solid was washed with MeOH (50 mL) to give **P2** as an off-white solid: M_n: 2.04 kDa, Đ: 1.21 (GPC). For the MS sample, the polymer was dissolved in minimal $CHCl_3$ (~2 mL) and filtered through a pipet column of basic, acidic, and neutral alumina to remove Pd. The solution was then concentrated in vacuo. The general procedure was followed for MALDI-TOF MS sample preparation (see General Experimental pS2).
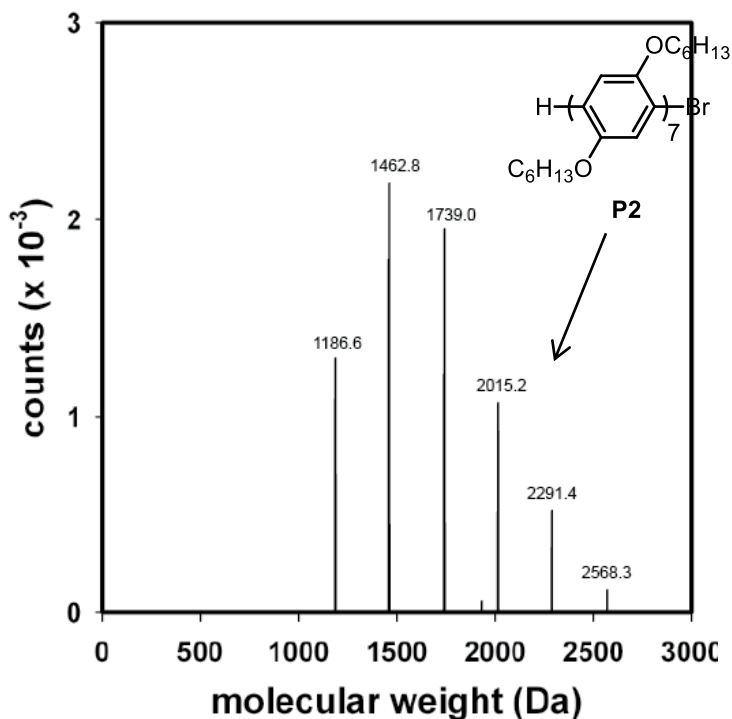
Figure S1.15 MALDI-TOF MS spectrum of **P2** initiated with precatalyst **1**.
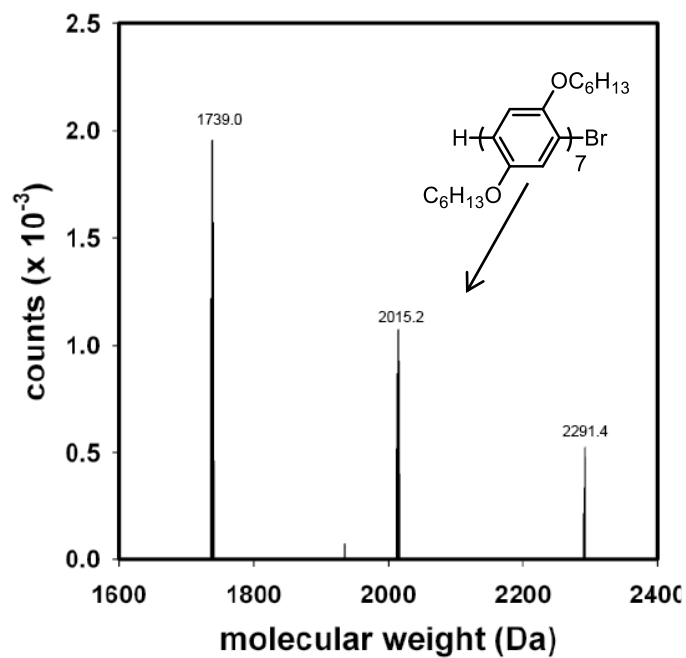
Figure S1.16 Expanded view of Figure S1.15.
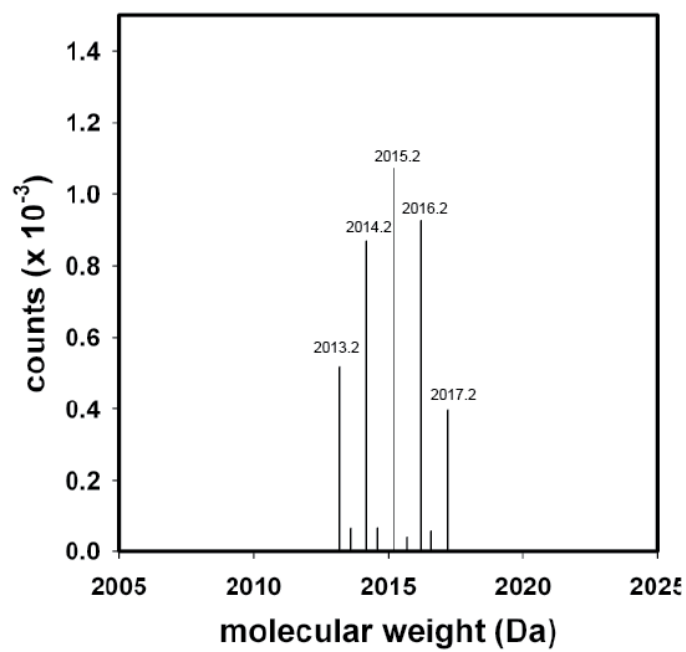
Figure S1.17 Expanded view of Figure S1.16.
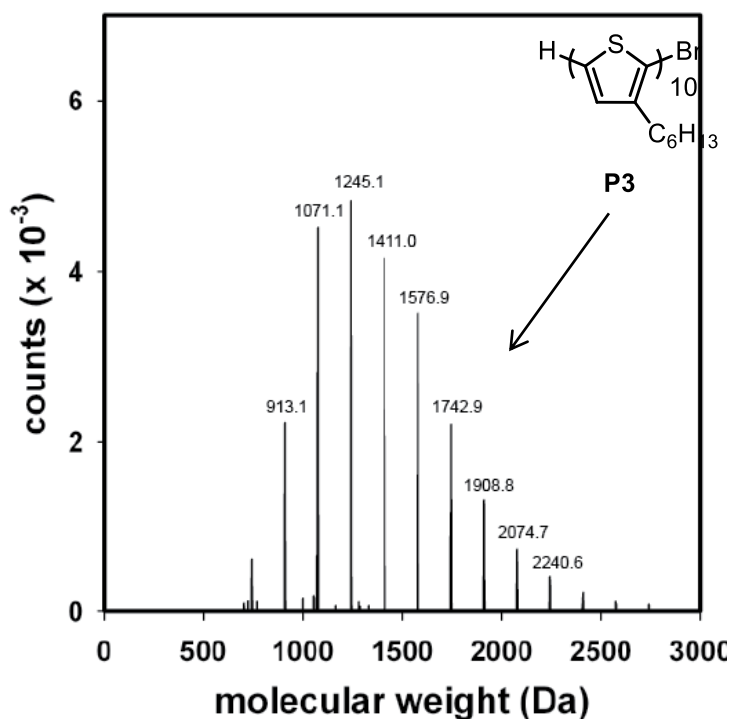
Figure S1.18 MALDI-TOF MS spectrum of **P3** initiated with precatalyst **1**.
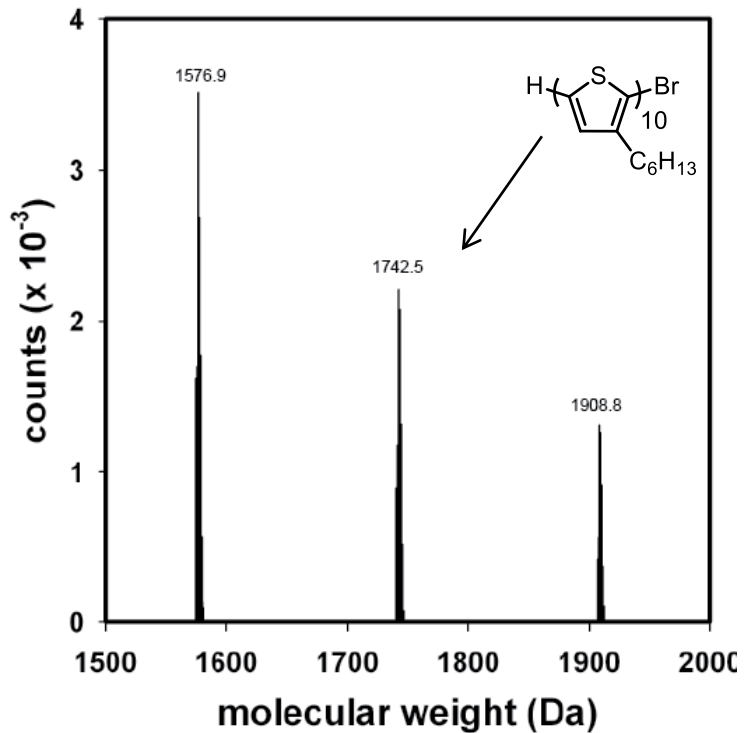
Figure S1.19 Expanded view of Figure S1.18.
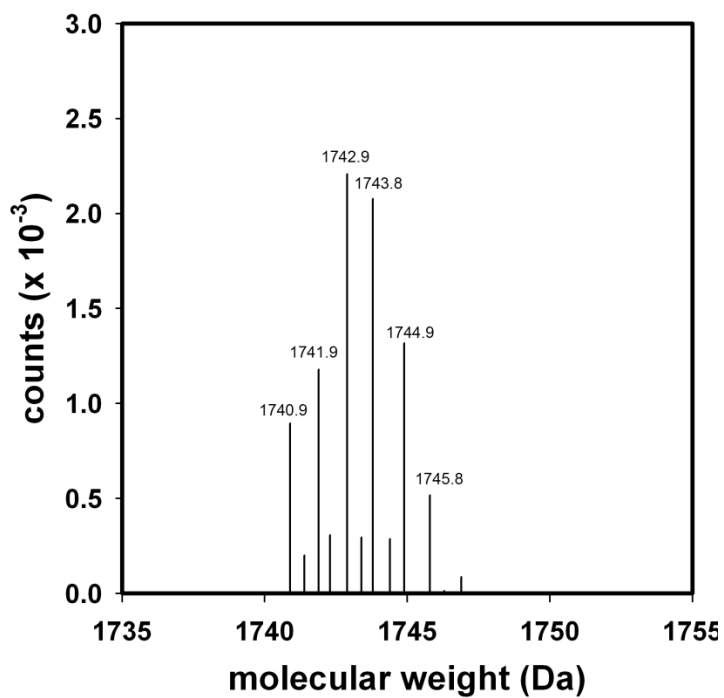
Figure S1.20 Expanded view of Figure S1.19.
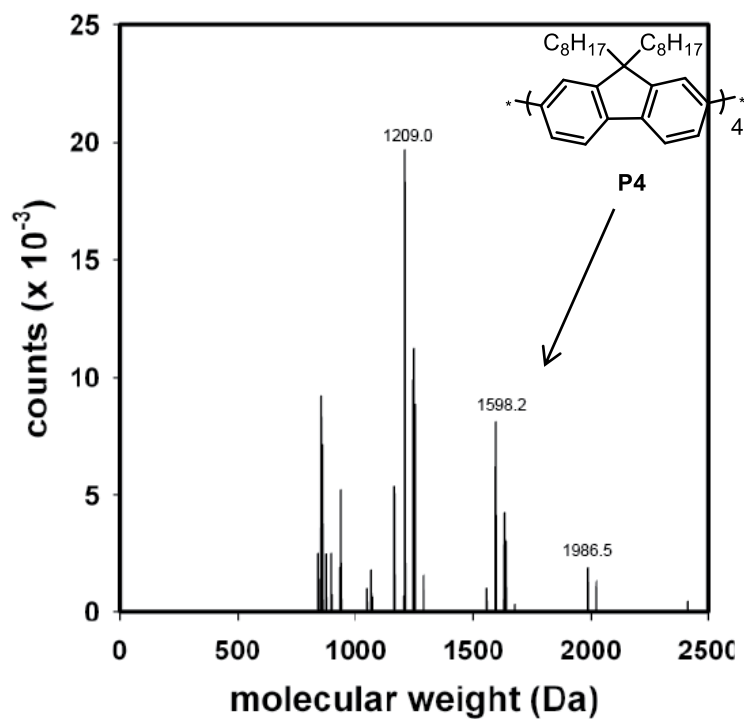
Figure S1.21 MALDI-TOF MS spectrum of **P4** initiated with precatalyst **1**.
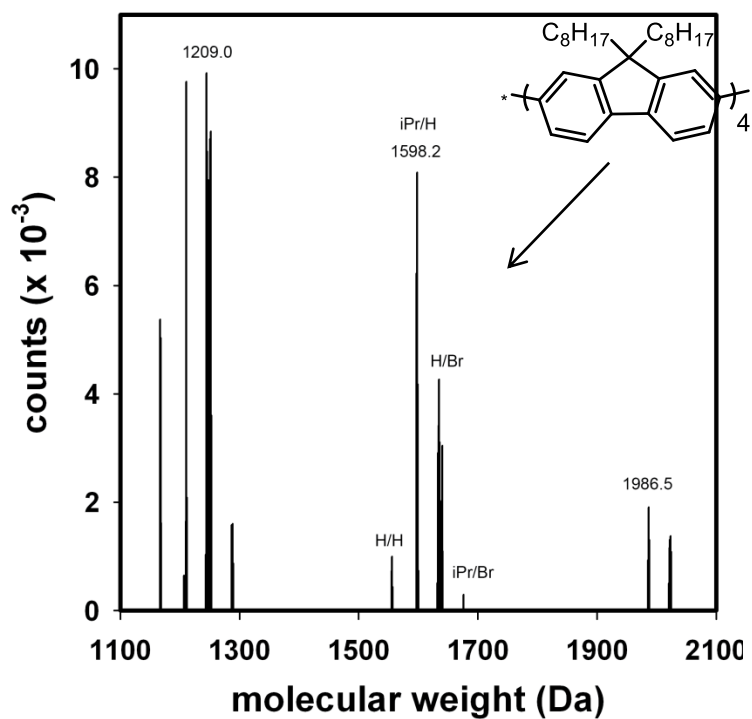
Figure S1.22 Expanded view of Figure S1.21.
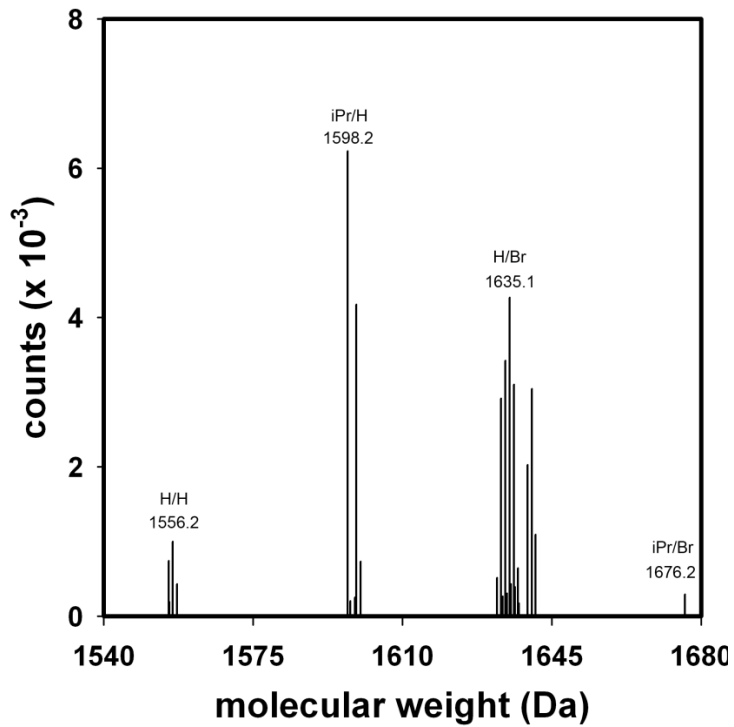
Figure S1.23 Expanded view of Figure S1.22.

X. Plot of ln([M]$_0$/[M]) versus Time

Representative Procedure for studies utilizing react IR:
The IR probe was inserted through an O-ring sealed 14/20 ground glass adapter (custom-made) into an oven-dried 50 mL 2-neck flask equipped with a stir bar. The other neck was fitted with a two-way adapter fitted with a septum for injections/aliquot sampling and an N$_2$ line. The oven-dried flask was cooled under vacuum. The flask was then filled with N$_2$ and evacuated again for a total of three cycles. The flask was charged with THF (6.75 mL). After recording a background spectrum, monomer **2** (2.25 mL, 0.466 M, 1.01 mmol, 67 equiv) was added by syringe. Precatalyst **1** (10.2 mg, 0.0150 mmol, 1 equiv), dissolved in THF (1 mL), was then injected and spectra were recorded every 30 s over the entire reaction. To account for mixing, spectra recorded in the first 60 s of the reaction were discarded. Aliquots (~0.5 mL) were withdrawn via syringe and immediately quenched with aq. HCl (12 M, 1 mL). Each aliquot was then extracted with CH$_2$Cl$_2$ (3 x 1 mL) with mild heating and the combined aliquots were dried over MgSO$_4$. Conversion was determined by absorbance readings relative to starting concentration. To measure molecular weight and molecular weight distribution, the organic phase was concentrated in vacuo, redissolved in THF (~1.5 mL) with mild heating and passed through a 0.2 µm PTFE filter for GPC analysis.

Although linear plots of ln([M]$_0$/[M]) have been used to provide evidence of a "living" polymerization,[4] this analysis assumes that the polymerization is first-order in monomer throughout the polymerization. If, on the other hand, the rate-determining step changes with conversion, then a non-linear plot can be observed, even under "living" conditions. Because the mechanism has not been established in this case, it is not possible to determine whether the observed non-linearity stems from chain termination pathways or a change in rate-determining step.
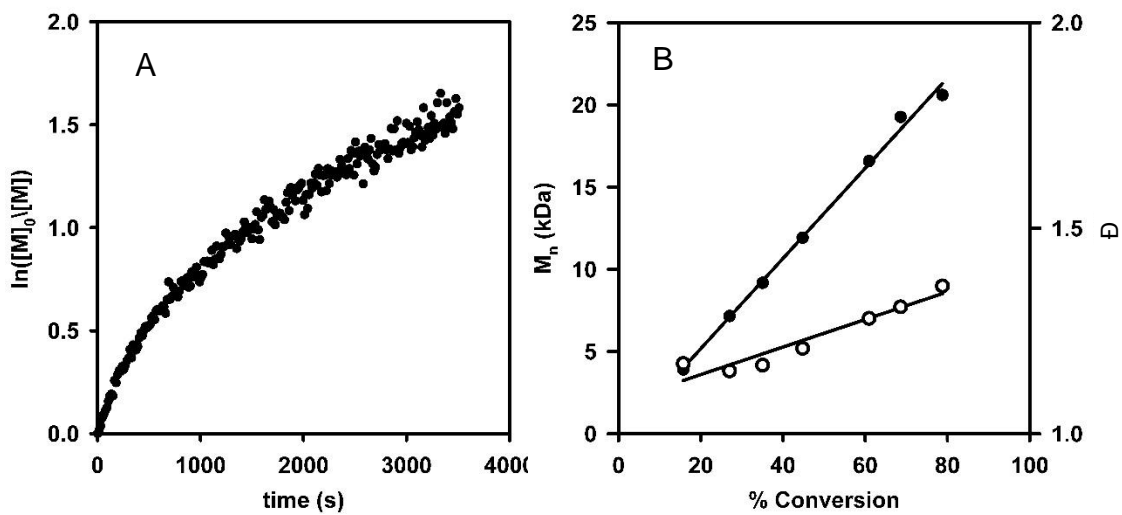
Figure S1.24 (A) Plot of ln([M]$_0$/[M]) versus time for polymerization of **2** ([**1**] = 1.5 mM, [**2**] = 101 mM, 25 °C, THF). (B) Corresponding plot of M_n (●) and Đ (○) versus conversion for the polymerization of **2**.

XI. Summary of Homopolymerizations
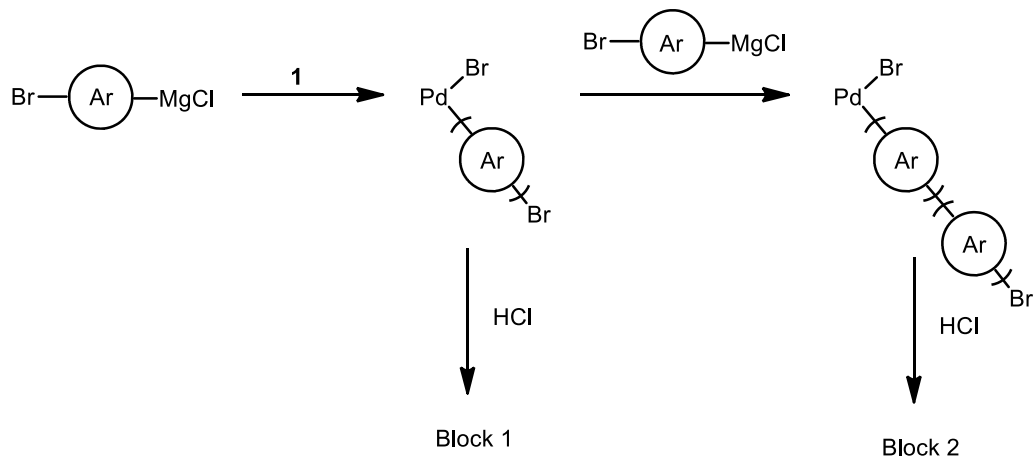
Table S1.14 Summary of GPC Data for Homopolymerizations.

Homopolymerization	M_n (kDa)	Đ
P2-b-P2 (Block 1)	13.8	1.13
P2-b-P2 (Block 2)	21.8	1.18
P3-b-P3 (Block 1)	11.2	1.22
P3-b-P3 (Block 2)	17.8	1.35
P4-b-P4 (Block 1)	7.0	1.97
P4-b-P4 (Block 2)	7.3	2.04

XII. Fluorene Side Reactions

(A) No consumption of *i*-PrBr was observed relative to internal standard (mesitylene), while complete consumption of *i*-PrMgCl was observed during polymerization of **4**.*
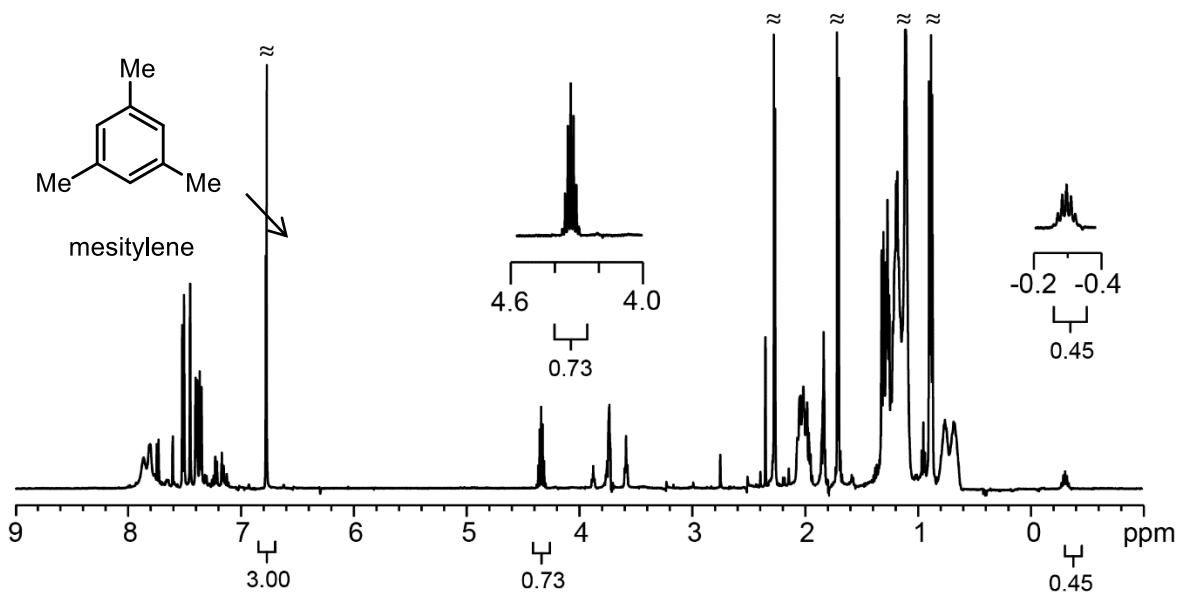
Figure S1.25 ^{1}H NMR spectrum for **4** (note: solvent suppresion was used). ^{1}H NMR (500 MHz, THF) δ 6.78 (s, 3H, Ar H), 4.36 (m, 1H, BrC*H*(CH$_3$)$_2$), -0.31 (m, 1H, ClMgC*H*(CH$_3$)$_2$).
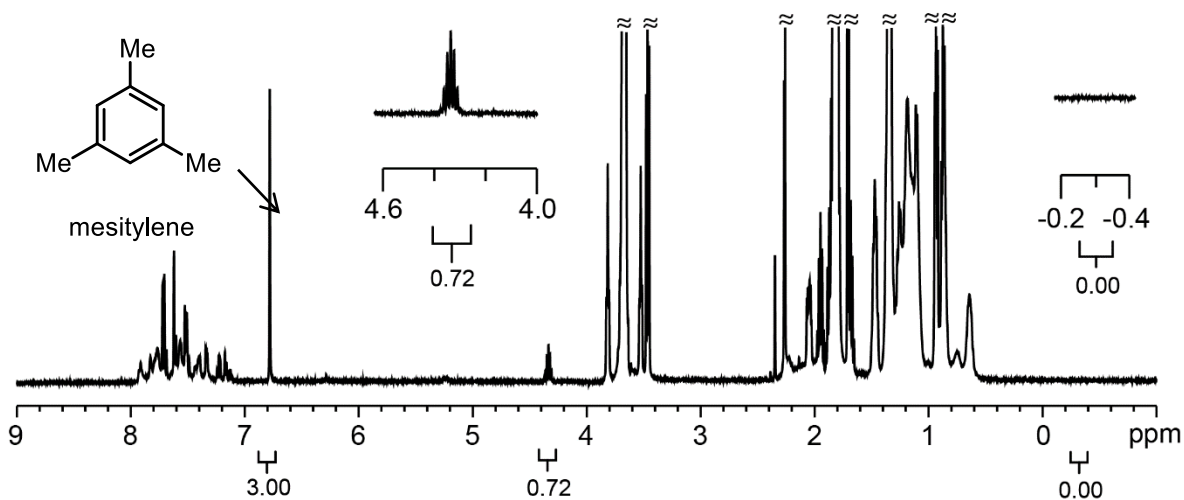
Figure S1.26 ^{1}H NMR spectrum for **P4** before quenching. ^{1}H NMR (500 MHz, THF) δ 6.78 (s, 3H, Ar H), 4.36 (m, 1H, BrC*H*(CH$_3$)$_2$), -0.31 (m, 1H, ClMgC*H*(CH$_3$)$_2$).

* These results are consistent with a control experiment wherein 1-bromodecane (20 equiv) was not consumed during the polymerization of **4** as evidenced by GC relative to internal standard.

(B) Consumption of the 2,7-dibromo-9,9-dioctylfluorene (**S3**) following Grignard metathesis was determined during the polymerization of **4**. Conversion was determined by GC relative to added internal standard (mesitylene).

Table S1.15 Conversion of 2,7-dibromo-9,9-dioctylfluorene (**S3**) during the polymerization of **4**.

Trial	% Conversion **S3**
Run 1	5
Run 2	10
Run 3	10
Run 4	11
Run 5	29

* All reactions showed > 85% monomer (**4**) conversion.

XII. References

(1) (a) Lanni, E. L.; McNeil, A. J. *J. Am. Chem. Soc.* **2009**, *131*, 16573–16579. (b) Lanni, E. L.; McNeil, A. J. *Macromolecules* **2010**, *43*, 8039–8044.

(2) Locke, J. R.; McNeil, A. J. *Macromolecules* **2010**, *43*, 8709–8710.

(3) Love, B. D.; Jones, E. G. *J. Org. Chem.* **1999**, *64*, 3755–3756.

(4) Penczek, S.; Kubisa, P.; Szymanski, R. *Makromol. Chem., Rapid Commun.* **1991**, *12*, 77–80.

Appendix 2

Supporting Information for Chapter 3
Impact of preferential π-binding in catalyst-transfer polymerization of thiazole
derivatives

I. Materials

Flash chromatography was performed on SiliCycle silica gel (40–63 μm). Thin layer chromatography was performed on Merck TLC plates (pre-coated with silica gel 60 F254). iPrMgCl (2M in THF) and 2,4,6-iPr$_3$PhMgBr (0.5M in THF) were purchased in 100 mL quantities from Aldrich. All other reagent grade materials and solvents were purchased from Aldrich, Acros, or Fisher and were used without further purification unless otherwise noted. THF was dried and deoxygenated using an Innovative Technology (IT) solvent purification system composed of activated alumina, copper catalyst, and molecular sieves. *N*-Bromosuccinimide was recrystallized from hot water and dried over P$_2$O$_5$. The glovebox in which specified procedures were carried out was an MBraun LABmaster 130 with a N$_2$ atmosphere and H$_2$O levels below 4 ppm. Compounds **S1**,[1] **S2**,[1] **1**,[2] **3**,[3] **5**,[4] **S3**,[5] **S4**,[6] and **6**[7] were prepared using modified literature procedures.

II. General Experimental

NMR Spectroscopy: Unless otherwise noted, ^{1}H, ^{13}C, and ^{31}P NMR spectra for all compounds were acquired at rt in CDCl$_3$ on a Varian vnmrs 500 spectrometer operating at 500, 126, and 202 MHz, respectively. Chemical shift data are reported in units of δ (ppm) relative to tetramethylsilane (TMS) and referenced with residual solvent. Multiplicities are reported as follows: singlet (s), doublet (d), triplet (t), multiplet (m). Residual water is denoted by an *.

Mass Spectrometry: High-resolution mass spectrometry data were obtained on a Micromass AutoSpec Ultima Magnetic Sector mass spectrometer.

Gel-Permeation Chromatography: Polymer molecular weights were determined by comparison with polystyrene standards (Varian, EasiCal PS-2 MW 580–377,400) at 40 °C in THF on a Malvern Viscotek GPCMax VE2001 equipped with two Viscotek LT-5000L 8 mm (ID) × 300 mm (L) columns and analyzed with Viscotek TDA 305 (with RI, UV-PDA Detector Model 2600 (190–500 nm), RALS/LALS, and viscometer). All presented data correspond to the absorbance

at 254 nm normalized to the highest peak. Samples were dissolved in THF (with mild heating), and passed through a 0.2 μm PTFE filter prior to analysis.

EPR Spectroscopy: Electron paramagnetic resonance spectra for all compounds were acquired in THF at -150 °C using quartz EPR tubes on a Bruker EMX electron spin resonance spectrometer operating in the X band with a Bruker 4102-ST general purpose cavity.

Gas Chromatography: Gas chromatography was carried out using a Shimadzu GC 2010 containing a Shimadzu SHRX5 (crossbound 5% diphenyl – 95% dimethyl polysiloxane; 15 m, 0.25 mm ID, 0.25 μm df) column.

MALDI-TOF Mass Spectrometry: MALDI-TOF-MS was carried out on a Bruker AutoFlex Speed MALDI-TOF in positive-ion linear mode using *trans*-2-[3-(4-*tert*-butylphenyl)-2-methyl-2-propenylidene]malononitrile (DCTB) as a matrix.

III. Synthetic Procedures
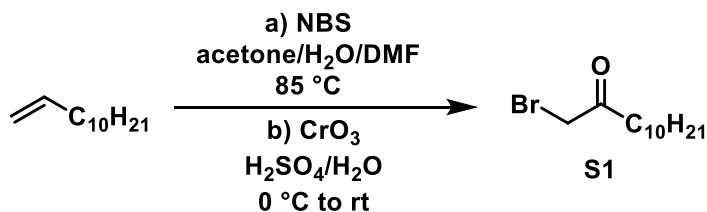
1-Bromododecan-2-one (S1).[1] In a 250 mL round-bottom flask with a stir bar, dodec-1-ene (22.7 g, 135 mmol, 1.00 equiv) was dissolved in DI H_2O/acetone (45 mL, 45:55 v/v). While stirring, the solution was heated to 85 °C. Subsequently, *N*-bromosuccinimide (35.1 g, 197 mmol, 1.46 equiv) was added to the solution, followed by DMF (8 mL). A reflux condenser was affixed and the reaction solution was stirred at 85 °C for 2 h. The reaction solution was then cooled to 0 °C using an ice-water bath. A mixture of CrO_3 (18.5 g, 185 mmol, 1.37 equiv) in H_2SO_4 (46.2 mL, 4.4M in DI H_2O) was prepared in an Erlenmeyer flask and cooled on ice. The heterogeneous CrO_3 mixture was added to the reaction flask over 10 min. An additional portion of H_2SO_4 (10 mL, 1.8M in DI H_2O) was used completely transfer the remaining CrO_3 mixture to the reaction flask. The reaction solution was warmed to rt while stirring over 16 h. The crude product was extracted with Et_2O (3 x 100 mL). The combined organic layers were washed with DI H_2O (50 mL), brine (2 x 50 mL), dried over $MgSO_4$, and concentrated to give a viscous dark oil. The crude oil was purified by flash column chromatography (97:3 v/v hexanes:EtOAc on silica) and then recrystallized from petroleum ether (100 mL) to give 22.6 g of **S1** as an off-white solid (63% yield). HRMS (EI): Calcd. for $C_{12}H_{23}BrO$ [M$^+$] 262.0932; found 262.0936.
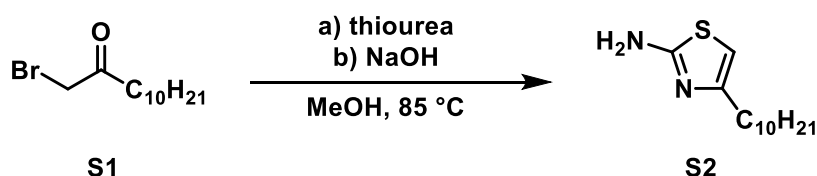
4-Decylthiazol-2-amine (S2).[1] In a 250 mL round-bottom flask with a stir bar, **S1** (22.2 g, 84.3 mmol, 1.00 equiv) was dissolved in MeOH (22.5 mL). While stirring, thiourea (7.19 g, 94.5 mmol, 1.12 equiv) was added to the reaction solution over 5 min. The mixture was heated at 85 °C for 2 h. Subsequently, solid NaOH (6.43 g, 161 mmol, 1.91 equiv) was added to the reaction solution. The mixture was heated at 85 °C for an additional 2 h. The reaction mixture was cooled to rt and filtered through filter paper to remove all solid material. The solution was extracted with Et_2O (4 x 50 mL). The combined organic layers were washed sequentially with DI H_2O (3 x 50 mL) and brine (3 x 50 mL), then dried over $MgSO_4$ and concentrated to a dark red oil. Recrystallization from petroleum ether

(300 mL) gave 14.2 g of **S2** as an orange powder (70% yield). HRMS (ESI+): Calcd. for $C_{13}H_{24}N_2S$ [M+H]$^+$ 241.1733; found 241.1731.
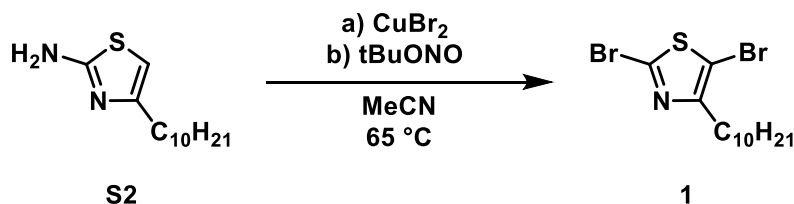
2,5-Dibromo-4-decylthiazole (1).[2] In a 500 mL round-bottom flask with a stir bar, **S2** (6.04 g, 25.1 mmol, 1.00 equiv) and copper(II) bromide (7.30 g, 32.7 mmol, 1.30 equiv) were dissolved in acetonitrile (250 mL). The reaction solution was heated at 65 °C for 2 h. *Tert*-butyl nitrite (4.78 mL, 40.2 mmol, 1.60 equiv) was added, and the reaction solution was heated at 65 °C for an additional 2 h. The reaction solution was cooled to rt, and the solvent was removed under reduced pressure. The dark brown solid was dissolved in Et$_2$O (250 mL), then washed with NH$_4$OH (50 mL, 5M in DI H$_2$O), followed by DI H$_2$O (50 mL), then brine (50 mL). The organic layer was dried over MgSO$_4$ and concentrated to give a viscous dark oil. The crude product was purified by flash column chromatography (0 to 10% EtOAc in hexanes gradient) to isolate 3.84 g of **1** as a colorless oil (40% yield). HRMS (ESI+): Calcd. for $C_{13}H_{21}Br_2NS$ [M+H]$^+$ 381.9834; found 381.9833.
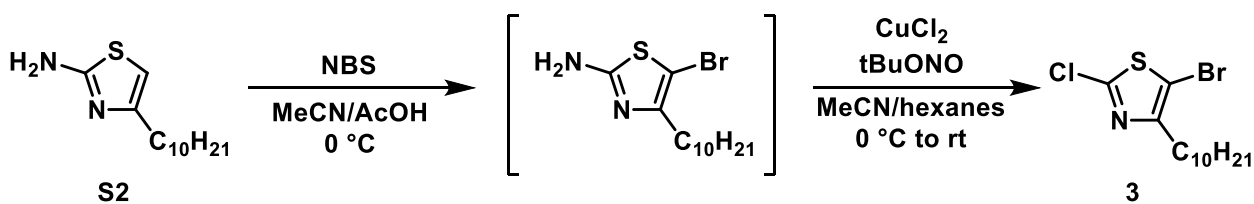
5-Bromo-2-chloro-4-decylthiazole (3).[3] To a 250 mL round-bottom flask equipped with a stir bar, **S2** (2.00 g, 8.32 mmol, 1.00 equiv), acetonitrile (25 mL), and acetic acid (1.5 mL, glacial) were added sequentially. After **S2** had completely dissolved, the solution was cooled to 0 °C using an ice-water bath. *N*-Bromosuccinimide (1.48 g, 8.32 mmol, 1.00 equiv) was added portionwise over 10 min. The reaction solution was kept at 0 °C for 2.5 h and then diluted with EtOAc (25 mL), then washed sequentially with NaHCO$_3$ (3 x 30 mL, satd. DI H$_2$O solution), DI H$_2$O (2 x 25 mL), and brine (2 x 25 mL). The organic layer was dried over MgSO$_4$ and concentrated to give a dark red oil. ^{1}H NMR spectroscopic analysis of the crude product showed quantitative conversion of **S2**. 5-Bromo-4-decylthiazol-2-amine decomposed when purified further; for this reason, the crude material was carried through to the chlorination without further purification.

Anhydrous copper(II) chloride (1.58 g, 11.7 mmol, 1.41 equiv) was added to a hot oven-dried 500 mL Schlenk flask with a stir bar, which was sealed with a septum

and cooled to rt under vaccum to remove adventitious H_2O. Acetonitrile (100 mL) was injected via syringe and the heterogeneous mixture was cooled to 0 °C using an ice-water bath. Subsequently, *tert*-butyl nitrite (2.52 mL, 21.2 mmol, 2.55 equiv) was injected into the mixture using a syringe, followed by crude 5-bromo-4-decylthiazol-2-amine (dissolved in 5 mL hexanes). The reaction mixture was warmed to rt and stirred for 19 h. The solvent was removed under vacuum. The resulting solid was dissolved in Et_2O (50 mL). The organic solution was washed sequentially with HCl (3 x 30 mL, 3M in DI H_2O), $NaHCO_3$ (2 x 30 mL, satd. in DI H_2O), DI H_2O (30 mL), brine (2 x 30 mL), dried over $MgSO_4$, and concentrated. The crude product was purified by column chromatography (eluting with hexanes) to give 0.876 g of **3** as a colorless oil (31% yield). HRMS (ESI+): Calcd. for $C_{13}H_{21}BrClNS$ [M+H]+ 338.0339; found 338.0332.
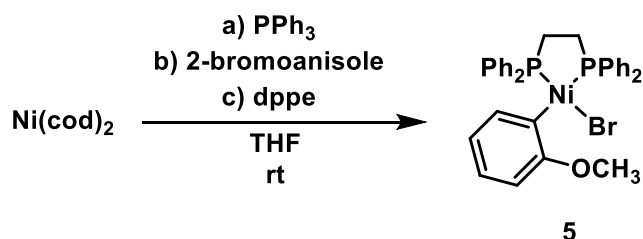
[1,2-bis(diphenylphosphino)ethane](2-methoxyphenyl)nickel(II) bromide (5).[4] In a glovebox, bis(1,5-cyclooctadiene)nickel(0) (84.9 mg, 0.309 mmol, 1.00 equiv) and triphenylphosphine (162 mg, 0.617 mmol, 2.00 equiv) were added to a 20 mL vial with a stir bar. The solids were dissolved in THF (4 mL), and the solution was stirred for 5 min. Subsequently, 2-bromoanisole (86.6 mg, 0.463 mmol, 1.50 equiv) was added and the reaction solution was stirred for 2 h. Then, 1,2-bis(diphenylphosphino)ethane (111 mg, 0.278 mmol, 0.900 equiv) was added and the reaction solution stirred for 2 h. Subsequently, hexanes (15 mL) were added, and the sealed vial was placed in a -30 °C glovebox freezer for 18 h. The resulting orange solid was isolated by filtration and recrystallized from 1:8 DCM/hexanes to give 134 mg of **5** as an orange solid (75% yield). HRMS (ESI+): Calcd. for $C_{33}H_{31}BrNiOP_2$ [M-Br]+ 563.1198; found 563.1200.
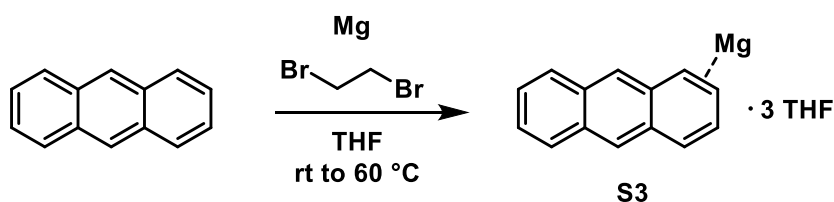
Magnesium anthracene · 3 THF (S3).[5] Magnesium turnings (98.6 mg, 4.06 mmol, 1.00 equiv) were added to a 20 mL vial with a stir bar in a glovebox. Subsequently, THF (10 mL) and 1,2-dibromoethane (0.25 mL, 2.9 mmol, 0.71 equiv) were added and the heterogeneous mixture was stirred overnight to activate the Mg. Anthracene (723 mg, 4.06 mmol, 1.00 equiv) was added in five

equal portions over 15 min, wherein the mild bubbling subsided before the next addition. The stirred solution remained colorless for approximately 90 min, after which time a rapid color change to dark blue occurred. The reaction mixture was stirred at rt for an additional 16 h, then heated at 60 °C for 12 h. An orange precipitate was then observed. The reaction mixture was cooled to rt and filtered to give an orange solid, which was washed with THF (4 x 20 mL) and dried under vacuum to give 1.33 g of **S3** as an orange-red powder (78% yield).
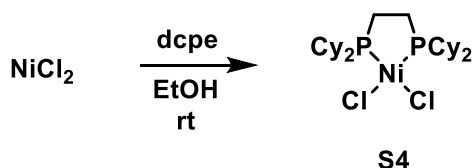
[1,2-bis(dicyclohexylphosphino)ethane]nickel(II) chloride (S4).[6] Nickel(II) chloride (103 mg, 0.795 mmol, 1.00 equiv) and 1,2-bis(dicyclohexylphosphino)ethane (305 mg, 0.722 mmol, 0.908 equiv) were added to a 100 mL Schlenk flask equipped with a stir bar in a glovebox. The reaction vessel was sealed with a septum, then brought out of the glovebox and placed under N_2 on a Schlenk line. Then, EtOH (35 mL, sparged for 1 h with N_2) was added via syringe. The reaction mixture was stirred at rt for 2 h, then filtered to isolate an orange solid. This solid was dissolved in DCM, filtered, and the solvent removed under vacuum to give 373 mg of **S4** as an orange solid (94% yield).
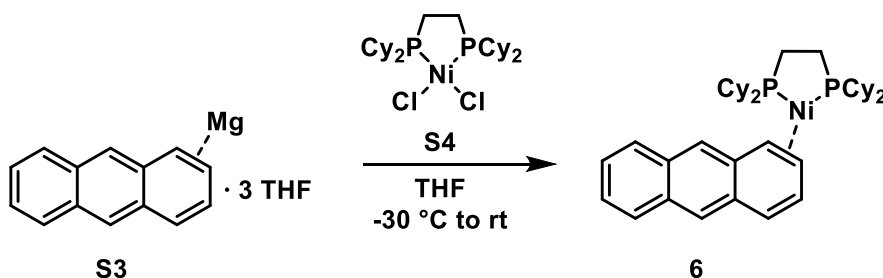
[1,2-bis(dicyclohexylphosphino)ethane]nickel(0)-anthracene π-complex (8).[7] In a glovebox, **S3** (41.5 mg, 0.0991 mmol, 1.00 equiv) and **S4** (54.7 mg, 0.0991 mmol, 1.00 equiv) were added to separate 20 mL vials with stir bars. To each vial, THF (3 mL) was added and then both vials were sealed and placed in a -30 °C glovebox freezer for 20 h. Immediately after removing the vials from the freezer, the nickel suspension was added dropwise to the magnesium suspension using a pipette. The reaction solution was warmed to rt over 90 min. Complete consumption of **S4** was confirmed by ^{31}P NMR spectroscopy. The solvent was removed under reduced pressure, and the dark purple solids were dissolved in hexanes and filtered. Hexanes were removed under reduced pressure to give 65.3 mg of **8** as a deep purple solid (56% yield).

S5
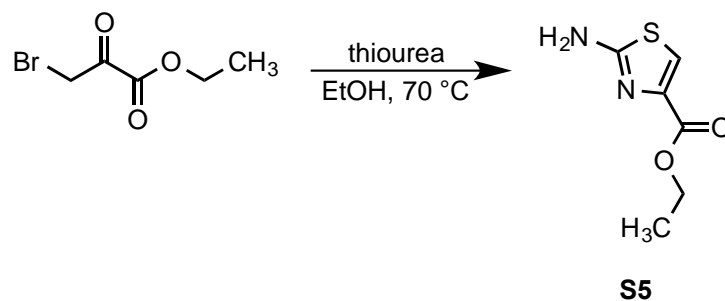
2-amino-4-(ethylcarboxy)-thiazole (S5) In a 250 mL round-bottom flask with a stir bar, thiourea (2.03 g, 26.7 mmol, 1.04 equiv) was added to a stirring solution of ethyl bromopyruvate (3.22 mL, 25.7 mmol, 1.00 equiv) and EtOH (50 mL). The mixture was stirred vigorously at reflux (70 °C) for 60 min. Then the reaction vial was moved to a -20 °C freezer to effect crystallization. After 18 h, the mother liquor was decanted and the remaining white solid was washed with Et_2O (3 x 20 mL), then DI H_2O (15 mL) and satd. aq. Na_2CO_3 (30 mL) were added to the solid in a 250 mL round-bottom flask. Agitating the mixture transformed the white solid into a less dense white solid. The solid was collected by filtration over a 500 mL Buchner funnel, washed with DI H_2O (3 x 20 mL), collected, and dried under reduced pressure. The original organic mother liquor was collected in a 250 mL round-bottom flask, concentrated under reduced pressure, then DI H_2O (10 mL) and satd. aq. Na_2CO_3 (20 mL) were added. Agitating the mixture led to a pale yellow solid. The solid was collected by filtration over a 500 mL Buchner funnel, washed with DI H_2O (3 x 20 mL), collected, and dried under reduced pressure. The solids were combined, yielding 3.98 g of **S5** (90% yield). HRMS (ESI+): Calcd. for $C_6H_8N_2O_2S$ [M+H]+ 173.0379; found 173.0375.
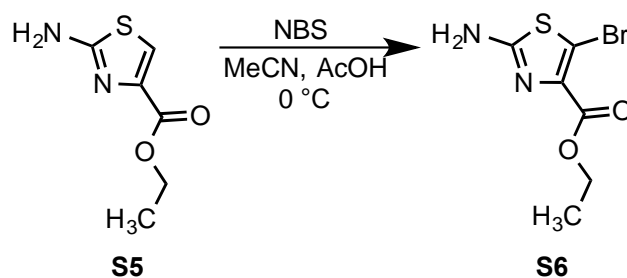
2-amino-5-bromo-4-(ethylcarboxy)-thiazole (S6) To a 250 mL round-bottom flask with a stir bar, **S5** (3.01 g, 17.5 mmol, 1.03 equiv), acetonitrile (51.5 mL), and AcOH (3.4 mL) were added. The pale yellow solution was cooled to 0 °C using an ice-water bath. *N*-Bromosuccinimide (3.03 g, 17.0 mmol, 1.00 equiv) was added to the reaction vial over 10 min, effecting color change from yellow to red. After 2.5 h, the solution was diluted with EtOAc (40 mL) and sequentially washed with satd. aq. Na_2CO_3 (4 x 50 mL), DI H_2O (1 x 50 mL), and brine (3 x 50 mL). The organic layer was dried over $MgSO_4$, filtered and moved to a -20 °C freezer to effect crystallization. After 18 h, a pale yellow solid was collected by

filtration and washed with cold EtOAc (3 x 10 mL), to yield a pale yellow solid. The filtrate was collected, concentrated by rotary evaporation, crystallized at -20 °C in EtOAc (10 mL), collected by filtration and washed with cold EtOAc (3 x 10 mL) to yield a pale yellow solid. The collected solids were combined and dried under reduced pressure to yield 2.77 g of **S6** (65% yield). HRMS (ESI+): Calcd. for $C_6H_7BrN_2O_2S$ [M+Na]+ 272.9304; found 272.9306.

S6   **S7**
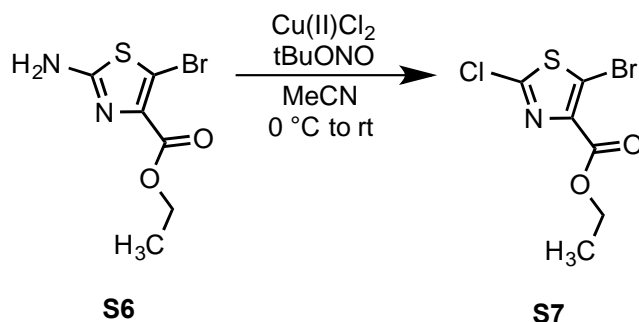
5-bromo-2-chloro-4-(ethylcarboxy)-thiazole (S7) To a hot, oven-dried 50 mL Schlenk flask with a stir bar was added $Cu(II)Cl_2$ (901 mg, 6.70 mmol, 1.50 equiv) which was sealed with a septum and cooled to rt under vacuum to remove adventitious H_2O, evidenced by color change from blue to brown. The flask was then filled with N_2. Dry, sparged acetonitrile (12 mL) was injected into the reaction flask via syringe and the heterogeneous mixture was cooled to 0 °C using an ice-water bath. Subsequently, tert-butyl nitrite (1.4 mL, 12 mmol, 2.7 equiv) was injected into the mixture using a syringe. A solution of **S6** (1.12 g, 4.50 mol, 1.00 equiv) in dry, sparged acetonitrile (22 mL) was injected dropwise into the flask using a syringe over 20 min. The flask was evacuated for 30 s to remove adventitious air, and then refilled with N_2. The reaction was warmed to rt and stirred for 14.5 h. The solvent was removed under reduced pressure resulting in a dark red viscous oil, which was dissolved in Et_2O (30 mL). The organic solution was washed sequentially with aq. 0.6M HCl (3 x 30 mL), DI H_2O (3 x 30 mL), satd. aq. Na_2CO_3 (3 x 30 mL), brine (3 x 30 mL), dried over $MgSO_4$, and concentrated to a red oil that was filtered over a silica plug using hexanes (10 mL), and concentrated to yield 910 mg of **S7** as an orange oil that becomes solid when cooled to 4 °C (73% yield). HRMS (ESI+): Calcd. for C_6H_5BrCl [M+H]+ 269.8986; found 269.8986.

S7   **S8**   **S9**
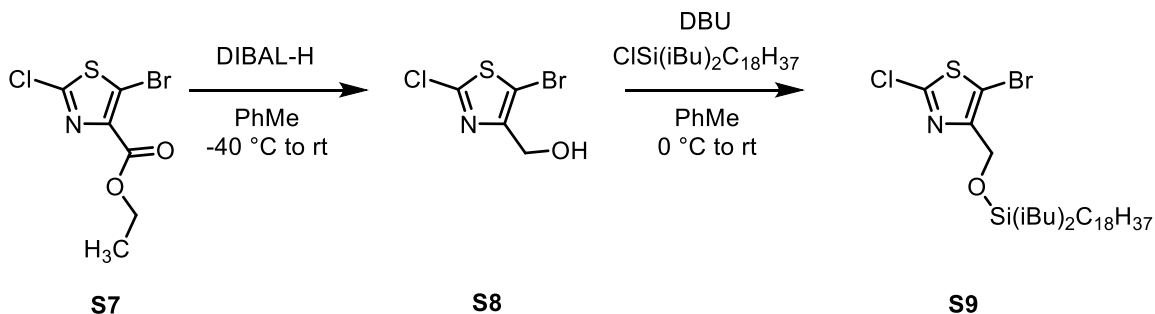
5-bromo-2-chloro-4-(methanolyl)-thiazole (S8) To an oven-dried 50 mL Schlenk flask with a stir bar was added **S7** (900 mg, 3.33 mmol, 1.00 equiv) which was sealed with a septum and cooled to rt under vacuum, then filled with N_2. The flask was charged with dry toluene (25 mL) and cooled to -40 ºC using an acetone/dry-ice bath over 5 min. Diisobutylaluminium hydride (DIBAL-H) (1.0 M in hexane, 6.7 mL, 6.7 mmol, 2.0 equiv) was injected into the **S7**/toluene solution dropwise. The solution was gradually warmed to rt while stirring for 20 h, and then quenched with DI H_2O (24 mL) and acidified with 12 M HCl (~0.5 mL) (initial pH = 5, final pH <1). The organic layer was separated and the aqueous layer was extracted with Et_2O (2 x 20 mL). The organic layers were combined and washed with brine (3 x 30 mL), dried over $MgSO_4$, concentrated, and dried under reduced pressure to yield 633 mg of **S8** as a brown viscous oil that forms a solid at 4 °C (83% crude yield). The resulting **S8** was carried through to silylation without further purification. HRMS (ESI+): Calcd. for $C_4H_3BrClNOS$ [M+] 226.8807; found 226.8806.

5-bromo-2-chloro-4-(diisobutyloctadecylsilyloxymethyl)-thiazole (S9)
An oven-dried 50 mL Schlenk flask with a stir bar was sealed with a septum and cooled to rt under vacuum, then filled with N_2. The flask was charged with a solution of **S8** (630 mg, 2.76 mmol, 1.00 equiv) in dry toluene (14.8 mL). Subsequently, 1,8-diazabicycloundec-7-ene (DBU) (2.0 mL, 13 mmol, 5.0 equiv) was injected into the **S8**/toluene solution. The solution was cooled to 0 °C using an ice-water bath. Then, chlorodiisobutyloctadecylsilane (1.3 mL, 2.7 mmol, 1.0 equiv) was added dropwise. The solution was stirred for 30 min at 0 °C, the ice-water bath was removed and the reaction was stirred for an additional 1 h. The reaction was quenched with DI H_2O (24 mL), transferred to a separatory funnel using Et_2O (30 mL). The organic layer was washed with DI H_2O (3 x 20 mL) and brine (3 x 20 mL), dried over $MgSO_4$, filtered, and concentrated to yield a yellow oil which was purified via column chromatography (deactivated neutral Al_2O_3, eluting with 99:1 hexanes:toluene (v/v)), which furnished 915 mg of **S9** as a clear, colorless oil (53% yield) HRMS (ESI+): Calcd. for $C_{30}H_{57}BrClNOSSi$ [M+H]+ 622.2875; found 622.2876.

10
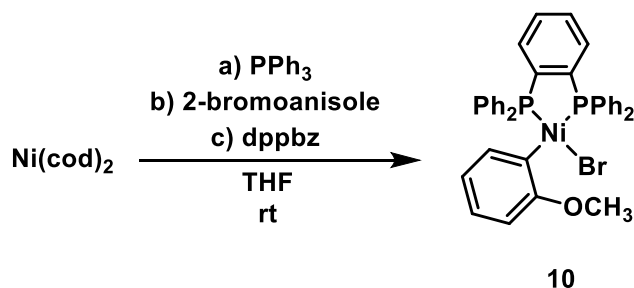
[1,2-bis(diphenylphosphino)benzene](2-methoxyphenyl)nickel(II) bromide (10). In a glovebox, Ni(cod)$_2$ (64.8 mg, 0.236 mmol, 1.00 equiv) and PPh$_3$ (124 mg, 0.471 mmol, 2.00 equiv) were added to a 20 mL vial with a stir bar. The solids were dissolved in THF (3 mL) and the solution was stirred for 5 min. Subsequently, 2-bromoanisole (66.1 mg, 0.353 mmol, 1.50 equiv) was added and the reaction solution was stirred for 2 h. Then, 1,2-bis(diphenylphosphino)benzene (94.7 mg, 0.212 mmol, 0.900 equiv) was added and the reaction solution was stirred for 2 h. Subsequently, hexanes (15 mL) were added and the sealed vial was placed in a -30 °C glovebox freezer for 18 h. The resulting orange solid was isolated by filtration and recrystallized from 1:8 DCM/hexanes to give 131 mg of **10** as an orange solid (80% yield). HRMS (ESI+): Calcd. for C$_{37}$H$_{31}$BrNiOP$_2$ [M-Br]$^+$ 611.1198; found 611.1200.

IV. NMR Spectra

Figure S2.1. ^1H and ^{13}C NMR spectra of **S1**. ^1H NMR (500 MHz, CDCl$_3$) δ 3.88 (s, 2H), 2.64 (t, J = 7.4 Hz, 2H), 1.65–1.56 (m, 2H), 1.38–1.15 (m, 14H), 0.88 (t, J = 6.9 Hz, 3H). ^{13}C NMR (126 MHz, CDCl$_3$) δ 202.16, 39.76, 34.17, 31.78, 29.44, 29.33, 29.21, 29.19, 28.94, 23.78, 22.57, 14.01.

114

Figure S2.2.2. ^{1}H and ^{13}C NMR spectra of **S2**. ^{1}H NMR (700 MHz, CDCl$_3$) δ 6.08 (s, 1H), 4.84 (s, 2H), 2.52 (t, J = 7.7 Hz, 2H), 1.70–1.53 (m, 2H), 1.40–1.11 (m, 14H), 0.88 (t, J = 6.9 Hz, 3H). ^{13}C NMR (126 MHz, CDCl$_3$) δ 167.37, 154.12, 102.58, 32.31, 32.16, 30.02, 30.00, 29.86, 29.74, 29.74, 29.23, 23.09, 14.52.

Figure S2.3. ¹H and ¹³C NMR spectra of **1**. ¹H NMR (500 MHz, CDCl₃) δ 2.69 (t, *J* = 7.6 Hz, 2H), 1.70–1.60 (m, 2H), 1.35–1.19 (m, 14H), 0.88 (t, *J* = 6.8 Hz, 3H). ¹³C NMR (126 MHz, CDCl₃) δ 157.07, 134.44, 105.79, 32.28, 32.24, 29.96, 29.91, 29.87, 29.70, 29.49, 28.99, 23.07, 14.51.
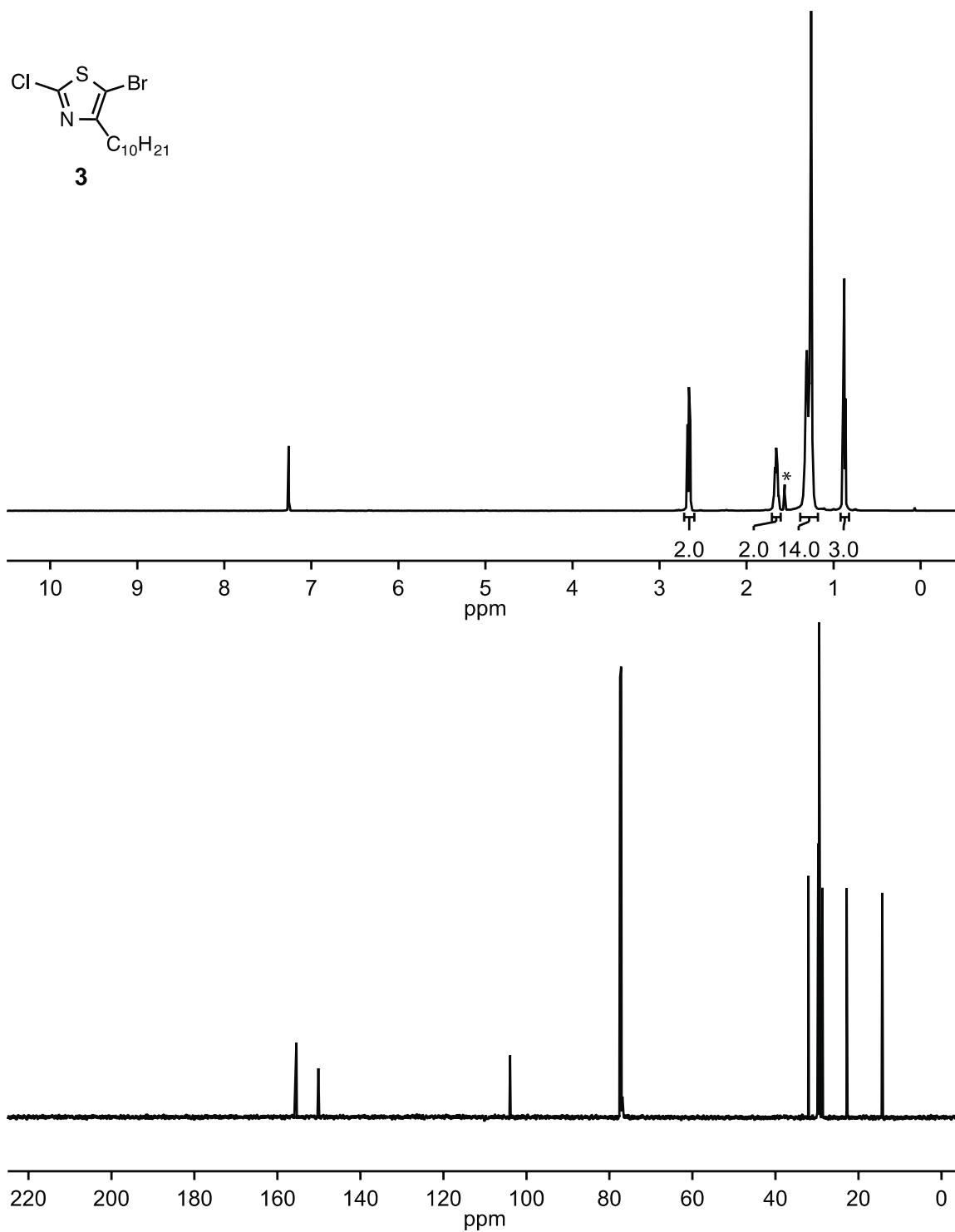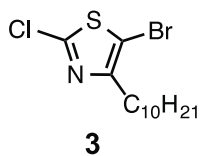
Figure S2.4. ^{1}H and ^{13}C NMR spectra of **3**. ^{1}H NMR (500 MHz, CDCl$_3$)δ 2.66 (t, J = 7.5 Hz, 2H), 1.71–1.60 (m, 2H), 1.37–1.20 (m, 14H), 0.88 (t, J = 6.8 Hz, 3H). ^{13}C NMR (126 MHz, CDCl$_3$) δ 155.43, 150.15, 103.93, 32.05, 29.73, 29.70, 29.67, 29.47, 29.47, 29.24, 28.69, 22.84, 14.27.
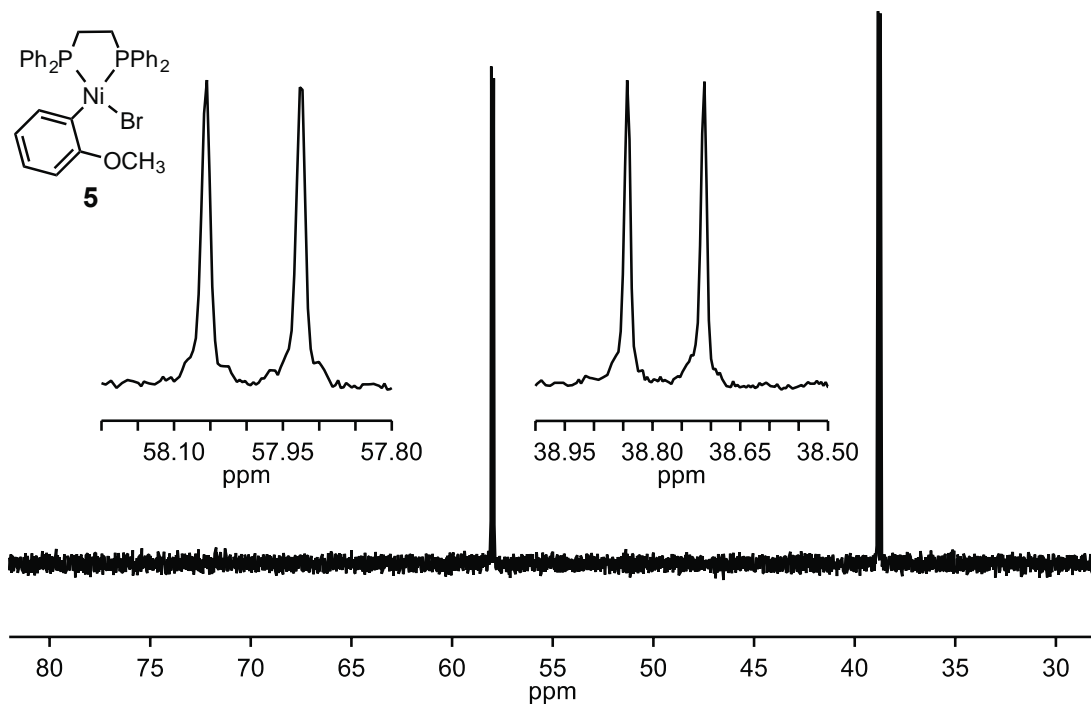
Figure S2.5. ^{31}P NMR spectrum of **5**. ^{31}P NMR (202 MHz, THF) δ 57.99 (d, J_{P-P} = 26.6 Hz), 38.78 (d, J_{P-P} = 26.6 Hz).
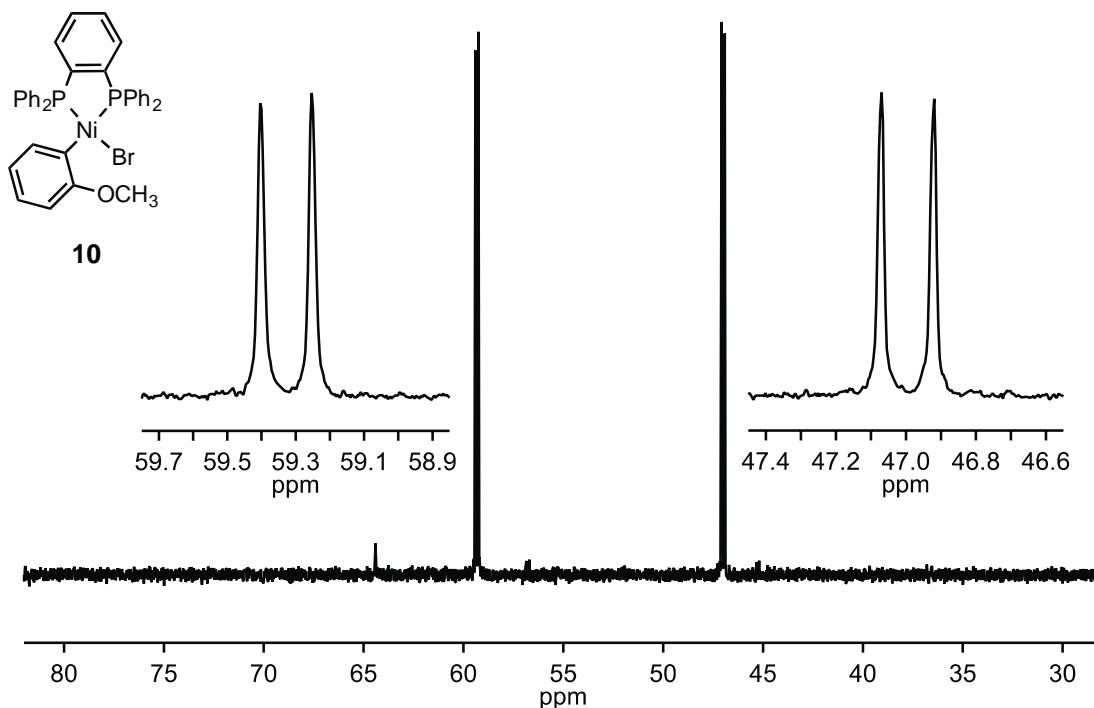
Figure S2.6. ^{31}P NMR spectrum of **10**. ^{31}P NMR (202 MHz, THF) δ 59.33 (d, J_{P-P} = 30.3 Hz), 46.97 (d, J_{P-P} = 30.3 Hz).
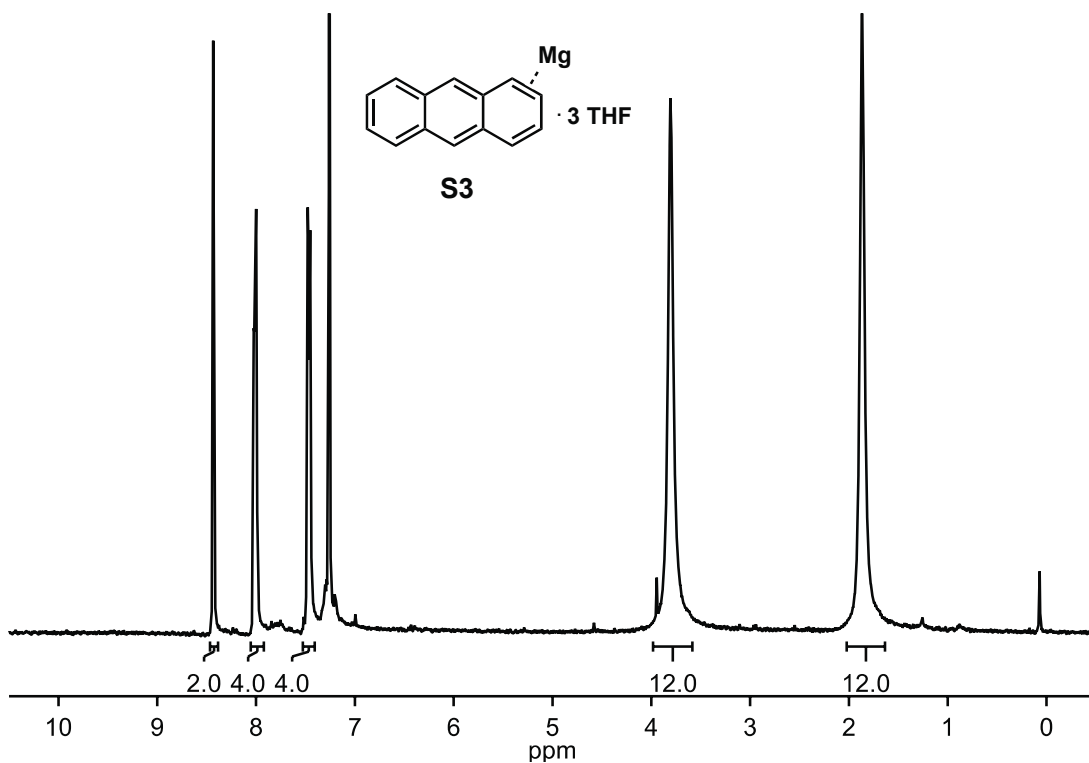
Figure S2.7. ^1H NMR spectrum of **S3**. ^1H NMR (400 MHz, CDCl$_3$) δ 8.43 (s, 2H), 8.05–7.95 (m, 4H), 7.53–7.41 (m, 4H), 3.81 (s, 12H), 1.87 (s, 12H).
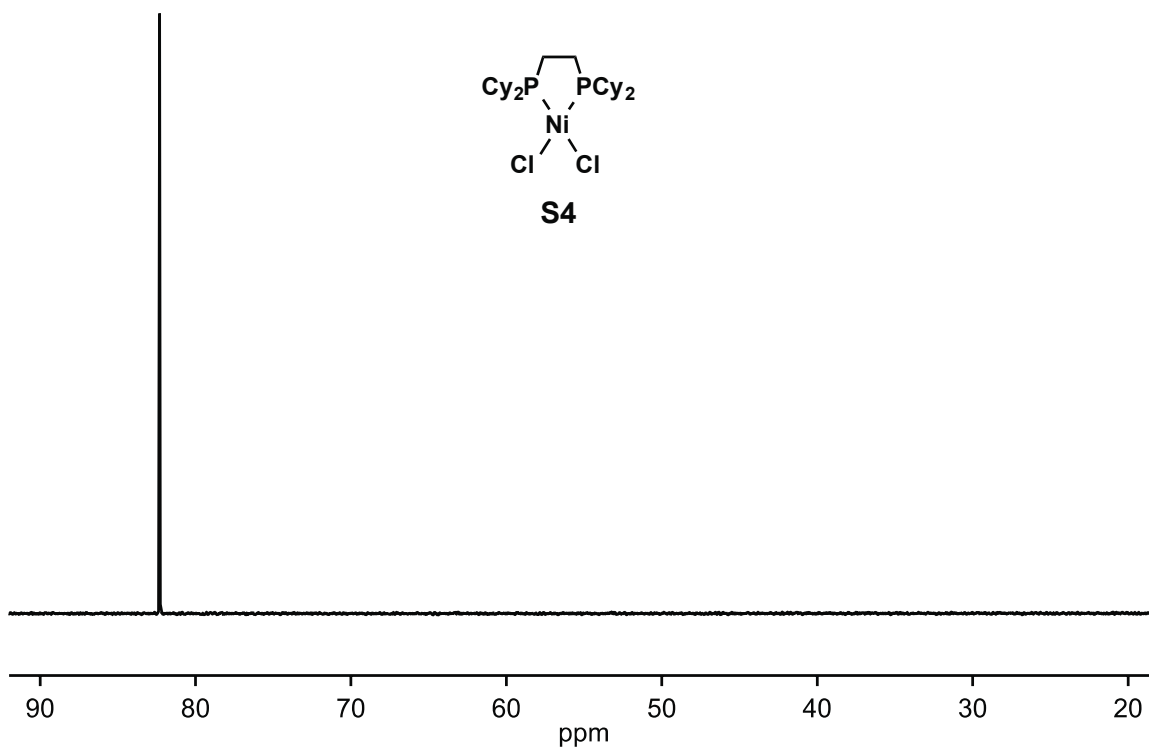
Figure S2.8. ^{31}P NMR spectrum of **S4**. ^{31}P NMR (283 MHz, CDCl$_3$) δ 82.30 (s).
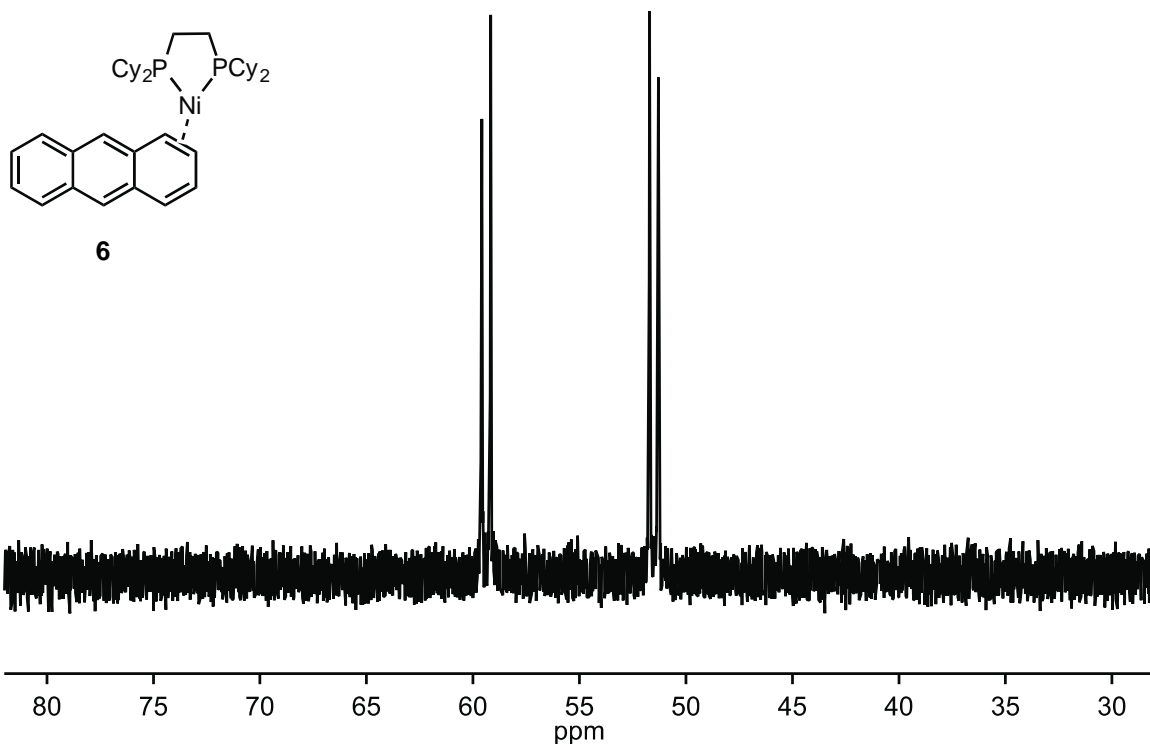
Figure S2.9. ^{31}P NMR spectrum of **6**. ^{31}P NMR (162 MHz, d$_8$-THF) δ 59.38 (d, $J_{P\text{-}P}$ = 68.0 Hz), 51.50 (d, $J_{P\text{-}P}$ = 68.0 Hz).
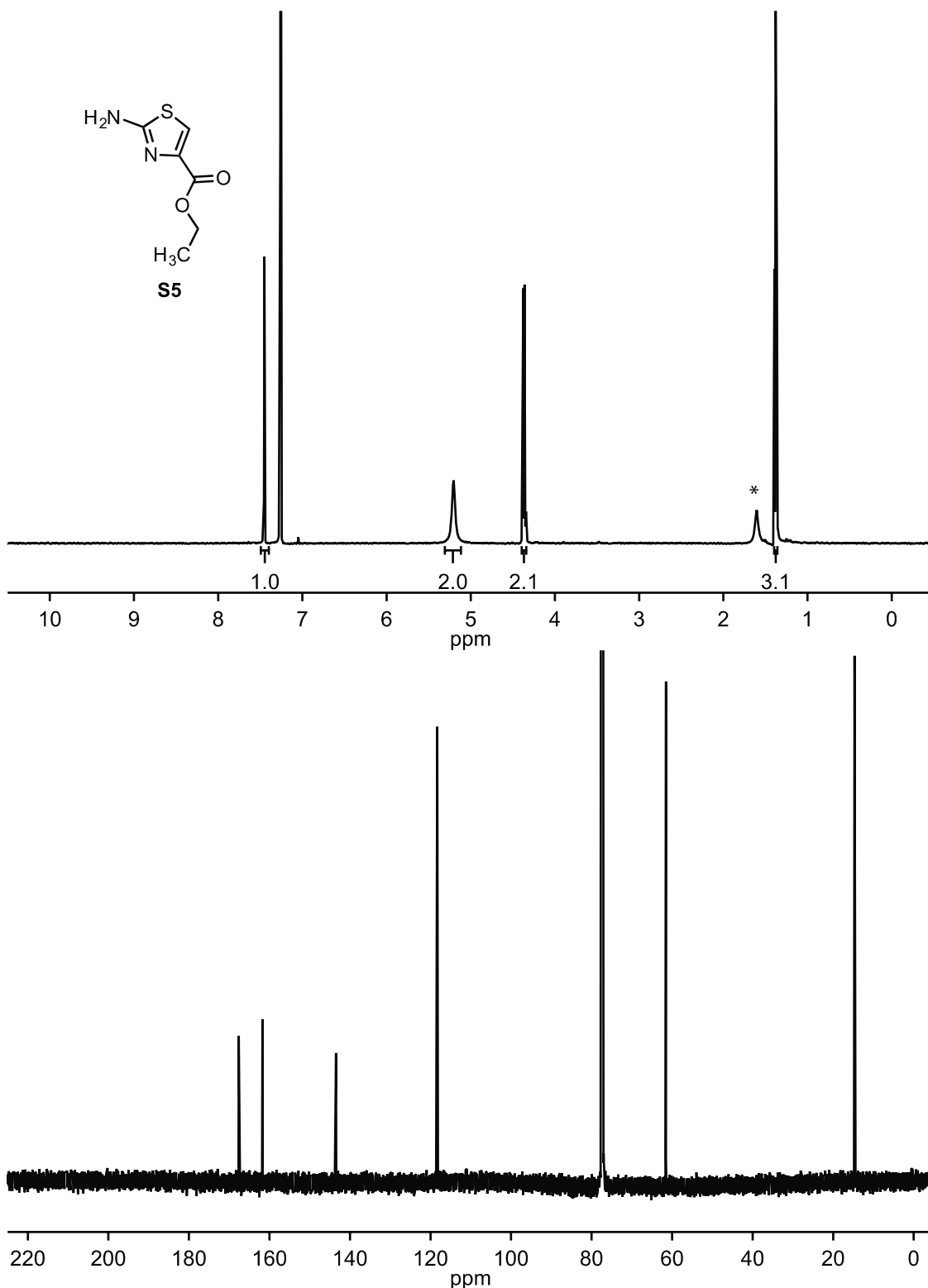
Figure S2.10. ¹H and ¹³C NMR spectra of **S5**. ¹H NMR (500 MHz, CDCl₃) δ 7.45 (s, 1H), 5.21 (s, 2H), 4.37 (q, *J* = 7.1 Hz, 2H), 1.38 (t, *J* = 7.1 Hz, 3H). ¹³C NMR (176 MHz, CDCl₃) δ 167.61, 161.75, 143.48, 118.31, 61.52, 14.71.
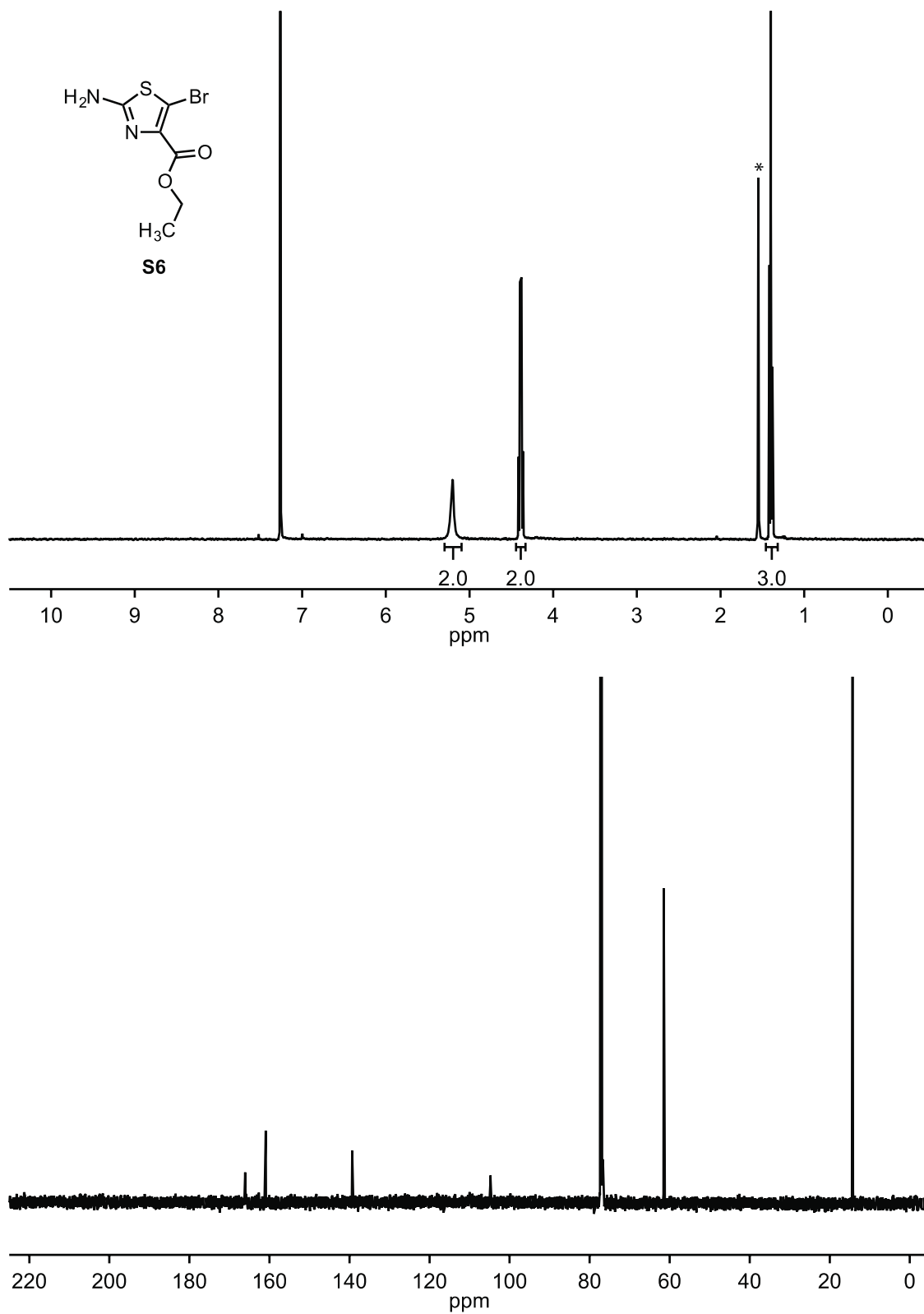
Figure S2.11. ^{1}H and ^{13}C NMR spectra of **S6**. ^{1}H (400 MHz, CDCl$_3$) δ 5.20 (s, 2H), 4.39 (q, J = 7.1 Hz, 2H), 1.40 (t, J = 7.1 Hz, 3H). ^{13}C NMR (126 MHz, CDCl$_3$) δ 166.50, 161.37, 139.76, 105.21, 61.89, 14.72.
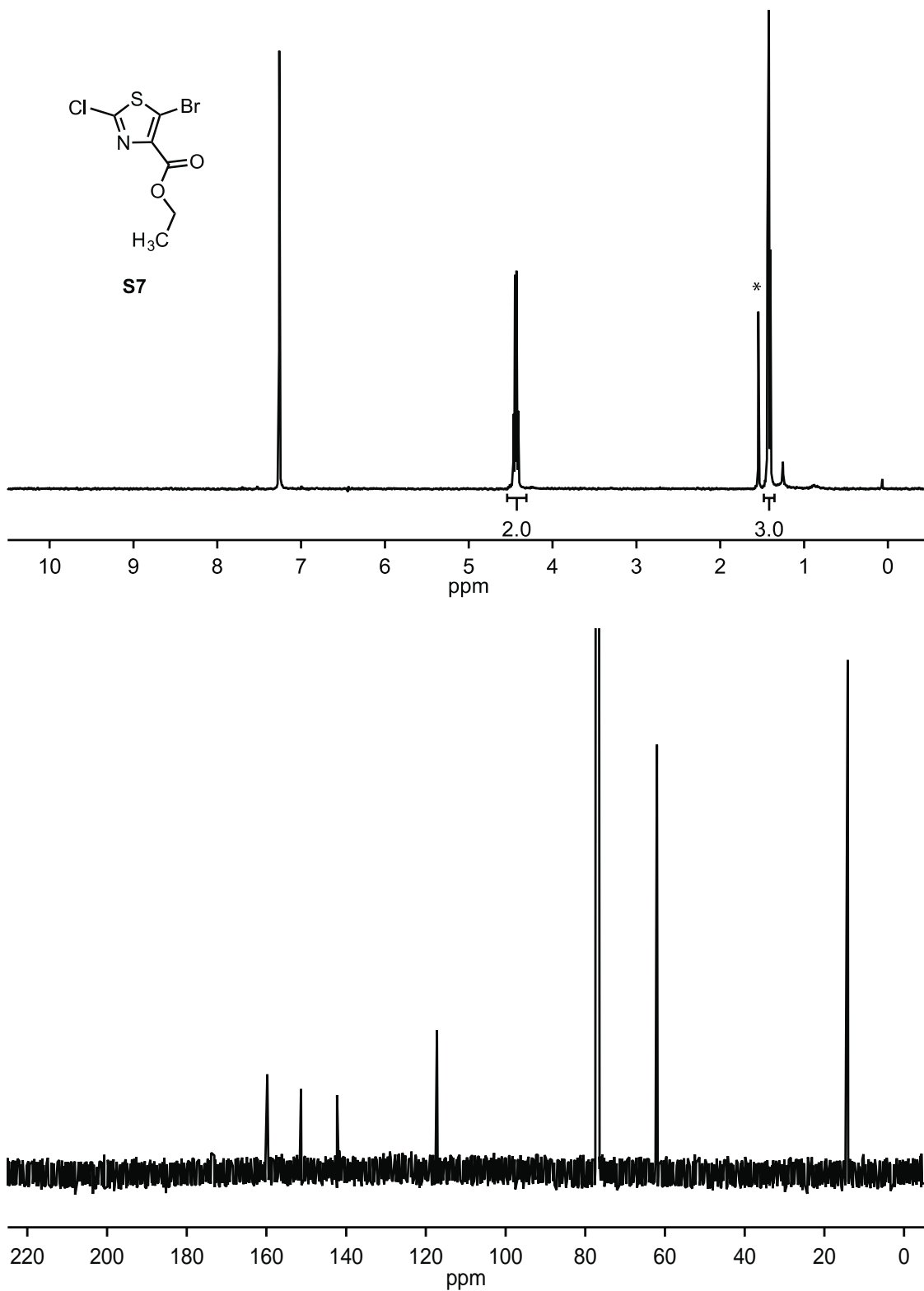
Figure S2.12. ^{1}H and ^{13}C NMR spectra of **S7**. ^{1}H NMR (400 MHz, CDCl$_3$) δ 4.44 (q, J = 7.1 Hz, 2H), 1.42 (t, J = 7.1 Hz, 3H). ^{13}C NMR (126 MHz, CDCl$_3$) δ 159.94, 151.68, 142.95, 117.71, 62.39, 14.27.
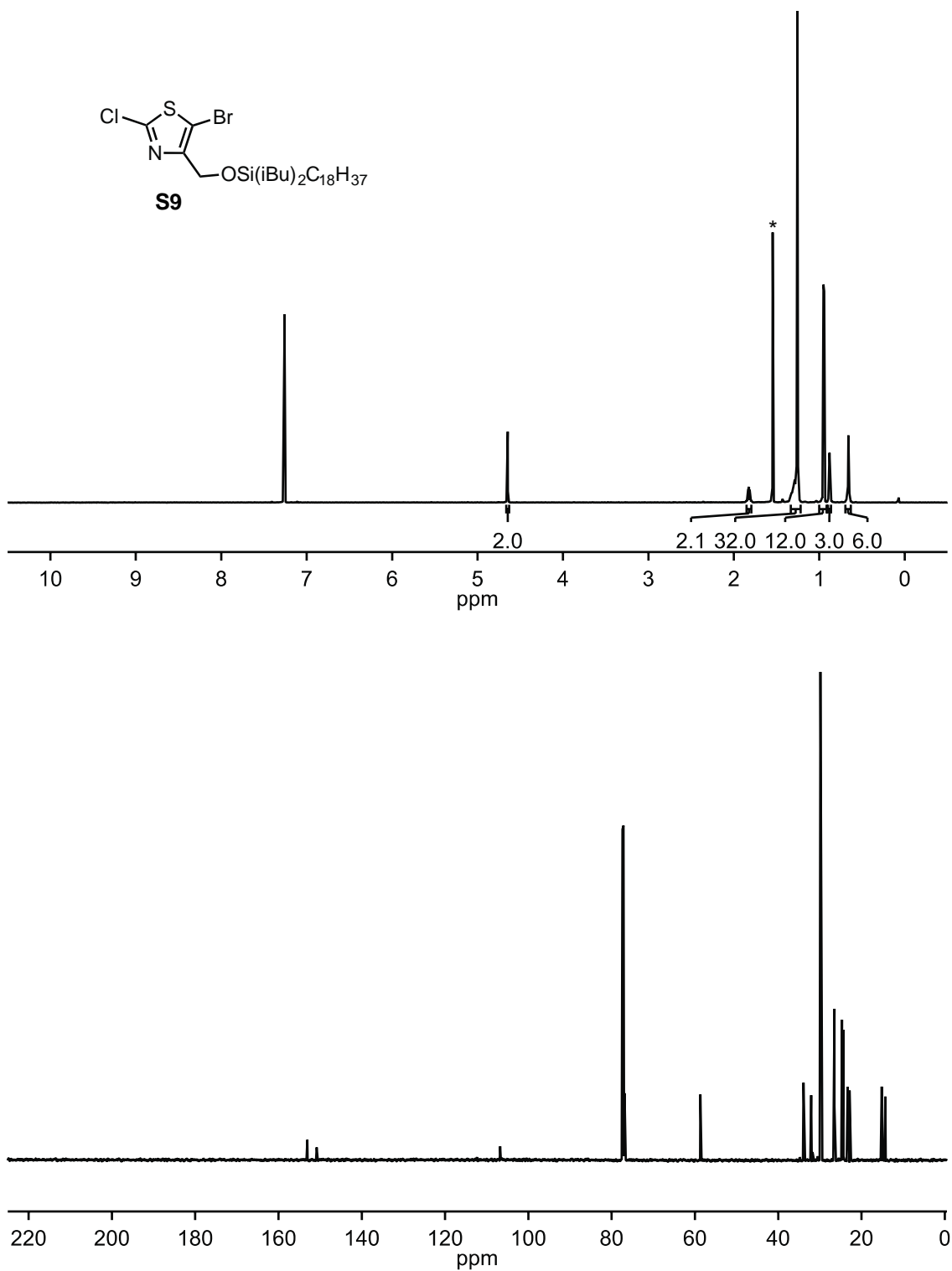
Figure S2.13. ^{1}H and ^{13}C NMR spectra of **S9**. ^{1}H NMR (700 MHz, CDCl$_3$) δ 4.65 (s, 2H), 1.89–1.77 (non, J = 6.7 Hz, 2H), 1.25 (m, 32H), 0.95 (d, J = 6.6 Hz, 12H), 0.88 (t, J = 7.0 Hz, 3H), 0.71–0.56 (m, 6H). ^{13}C NMR (126 MHz, CDCl$_3$) δ 153.08, 150.82, 106.76, 58.70, 33.92, 32.09, 29.82, 29.77, 29.53, 29.48, 26.54, 26.50, 24.70, 24.33, 23.35, 22.85, 15.14, 14.28.

V. Monomer Activation Experiments: Regioselectivity and Oligomer Formation

A. Regioselectivity of the reaction of 1 with iPrMgCl
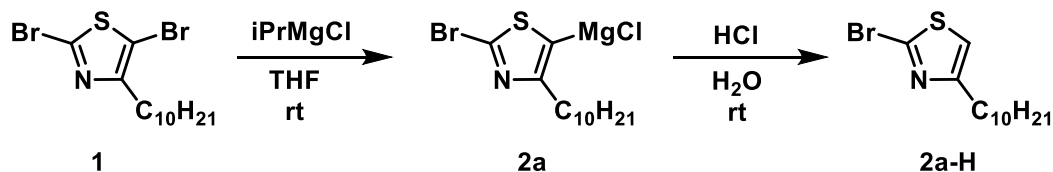
In a glovebox, **1** (400 mg, 1.04 mmol, 1.00 equiv) was added to a 4 mL vial with a stir bar. THF (3 mL) was added. Subsequently, iPrMgCl (0.47 mL, 2M in THF, 0.94 mmol), 0.9 equiv) was added to this solution. The reaction solution was stirred for 10 min, then removed from the glovebox and poured into HCl (5 mL, 5M in DI H_2O). The organic products were extracted from the resulting aqueous mixture with $CHCl_3$ (5 mL). Column chromatography (2 to 15% EtOAc in hexanes solvent gradient) was used to isolate 47.2 mg of **2a-H** (2-bromo-4-decylthiazole) as a colorless oil (16% yield).
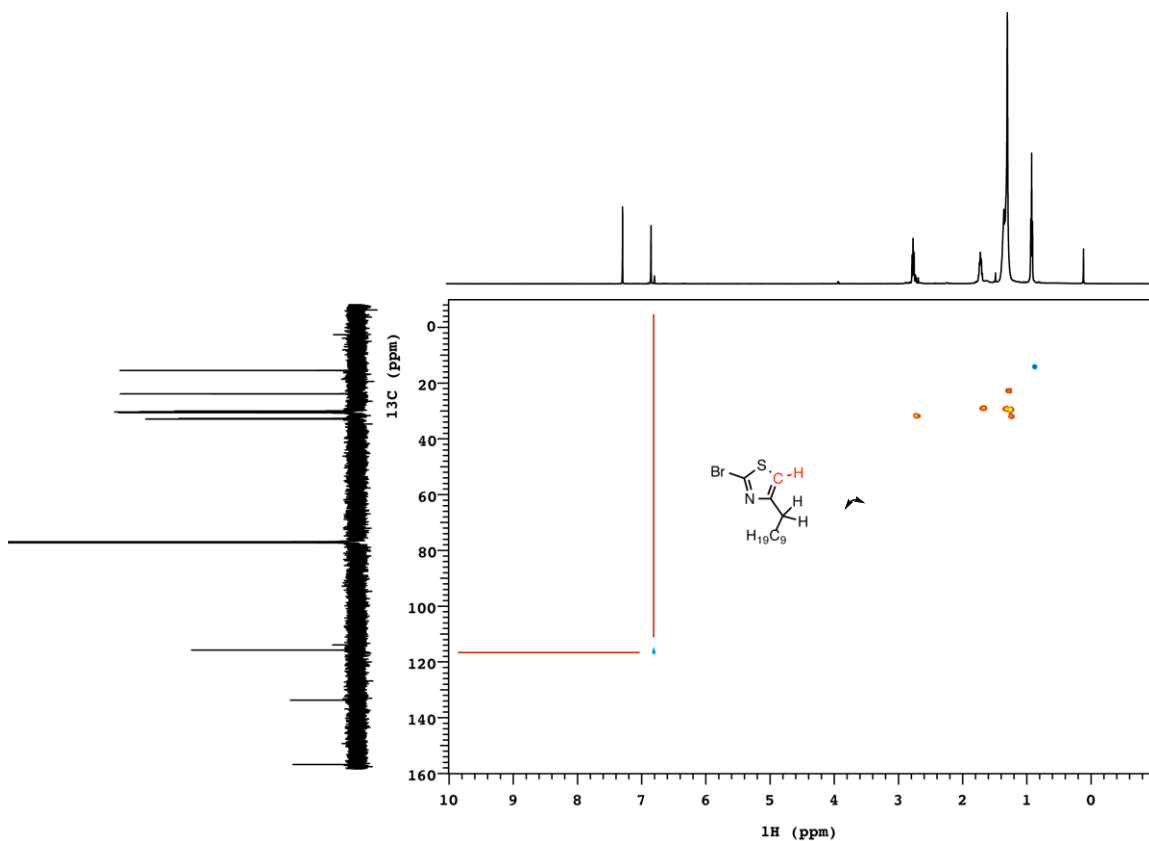
Figure S2.14. gHSQC of **2a-H**. F2 = ^{1}H (500 MHz, $CDCl_3$), F1 = ^{13}C.

Figure S2.15. gHMBC of **2a-H**. F2 = ^{1}H (500 MHz, CDCl$_3$), F1 = ^{13}C.
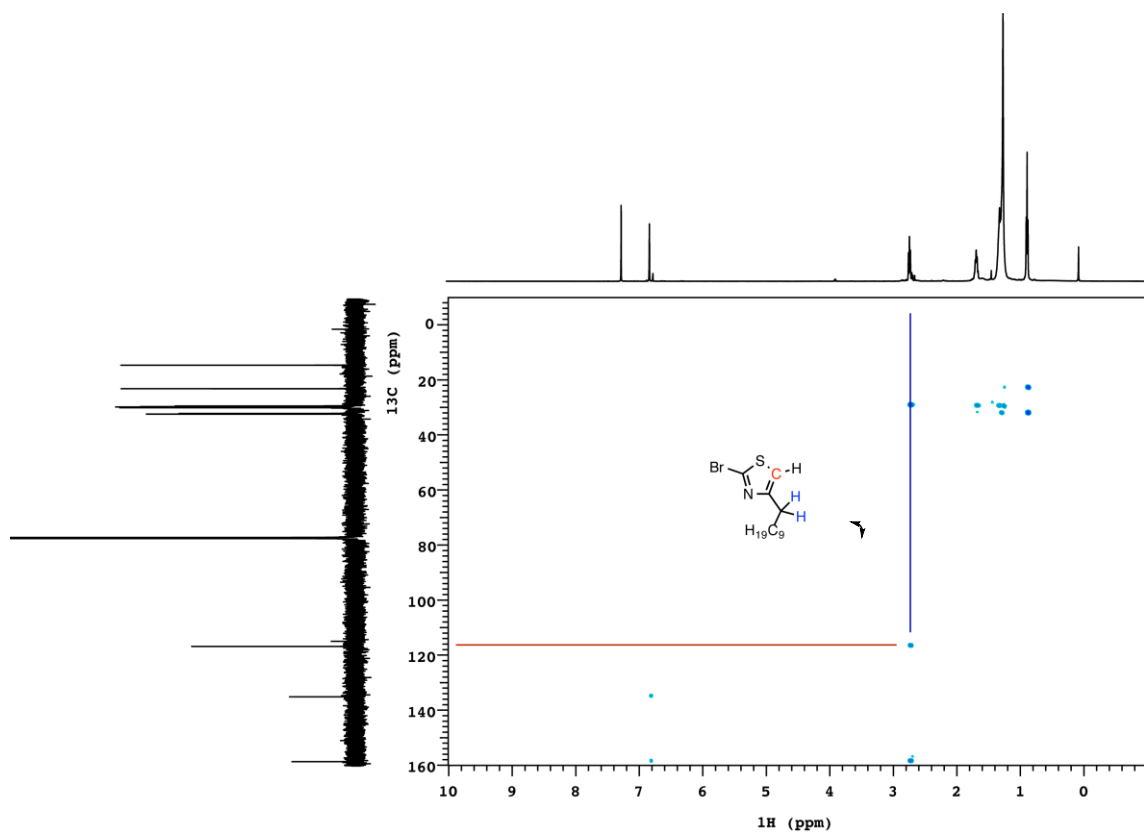
B. Formation of oligomers in the reaction of 1 with iPrMgCl
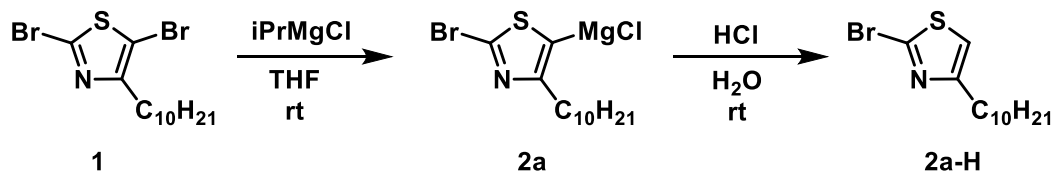
In a glovebox, **1** (59.2 mg, 0.154 mmol, 1.00 equiv) was added to a 4 mL vial with a stir bar. THF (2 mL) was added. Subsequently, iPrMgCl (69.5 µL, 2M in THF, 0.139 mmol, 0.903 equiv) was added to this solution. The reaction solution was stirred for 16 h, then removed from the glovebox and poured into HCl (5 mL, 5M in DI H_2O). The organic products were extracted from the resulting aqueous mixture with $CHCl_3$ (5 mL). The solvent was removed under vacuum, and then the organic products were redissolved in THF, dried over $MgSO_4$, filtered, and analyzed by GPC. M_n = 1.4 kDa, Đ = 1.5.
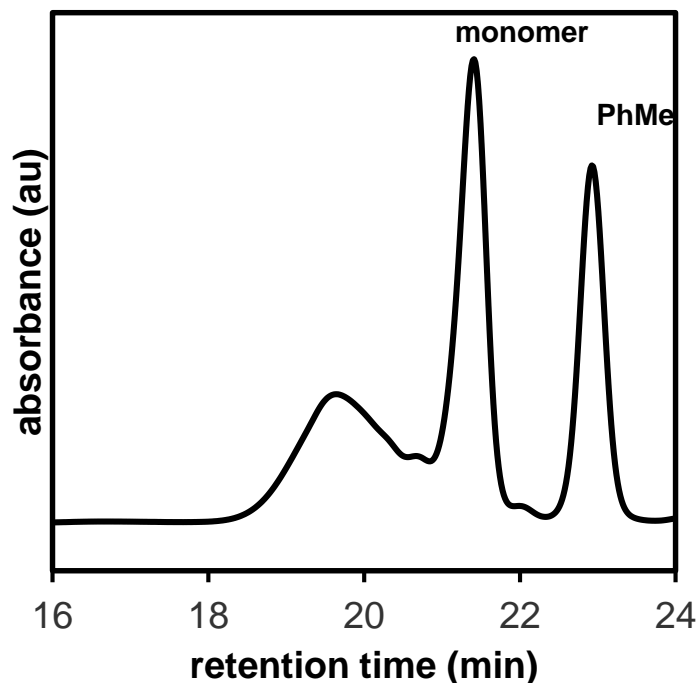
Figure S2.16. GPC trace of the reaction of **1** with iPrMgCl after 16 h at rt.

C. Regioselectivity and formation of oligomers in reaction of 1 with iPr₃PhMgBr
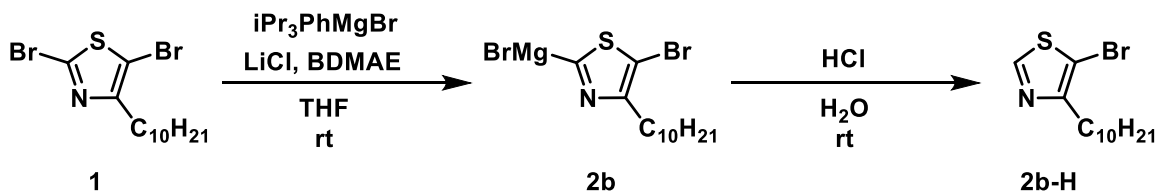
In a glovebox, **1** (51.8 mg, 0.135 mmol, 1.00 equiv) and LiCl (5.8 mg, 0.13 mmol, 0.95 equiv) were added to a 4 mL vial with a stir bar. THF (2 mL) was added, then bis(2-dimethylaminoethyl) ether (24.0 µL, 0.128 mmol, 0.948 equiv) was added. Subsequently, 2,4,6-iPr₃PhMgBr (0.257 mL, 0.5M in THF, 0.128 mmol, 0.948 equiv) was added to this mixture. The reaction solution darkened over the course of 10 min, and was then removed from the glovebox and poured into HCl (5 mL, 5M in DI H₂O). The organic products were extracted from the resulting aqueous mixture with CHCl₃ (5 mL). The solvent was removed under vacuum, and then the organic products were redissolved in THF, dried over MgSO₄, filtered, and analyzed by GPC. M_n = 0.85 kDa, Đ = 1.4. Following GPC analysis, the product was purified using column chromatography with a 2 to 15% EtOAc in hexanes solvent gradient to isolate 3.5 mg of **2b-H** as a colorless oil (9% yield).
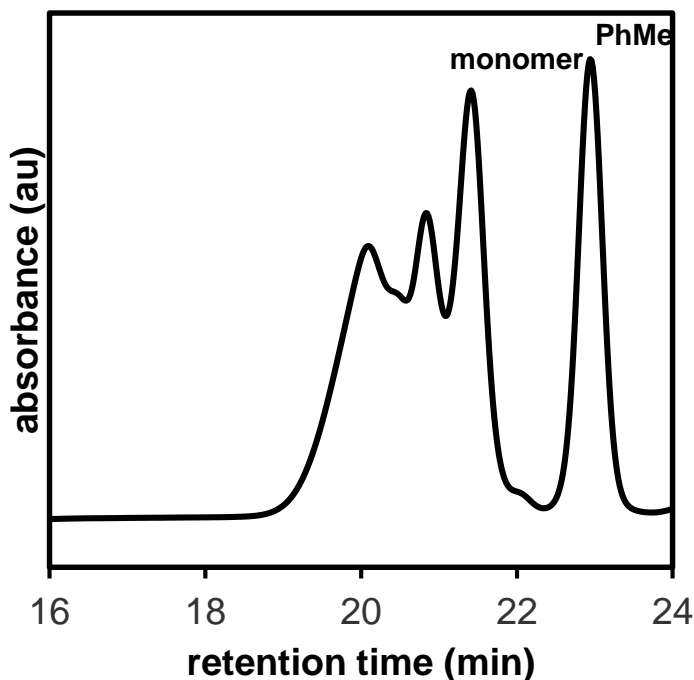
Figure S2.17. GPC trace of the reaction of **1** with iPr₃PhMgBr after 10 min.
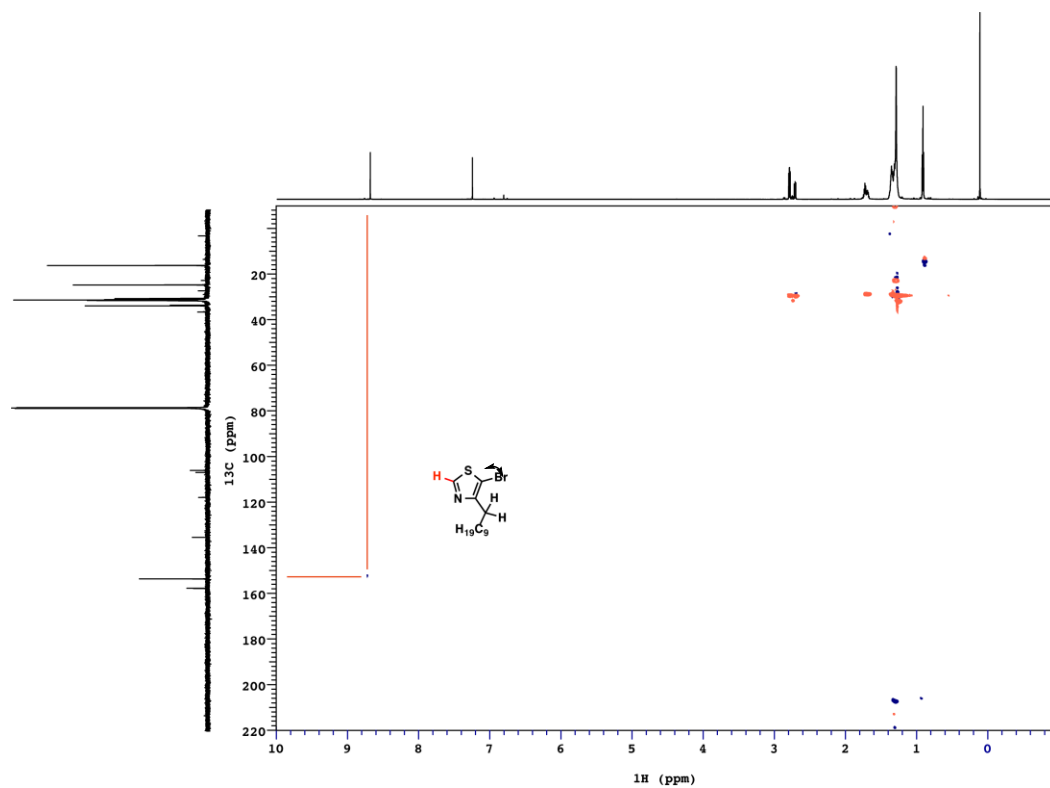
Figure S2.18. gHSQC of **2b-H**. F2 = ^{1}H (500 MHz, CDCl$_3$), F1 = ^{13}C.
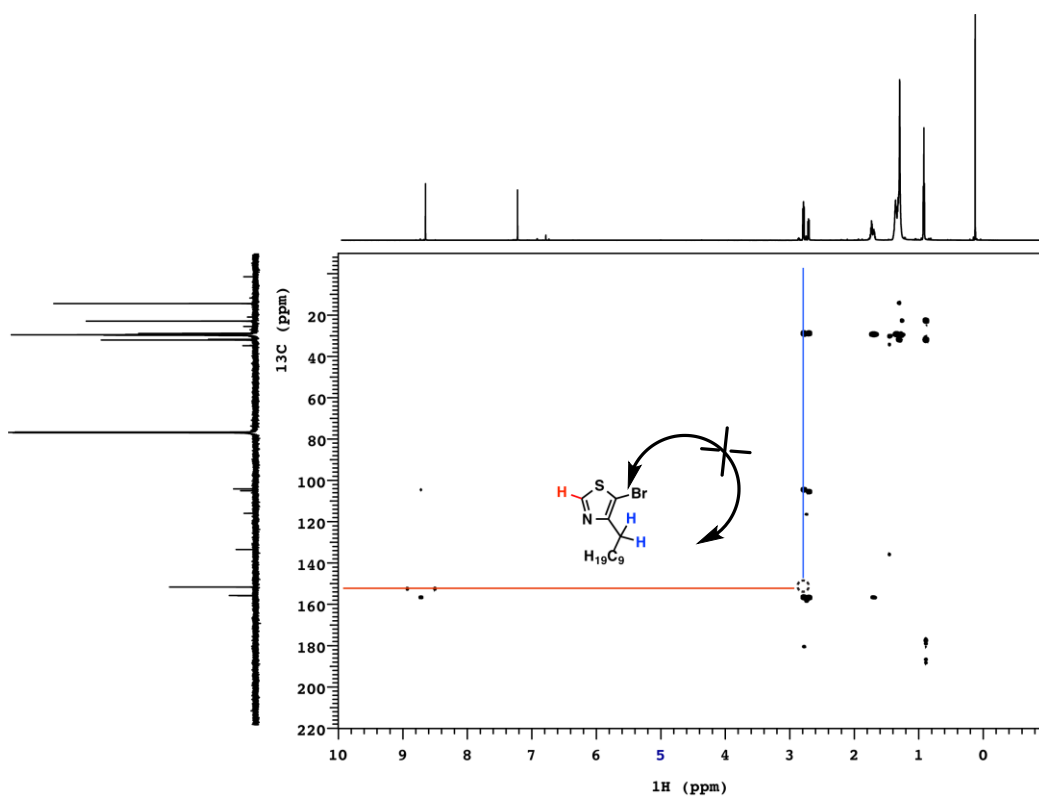
Figure S2.19. gHMBC of **2b-H**. F2 = ^{1}H (500 MHz, CDCl$_3$), F1 = ^{13}C.

129

D. EPR spectroscopy during the reaction of 1 with iPr₃PhMgBr
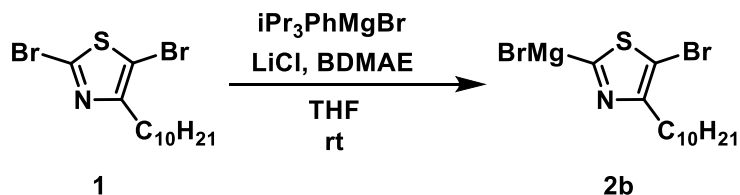
EPR spectra were recorded on solutions containing **1**, iPr₃PhMgBr, and the combined reaction solution.

2b. In a glovebox, **1** (224 mg, 0.585 mmol, 1.00 equiv) and THF (0.7 mL) were added to a 4 mL vial. To a separate 4 mL vial with a stir bar, LiCl (29.8 mg, 0.703 mmol, 1.20 equiv), bis(2-dimethylaminoethyl) ether (0.12 mL, 0.63 mmol, 1.1 equiv), and iPr₃PhMgBr (1.1 mL, 0.5M in THF, 0.55 mmol, 0.94 equiv) were added. Separately, half of each solution was transferred by syringe to an individual quartz EPR tube. The remaining half of the solution of **1** was transferred by syringe to the vial containing the Grignard solution. The reaction solution darkened over the course of 10 min. This solution was transferred by pipette to a quartz EPR tube. The EPR tubes were all sealed with a Teflon stopcock, removed from the glovebox, and immediately frozen in liquid nitrogen for analysis via EPR spectroscopy (**Figure S2.17A**).

The above reaction was performed in triplicate and the integrated area in the EPR spectra were compared to external TEMPO standards (**Figure S2.17B**).

2b-A. In a glovebox, **1** (99.8 mg, 0.260 mmol, 1.00 equiv) and LiCl (12.5 mg, 0.295 mmol, 1.13 equiv) were added to a 20 mL vial with a stir bar. THF (0.35 mL) was added, then BDMAE (54.0 µL, 0.284 mmol, 1.09 equiv) was added to the reaction solution. Finally, 2,4,6-iPr₃PhMgBr (0.49 mL, 0.5M in THF, 0.245 mmol, 0.942 equiv) was added to the reaction solution. The solution was darkened over the course of 10 min. This solution was transferred by pipette to a quartz EPR tube, which was sealed with a Teflon stopcock, removed from the glovebox, and immediately frozen in liquid nitrogen for analysis via EPR spectroscopy.

2b-B. Following the procedure for **2b-A**, with the following quantities: **1** (97.6 mg), LiCl (11.3 mg), BDMAE (55.0 µL), 2,4,6-iPr₃PhMgBr (0.48 mL, 0.5M in THF), THF (0.35 mL).

2b-C. Following the procedure for **2b-A**, with the following quantities: **1** (133.1 mg), LiCl (14.1 mg), BDMAE (70.0 µL), 2,4,6-iPr₃PhMgBr (0.66 mL, 0.5M in THF), THF (0.48 mL).
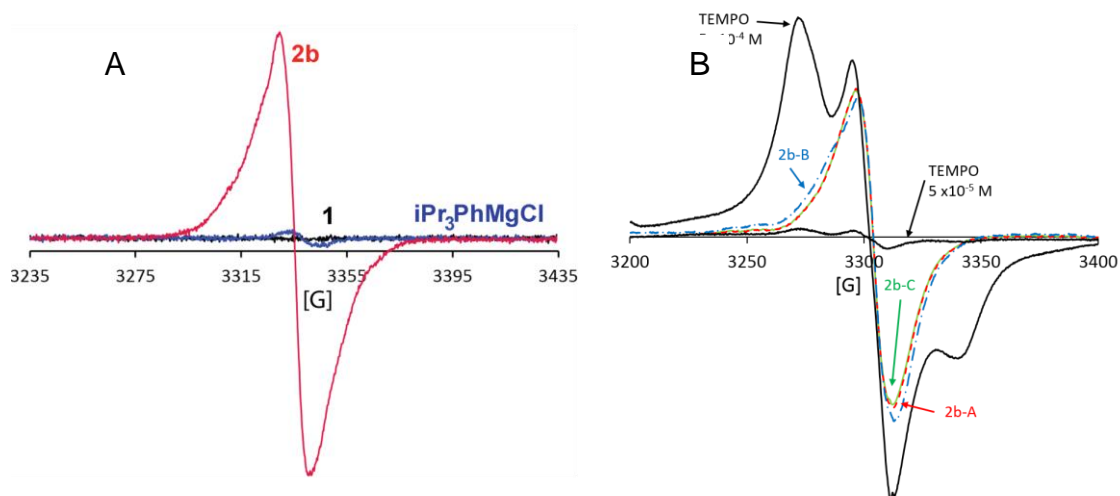
Figure S2.20. EPR spectra of the reaction of **1** with iPr₃PhMgBr. A. Overlaid spectra of THF solutions of the reagents and the reaction mixture. Black: A solution of **1** (0.84M); blue: a solution of iPr₃PhMgBr (0.45M), BDMAE (0.51M), and LiCl (0.58M); red: the preceding solutions were combined to generate a solution of **2b** (0.30M). B. Comparison of the reaction mixture to external standards for quantification. Black: Solutions of TEMPO (5 x 10^{-4}M and 5 x 10^{-5} M); dashed red: A solution of **2b-A** (0.29M); dash-dot blue: **2b-B** (0.29M); solid green: **2b-C** (0.30M).

Table S2.1. Measured areas and their corresponding concentrations for the data in **Figure S2.20B**.

	integrated area	[radical] (M x10^{-5})	[2b] (M)	% radical
TEMPO	4.39 x 10^5	50.0	–	–
TEMPO	2.01 x 10^4	5.00	–	–
2b-A	1.61 x 10^5	21.3	0.29 M	0.073%
2b-B	1.63 x 10^5	18.4	0.29 M	0.063%
2b-C	1.86 x 10^5	18.6	0.30 M	0.064%
Average (std dev) (0.006%)				0.067%

E. Regioselectivity and formation of oligomers in the reaction of 3 with iPrMgCl.
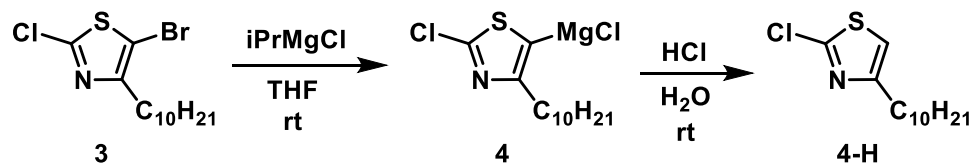
In a 20 mL vial equipped with a stir bar in a glovebox, **3** (199.8 mg, 0.590 mmol, 1.00 equiv) was dissolved in THF (3.2 mL), then iPrMgCl (0.31 mL, 1.7M in THF, 0.53 mmol, 0.90 equiv) was added. The reaction solution was kept at rt in the glovebox for 24 h. The reaction solution was removed from the glovebox and poured into HCl (5 mL, 5M in DI H_2O). The organic products were extracted from the resulting aqueous mixture with $CHCl_3$ (5 mL). The solvent was removed under vacuum, and then the organic products were redissolved in THF, dried over $MgSO_4$, filtered, and analyzed by GPC (**Figure S2.22**).
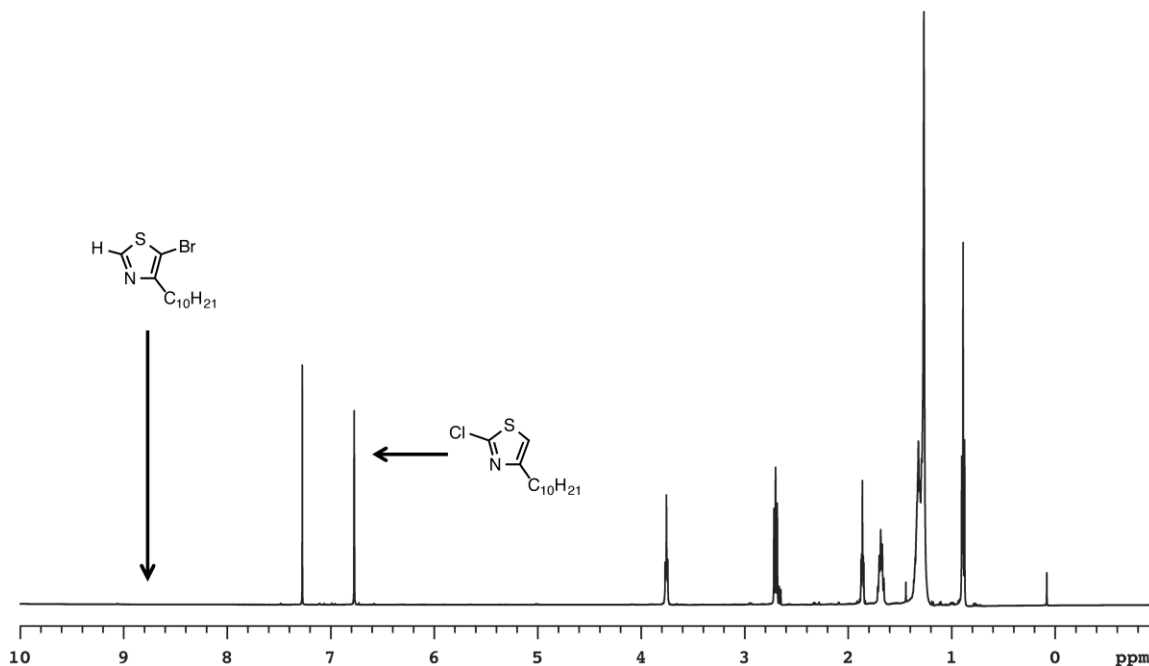
Figure S2.21. ^1H NMR spectrum of crude **4-H**. ^1H NMR (500 MHz, $CDCl_3$)
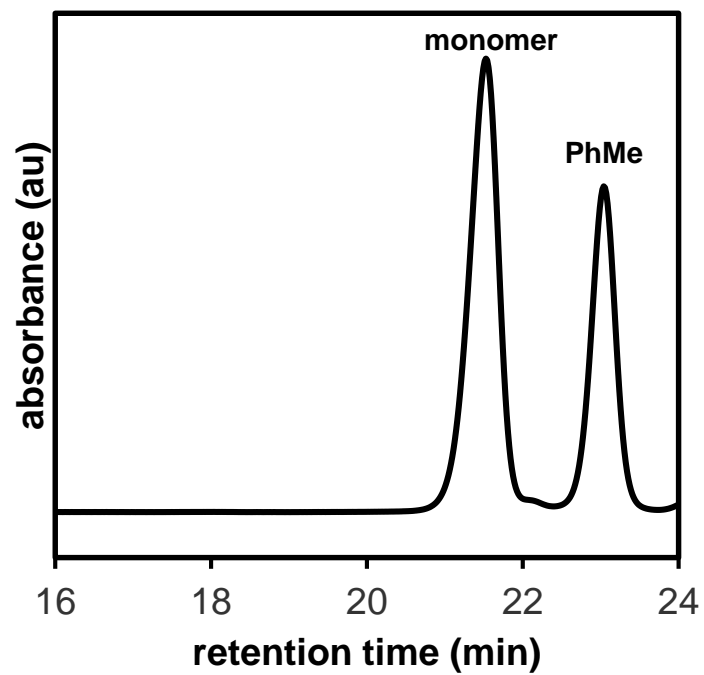
Figure S2.22. GPC trace of the reaction of **3** with iPrMgCl.

VI. Polymerizations of Monomer 4

Polymerization of 4 with precatalyst 5
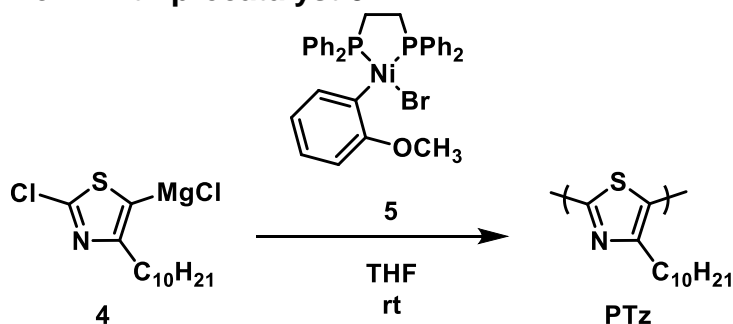
In a 20 mL vial equipped with a stir bar in a glovebox, precatalyst **5** (2.1 mg, 0.0033 mmol, 1.0 equiv) was dissolved in THF (0.54 mL). Subsequently, monomer **4** (1.09 mL, 0.15M in THF, 0.163 mmol, 50 equiv) was added in one portion. The reaction mixture was held at rt for 16 h, then poured into HCl (5 mL, 5M in DI H_2O). The organic products were extracted from the resulting aqueous mixture with $CHCl_3$ (5 mL) to obtain a dark red solid. Relative to an n-docosane internal standard, 42% of monomer was consumed. Of this, 10% was incorporated into insoluble polymer (1.8 mg recovered), and the remainder into soluble oligomers. The soluble fraction was dissolved in THF, dried over $MgSO_4$, filtered, and analyzed by GPC. M_n = 0.88 kDa, Đ = 1.4.
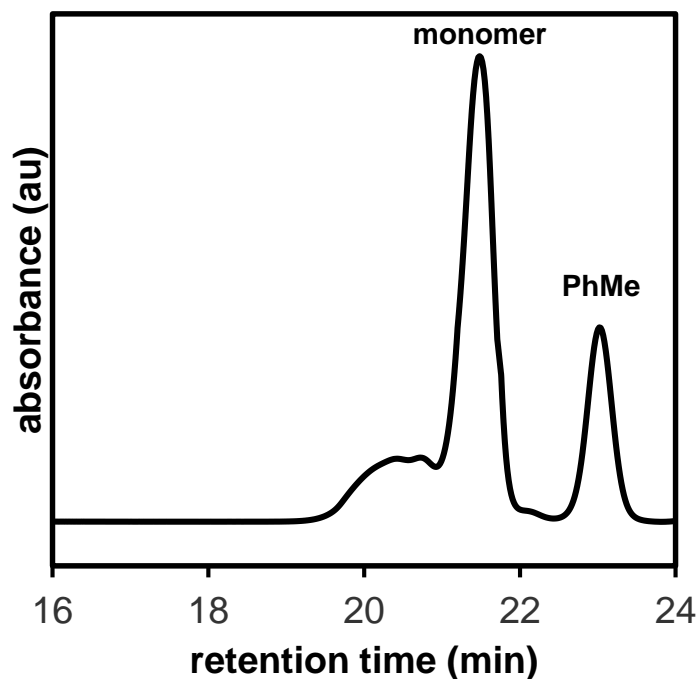
Figure S2.23. GPC trace of the polymerization of **4** with precatalyst **5**.
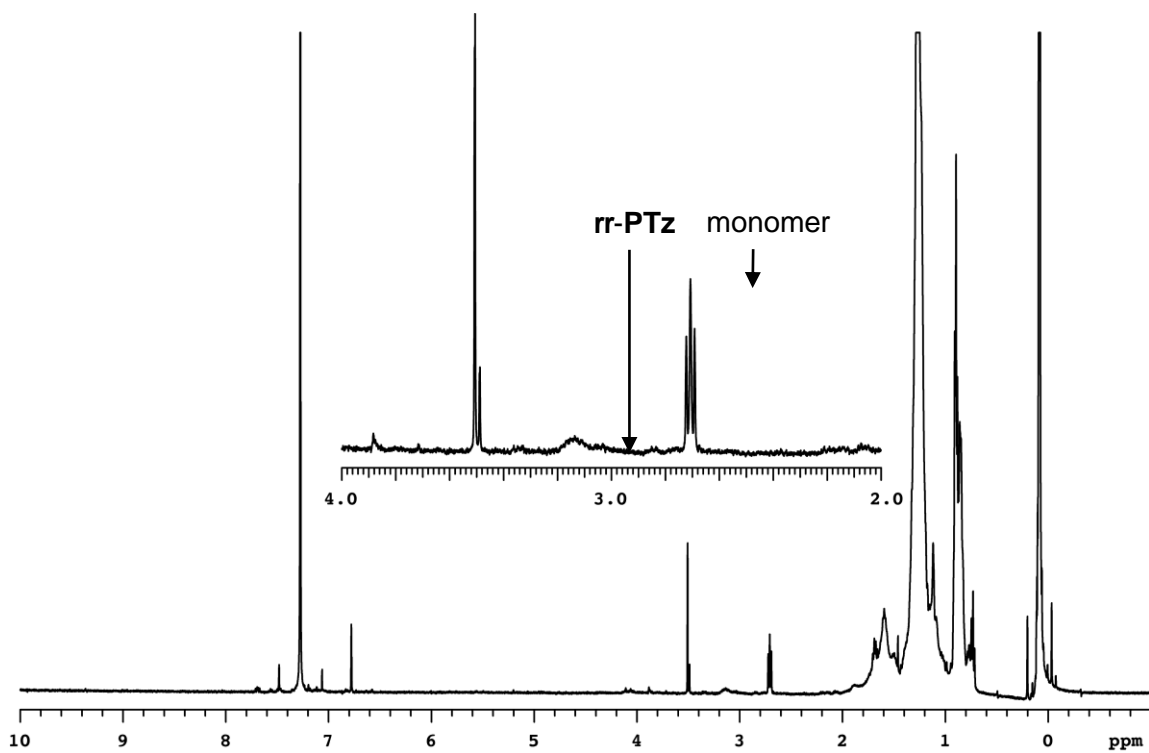
Figure S2.24. ^{1}H NMR spectrum of **PTz** generated with precatalyst **5**.

VII. π-Complex Model System
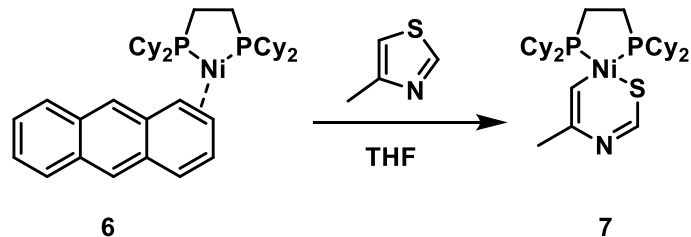
In separate 4 mL vials in a glovebox, **6** (3.7 mg, 0.0056 mmol, 1.0 equiv) was dissolved in d_8-THF (0.7 mL) and 4-methylthiazole (1.1 mg, 0.011 mmol, 2.0 equiv) was dissolved d_8-THF (0.3 mL). Both solutions were transferred to the same J-Young tube and a teflon stopcock was affixed. ^1H and ^{31}P NMR spectra were taken.
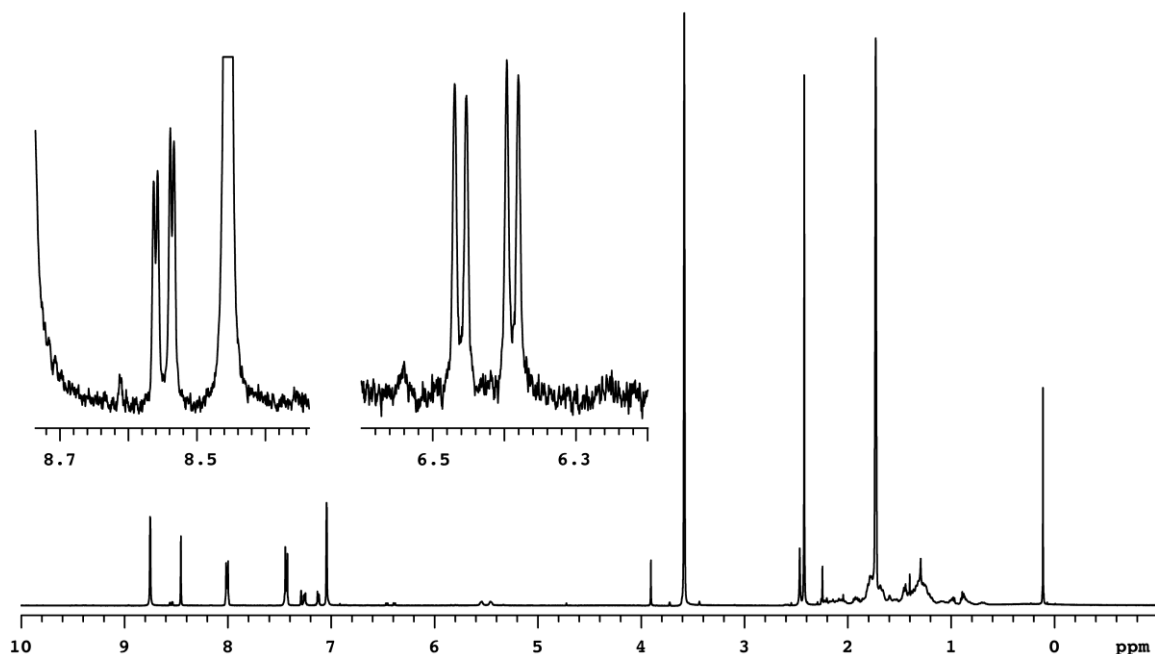

Figure S2.25. ^1H NMR spectrum of the reaction of **6** with 4-methylthiazole. ^1H NMR (d_8-THF, 500 MHz): 8.75 (s, 15 H, 4-methylthiazole), 8.54 (dd, J_{H-H} = 2.0 Hz, J_{P-H} = 11.9 Hz, 1 H, **9**), 8.45 (s, 6.5 H, anthracene), 8.01 (m, 12.5 H, anthracene), 7.43 (m, 14 H, anthracene), 7.29 (s, 2 H, **8**), 7.26 (m, 3 H, **8**), 7.12 (m, 3 H, **8**), 7.05 (s, 17 H, 4-methylthiazole), 6.43 (dd, J_{H-H} = 7.3 Hz, J_{P-H} = 36.5 Hz, 1 H, **9**), 5.54 (br. s, 2 H, **8**), 5.45 (br. s, 2 H, **8**), 3.90 (s, 3.5 H), 2.47 (s, 11 H), 2.42 (s, 51 H, 4-methylthiazole), 2.3–0.6 (m, 329, multiple species incl. THF).
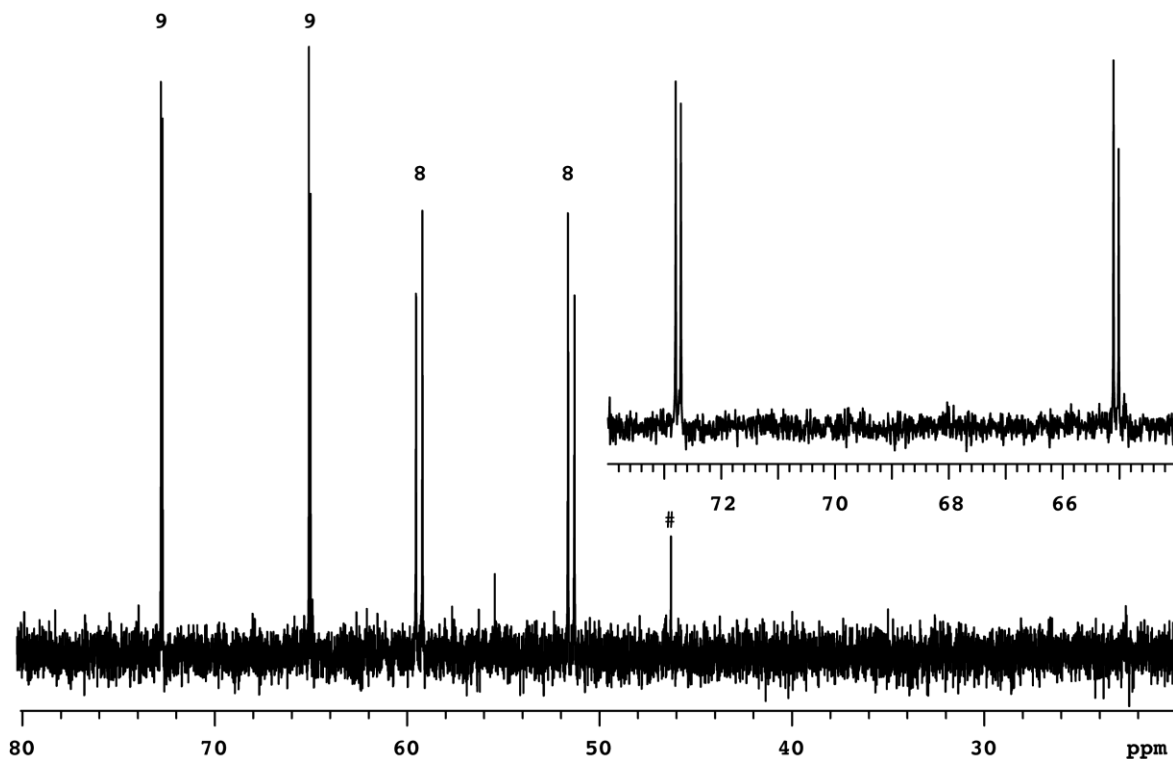
Figure S2.26. ^{31}P NMR spectrum of the reaction of **6** with 4-methylthiazole. ^{31}P NMR (202 MHz, d_8-THF): δ 72.77 (d, J_{P-P} = 18.5 Hz), 65.05 (d, J_{P-P} = 18.5 Hz), 59.38 (d, J_{P-P} = 68.0 Hz), 51.50 (d, J_{P-P} = 68.0 Hz). # denotes Ni(dcpe)$_2$.
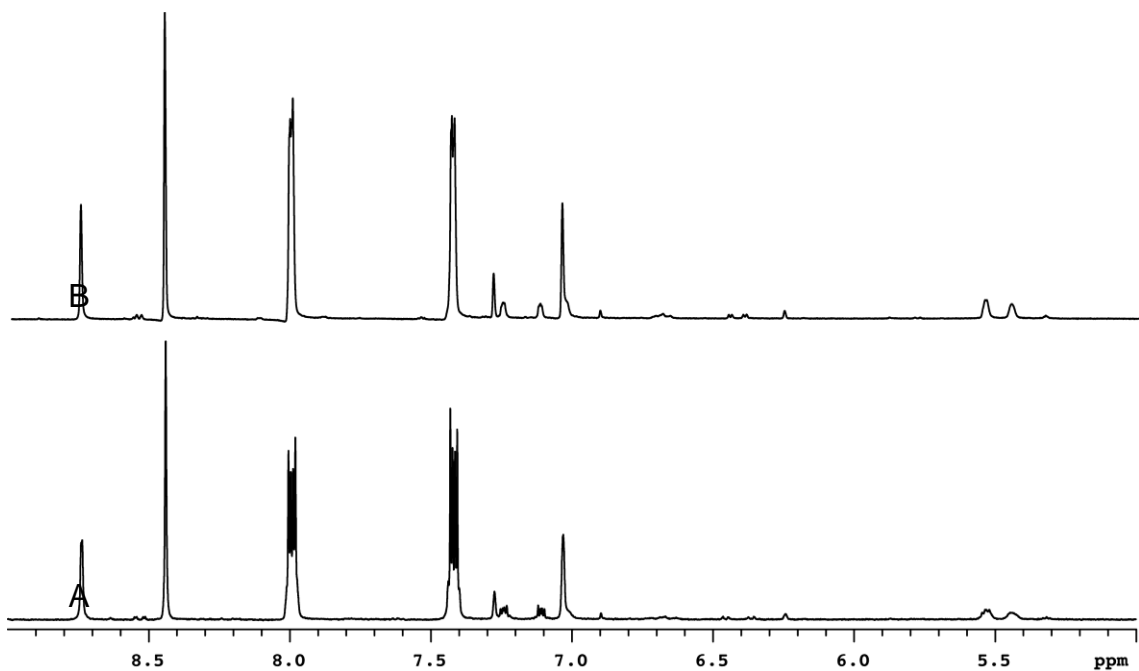
Figure S2.27. ^1H NMR spectra of **7** at varying field strength. A: ^1H NMR (d_8-THF, 400 MHz): 8.54 (dd, J_{H-H} = 2.0 Hz, $J_{P-H}$ = 11.9 Hz, 1 H), 6.43 (dd, J_{H-H} = 7.3 Hz, J_{P-H} = 36.5 Hz, 1 H). B: ^1H NMR (d_8-THF, 700 MHz): 8.54 (dd, J_{H-H} = 2.0 Hz, J_{P-H} = 11.9 Hz, 1 H), 6.43 (dd, J_{H-H} = 7.3 Hz, J_{P-H} = 36.5 Hz, 1 H).
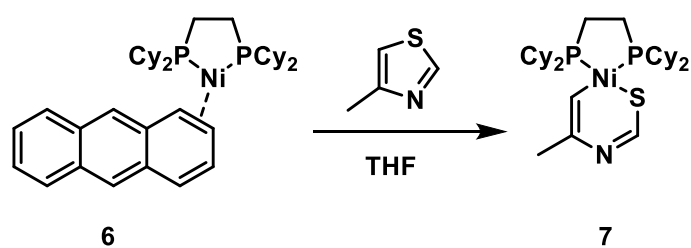
In separate 4 mL vials in a glovebox, **6** (4.3 mg, 0.0065 mmol, 1.0 equiv) and 4-methylthiazole (1.9 mg, 0.019 mmol, 2.9 equiv) each dissolved d_8-THF (0.4 mL each). Both solutions were transferred to the same J-Young tube and a teflon stopcock was affixed. ^1H, ^{31}P, and ^1H-^{31}P gHMBC NMR spectra were taken.
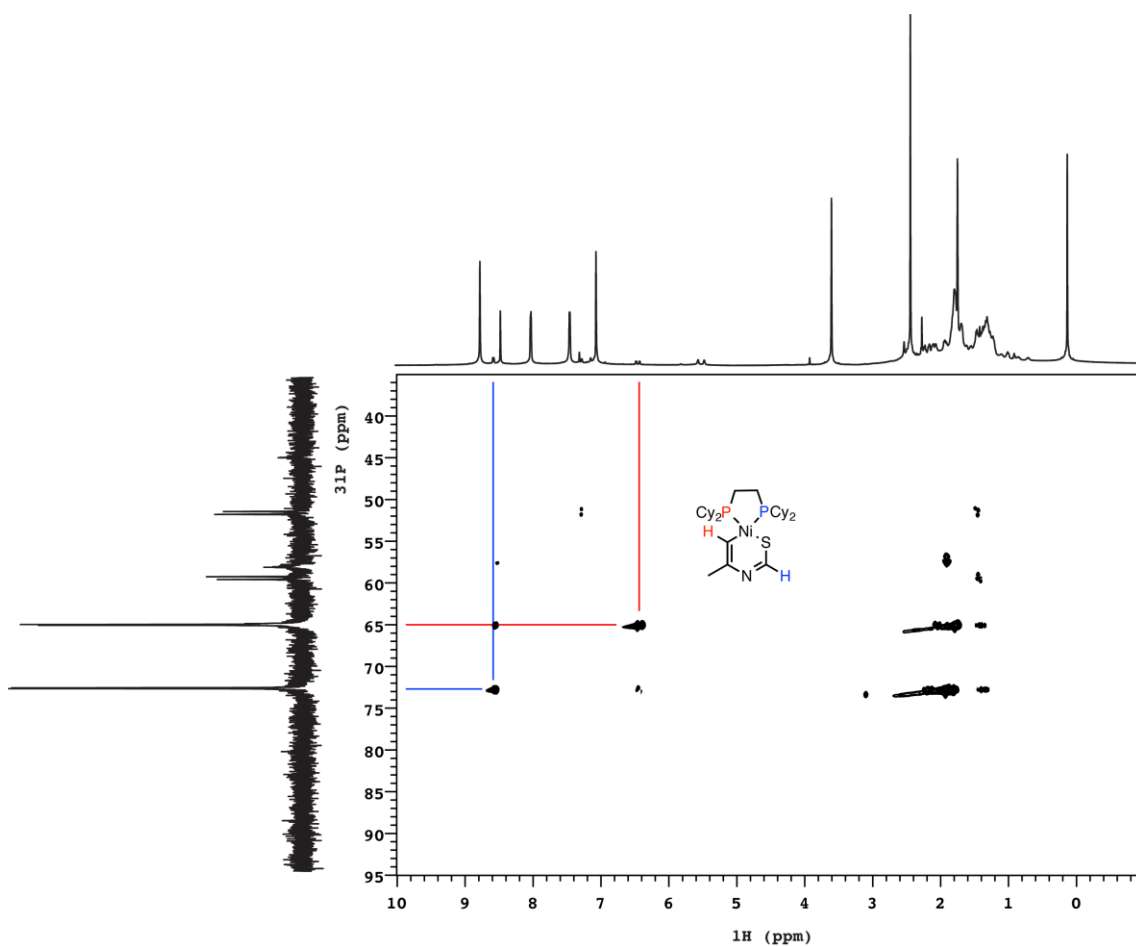
Figure S2.28. ^1H-^{31}P gHMBC spectrum for the reaction of **6** with 4-methylthiazole. A solution of **6** (0.0081 M) and 4-methylthiazole (0.024M) at rt. F2 = ^1H (500 MHz, d_8-THF), F1 = ^{31}P.

VIII. Polymerizations of Monomer 9

Activation of monomer 9 (representative procedure)
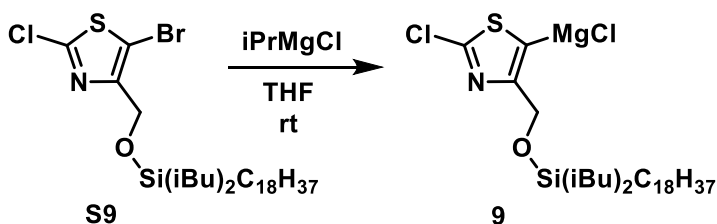
In a 4 mL vial equipped with a stir bar in a glovebox, **S9** (180 mg, 0.289 mmol, 1.00 equiv) and docosane (internal standard for measuring conversion, 82.2 mg) were dissolved in THF (1.11 mL). Then, iPrMgCl (123 µL, 2.0M in THF, 0.246 mmol, 0.85 equiv) was added. After stirring at rt in the glovebox for 1 h, the resulting monomer solution was used in polymerizations.

Polymerizing monomer 9 with precatalyst 5

[9] = 5mM. In a 20 mL vial equipped with a stir bar in a glovebox, monomer **9** (0.125 mL, 0.20M in THF, 0.0250 mmol, 29 equiv) was diluted with THF (4.7 mL). Then, precatalyst **5** (170 µL, 5.0mM in THF, 0.000850 mmol, 1.0 equiv) was added. The reaction solution was quickly divided equally between five 4 mL vials equipped with stir bars. After 3, 6, 12, 20, and 30 min, one of these vials was removed from the glovebox and quenched by pouring into HCl (0.5 mL, 0.3% in MeOH) followed by dilution with MeOH (2 mL) and H_2O (2 mL). The organic products were extracted from each quenched vial with $CHCl_3$ (3 mL). Solvent was removed under vacuum, then the organic products were dissolved in THF, dried over $MgSO_4$, filtered, and analyzed by GPC. Decomposition of remaining monomer prevented determining conversion by GC.

[9] = 10mM. The reaction was performed as described above, with monomer **9** (0.250 mL, 0.20M in THF, 0.0500 mmol, 59 equiv), THF (4.6 mL), and **5** (170 µL, 5.0mM in THF, 0.000850 mmol, 1.0 equiv). Aliquots were removed after 2, 4, 6, 12, and 30 min and worked up as above.

*[9] = 15mM.* The reaction was performed as described above, with monomer **9** (0.250 mL, 0.20M in THF, 0.0500 mmol, 88 equiv), THF (3.0 mL), and **5** (113 µL, 5.0mM in THF, 0.00570 mmol, 1.0 equiv). Aliquots were removed after 2, 4, 6, 12, and 30 min and worked up as above.

Table S2.2. GPC data for polymerizing **9** with precatalyst **5**.

| [**9**] (mM)	time (min)	Trial 1 M_n (kDa)	Đ	Trial 2 M_n (kDa)	Đ	Trial 3 M_n (kDa)	Đ	Trial 4 M_n (kDa)	Đ
5	3	6.7	1.61	5.7	1.29				
	6	13.3	1.30	13.3	1.30				
	12	13.1	1.28	14.6	1.28				
	20	13.7	1.27	14.7	1.30				
	30	13.4	1.34	14.6	1.29				
10	2	4.3	1.27	4.7	1.18	4.5	1.25	4.2	1.30
	4	8.8	1.29	8.8	1.28	8.8	1.28	8.4	1.31
	6	14.8	1.28	14.7	1.27	14.5	1.26	14.8	1.28
	12	25.9	1.24	26.6	1.26	22.6	1.28	24.4	1.30
	30	26.9	1.26	27.0	1.26	23.4	1.26	24.2	1.30
15	2	8.0	1.29	6.5	1.19				
	4	17.6	1.22	15.8	1.24				
	6	24.8	1.22	21.0	1.21				
	12	44.1	1.27	42.5	1.22				
	30	40.9	1.28	41.2	1.20				
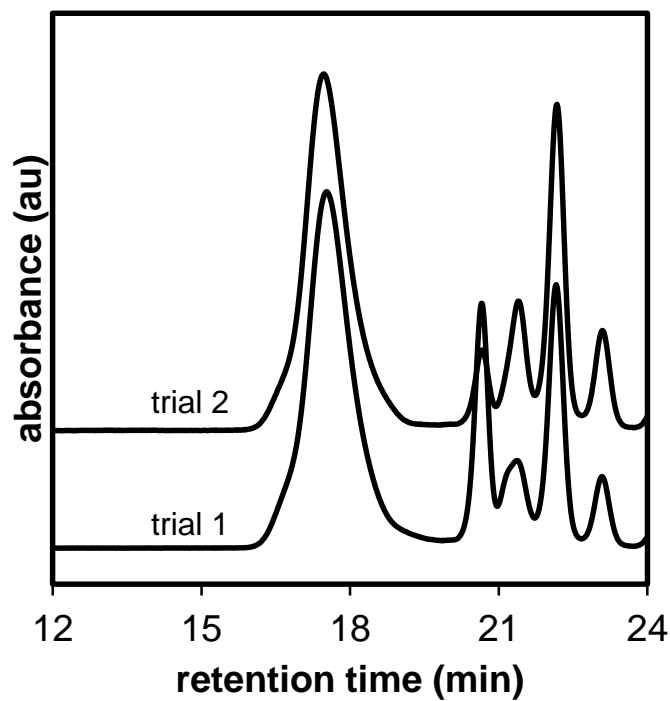
Figure S2.29. GPC traces for polymerizing monomer **9** (5mM) with precatalyst **5**.
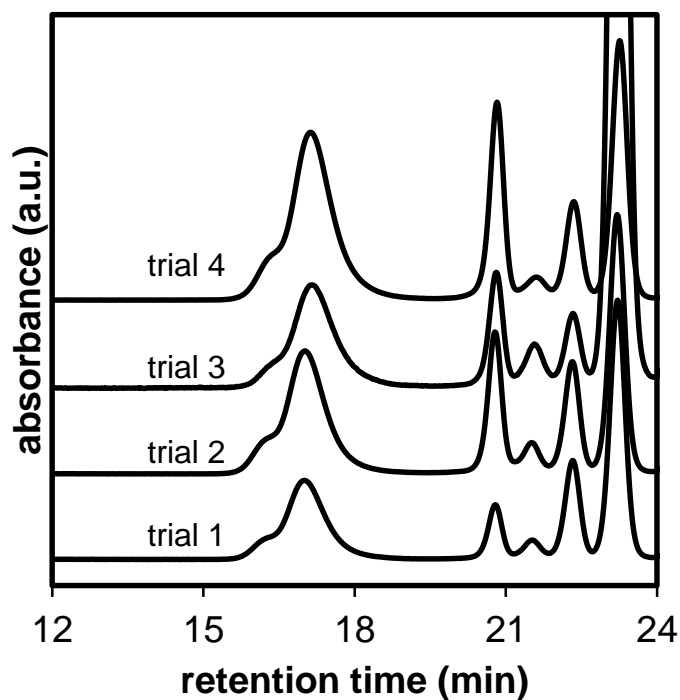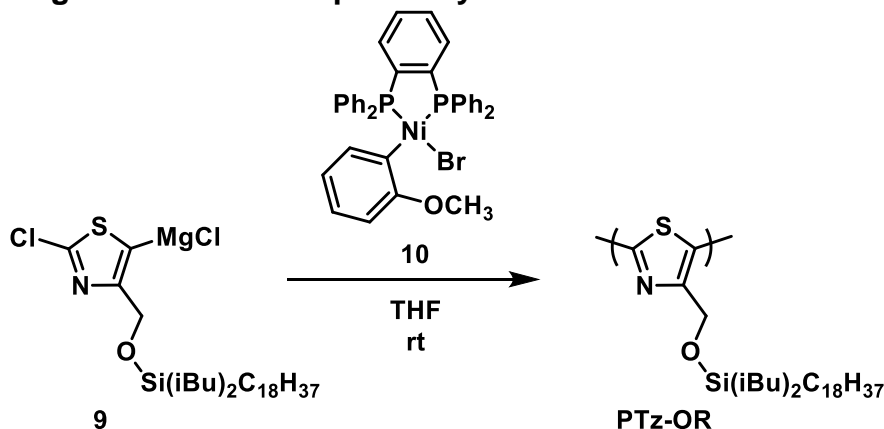

Figure S2.30. GPC traces for polymerizing monomer **9** (10mM) with precatalyst **5**.
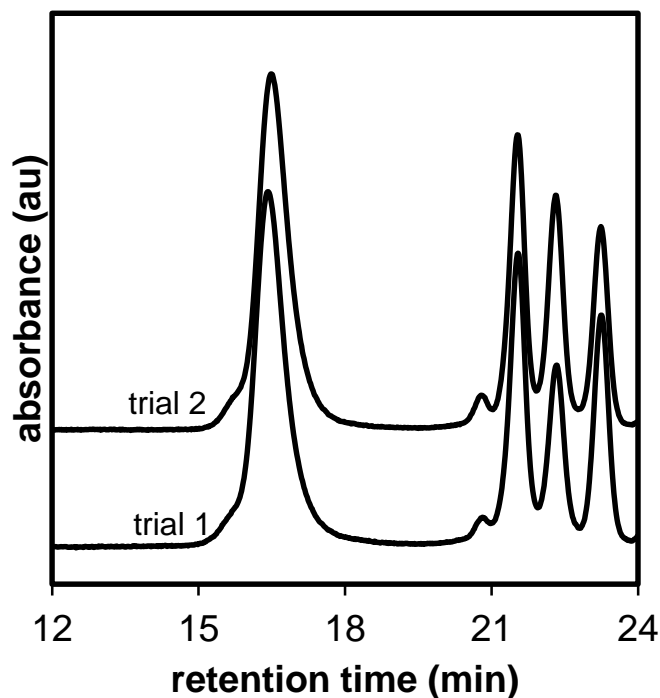
Figure S2.31. GPC traces for polymerizing monomer **9** (15mM) with precatalyst **5**.

Polymerizing monomer 9 with precatalyst 10

[9] = 5mM. In a 20 mL vial equipped with a stir bar in a glovebox, monomer **9** (0.125 mL, 0.20M in THF, 0.0250 mmol, 29 equiv) was diluted with THF (4.7 mL). Then precatalyst **10** (170 µL, 5.0mM in THF, 0.000850 mmol, 1.0 equiv) was added. The reaction solution was quickly divided equally between five 4 mL vials equipped with stir bars. After 3, 6, 12, 20, and 30 min, one of these vials was removed from the glovebox and quenched by pouring into HCl (0.5 mL, 0.3% in MeOH) followed by dilution with MeOH (2 mL) and H_2O (2 mL). The organic products were extracted from each quenched vial with $CHCl_3$ (3 mL). Solvent was removed under vacuum, then the organic products were dissolved in THF,

dried over MgSO$_4$, filtered, and analyzed by GPC. Decomposition of remaining monomer prevented determining conversion by GC.

[9] = 10mM. The reaction was performed as described above, with monomer **9** (0.250 mL, 0.20M in THF, 0.0500 mmol, 59 equiv), THF (4.6 mL), and **10** (170 µL, 5.0mM in THF, 0.000850 mmol, 1.0 equiv). Aliquots were removed after 2, 4, 6, 12, and 30 min and worked up as above.

[9] = 15mM. The reaction was performed as described above, with monomer **9** (0.250 mL, 0.20M in THF, 0.0500 mmol, 88 equiv), THF (3.0 mL), and **10** (113 µL, 5.0mM in THF, 0.00570 mmol, 1.0 equiv). Aliquots were removed after 2, 4, 6, 12, and 30 min and worked up as above.

**Table S2.3**. GPC data for polymerizing **9** with precatalyst **10**.

| [**9**] (mM)	time (min)	Trial 1 M_n (kDa)	Đ	Trial 2 M_n (kDa)	Đ	Trial 3 M_n (kDa)	Đ
5	3	8.0	1.36	7.8	1.27		
	6	16.5	1.32	15.8	1.23		
	12	26.9	1.24	24.1	1.25		
	20	26.1	1.26	25.8	1.20		
	30	24.6	1.23	25.8	1.20		
10	2	5.6	1.20	5.0	1.18		
	4	11.0	1.24	11.1	1.24		
	6	17.3	1.20	16.7	1.24		
	12	32.6	1.17	29.5	1.15		
	30	36.0	1.18	32.2	1.16	38.0	1.23
15	2	9.4	1.21	7.8	1.20		
	4	24.2	1.22	20.6	1.19		
	6	32.3	1.16	27.3	1.19		
	12	63.8	1.19	52.9	1.28		
	30	66.4	1.19	63.5	1.29		
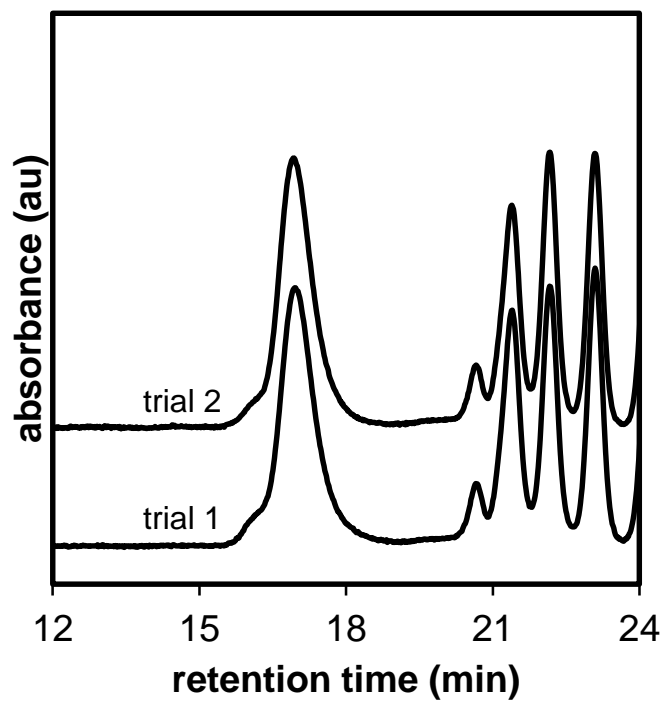
Figure S2.32. GPC traces for polymerizing monomer **9** (5mM) with precatalyst **10**.
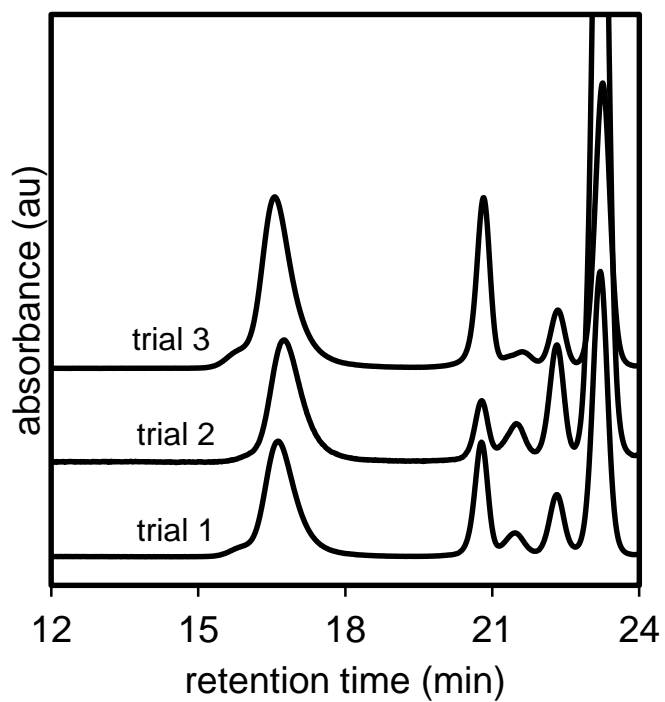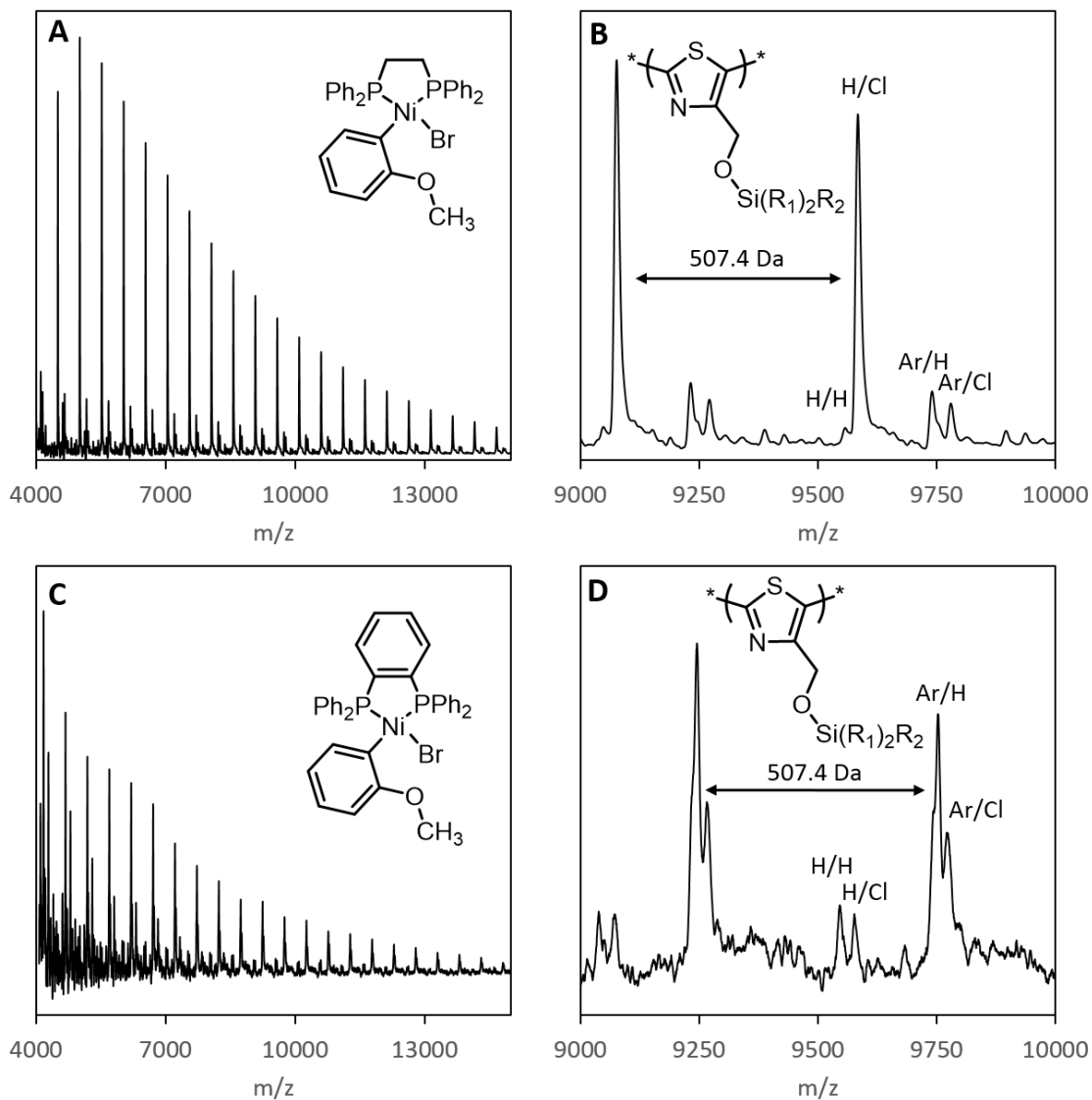

Figure S2.33. GPC traces for polymerizing monomer **9** (10mM) with precatalyst **10**.
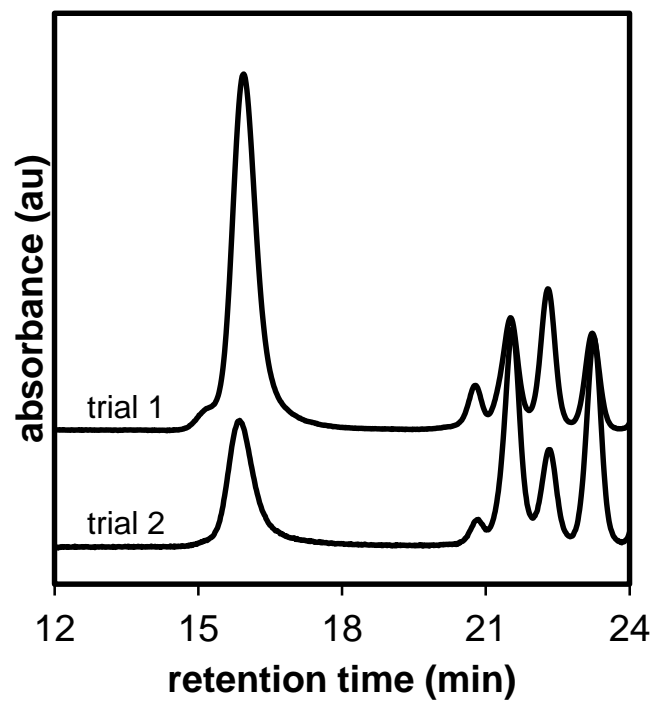
Figure S2.34. GPC traces for polymerizing monomer **9** (15mM) with precatalyst **10**.
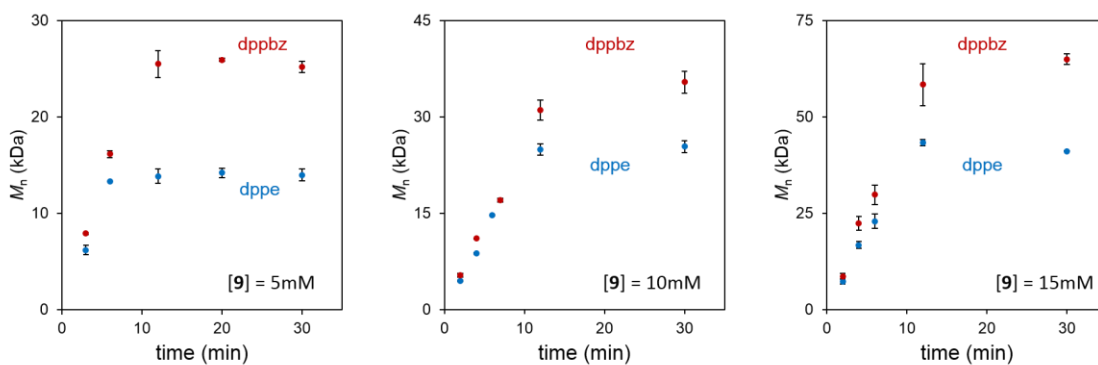
Figure S2.35. M_n versus time for polymerizing monomer **9** with precatalysts **5** and **10**. Error bars denote the standard error of the mean.

Figure S2.36. MALDI-TOF-MS data of **PTz-OR** generated with precatalysts **5** (A, B) and **10** (C, D).

IX. Computational Details

Simulations were performed using a development version of the Q-Chem 4.3 quantum chemistry suite.[8] The hybrid B3LYP density functional[9] in the spin restricted formulism and the double-zeta, LANL2DZ basis set[10] were used for all optimizations. The long range corrected, empirical dispersion corrected ωB97X-D functional[11] was used for single point energies with the SMD solvation model using THF as the implicit solvent.[12,13] The solvent-corrected single point energies were computed using the triple-zeta, polarized cc-pVTZ basis set.[14] Thermodynamic corrections were applied to the enthalpies at 298.15 K to all single point energies. In one transition state (Displacement TS 3), 2kT was added to the enthalpies to correct for the presence of two small imaginary frequencies. Energies reported in this paper therefore are free energies at the SMD(THF)/ωB97X-D/cc-pVTZ level of theory.

Reaction discovery simulations were used to locate the chain transfer pathway. These techniques were developed by the Zimmerman group to systematically search through a combinatorial set of plausible reaction coordinates for the lowest barrier reaction pathways. These reaction coordinates include addition or subtraction of interatomic connections as well as angular coordinates (at the transition metal). Details of this method are available in references.[15] Examples of previous use of the method to transition metal reactions are available in references.[16,17]

Over 4,000 reaction path searches were performed in this study, the majority of which were automatically hypothesized and evaluated by the reaction discovery tools. While many of these pathways were uncompetitive, the remaining pathways were analyzed in detail and the most competitive paths are discussed in the paper.

The latest version of the Growing String Method (GSM) optimized the exact transition states and minimum energy reaction paths.[18] By optimizing the reaction path, GSM provides verification that the saddle point connects the reactant to product geometries through a single transition state. Frequency computations verified that all transition states have the correct negative eigenvalue corresponding to the indicated path. GSM was considered converged when the RMS gradient at the transition state node reached less than 0.0005 HT/Å. When needed, transition states were refined using an eigenvector algorithm in Q-Chem to eliminate spurious negative eigenvalues in the Hessian.

A. Reaction pathway for chain-growth pathway
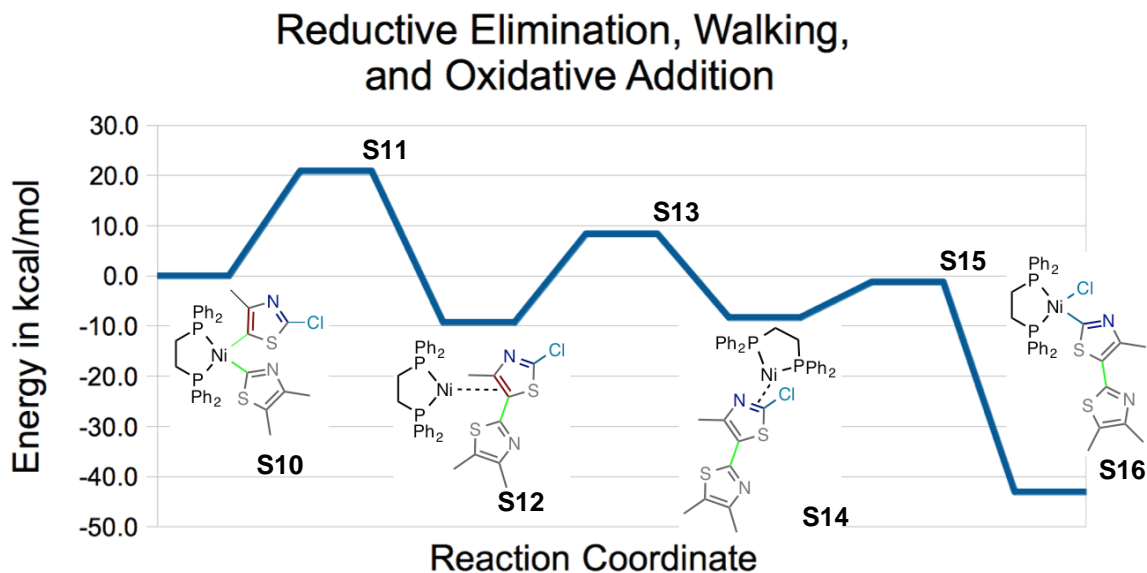
Figure S2.37. Chain-growth pathways from (dppe)Ni(thiazole)₂ through oxidative addition. Energies are solvated (THF) free energies at 298K.
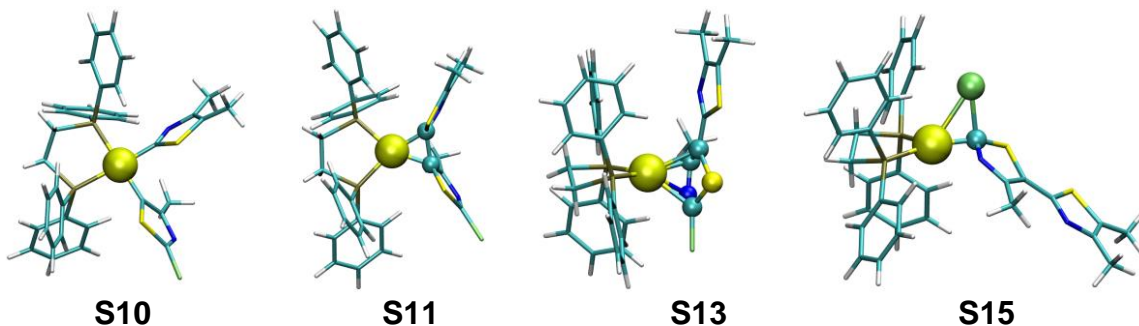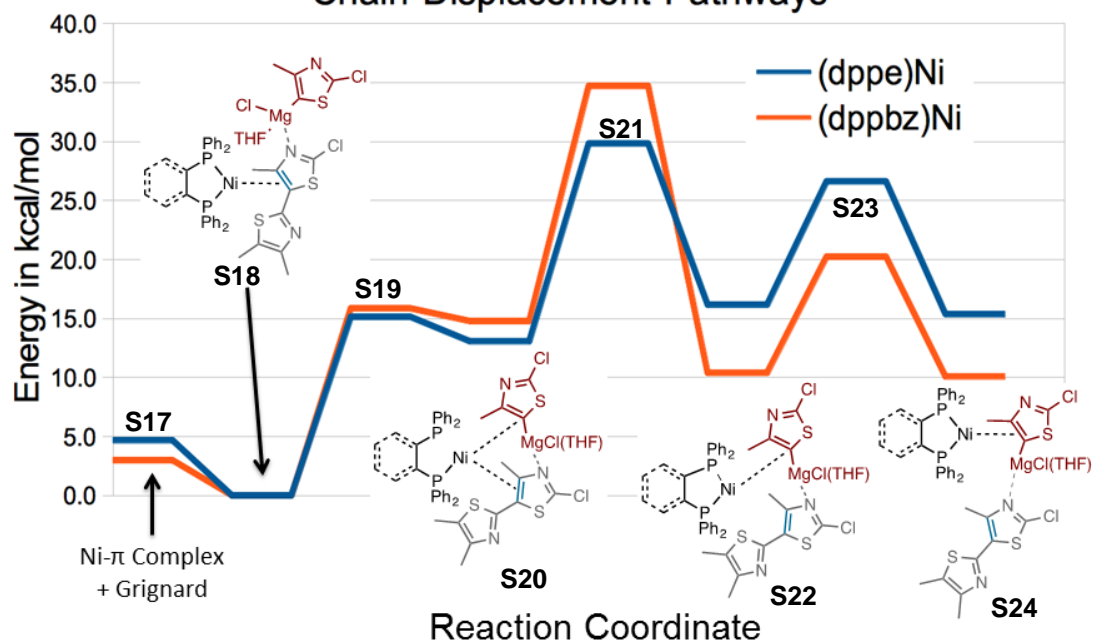

Figure S2.38. Selected 3D structures for chain-growth pathway.

Table S2.4. Simulated total energies for chain-growth pathway (SMD/ωB97X-D/cc-pVTZ). E_{rel} is calculated as follows: $E-E_0 * 627.5 + H-H_0$
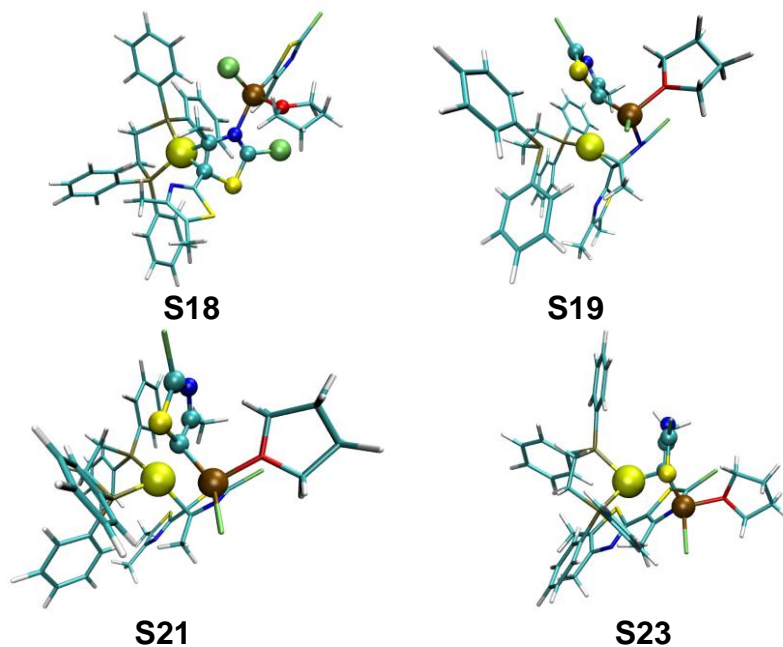
Structure	E (Hartree)	H (kcal/mol)	E_{rel} (kcal/mol)
S10	-3571.68886	400.328	0
S11	-3571.65478	399.821	20.9
S12	-3571.70516	401.294	-9.3
S13	-3571.67587	400.543	8.4
S14	-3571.70314	400.984	-8.3
S15	-3571.69238	401.312	1.2
S16	-3571.75693	402.049	-41.0

B. Reaction pathway for chain-displacement pathway

Figure S2.39. Chain-displacement pathways for dppe and dppbz Ni species, starting from the π-complex and separated Grignard. Energies are solvated (THF) free energies at 298K. Numbered complexes refer to the dppe-containing version.

Figure S2.40. Selected 3D structures for chain-displacement pathway.
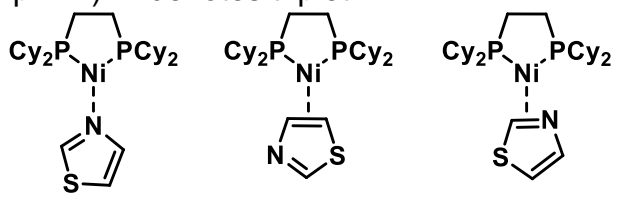
Table S2.5. Simulated total energies for chain-displacement pathway (SMD/ωB97X-D/cc-pVTZ). E_{rel} is calculated as follows: $E-E_0 * 627.5 + H-H_0$

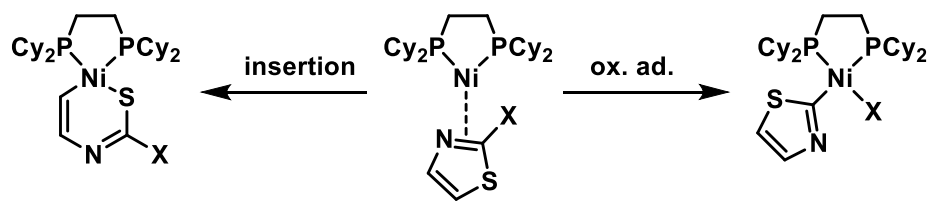| Structure	E (Hartree)	H (kcal/mol)	E_{rel} (kcal/mol)
S18	-5531.98512	528.6	0
S19	-5531.95783	526.6	15.1
S20	-5531.96521	529.1	13.0
S21	-5531.93634	527.8	29.8
S22	-5531.96118	529.7	16.1
S23	-5531.94208	528.2	26.6
S24	-5531.96199	529.4	15.3
S18$_{dppbz}$	-5684.39	546.2	0
S19$_{dppbz}$	-5684.36	545.3	16.0
S20 $_{dppbz}$	-5684.37	546.0	14.9
S21 $_{dppbz}$	-5684.33	545.1	34.7
S22 $_{dppbz}$	-5684.37	546.4	10.9
S23 $_{dppbz}$	-5684.36	545.3	20.4
S24 $_{dppbz}$	-5684.37	546.2	10.0

C. Ni(dcpe) associative and insertion complexes with thiazole

Table S2.6. Simulated total energies for Ni(dcpe)-thiazole associative complexes (SMD/ωB97X-D/cc-pVTZ). T denotes triplet.

Structure	E (Hartree)	E_{rel} (kcal/mol)
S25	-2440.85589	0
S25, T	-2440.81713	24.3
S26	-2440.88992	-21.4
S26, T	-2440.81893	23.2
S27	-2440.88373	-17.5
S27, T	-2440.81713	24.3

Table S2.7. Simulated barriers for Ni(dcpe) insertion thiazole (SMD/ωB97X-D/cc-pVTZ).

Pathway	X =	$\Delta G^{\ddagger}$ (kcal/mol)	ΔG (kcal/mol)
Ox. Ad.	Cl	0.4	-36.9
Ox. Ad.	H	17.4	7.7
Insertion	H	23.2	-7.2

X. References

(1) Cardwell, H. M. E.; Kilner, A. E. H. *J. Chem. Soc.* **1951**, 2430–2441.

(2) Simeon, F. G.; Wendahl, M. T.; Pike, V. W. *J. Org. Chem.* **2009**, *74*, 2578–2580.

(3) Fan, P.; Goto, H.; He, X.; Kakutani, M.; Labelle, M.; McMinn, D. L.; Powers, J. P.; Rew, Y.; Sun, D.; Yan, X. US Patent WO2005110980 A2, Nov 24, 2005.

(4) Pammer, F.; Jäger, J.; Rudolf, B; Sun, Y. *Macromolecules* **2014**, *47*, 5904–5912.

(5) Bogdanović, B; Liao, S-T.; Mynott, R.; Schlichte, K.; Westeppe, U. *Chem. Ber.* **1984**, *117*, 1378–1392.

(6) Jonas, K.; Wilke, G. *Angew. Chem. Int. Ed.* **1970**, *9*, 312–313.

(7) Lanni, E. L.; McNeil, A. J. *J. Am. Chem. Soc.* **2009**, *131*, 16573–16579.

(8) Shao, Y.; Gan, Z.; Epifanovsky, E.; Gilbert, A. T. B.; Wormit, M.; Kussmann, J.; Lange, A. W.; Behn, A.; Deng, J.; Feng, X.; Ghosh, D.; Goldey, M.; Horn, P. R.; Jacobson, L. D.; Kaliman, I.; Khaliullin, R. Z.; Kuś, T.; Landau, A.; Liu, J.; Proynov, E. I.; Rhee, Y. M.; Richard, R. M.; Rohrdanz, M. A.; Steele, R. P.; Sundstrom, E. J.; Woodcock, H. L.; Zimmerman, P. M.; Zuev, D.; Albrecht, B.; Alguire, E.; Austin, B.; Beran, G. J. O.; Bernard, Y. A.; Berquist, E.; Brandhorst, K.; Bravaya, K. B.; Brown, S. T.; Casanova, D.; Chang, C.-M.; Chen, Y.; Chien, S. H.; Closser, K. D.; Crittenden, D. L.; Diedenhofen, M.; DiStasio, R. A.; Do, A. D.; Dutoi, A. D.; Edgar, R. G.; Fatehi, S.; Fusti-Molnar, L.; Ghysels, A.; Golubeva-Zadorozhnaya, A.; Gomes, J.; Hanson-Heine, M.; Harbach, P. H.; Hauser, A. W.; Hohenstein, E. G.; Holden, Z. C.; Jagau, T.-C.; Ji, H.; Kaduk, B.; Khistyaev, K.; Kim, J.; Kim, J.; King, R. A.; Klunzinger, P.; Kosenkov, D.; Kowalczyk, T.; Krauter, C. M.; Lao, K. U.; Laurent, A. D.; Lawler, K. V.; Levchenko, S. V.; Lin, C. Y.; Liu, F.; Livshits, E.; Lochan, R. C.; Luenser, A.; Manohar, P.; Manzer, S. F.; Mao, S.-P.; Mardirossian, N.; Marenich, A. V.; Maurer, S. A.; Mayhall, N. J.; Neuscamman, E.; Oana, C. M.; Olivares-Amaya, R.; O'Neill, D. P.; Parkhill, J. A.; Perrine, T. M.; Peverati, R.; Prociuk, A.; Rehn, D. R.; Rosta, E.; Russ, N. J.; Sharada, S. M.; Sharma, S.; Small, D. W.; Sodt, A; Stein, T.; Stück, D.; Su, Y.-C.;Thom, A. J. W.; Tsuchimochi, T.; Vanovschi, V.; Vogt, L.; Vydrov, O.; Wang, T.; Watson, M. A.; Wenzel, J.; White, A.; Williams, C. F.; Yang, J.; Yeganeh, S.; Yost, S. R.; You, Z.-Q.; Zhang, I. Y.; Zhang, X.; Zhao, Y.; Brooks, B. R.; Chan, G. K. L.; Chipman, D. M.; Cramer, C. J.; Goddard, W. A.; Gordon, M. S.; Hehre, W. J.; Klamt, A.; Schaefer, H. F.; Schmidt, M. W.; Sherrill, C. D.; Truhlar, D. G.; Warshel, A.; Xu, X.; Aspuru-Guzik, A.; Baer, R.; Bell, A. T.; Besley, N. A.; Chai, J.-D.; Dreuw, A.; Dunietz, B. D.; Furlani, T. R.; Gwaltney, S.R.; Hsu, C.-P.; Jung, Y.; Kong, J.; Lambrecht, D. S.; Liang, W.; Ochsenfeld, C.; Rassolov, V. A.;

Slipchenko, L. V.; Subotnik, J.E.; Voorhis, T.V.; Herbert, J.M.; Krylov, A. I.; Gill, P. M.W.; Head-Gordon, M. *Mol. Phys.* **2015**, *113*, 184–215.

(9) (a) Becke A. D. *J. Chem. Phys.* **1993**, *98*, 5648–5652. (b) Lee, C.; Yang, W.; Parr, R. G. *Phys. Rev. B* **1998**, *37*, 785–789.

(10) (a) Hay, P. J. Wadt, W. R. *J. Chem. Phys.* **1985**, *82*, 270–283. (b) Wadt, W. R.; Hay, P. J. *J. Chem. Phys.* **1985**, *82*, 284–298. (c) Wadt, P. J.; Wadt, W. R. *J. Chem. Phys.* **1985**, *82*, 299–310.

(11) Chai, J. D.; Head-Gordon, M. *Phys. Chem. Chem. Phys.* **2008**, *10*, 6615–6620.

(12) Cossi, M.; Rega, N.; Scalmani, G.; Barone, V. *J. Comput. Chem.* **2003**, *24*, 669–681.

(13) Marenich, A. V. Cramer, C. J.; Truhlar, D. G. *J. Phys. Chem. B* **2003**, *113*, 6378–6396.

(14) (a) Dunning Jr., T. H. *J. Chem. Phys.* **1989**, *90*, 1007–1023. (b) Woon, D. E.; Dunning Jr., T. H. *J. Chem. Phys.* **1993**, 98, 1358–1371. (c) Balabanov, N. B.; Peterson, K. A. *J. Chem. Phys.* **2005**, *123*, 064107.

(15) (a) Zimmerman, P. M. *J. Comput. Chem.* **2013**, *34*, 1385–1392. (b) Zimmerman, P. M. *J. Comput. Chem.* **2015**, *36*, 601–611.

(16) Nett, A. J.; Zhao, W.; Zimmerman, P. M.; Montgomery, J. A. *J. Am. Chem. Soc.* **2015**, *137*, 7636–7639.

(17) Ludwig, J R.; Zimmerman, P. M.; Gianino, J. B.; Schindler, C. S. *Nature*, **2016**, *533*, 374–379.

(18) (a) Zimmerman, P. M. *J. Chem. Phys.* **2013**, *138*, 184102; (b) Zimmerman, P. M. *J. Chem. Theory Comput.* **2013**, *9*, 3043–3050.

Appendix 3

Supporting Information for Chapter 4
Synthesis of P3HT with targeted dispersity and its role in thin-film morphology

I. Materials

iPrMgCl (2M in THF) was purchased in 100 mL quantities from Aldrich. 2,5-Dibromo-3-hexylthiophene was purchased from and purified by stirring with decolorizing carbon followed by filtration through a silica plug with hexanes as an eluent. All other reagent grade materials and solvents were purchased from Aldrich, Acros, or Fisher and were used without further purification unless otherwise noted. THF was dried and deoxygenated using an Innovative Technology (IT) solvent purification system composed of activated alumina, copper catalyst, and molecular sieves. The glovebox in which specified procedures were carried out was an MBraun LABmaster 130 with a N_2 atmosphere and H_2O levels below 4 ppm. Compound **2**[1] was prepared via literature procedure.

II. General Experimental

NMR Spectroscopy: Unless otherwise noted, ^{1}H, and ^{31}P NMR spectra for all compounds were acquired at rt in $CDCl_3$ on a Varian vnmrs 500 spectrometer operating at 500, and 202 MHz, respectively. Chemical shift data are reported in units of δ (ppm) relative to tetramethylsilane (TMS) and referenced with residual solvent. Multiplicities are reported as follows: singlet (s), doublet (d), triplet (t), multiplet (m). Residual water is denoted by an asterisk (*).

Mass Spectrometry: High-resolution mass spectrometry data were obtained on a Micromass AutoSpec Ultima Magnetic Sector mass spectrometer.

Gel-Permeation Chromatography: Polymer molecular weights were determined by comparison with polystyrene standards (Varian, EasiCal PS-2 MW 580–377,400) at 40 °C in THF on a Malvern Viscotek GPCMax VE2001 equipped with two Viscotek LT-5000L 8 mm (ID) × 300 mm (L) columns and analyzed with Viscotek TDA 305 (with RI, UV-PDA Detector Model 2600 (190–500 nm), RALS/LALS, and viscometer). All presented data correspond to the absorbance at 254 nm normalized to the highest peak. Samples were dissolved in THF (with mild heating), and passed through a 0.2 μm PTFE filter prior to analysis.

Gas Chromatography: Gas chromatography was carried out using a Shimadzu GC 2010 containing a Shimadzu SHRX5 (crossbound 5% diphenyl – 95% dimethyl polysiloxane; 15 m, 0.25 mm ID, 0.25 μm df) column.

*UV-Vis Spectroscopy*: UV-vis spectra were acquired using a Perkin Elmer Lambda 850 UV-vis Spectrometer.

X-Ray Diffraction: Samples were analyzed using a Rigaku SmartLab in the 2-theta geometry. Samples were scanned at a rate of 2 sec/step from $2\theta = 4$ to 40° with a step size of 0.01°.

III. Synthetic Procedures

a) PPh$_3$
b) 2-bromoanisole
c) dppe

Ni(cod)$_2$ → THF, rt

2
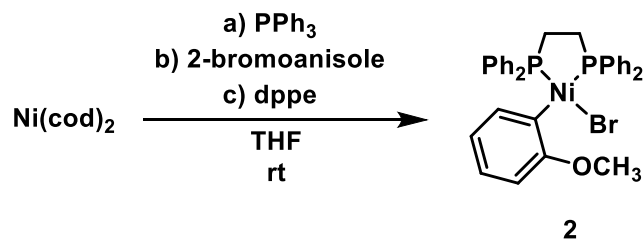
[1,2-bis(diphenylphosphino)ethane](2-methoxyphenyl)nickel(II) bromide (2).[1] In a glovebox, bis(1,5-cyclooctadiene)nickel(0) (84.9 mg, 0.309 mmol, 1 equiv) and triphenylphosphine (162 mg, 0.617 mmol, 2 equiv) were added to a 20 mL vial with a stir bar. The solids were dissolved in THF (4 mL), and the solution was stirred for 5 min. Subsequently, 2-bromoanisole (86.6 mg, 0.463 mmol, 1.5 equiv) was added and the solution was stirred for 2 h. Then, 1,2-bis(diphenylphosphino)ethane (111 mg, 0.278 mmol, 0.9 equiv) was added and the solution was stirred for 2 h. Subsequently, hexanes (15 mL) were added, and the sealed vial was placed in a -30 °C glovebox freezer for 18 h. The resulting orange solid was isolated by filtration and recrystallized from 1:8 DCM/hexanes to give 134 mg of **5** as an orange solid (75% yield). HRMS (ESI+): Calcd. for C$_{33}$H$_{31}$BrNiOP$_2$ [M-Br]$^+$ 563.1198; found 563.1200.

IV. NMR Spectra
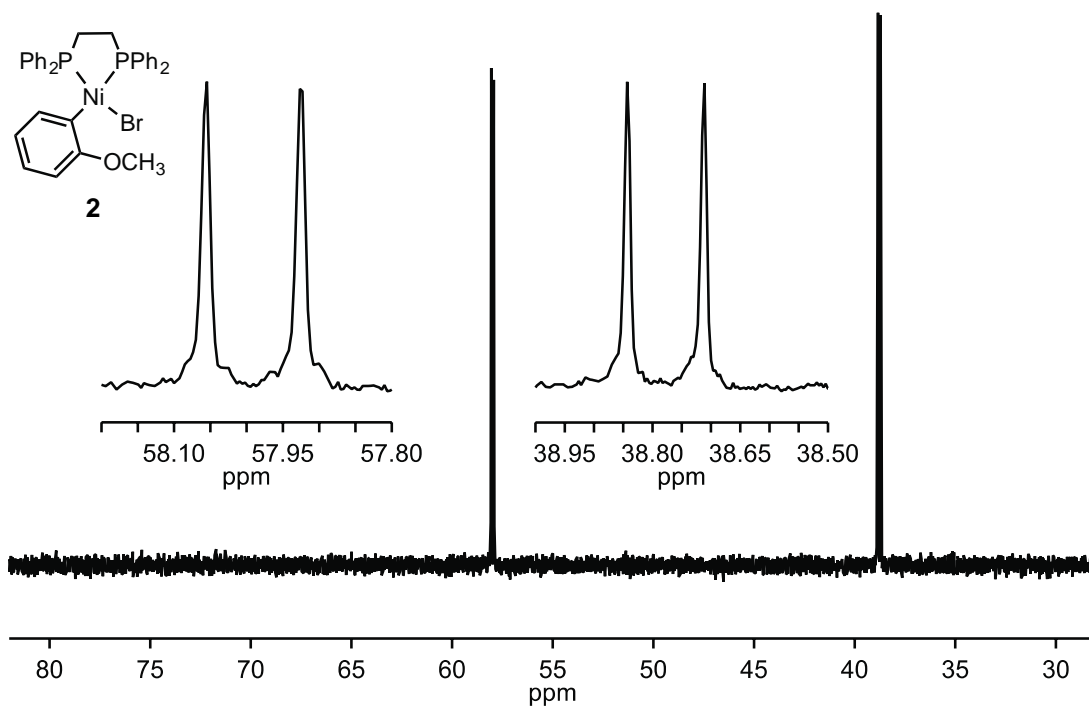
Figure S3.1. ^{31}P NMR spectrum of **2**. ^{31}P NMR (202 MHz, THF) δ 57.99 (d, J_{P-P} = 26.6 Hz), 38.78 (d, J_{P-P} = 26.6 Hz).

V. Batch Polymerizations

Representative procedure for the activation of monomer 1
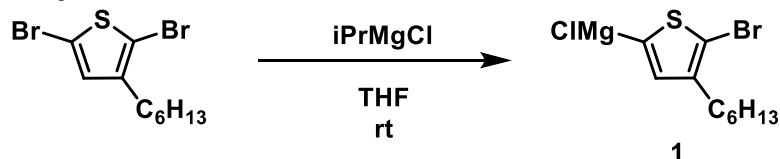
In a 20 mL vial equipped with a stir bar in a glovebox, 2,5-dibromo-3-hexylthiophene (1.04 g, 3.19 mmol, 1.00 equiv) and docosane (internal standard for measuring conversion, 140 mg) were dissolved in THF (5.43 mL). Then, iPrMgCl (1.36 mL, 2.0M in THF, 2.71 mmol, 0.85 equiv) was added. After stirring at rt in the glovebox for 40 min, the resulting monomer solution's concentration was determined by titration with salicylaldehyde phenylhydrazone.[2] It was then used in polymerizations within 30 min.

Polymerization of 1 with rapid addition of precatalyst 2
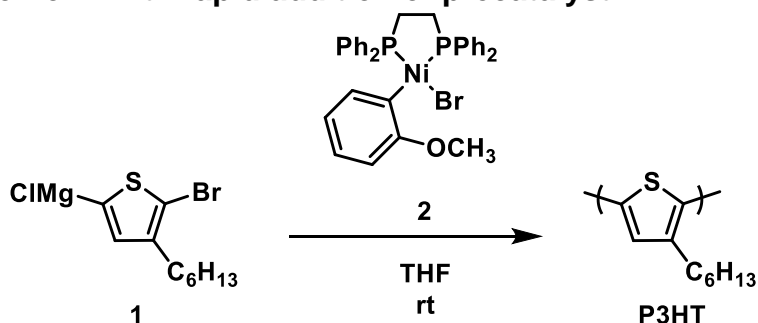
P3HT-A. In a 100 mL Schlenk flask equipped with a stir bar in a glovebox, monomer **1** (2.00 mL, 0.292 M in THF, 0.584 mmol, 60 equiv) was diluted with THF (70 mL). Precatalyst **2** (1.94 mL, 5.0 mM in THF, 9.69 µmol, 1.00 equiv) was injected. After 1 h, the solution was removed from the glovebox and poured into HCl (20 mL, 5M in DI H_2O). The organic products were extracted from the resulting aqueous mixture with $CHCl_3$ (50 mL) and conversion analyzed by GC. The polymer was precipitated from $CHCl_3$ into cold methanol and subjected to Soxhlet extraction with methanol, acetone, and $CHCl_3$ until each fraction ran clear (2-8 h). The $CHCl_3$ fraction was concentrated to a solid, then dissolved in THF (15 mL), dried over $MgSO_4$, filtered, and analyzed by GPC. M_n = 13.4 kDa, Đ = 1.18.

P3HT-B. As **P3HT-A**, with monomer **1** (2.00 mL, 0.292 M in THF, 0.584 mmol, 120 equiv), THF (70 mL), precatalyst **2** (0.971 mL, 5.0 mM in THF, 4.86 µmol, 1.00 equiv). , M_n = 18.5 kDa, Đ = 1.46.

P3HT-C. As **P3HT-A**, with monomer **1** (2.50 mL, 0.383 M in THF, 0.958 mmol, 180 equiv), THF (70 mL), precatalyst **2** (1.061 mL, 5.0 mM in THF, 5.30 µmol, 1.00 equiv). M_n = 33.8 kDa, Đ = 1.34.

P3HT-D. As **P3HT-A**, with monomer **1** (1.50 mL, 0.300 M in THF, 0.450 mmol, 240 equiv), THF (70 mL), precatalyst **2** (0.374 mL, 5.0 mM in THF, 1.87 µmol, 1.00 equiv). The crude polymer was additionally subjected to Soxhlet extraction with hexanes between acetone and CHCl$_3$. M_n = 41.9 kDa, Đ = 1.54.

P3HT-E. As **P3HT-D**, with monomer **1** (1.50 mL, 0.300 M in THF, 0.450 mmol, 300 equiv), THF (70 mL), precatalyst **2** (0.299 mL, 5.0 mM in THF, 1.50 µmol, 1.00 equiv). M_n = 51.0 kDa, Đ = 1.36.
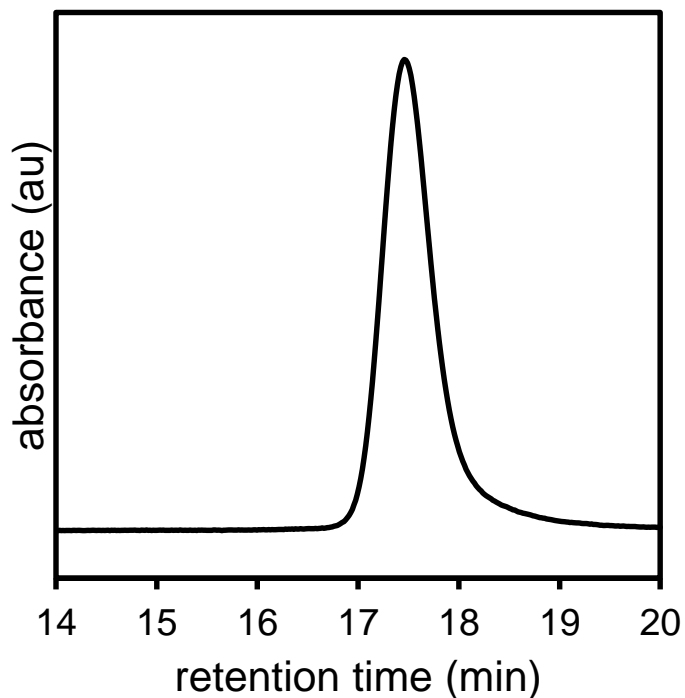
Figure S3.2. GPC trace of **P3HT-A**.
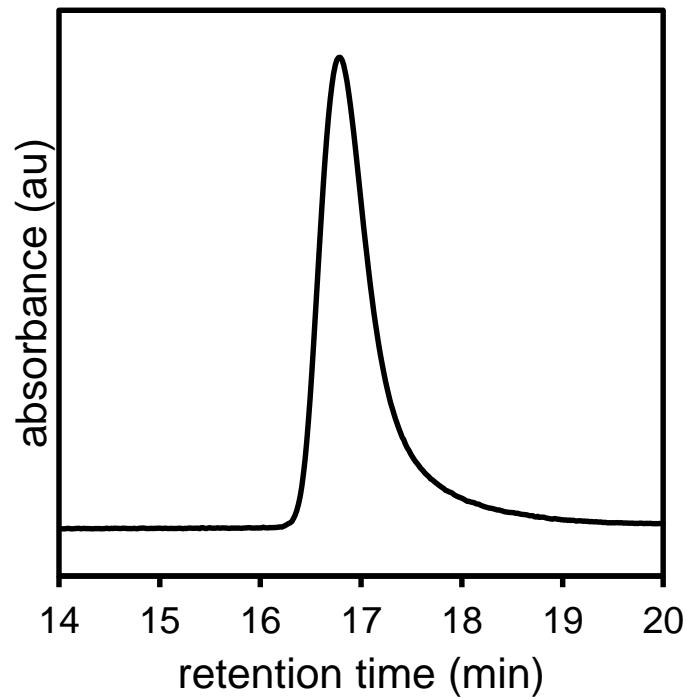
Figure S3.3. GPC trace of **P3HT-B**.
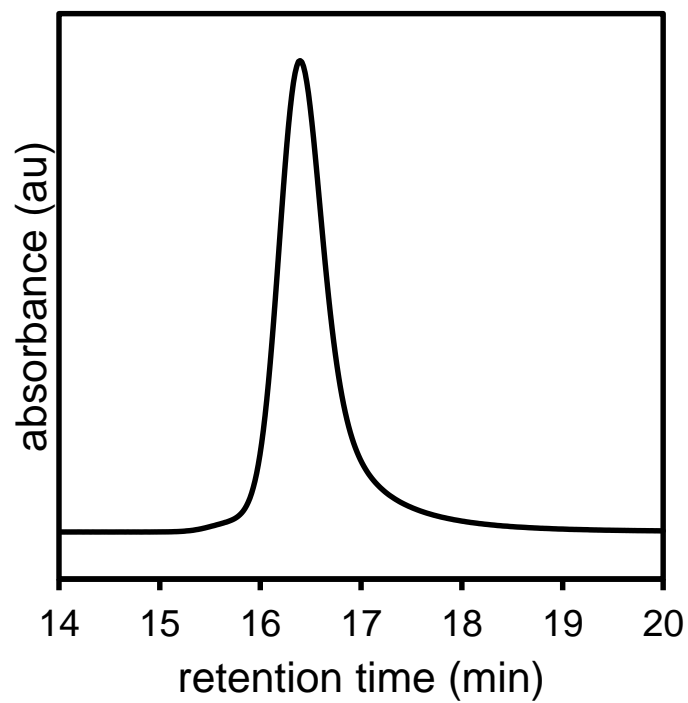
Figure S3.4. GPC trace of **P3HT-C**.
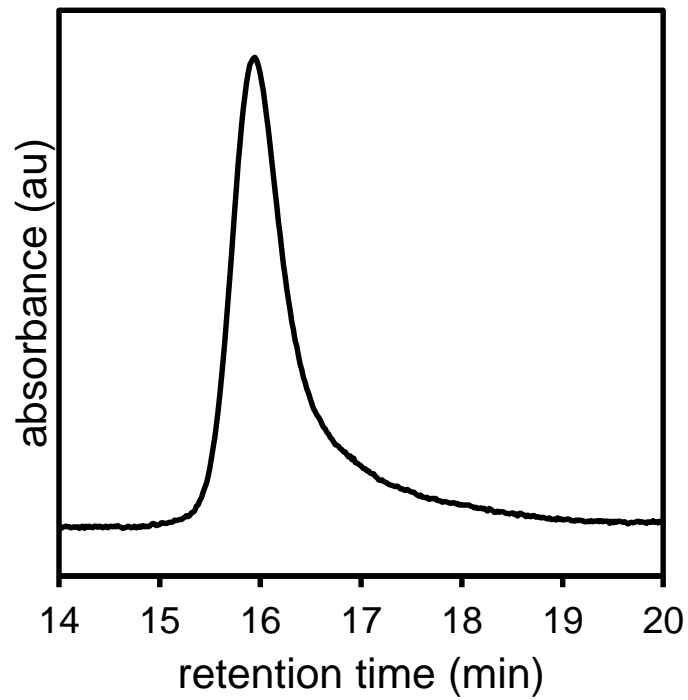
Figure S3.5. GPC trace of **P3HT-D**.
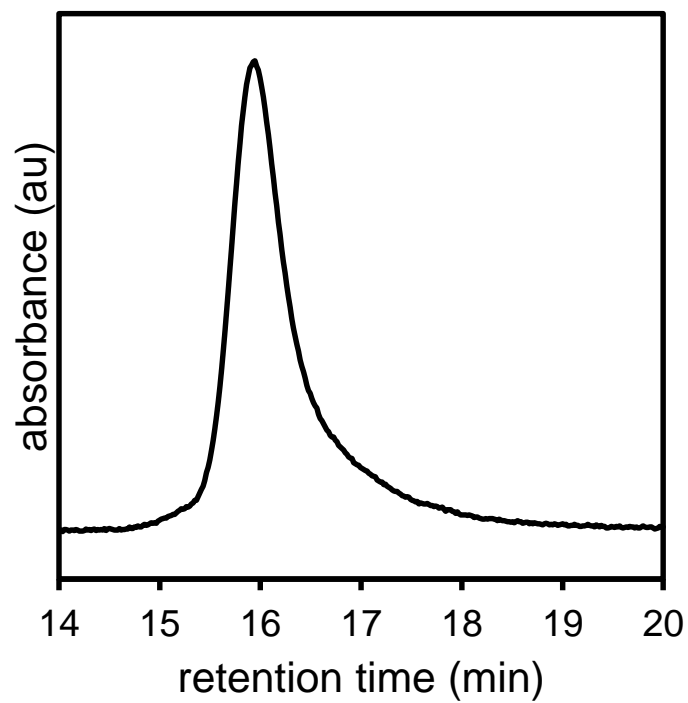
Figure S3.6. GPC trace of **P3HT-E**.
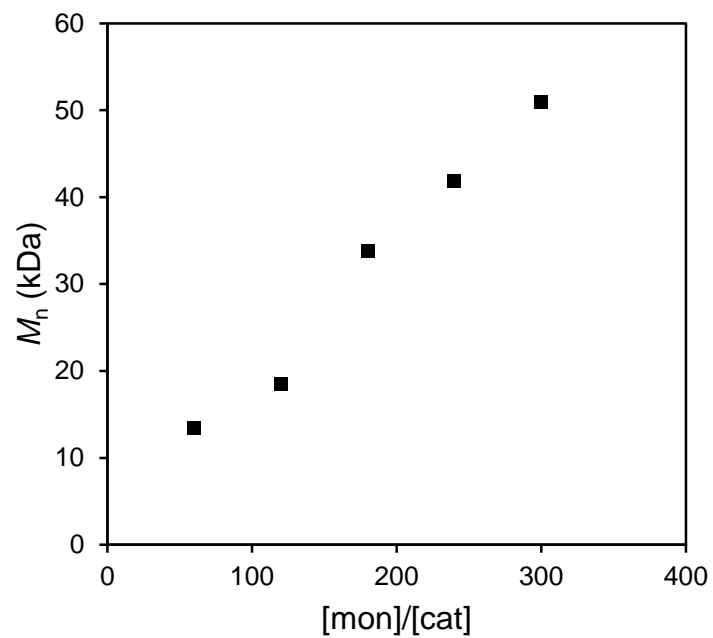
Figure S3.7 M_n vs [mon]/[cat] in the polymerization of **1** with **2**.

VI. Polymer Blending

Polymer samples **P3HT-A**, **-B**, **-C**, **-D**, and **-E** were dissolved in CHCl$_3$ at a concentration of 20 mg/mL. These solutions were combined in the ratios found in Table S3.1 to give constant M_n and increasing Đ (**-NX**), or constant M_w and increasing Đ (**-WX**). The blended samples were analyzed by GPC.

Table S3.1. Component ratios and GPC data for blended P3HT samples

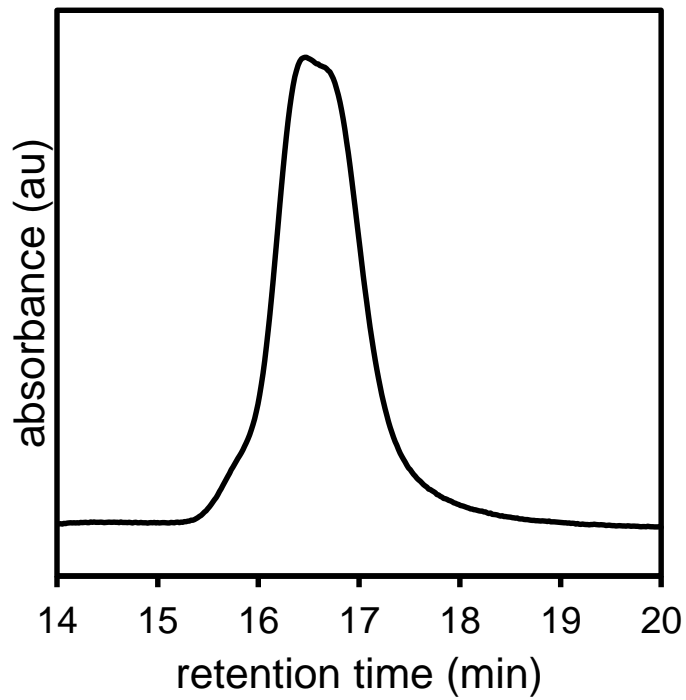|	A : B : C : D : E (wt%)	M_n (kDa)	M_w (kDa)	Đ
P3HT-N2	0 : 34.2 : 33.3 : 32.5 : 0	36.6	50.9	1.39
P3HT-N3	18.1 : 20.9 : 19.9 : 19.4 : 21.7	36.0	60.1	1.67
P3HT-N4	30.3 : 0 : 33.3 : 0 : 36.3	33.2	61.8	1.86
P3HT-W2	0 : 14.0 : 49.5 : 36.5 : 0	29.9	46.0	1.54
P3HT-W3	6.5 : 9.0 : 27.0 : 24.5 : 33.1	24.3	39.9	1.64
P3HT-W4	11.0 : 0 : 33.4 : 0 : 55.6	20.9	37.8	1.81
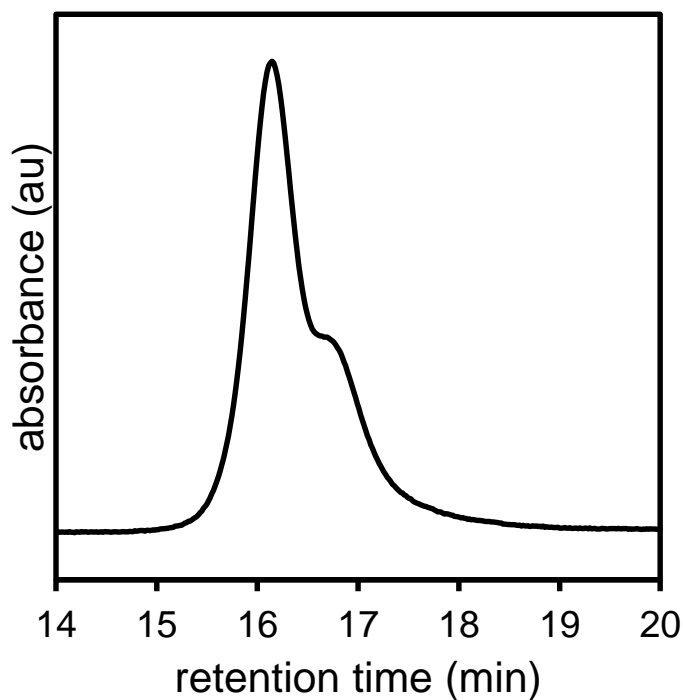
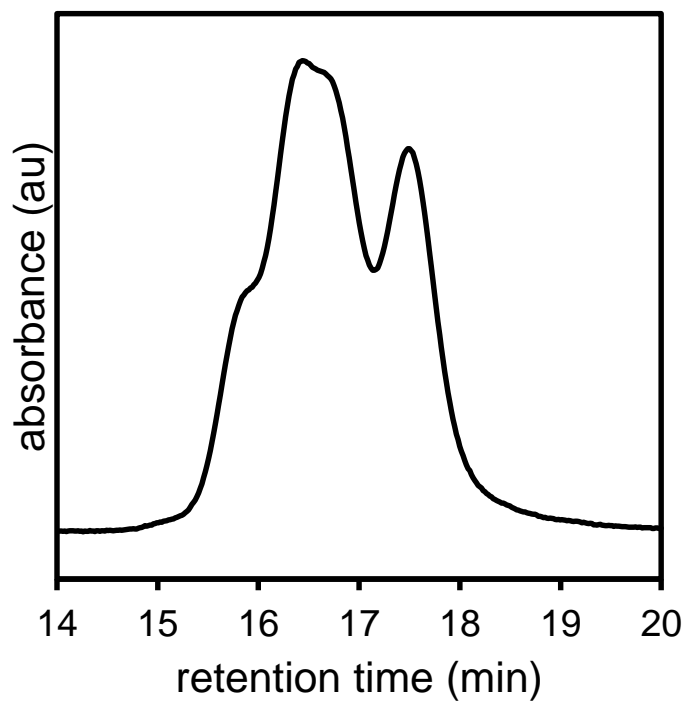**Figure S3.8** GPC trace of **P3HT-N2**.
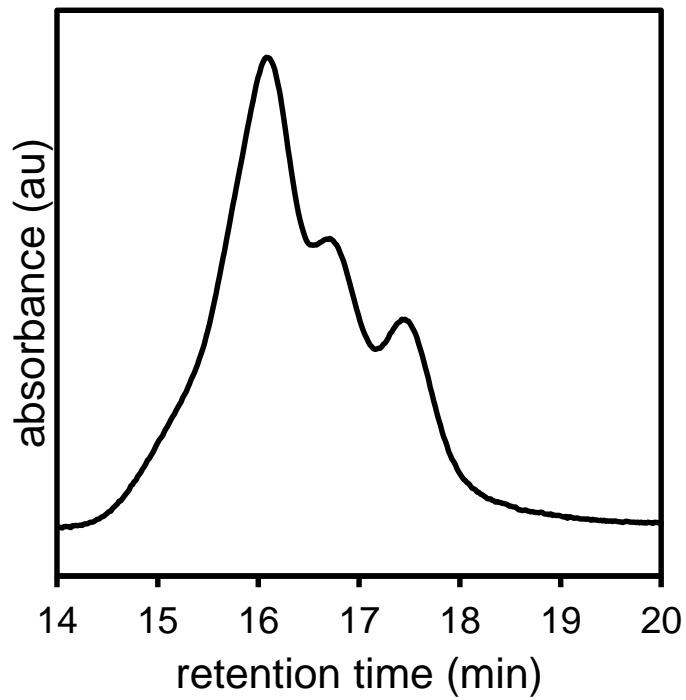
Figure S3.9 GPC trace of **P3HT-N3**.
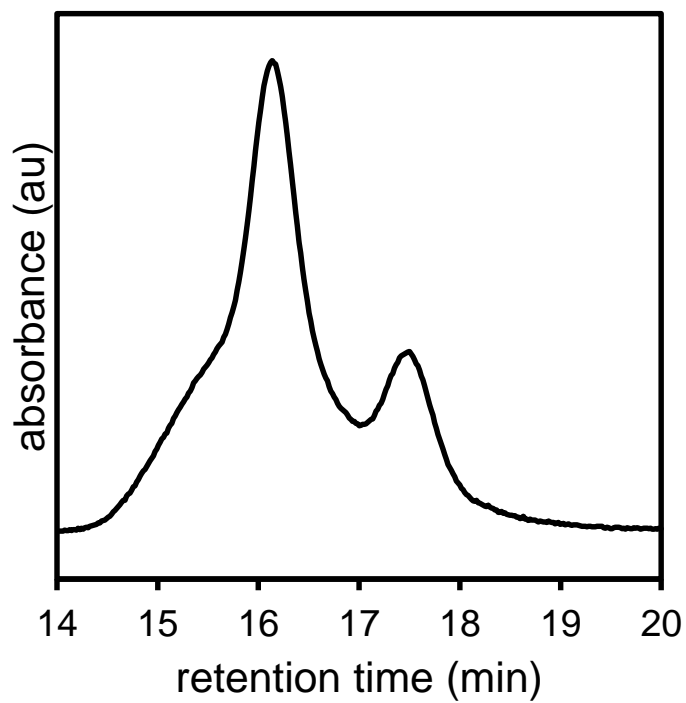
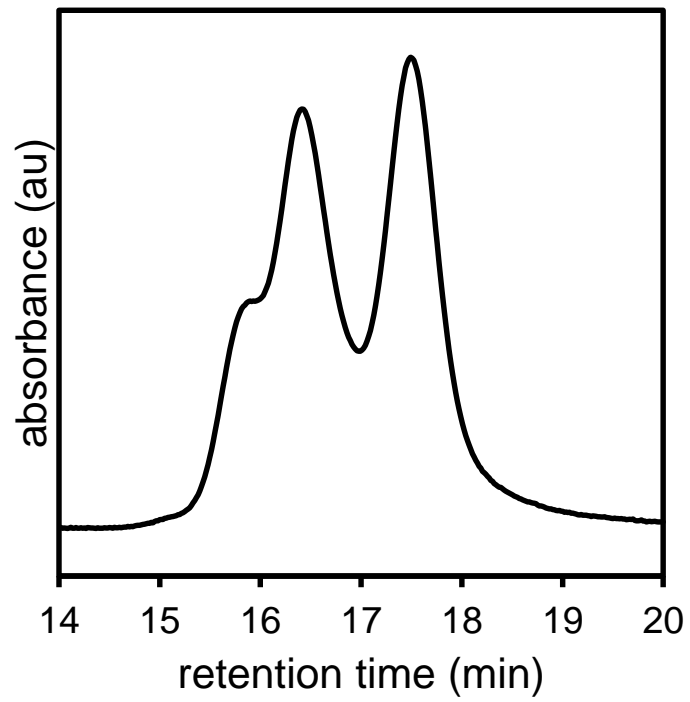**Figure S3.10** GPC trace of **P3HT-N4**.
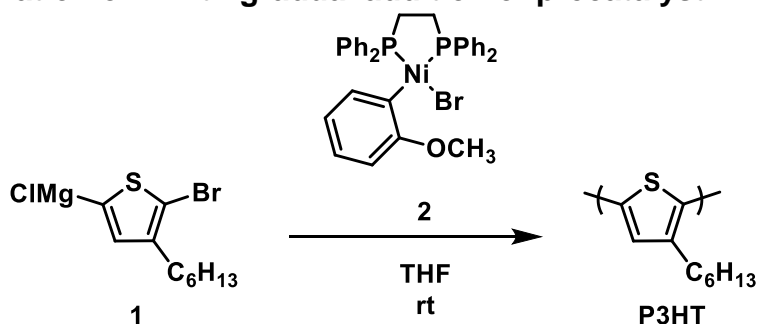
Figure S3.11 GPC trace of **P3HT-W2**.

Figure S3.12 GPC trace of **P3HT-W3**.
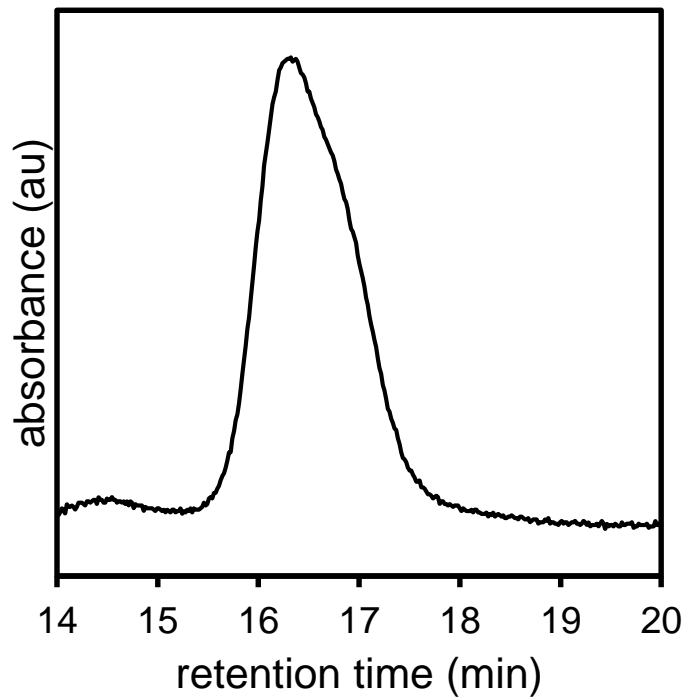
Figure S3.13 GPC trace of **P3HT-W4**.

## VII. Polymerization of 1 with gradual addition of precatalyst 2

P3HT-G1. In a 500 mL Schlenk flask equipped with a stir bar in a glovebox, monomer **1** (1.00 mL, 0.367 M in THF, 0.367 mmol, 180 equiv) was diluted with THF (35 mL), then removed from the glovebox and placed under N_2. Precatalyst **2** (1.00 mL, 2.03 mM in THF, 2.03 μmol, 1.0 equiv) was injected dropwise over 5 min using a syringe pump. After 1 h, the solution was poured into HCl (20 mL, 5M in DI H_2O). The organic products were extracted from the resulting aqueous mixture with $CHCl_3$ (50 mL) and the conversion analyzed by GC. The polymer was precipitated from $CHCl_3$ into cold methanol and subjected to Soxhlet extraction with methanol, acetone, and $CHCl_3$ until each fraction ran clear (2-8 h). The $CHCl_3$ fraction was concentrated to a solid, then dissolved in THF (15 mL), dried over $MgSO_4$, filtered, and analyzed by GPC. M_n = 39.1 kDa, Đ = 1.20.

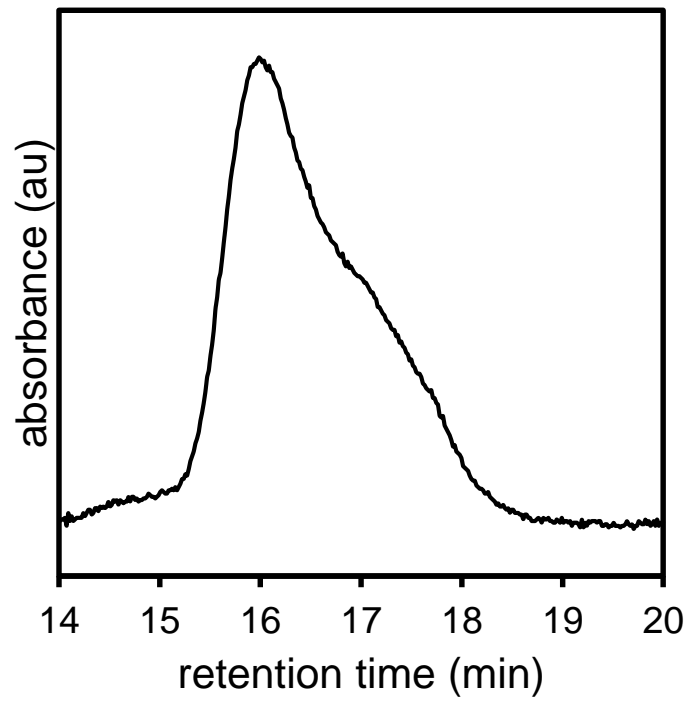**P3HT-G2**. As **P3HT-G1**, except catalyst added over 10 min. M_n = 42.1 kDa, Đ = 1.38.

P3HT-G3. As **P3HT-G1**, except catalyst added over 15 min. M_n = 35.7 kDa, Đ = 2.15.

Figure S3.14 GPC trace of **P3HT-G1**.
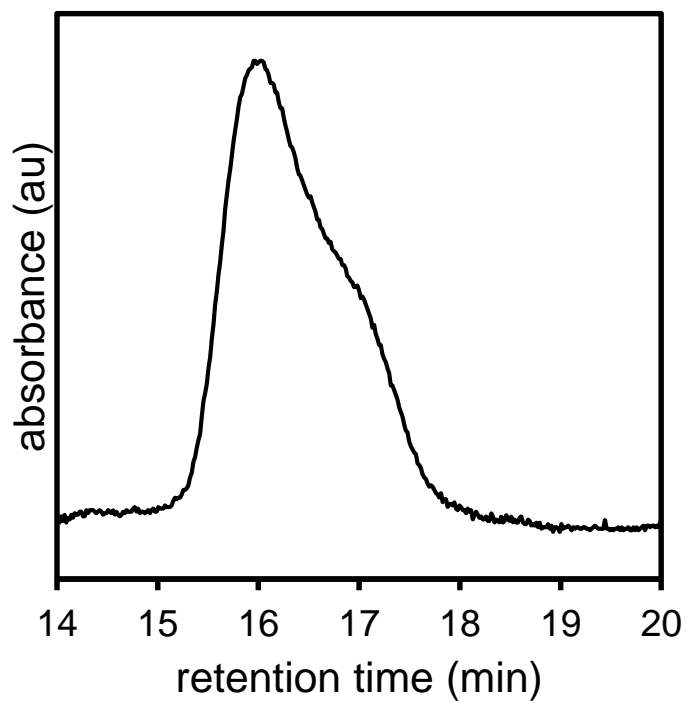
Figure S3.15 GPC trace of **P3HT-G2**.

Figure S3.16 GPC trace of **P3HT-G3**.

VIII. Thin-film Preparation and Analysis

Spin-coating of thin films

The narrowly disperse polymer sample **P3HT-C**, the blended samples **P3HT-N2**, **-N3**, **-N4**, **-W2**, **-W3**, and **-W4**, and the gradual addition samples **P3HT-G1**, **-G2**, and **-G3** were dissolved in 1,2-dichlorobenzene at a concentration of 17 mg/mL. Approximately 100 mg of each polymer sample was used. Separately, $PC_{61}BM$ was dissolved in 1,2-dichlorobenzene at a concentration of 17 mg/mL. Each polymer solution (0.1 mL) was combined with fullerene solution (0.1 mL) and stirred for 1 h at 60 °C. The 1 cm x 1cm glass slides were cleaned with Hellmanex III detergent in DI water, followed by sonication for 15 min in, sequentially, acetone and 2-propanol. Approximately 0.1 mL of each polymer solution and polymer+fullerene solution was spin-coated onto a glass slide using a rate of 2000 rpm for 60 s. Films were then annealed in a vacuum oven at 150 °C for 30 min.

Films containing fullerene are denoted by an appended **F**.

UV-vis analysis of thin films

To interpret the UV-vis spectra following Spano's H-aggregate model, it is useful to quantify the intensities of each relevant absorbance.[3] Spectra were deconvoluted via iterative fitting of Gaussians corresponding to π-π*, 0-1, 0-0, and (when present) PCBM absorption.[4]

Table S3.2 Selected parameters from Gaussian fitting

|	π-π* λ_{max} (nm)	π-π* amplitude	0-0 amplitude	0-1 amplitude	PCMB amplitude
P3HT-C	541.4	0.9239	0.3356	0.1313	--
P3HT-N2	547.2	0.7958	0.4044	0.2479	--
P3HT-N3	536.0	0.8847	0.4087	0.1916	--
P3HT-N4	535.4	0.8874	0.3814	0.1813	--
P3HT-W2	544.3	0.9566	0.3115	0.1116	--
P3HT-W3	544.4	0.9314	0.3638	0.1391	--
P3HT-W4	537.4	0.8559	0.4313	0.2121	--
P3HT-G1	536.18	0.8840	0.3393	0.1905	--
P3HT-G2	534.5	0.9081	0.3746	0.1727	--
P3HT-G3	536.6	0.8664	0.3506	0.2276	--
P3HT-CF	536.0	0.9057	0.4326	0.1749	0.1368
P3HT-N2F	516.6	0.9414	0.3988	0.2572	1.1358
P3HT-N3F	520.6	0.9981	0.3476	0.1812	0.9156
P3HT-N4F	531.1	0.9244	0.3660	0.1723	0.6931
P3HT-W2F	531.2	0.9208	0.2913	0.1420	0.5824
P3HT-W3F	534.5	0.8995	0.3670	0.1697	0.4957
P3HT-W4F	534.5	0.9570	0.3492	0.1345	0.4575
P3HT-G1F	514.6	0.9509	0.3100	0.2525	0.9428
P3HT-G2F	519.4	0.9628	0.2717	0.1842	0.8185
P3HT-G3F	506.3	0.9568	0.2737	0.2438	1.3100
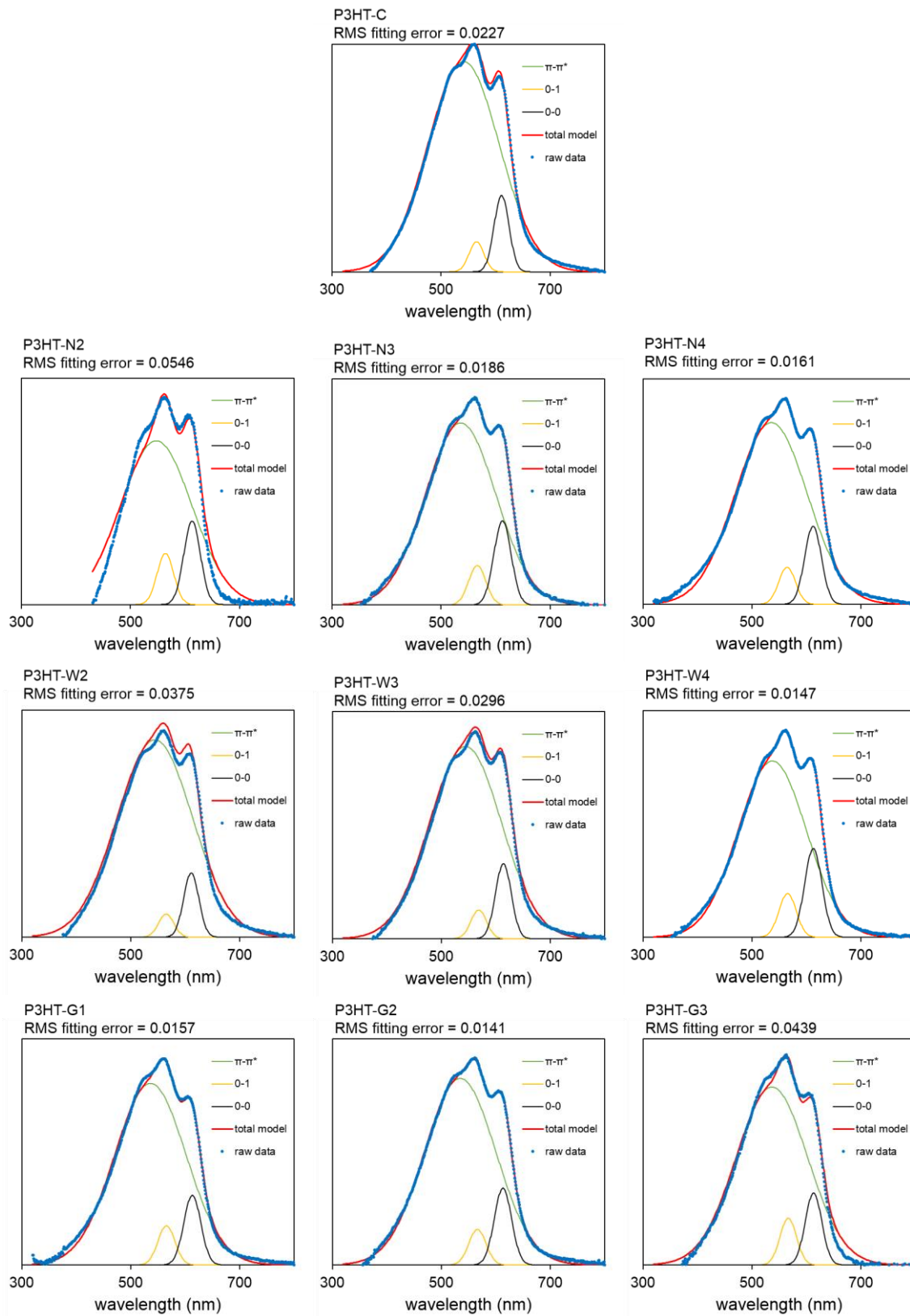
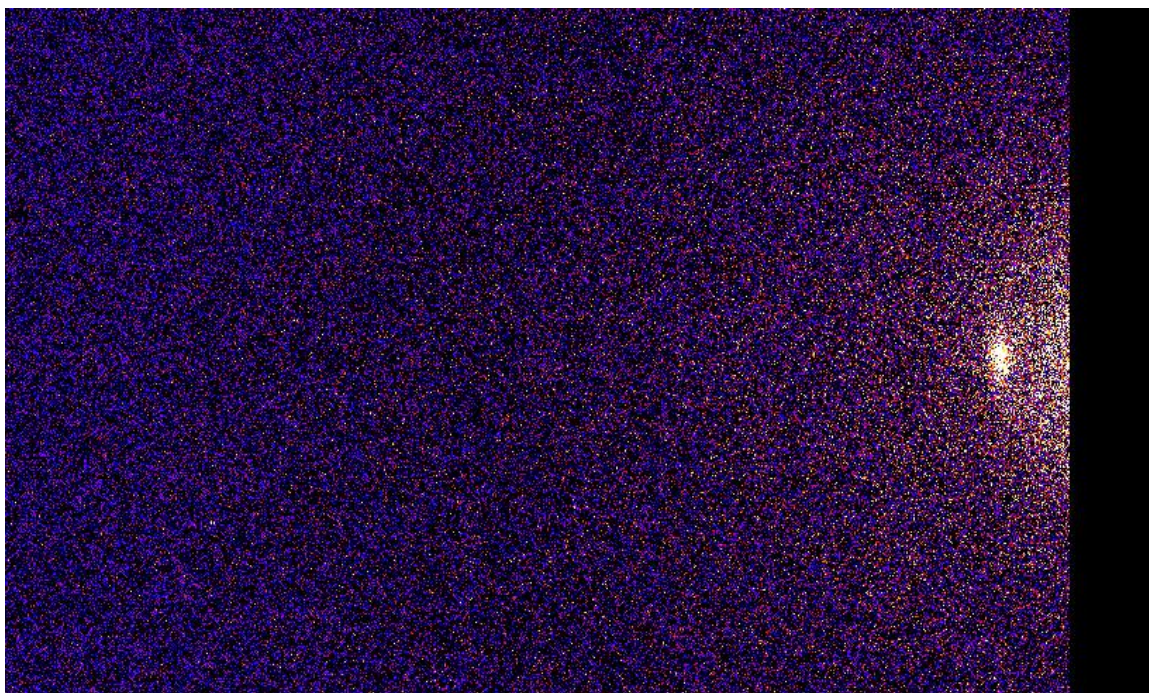**Figure S3.17** UV-Vis spectra for polymer thin films with Gaussian fits
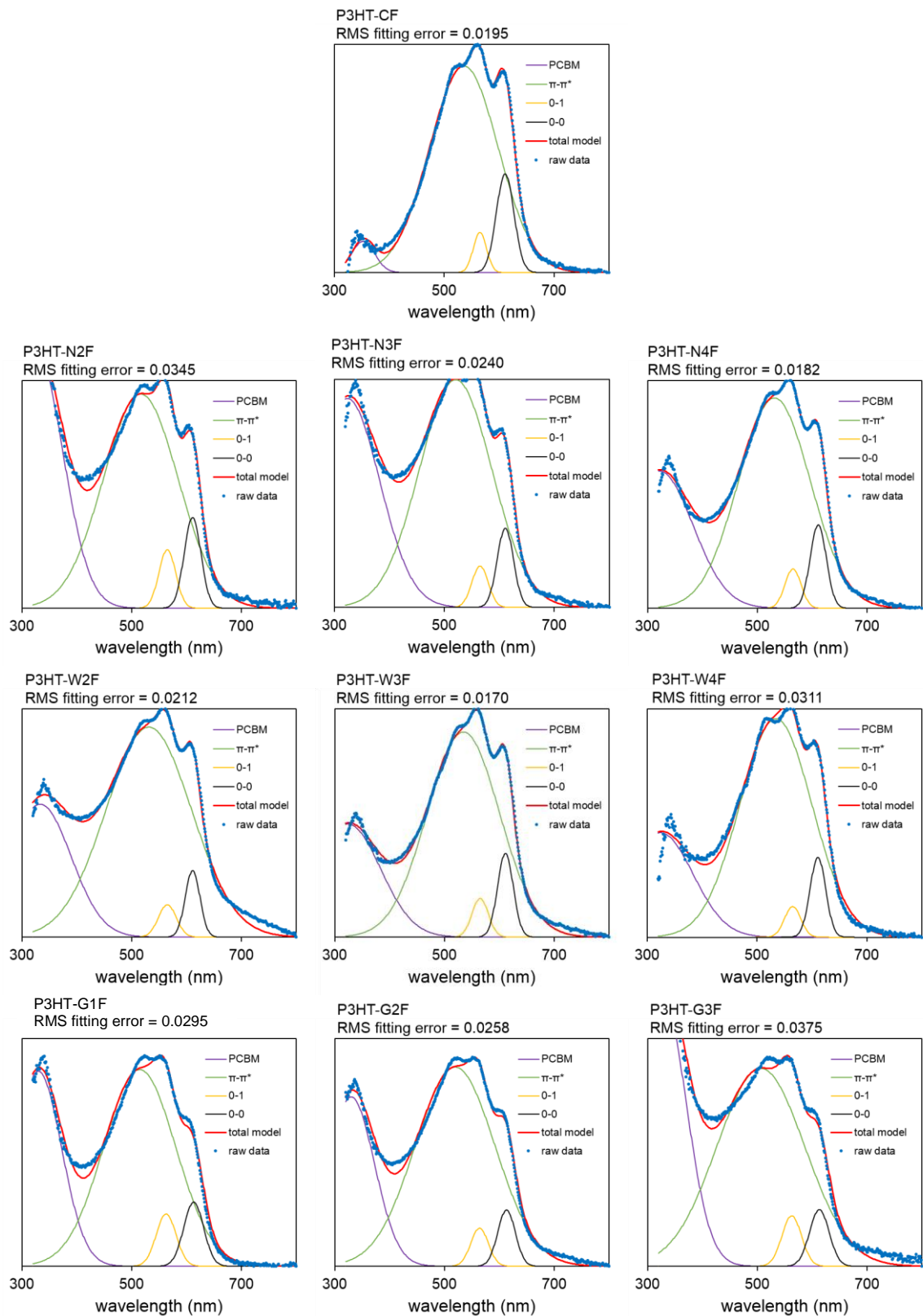
Figure S3.18 UV-Vis spectra for polymer-fullerene thin films with Gaussian fits
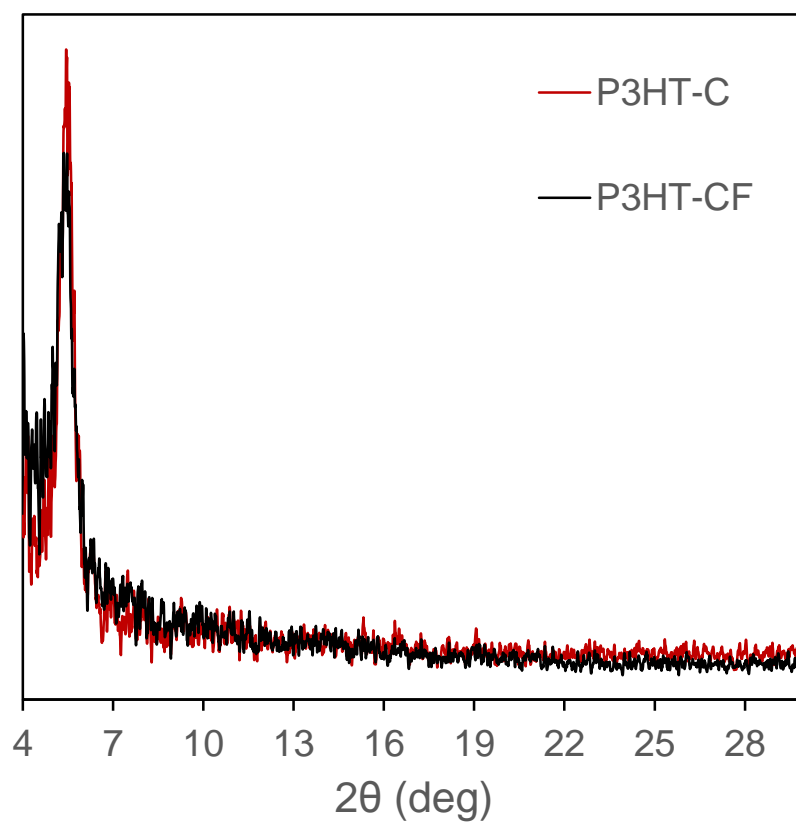
Preliminary XRD of thin films
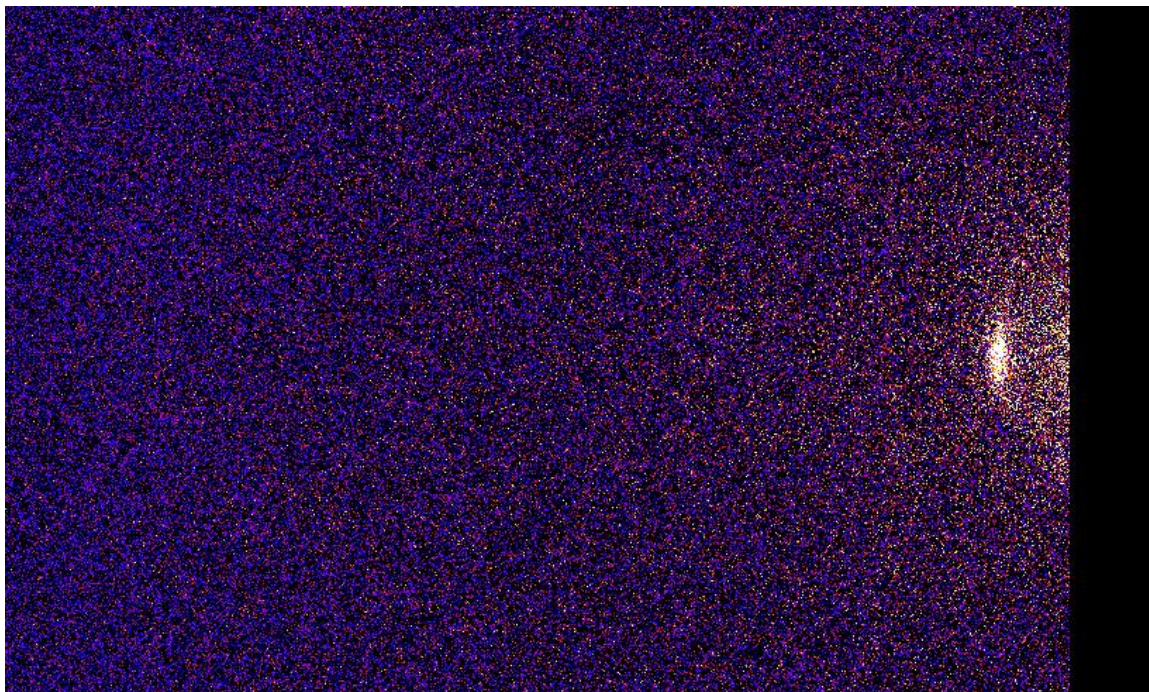
Figure S3.19 Diffraction pattern of P3HT-C film. Glass slide background has been subtracted.

Figure S3.20 Diffraction pattern of **P3HT-CF** film. Glass slide background has been subtracted.

Figure S3.21 Diffractograms of **P3HT-C** and **P3HT-CF** films.

IX. References

(1) Smith, M. L.; Leone, A. K.; Zimmerman, P. M.; McNeil, A. J. *ACS Macro Lett.* **2016**, *5,* 1411-1415, which modifies a procedure from Pammer, F.; Jäger, J.; Rudolf, B; Sun, Y. *Macromolecules* **2014**, *47*, 5904–5912.

(2) Love, B.E.; Jones, E. G. *J. Org. Chem.* **1999** *64*, 3755–3756.

(3) Spano, F. C.; *J. Chem. Phys.* **2005**, *122*, 234701.

(4) We employed an Excel spreadsheet modified from O'Haver, T. "Non-Linear Iterative Curve Fitting." in *A Pragmatic Introduction To Signal Processing*." Retrieved 20 December 2016. Available online at: https://terpconnect.umd.edu/~toh/spectrum/